The Biochemistry behind anthocyanins bioavailability

Hélder José Couto Oliveira
PhD in Sustainable Chemistry
Department of Chemistry and Biochemistry
2018

Supervisor
Professor Nuno Mateus, Associate Professor, Faculty of Sciences University of Porto

Co-supervisors
Professor Conceição Calhau, Associate Professor, Nova Medical School, Medical Sciences Faculty New University of Lisbon

Doctor Iva Fernandes, Post-Doctoral Researcher, Faculty of Sciences University of Porto

PUBLICATIONS LIST

This research was developed at LAQV-REQUIMTE, Department of Chemistry and Biochemistry of the Faculty of Sciences University of Porto, with the financial support of a PhD fellowship (PD/BD/106062/2015) attributed by the Medical Biochemistry and Biophysics Doctoral Programme (M2B-PhD).

This dissertation contains results that were published in international scientific conferences trough oral and panel communications, and in international scientific journals:

Articles in international scientific journals

5. **Oliveira, H.,** Basílio, N., Pina, F., de Freitas, V., Mateus, N., Fernandes, I., "Physical and Chemical Properties of Anthocyanins from Purple-fleshed Sweet Potato", Submitted for publication.

4. **Oliveira, H.,** Roma-Rodrigues, C., Santos, A., Veigas, B., Brás, N., Faria, A., Calhau, C., de Freitas, V., Baptista, P. V., Mateus, N., Fernandes, A. R., Fernandes, I., (2018) "GLUT1 and GLUT3 involvement in anthocyanin gastric transport – Nanobased targeted approach", Submitted for publication.

3. **Oliveira, H.,** Perez-Gregório, R., de Freitas, V., Mateus, N., Fernandes, I. (2018) "Comparison of the in vitro gastrointestinal bioavailability of acylated and non-acylated anthocyanins: Purple-Fleshed Sweet Potato vs Red Wine.", Food Chemistry accepted manuscript, DOI: 10.1016/j.foodchem.2018.09.159

2. **Oliveira, H.,** Cai, X., Zhang, Q., de Freitas, V., Mateus, N., He, J., Fernandes, I. (2017). "Gastrointestinal absorption, antiproliferative and anti-inflammatory effect of the major carotenoids of *Gardenia Jasminoides* Ellis on cancer cells", Food and Function, 8, 1672-1679. DOI: 10.1039/c7fo00091j

1. **Oliveira, H.,** Wu, N., Zhang, Q., Wang, J., Oliveira, J., de Freitas, V., Mateus, N., He, J., Fernandes, I. (2016). "Bioavailability studies and anticancer properties of malvidin based anthocyanins, pyranoanthocyanins and non-oxonium derivatives", Food and Function, 7, 2462-2468. DOI: 10.1039/c6fo00445h.

Oral communications in international conferences

4. **Oliveira, H.,** Fernandes, I., de Freitas, V., Mateus, N., "Nanobased targeted approach to study anthocyanins transport through MKN-28 Cells: putative involvement of Glucose Transporters", 2nd International Conference on Food Bioactives and Health, Lisbon, Portugal, 26-28 September 2018.

3. **Oliveira, H.,** Fernandes, I., de Freitas, V., Mateus, N. "Unveiling the molecular mechanism of acylated anthocyanins gastrointestinal absorption", 29th International Conference on Polyphenols, Madison, United States of America, 16-20 July 2018.

2. **Oliveira, H.,** Fernades, I., He, J., de Freitas, V., Mateus, N., "Complex Anthocyanins from Purple Sweet Potato towards novel technological applications", 23th Galician-Portuguese Meeting of Chemistry, Ferrol, Spain, 15-17 November 2017.

1. **Oliveira, H.,** Fernandes, I., de Freitas V., Mateus, N., "The biochemistry behind food polyphenols bioavailability and bioactivity", 3th Medical Biochemistry and Biophysics Doctoral Programme International Meeting, Coimbra, Portugal, 16-18 October 2017.

ACKNOWLEDGMENTS

The success of this work was not possible without the collaboration and support of several important people and institutions. Thus, I would like to formally express my deep gratitude:

To Professor Nuno Mateus, supervisor of this work, for the constant support and availability, for the critical reviews and suggestions during the entire project, for the motivation, and for the trust.

To Doctor Iva Fernandes, co-supervisor of this work, for all the support, commitment, motivation and trust. Thank you for living this with an enormous enthusiasm and, above all, for being more than a supervisor, for being a friend.

To Professor Victor de Freitas, for always having the right opinion and for the transmission of knowledge on a daily basis that truly helped me during this path. And for trust me as a multi-tasker on areas far from scientific research.

To Professor Jingren He, from the Polytechnic University of Wuhan, for making me feel home every single day during my internship in China.

To Nuno Basílio and Professor Fernando Pina, from the New University of Lisbon, for all the help and knowledge transmitted. Always ready to make me feel amazed with the wonders of photochemistry. Also thank you for the precious knowledge on fluorescence studies.

To Professors Pedro Viana Baptista and Alexandra Fernandes, from the New University of Lisbon, for receiving me in their research group, for the precious knowledge on molecular biology, advises and collaborations.

To Professor Conceição Calhau for the supervision of this work.

To all the elements of the Department of Chemistry and Biochemistry of the Faculty of Sciences that somehow contributed for the success of this work.
To Faculty of Sciences of University of Porto for being responsible for my academic and scientific growth.
To Professors Nuno Santos, Miguel Castanho and Graça Soveral, for giving me the chance to perform this work through the attribution of the M2B-PhD scholarship.
To Professors Artur Silva, Baltazar Castro and Manuel Nunes da Ponte, for accepting me as a student on the Sustainable Chemistry Doctoral Programme.
To Fundação para a Ciência e Tecnologia (FCT) for the financial support through the M2B-PhD programme with a scholarship (PD/BD/106062/2015).

To all the people that work on the Food Polyphenol Lab, for help me growing at all levels.
In special, to my dear “dinosaurs” friends, Ana Luísa, Joana Azevedo, Joana Oliveira, Susana Soares, Rosa Perez-Gregorio, Luís Cruz and Natércia Teixeira, that in a way or another helped me, being always available when needed. For all the moments together and for always let me be the clown.
To the younger generation of the lab, Paulinha, Elsa, Vânia, Marta, Ricardo and Telmo, for the coffees, beers, and scientific discussions.
To all my friends, for living with me the good and the bad of life, for the laughs and love, for the ups and downs. 2 miles or 20000 miles away, there’s no difference. The world is ours!
To my dear girlfriend for all the comprehension and love.
To my dear sister for being always there, for giving me guidance through the years, and for being like a mother to me and my dad.
To Paula and Francisco for making my dad’s life shine again.
And finally, to my dad for being my best friend and idol, my number one fan, for always giving me the most amazing perspective of life, for all the efforts to make me a better person and for always trust me.

To Mom,
I made myself to your image.
Look for us wherever you are,
Hope you're proud.

ABSTRACT

Anthocyanins are amazing compounds that belong to the class of flavonoids. They are water soluble and have well-known health benefits. Although all over the years a panoply of evidences suggests that anthocyanins have an overall poor bioavailability, a lot is yet to discover to reach a full understanding on this matter.

Anthocyanins from Purple-Fleshed Sweet Potato were used and characterized, due to the fact that these anthocyanins have a higher degree of complexity and are less studied than the common anthocyanins.

The anthocyanins were extracted and the content analysed by analytical methods and were identified as Peonidin and Cyanidin derivatives with multiple glucosylations and acylations. Two of the main anthocyanins were isolated and their structure characterized by the analysis of LC-MS fragmentation patterns and one and two-dimensional NMR analysis. The anthocyanins were identified as being *Peonidin-3-(6'-hydroxybenzoyl)-sophoroside-5-glucoside* and *Peonidin-3-(6'-hydroxybenzoyl-6''-caffeoyl)-sophoroside-5-glucoside*. Furthermore, the acid-base network of these two acylated anthocyanins was evaluated by means of *pH jump* techniques and the results suggested a higher resistance to pH variations than the parent anthocyanin Peonidin-3-*O*-glucoside. The fluorescence properties of these two anthocyanins were evaluated. Overall, the species present at higher pH values (from neutral to slightly basic) showed the most interesting fluorescence characteristics for both anthocyanins. An optimum $\lambda_{ex}/\lambda_{em}$ pair was set at λ_{ex} 610 nm/ λ_{em} 640 nm. This finding was very interesting due to the fact that is rare for anthocyanins to have clear fluorescence properties.

Simulated oral, gastric and intestinal digestions were performed, for Purple-Fleshed Sweet Potato anthocyanins and for Red Wine anthocyanins, for comparison. Overall, the results suggest that anthocyanins are degraded only at the intestinal level, also a protective effect of matrix components against the degradation through digestive

processes was observed. Purple-Fleshed Sweet Potato anthocyanins showed higher resistance to digestions when compared to Red Wine anthocyanins.

Transepithelial transport of Purple-Fleshed Sweet Potato anthocyanins was assayed using two different cell lines, MKN-28 (gastric cavity) and Caco-2 (intestinal cavity). The determination of the kinetic parameters suggested a similar absorption, however, anthocyanins from Purple-Fleshed Sweet Potato showed more ability to cross MKN-28 cells, with a higher $V_{máx}$ and K_M when compared to Caco-2 cells.

The effect of food matrix on the transport efficiency of these anthocyanins was also evaluated. Overall, starch did not affect the transport in both cell lines, however, the presence of glucose and proteins significantly reduced the transport efficiency. The intracellular localization of the anthocyanins was assayed, by fluorescence microscopy. It was possible to see that anthocyanins localize inside cells, mainly accumulated in specific regions (probably vesicles) of both MKN-28 and Caco-2 cells.

A nano-approach to assess the mechanism of absorption of anthocyanins in MKN-28 cells was also used. The effect of temperature was evaluated and the results demonstrated a very significant reduction of the transport efficiency at 4ºC.

Gold nanoparticles were used to deliver anti-sense sequences to the target mRNAs selected for this work: the mRNA responsible for the synthesis of the glucose transporters GLUT1 and GLUT3.

The results demonstrated that the transport efficiency of all the anthocyanins tested was reduced in the presence of both anti-GLUT1 and anti-GLUT3 nanoparticles. Efflux and organic transporters inhibition was also performed, suggesting that other transporters besides GLUTs may be involved in the absorption of anthocyanins at the gastric level. Computational biochemical studies were performed, and the results corroborate with the previous experimental results.

Overall the results presented and discussed give new insights to better understand the complexity involved in anthocyanins bioavailability.

Furthermore, other sources of anthocyanins and other natural compounds were used to evaluate specific aspects of bioavailability and bioactivity.

The gastric transport efficiency of malvidin-3-glucoside and several derivatives was assayed on MKN-28 cell model. It was possible to observe that pyranoanthocyanins may slightly impair transport efficiency levels in comparison with native anthocyanins. The work

focused on the structural differences between the compounds tested and among the pyranoanthocyanin derivatives the presence of the carbonyl group and the absence of charge were important for the transport efficiency percentage of oxovitisin A and apparently compensated the negative effect associated with the additional ring.

Moreover, and after proving the ability to cross MKN-28 cell line barrier, the antiproliferative properties of these compounds in MCF-7 cancer cell line were assayed.

Oxovitisin A showed the highest efficiency in inhibiting the proliferation of MCF-7 cells.

A study of the fluorescence properties of oxovitisin A was performed and a kinetic incorporation of oxovitisin A was assayed revealing that this pyranoanthocyanin is quickly incorporated into cells.

This study confirmed the importance of the natural micro-oxidative processes that occur during ageing of anthocyanin-containing food and their impact on their bioavailability and bioactivity properties.

Finally, the gastrointestinal absorption of the main carotenoids present in *Gardenia jasminoides Ellis*, crocetin, crocin-1 and crocin-2, through transport studies on MKN-28 and caco-2 cell lines.

Overall, crocetin was the compound that presented the highest gastrointestinal transport efficiency.

Additionally, and since, after absorption, crocins is metabolized into crocetin, the antiproliferative capacity of crocetin was assayed in MKN-28 (stomach), MCF-7 (breast) and caco-2 (colon) cancer cell lines.

The results point to an antiproliferative effect of crocetin on the three cell lines tested.

Anti-inflammatory properties were also assayed. Overall, crocetin showed a potential involvement in the downregulation of IL-1β and TNF-α but not IL-6.

Altogether, the results suggest that these compounds can have an important role against cancer proliferation, highlighting the importance of *Gardenia Jasminoides Ellis* as a nutraceutical food source.

Keywords: Anthocyanins, Bioavailability, Transepithelial Transport, Polyphenols, Glucose Transporters, Purple-Fleshed Sweet Potato

INDEX

LIST OF FIGURES

LIST OF TABLES

LIST OF ATTACHMENTS

LIST OF ABBREVIATIONS

All the abbreviations are indicated during the text.
The list will just include the most relevant.

Caco-2	cell line derived from human colon carcinoma with enterocite differentiation
MCF-7	cell line derived from human breast cancer
MKN-28	cell line derived from human gastric epithelial adenocarcinoma
HPLC-DAD	High Pressure Liquid Chromatography with diode array detector
LC-MS	Liquid Chromatography coupled with Mass Spectrometry
GLUT1	Glucose Transporter 1
GLUT3	Glucose Transporter 3
PFSP	Purple-Fleshed Sweet Potato
Pn3hbsoph5lgc	Peonidin-3-(6'-hydroxybenzoil)-sophoroside-5-glucoside
Pn3hbcsoph5glc	Peonidin-3-(6'-hydroxybenzoil-6''-caffeoyl)-sophoroside-5-glucoside

GENERAL INTRODUCTION

1. POLYPHENOLS

Thousands of years ago, there was a tree in Eden garden, known for being the source of all knowledge. The fruit, an apple, was forbidden to all humans. Some thousands of years passed, and the Viking Gods were believed to owe their immortality to apples. Two different Eras, two distinct beliefs and cultures, but with one thing in common: what we know now to be a “superfood” due to the high content in polyphenols.

Polyphenols are found in the plant kingdom as secondary metabolites, constituting the largest class of natural compounds and are composed by a broad set of molecules divided into flavonoids, phenolic acids and its derivatives, lignans and stilbenes. The range of these compounds will always be incomplete due to the continuous gene evolution; result of the changes our planet systematically suffers. Over than 8000 compounds belonging to polyphenols class have been identified [1].

These molecules have important roles in plants in response to several external stimuli, in several processes: cellular growth; coloration and maturation of fruits; protection against external threats such as bacteria and bugs; UV and sun protection; chelation of toxic heavy metals and antioxidant protection during photosynthesis [2, 3].

Nowadays, most people are aware of the dangers surrounding them that are not visible to the eye. The evolution of humanity led to a bunch of new diseases and threats that no shelters are effective against. However, with these changes came the adaption process, and fortunately, many people search and demand for healthier food habits.

Growing evidence from epidemiological, *in vivo* and *in vitro* studies, as well as clinical trials and meta-analyses correlates the high intake of polyphenols, largely present in Mediterranean diet, with a reduction of the risk of a broad range of chronic diseases, improving human health [4].

Numerous studies have attributed several biological and pharmacological activities to polyphenols, including antioxidant, anti-inflammatory, anticancer, antiviral and antiallergenic effects. Due to their biological actions, polyphenols may exert beneficial effects and there is increasing evidence providing a basis for considering the use of phytochemical compounds in the development of novel therapies for the treatment of human diseases [5-7]. A good example of that, is the deep knowledge already reported about anticancer properties of polyphenols. From the, probably most famous polyphenol, resveratrol, to flavonoids, thousands of reports are published every year presenting new insights about the biological activities of this family of compounds against several types of

cancers [8-13]. And in fact, cancer prevention can be probably obtained with easier, faster and less financial strains by pursuing educational programs aimed to induce changes in lifestyle, starting from dietary habits.

Also, in the food industry polyphenols are widely used for the enrichment of dairy products from both nutritional and sensorial improvement [14]. And in fact, the enrichment of dairy foods with bioactive compounds from natural sources has become particularly intense over the past decade as a result of consumer demands for healthier and functional foods. Despite the fact that many studies on the bioactivities are performed, a full comprehension of how polyphenols exert they beneficial effects has not yet been achieved. Their effects are frequently attributed to their antioxidant capacity, and the ability to contradict the oxidative stress normally present in chronic and acute diseases. The complexity of the network that involves the bioactivity of polyphenols is enormous, making the job of scientists much more difficult. In addition, account has to be taken to the bioavailability, the biochemistry of food components and the overall effect on the absorption of polyphenols. Although the metabolism of several polyphenols is now well understood, absorption and bioavailability in humans still are controversial themes [15]. Generally, the aglycons can be absorbed from the small intestine, however, most polyphenols are present in food in form of esters, glycosides, or polymers that cannot be absorbed in the native form. During the course of the absorption processes polyphenols undergo a series of modifications, adding even more complexity to the already complex network.

The main goal of bioavailability studies is to answer three main questions: which are the better absorbed polyphenol; which are the active metabolites; and which polyphenols lead to the formation of the active metabolites. The chemical structure of polyphenols, more than the concentration, determines the rate and extent of absorption and the nature of the metabolites circulating in the plasma. The most common polyphenols in our diet are not necessarily those leading to the highest concentrations of active metabolites in target tissues; consequently, the biological properties of polyphenols greatly differ from one polyphenol to another. Although the intestine is considered the main absorption site of nutrients, several studies reported an absorption of polyphenols at the gastric level, facts corroborated with the findings of *in vivo* studies and early antioxidant plasma increasing after consumption of polyphenol-rich foods [16, 17]. In fact, growing evidences shows that polyphenols can be absorbed by the human organism in doses that are effective at exerting the several biological properties demonstrated by this family of compounds [18].

Altogether, the information available clearly justifies the impact of polyphenols in the society of today and the need to keep a deep focus in research areas related with these compounds. It is estimated that the daily intake of polyphenols is of about 1g [19].
The motto “an apple a day keeps the doctor away” can very well now change to “1g of polyphenols taken with ease, certainly puts you away from disease”.

2. FLAVONOIDS

As previously referred, polyphenols can be divided into several groups and may be classified into flavonoids or non-flavonoids. Flavonoids represent, perhaps, the most significant and widely studied group of the polyphenols families (Table 1). Fuelled by the recognized importance of having a daily consumption of fruits and vegetables to achieve high patterns of health, researchers became interested in the behaviour of these compounds and whether they can truly enhance human health.
In the early years of the twentieth century, flavonoids and related substances were chemically characterized in multiple plants and synthetized in the laboratory. Most interest was centralized on their role as pigments and research was mainly focused on the flavonoid family of anthocyanins.
In his Nobel lecture of 1937, Albert Szent-Györgyi, stated about a particular group of flavonoids: *“…I investigated with my friend St. Rusznyák and his collaborators Armentano and Bentsáth the effect of the other link in the chain, the flavones. Certain members of this group of substances, the flavanone hesperidin and the formerly unknown eriodictyolglycoside, a mixture of which we had isolated from lemons and named citrin, now had the same therapeutic effect as paprika itself. It is still too early in our experience for us to make any definitive statements. But it does seem that these substances possess great biological activity.”* [20].
The chemistry of these compounds is based on the flavanic core they possess (Figure 1), this core presents a C6-C3-C6 structure, constituted by two aromatic rings connected to a heterocyclic ring. Flavonoids can be divided in several classes, such as flavonols, flavanols, flavones, flavanones, isoflavanones, anthocyadinins and chalcones, accordingly to the level of oxidation of ring C e it substituents [19]. Table 1 shows examples of the different classes of the flavonoids.
They are normally found in their glycosylated form, however may also appear as aglycons in plants.

Table 1. General structures of flavonoids classes.

Flavonoids	**Flavonols**	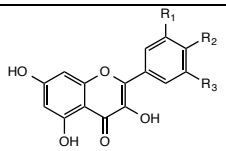	R_1=H; R_2=OH, R_3=H: Kaempferol R_1=OH; R_2=OH; R_3=H: Quercetin R_1=OH; R_2=OH; R_3= OH: Miricetin
	Flavones	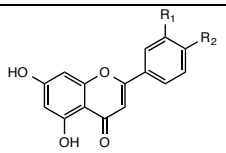	R_1=H; R_2=OH: Apigenine R_1=OH; R_2=OH: Luteoline
	Flavanols	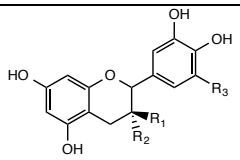	R_1=H; R_2=OH, R_3=H: Catechin R_1=OH; R_2=H; R_3=H: Epicatechin R_1=OH; R_2=OH; R_3= OH: Gallocatechin
		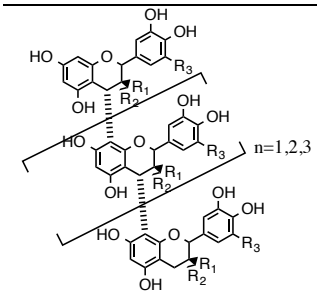	
	Isoflavones	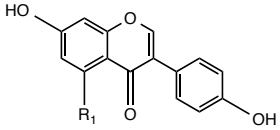	R_1=H: Daidzeine R_1=OH: Genisteine
	Flavanones	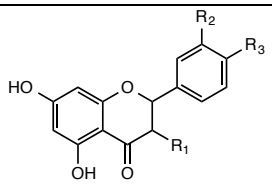	R_1=H; R_2=H, R_3=OH: Naringenine R_1=OH; R_2=OH; R_3=OMe: Hesperetine
	Chalcones	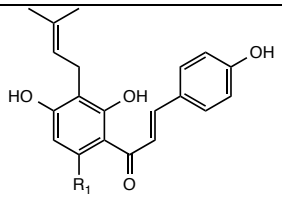	R_1=OMe: Xantumol R_1=OH: 8-Prenilnaringenin
	Anthocyanidins	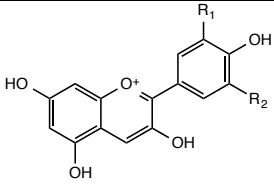	R_1=H; R_2=H: Pelargonidin (Pg) R_1=OH; R_2=H: Cyanidin (Cy) R_1=OH; R_2=OH: Delfinidin (Dp) R_1=OMe; R_2=OH: Petunidin (Pt) R_1=OMe; R_2=H: Peonidin (Pn) R_1=OMe; R_2=OMe: Malvidin (Mv)

Flavonoids research is normally supported by their well-known antioxidant capacities and their potential against free radicals and role in diseases. However, there are gaps in several areas that need to be closed to fully understand these compounds.

A very recent work reviewed the trends in flavonoid research from 1991 to 2016 [21]. Bioavailability and microbiota were amongst the top 5 topics researched on flavonoids theme. And this is easily understandable, once bioactivity studies are not accompanied by bioavailability studies, making this area and related areas emerging trends on the actual scientific society.

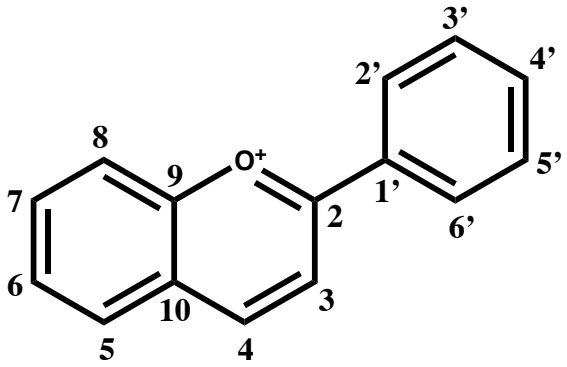

Figure 1. Structure of the flavanic core typical from flavonoids.

3. ANTHOCYANINS

Anthocyanin are part of the plant-derived flavonoid compounds and are the responsible for most of the colors ranging from pink through red, and violet to dark blue of several fruits, vegetables and flowers. Their characteristic glycoside structure makes them the main water soluble group of natural compounds.

The research on anthocyanidins and their glycosides anthocyanins deserves special consideration. Traditionally, these compounds have been studied as natural colorants, and there is great interest in wine industry for them, because they are responsible for the colors of red wine. As anthocyanins are hydrophilic due to their glycosylation, their ability to cross membrane barriers was thought to be especially limited. However, multiple studies have shown that they have clear biological activity *in vivo,* which correlates with either their ability to cross membranes using active transporters or their metabolism into more lipophilic and readily-absorbable compounds. Therefore, the interest on these compounds has grown and now, not only their colorimetric properties are studied but also the research on their biological properties and bioactivities has risen impressively in the last few years [22].

3.1. THE CHEMISTRY OF ANTHOCYANINS

Anthocyanidins represent the basic structures of the anthocyanins. These molecules (anthocyanidins or aglycons) consist of an aromatic ring (A) bonded to a heterocyclic ring (C) that contains oxygen (pyran ring), which is also bonded by a carbon–carbon bond to a third aromatic ring (B). When the anthocyanidins are found in their glycoside form (bonded to a sugar moiety) they are known as anthocyanins (Figure 2).

These amazing compounds are spread in nature in a huge variety. The number of hydroxylated groups, the nature and the number of sugar moieties linked to the aglycone structure, the acyl groups linked to the sugar moieties, and the distribution off all these in the flavanic core, determines the type of anthocyanin [23]. More than 635 different anthocyanins and 27 anthocyanidins based on the same carbon-C_{15} skeleton have been reported [24, 25]. The structures of the most common anthocyanidins present in nature are represented in Table 2.

Most anthocyanins found in plants are based on Cy, Dp, Pg, Pn, Mv and Pt, which have different substitutions on their B-rings. The glycoside derivatives of the three non-methylated anthocyanidins (Cy, Dp and Pg) are the most common in nature, being found in 80% of pigmented leaves, 69% in fruits and 50% in flowers [26].

The distribution of the six more common anthocyanidins in fruits and vegetables is: Cy 50%, Dp 12%, Pg 12%, Pn 12%, Pt 7% and Mv 7%. The glycoside derivatives more widespread in nature are 3-monosides, 3-biosides, 3,5- and 3,7-diglucosides. The presence of the 3-glucoside derivatives is 2.5 times more frequent than the 3,5-diglucosides and the most common anthocyanin is the Cyanidin-3-*O*-glucoside [23].

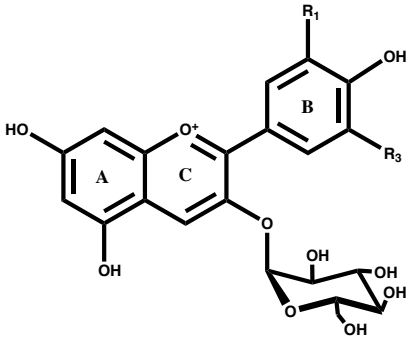

Figure 2. Representative structure for the most common anthocyanins present in nature. R1 and R3 differ accordingly to each anthocyanin. This substitution pattern can be found in Table 2.

Table 2. Structures of naturally occurring anthocyanidins based on the same carbon skeleton, 2-phenylbenzopyrylium. Adapted from [24].

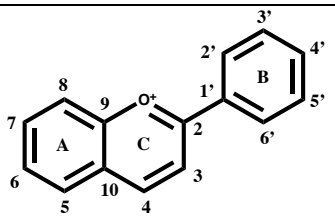

Anthocyanidins	Substitution pattern						
	3	5	6	7	3'	4'	5'
Common Anthocyanidins							
Pelargonidin (Pg)	OH	OH	H	OH	H	OH	H
Cyanidin (Cy)	OH	OH	H	OH	OH	OH	H
Delphinidin (Dp)	OH	OH	H	OH	OH	OH	OH
Peonidin (Pn)	OH	OH	H	OH	OMe	OH	H
Petunidin (Pt)	OH	OH	H	OH	OMe	OH	OH
Malvidin (Mv)	OH	OH	H	OH	OMe	OH	OMe
A-Ring Methoxylated Anthocyanidins							
5-*O*-MethylCy	OH	OMe	H	OH	OH	OH	H
7-*O*-MethylCy	OH	OH	H	OMe	OH	OH	H
7-*O*-MethylPn	OH	OH	H	OMe	OMe	OH	H
7-*O*-MethylDp	OH	OH	H	OMe	OH	OH	OH
7-*O*-MethylPt	OH	OH	H	OMe	OMe	OH	OH
7-*O*-MethylMv	OH	OH	H	OMe	OMe	OH	OMe
5,7-Di-*O*-MethylDp	OH	OMe	H	OMe	OH	OH	OH
5,7-Di-*O*-MethylPt	OH	OMe	H	OMe	OMe	OH	OH
5,7-Di-*O*-MethylMv	OH	OMe	H	OMe	OMe	OH	OMe
6-Hydroxylated Anthocyanidins							
6-HydroxyPg	OH	OH	OH	OH	H	OH	H
6-HydroxyCy	OH	OH	OH	OH	OH	OH	H
6-HydroxyDp	OH	OH	OH	OH	OH	OH	OH
3-Deoxyanthocyanidins							
Apigeninidin (Ap)	H	OH	H	OH	H	OH	H
Luteolinidin (Lt)	H	OH	H	OH	OH	OH	H
Tricetinidin (Tr)	H	OH	H	OH	OH	OH	OH
7-*O*-MethylAp	H	OH	H	OMe	H	OH	H
5-*O*-MethylLt	H	OMe	H	OH	OH	OH	H
6-Hydroxy-5-*O*-methylAp	H	OMe	OH	OH	H	OH	H
6-Hydroxy-5,4'-di-*O*-methylAp	H	OMe	OH	OH	H	OMe	H
6-Hydroxy-5-*O*-methylLt	H	OMe	OH	OH	OH	OH	H
6-Hydroxy-5-4'-di-*O*-methylLt	H	OMe	OH	OH	OH	OMe	H

The sugar moieties are mainly linked at position C3 or C5 of the aglycone, and less frequently at C7. The several saccharides found in anthocyanins are formed by glucosyl, galactosyl, rhamnosyl, arabinosyl, xylosyl, glucuronosyl and apiosyl units. They can still be linked in the form of mono, di or trisaccharides. And in fact, one or more glycosyl units

have been identified in more than 90% of the panoply of anthocyanins [27]. Figure 3 shows the structures of these sugars.

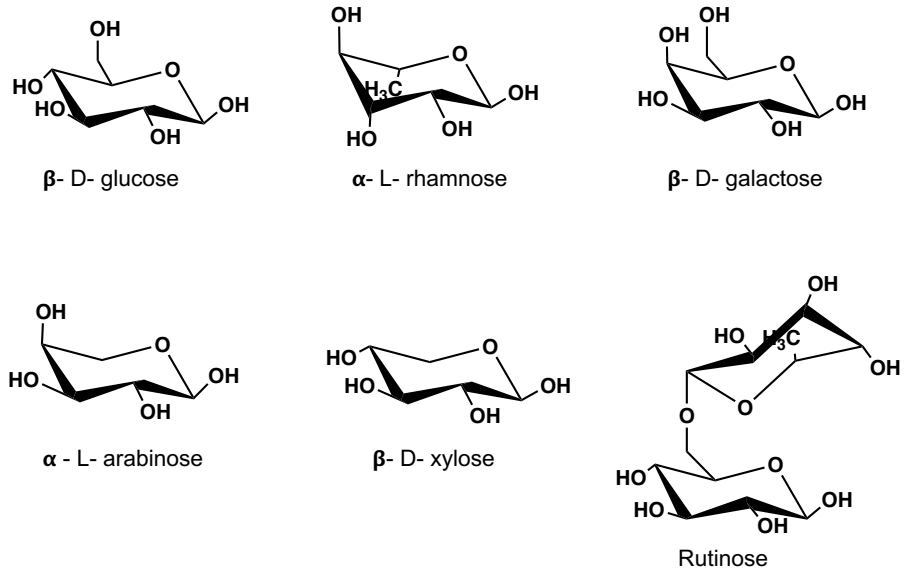

Figure 3. The most common sugar moieties linked to anthocyanidins, present in nature.

The glycosyl moieties of anthocyanins help to increase the water solubility and also to improve anthocyanidin stability. More than 69% of the reported anthocyanins present in their structure at least one acyl group, linked to the sugar moiety, and as previously referred, anthocyanins are highly affected by the nature, number and position of these groups. Hydroxycinnamic and hydroxybenzoic acids are the most frequent substituents found in acylated anthocyanins. These include aromatic compounds such as *p*-cumaroyl, *p*-hydroxybenzoyl, galloyl, sinapoyl, caffeoyl, feruloyl, and others. Figure 4 shows the structures of some aromatic and aliphatic acyl units normally found in acylated anthocyanins.

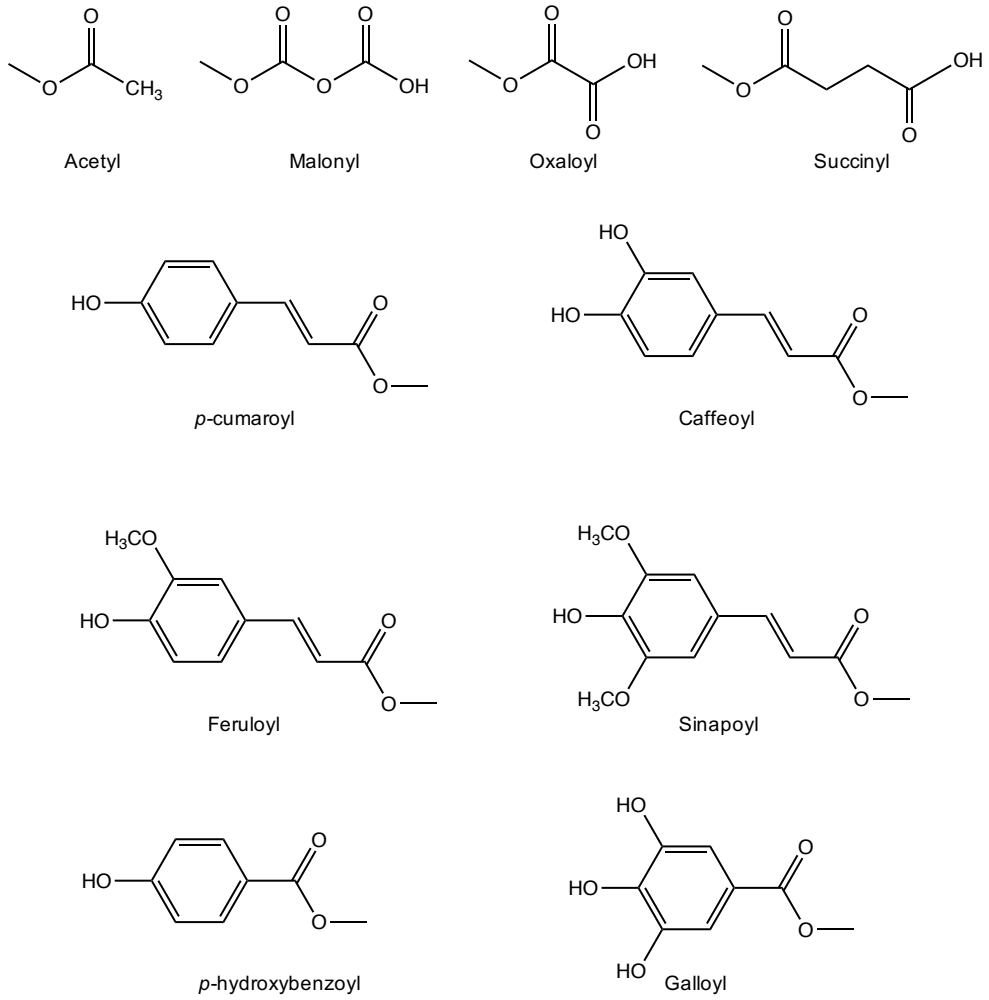

Figure 4. Structures of the aromatic and aliphatic acyl units, which have been found connected to a glycosyl moiety of acylated anthocyanins.

The high number of conjugated double bounds that are found in anthocyanins, results in a chromophore with a positive charge that in acidic conditions, the flavylium cation form. The maxima wavelengths of UV-Vis absorption for these compounds is usually located, for acidic conditions, at 465-550 nm (visible region) and at 270-280 nm (UV region).

3.2. FACTORS AFFECTING ANTHOCYANINS STABILITY

Anthocyanins extracted from natural sources are normally unstable and susceptible to degradation. Their reactivity, and therefore, stability is affected by several factors which includes: pH of the solutions, the temperature of storage and manipulation, chemical structure, concentration, light, oxygen, solvents, the presence of enzymes, the presence

of other polyphenols and metallic ions [28]. The flavanic core, has a structure suitable for reactions. Ring A, a structure common to all flavonoid group, usually have two nucleophilic regions at C6 and C8 due to the presence of the hydroxyl groups at C5/C7. The central pyran ring (Ring C) has a positive charge, and therefore, behaves as an electrophilic agent. Ring B, depending on the pattern of hydroxylation, can act as a reduction agent [29]. Figure 5 shows the different reactivity regions in a common anthocyanidin.

Due to the enormous potential of anthocyanins in both health benefits and technological applications, the stability of these compounds has received special attention in the last years. Stability is an important parameter considering the role of anthocyanins, for example, in human metabolism. Thermal processing and pH adjustment are among the commonly used unit operations in the food industry. For example, thermal processing is the most widely used preservation method in industrial beverage production [30]. However, thermal treatment can cause organoleptic and nutritional loss, as well as changes in the levels of phenolic compounds, thereby leading to decreased antioxidant capacity and other effects on bioactivities. Anthocyanin degradation may also give rise to the appearance of new molecules such as aromatic aldehydes (normally formed after the loss of the sugar moiety, resulting in the formation of the aglycone) that are dangerous for human health [31].

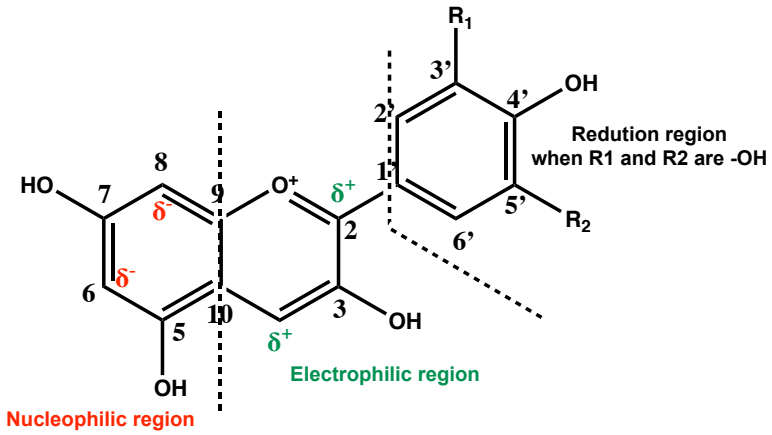

Figure 5. Scheme of reactivity on anthocyanins (anthocyadinin structure).

Anthocyanins themselves have strategies to enhance their stability. Some investigations suggest that the co-pigmentation of anthocyanins with other compounds is the main mechanism by which anthocyanins stabilise their color in plants [32]. Also, the acylation pattern in numerous anthocyanins, seems to confer an overall improved resistance to the several degradation factors [33].

Oxygen is also a factor capable of degrade anthocyanins. Together with temperature, these are the main factors responsible for the degradation of anthocyanins in foods. The deleterious action of the oxygen is as bigger as the pH of the solution and can occur through a mechanism of direct oxidation or through the formation of radicals, that may then oxidize anthocyanins.

Light has a double role in the stability of anthocyanins [34]. In one hand, it is essential for the biosynthesis of these compounds, on the other hand, accelerates its degradation. Studies demonstrated that similar degradation products are present by light and thermal degradation processes [35].

The pH of anthocyanin solutions, is, probably, the factor with the highest impact in anthocyanins stability. Anthocyanins are such amazing compounds that, due to their characteristic flavanic core, have the ability to adapt to different pH conditions by changing their structure in a series of reversible equilibrium reactions, giving rise to secondary anthocyanin forms.

At pH 1, these compounds are at their most stable from, the flavylium cation with a positive charged pyran ring (ring C). When the pH rises, a proton-transfer reaction occurs and a quinoidal base appears. This reaction forms a dynamic system that occurs extremely fast. In moderately acidic solutions (pH > 2) occurs the hydration (slower than proton-transfer) of the flavylium cation through a nucleophilic attack of water molecules in positions C2 and C4 (Figure 5), originating the hemiketal neutral forms, that becomes the predominant species for the slightly acidic pH ranges. However, other reactions occur, such as the opening of B ring on the hemiketal neutral base to give origin to chalcones. At pH values higher than 7, the anthocyanins are either degraded or suffer a deprotonation reaction to originate the respective anionic bases of each structure in equilibrium, depending on their substituents. Figure 6 shows the multistate equilibrium of a typical anthocyanin.

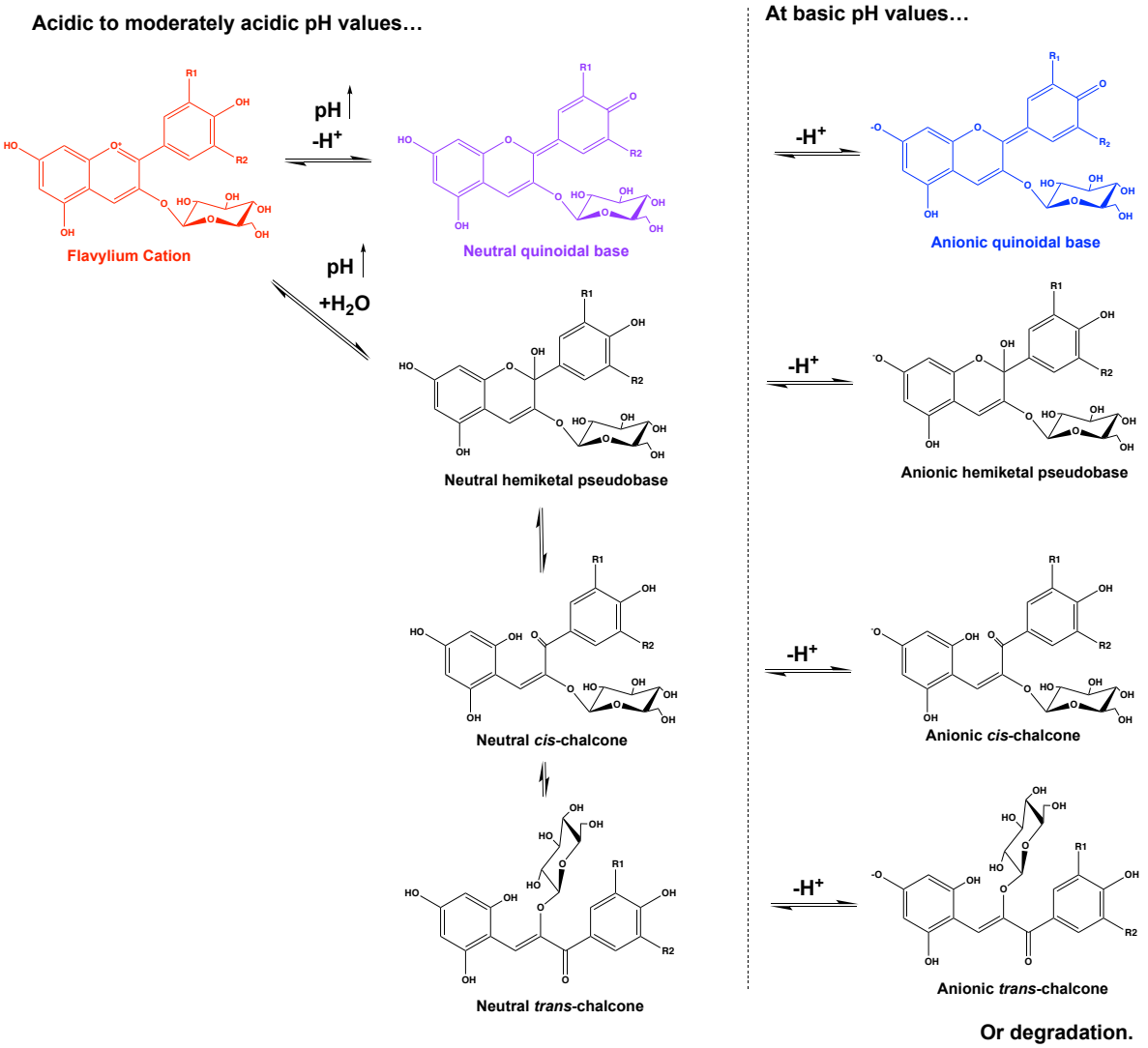

Figure 6. Representative chemical equilibrium of anthocyanins in aqueous solution. R1 and R2 can be H, OH or OMe depending on the anthocyanin.

Color as a sign of beauty and degradation…

Every transformation cited has profound alterations in colour of anthocyanins. The flavylium cation and the quinoidal base are the only colored structures, due to their characteristic absorption at the visible region in the electromagnetic spectrum (Figure 6). Normally, flavylium cation absorbs at lower wavelengths (transmitting reddish colors), while quinoidal base absorbs at higher wavelengths (transmitting bluish colors) [36]. Therefore, the color of the anthocyanins can be related to their stability. Under near neutral conditions (pH 6 and pH 6.5), Malvidin-3-*O*-glucoside showed an almost completely loss of color, while at acidic conditions the same anthocyanin maintained the red coloration for weeks at room temperature [37]. At these pH values the predominant forms will be

hemiketal neutral bases and chalcones. Thus, the formation of the hemiketal structure followed by the appearance of chalcone is postulated by some authors as the initial step for the degradation of anthocyanins [24]. The pattern of substitution in anthocyanins is also crucial to determine the degradation rate. The presence of acylated groups in the anthocyanin appears to inhibit the hydration of flavylium cation, keeping the anthocyanidin in their stable flavylium form, therefore prevailing the formation of the quinoidal base and causing a bathochromic shift towards the blue end of the spectrum [38-40].

As mentioned before, the high number of conjugated double bounds results in a chromophore with a positive charge that predominates in acidic conditions, and contributes to their intense colorations under these conditions. The maxima wavelengths of UV-Vis absorption for these compounds is usually located, for acidic conditions, at 465-550 nm (visible region) and at 270-280 nm (UV region). Anthocyanins are readily distinguished by their colour range, which is determined by the degree of hydroxylation of the B-ring of the C-6 (A-ring)–C-3 (C-ring)–C-6 (B-ring) carbon skeleton [41]. Aglycons exhibit different colors ranging from the orange-reds passing through magentas to purple-blues can appear at pH values such as 1, depending on the type of substitution. Normally, a direct relation is found between the number of hydroxyl groups and the batochromic effect, while for the methylation an inverse relation happens [42]. Figure 7 shows an example of flowers with different colours due to the presence of different anthocyanidins. All of these factors make anthocyanins extremely complex and beautiful, but also very susceptible to degradation.

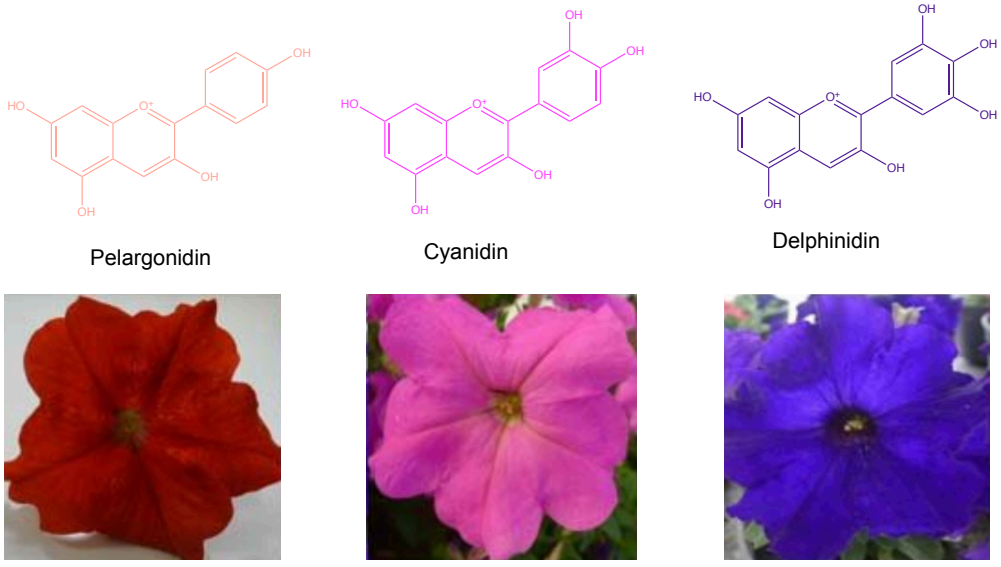

Figure 7. Structures of three major anthocyanidins that are responsible for the range of different colors presented in *Petunia hybrida*. Adapted from [43]

3.3. ANTHOCYANIN OCCURRENCE IN FOOD AND DIETARY INTAKE

Anthocyanins are present in a broad number of plants, fruits and vegetables being, therefore, present in our diet on daily basis. Anthocyanins content in foods depend on several factors, from genetics to ambience and either the agricultural processes and may even vary between the same species (as exemplified in Figure 7). For example, the amounts of anthocyanins reported for purple carrot vary from 4-1799 mg /100g [44-46].

Most of the anthocyanins present in foods are derived from the six more common anthocyanidins referred above: cyanidin, delphinidin, petunidin, peonidin, pelargonidin and malvidin. Cyanidin glycosides are the most commonly found anthocyanins in fruits, and in fact the major diet source of these compounds are the fruits of the Rosaceae family such as blackberries, raspberries, strawberries, cherries, plums and apples (whose composition is mainly based on cyanidin derivatives) [24]. Anthocyanin content in the different food sources can vary from a few miligrams to more than 1000 mg per 100 g [47]. Anthocyanins are also abundantly present in cereals and leafy or root vegetables. Pigmented potatoes, eggplant, cabbage, beans, or red onion are examples of anthocyanin-rich foods. Purple potato and purple sweet potato, for instance, have been reported with amounts of 1383 mg and 1407 mg/ 100g [48, 49].

Anthocyanins in vegetables differ from fruits in the sense that they are considerably more complex than those present on fruits. The proportion of anthocyanins without acyl groups and just one or two monosaccharide units is 74% in fruits, whereas above 77% of the anthocyanins in the vegetables have one or more acyl groups, generally aromatic acyl groups. Vegetables such as red cabbage, purple carrot or purple sweet potato are especially rich in anthocyanins with aromatic acylation. Among the anthocyanins of fruits, only 23% contains acyl groups and 11% have just one aromatic acyl group [24]. Table 3 summarizes the content of anthocyanins in some fruits and vegetables.

Table 3. Anthocyanin content in some fruits and vegetables present in the human diet. Adapted from [24].

Food Source	Major Anthocyanins	Content (mg /100g DW)
Blueberry	Cy3glc; Cy3gal; Dp3glc; Dp3gal; Dp3ara; Mv3glc; Mv3gal; Mv3ara; Pt3glc; Pt3gal; Pt3ara	2762
Cranberry	Cy3glc; Cy3ara; Cy3gal; Pn3gal; Pn3ara	396-480
Black currant	Cy3glc Cy3-(6rhaglc); Dp3glc; Dp3(6rhaglc)	744-2120

Pomegranate	Cy3glc; Cy3,5diglc; Dp3glc	6100-8600
Black Olive	Cy3glc	48-443
Black Rice	Cy3glc; Pn3glc	10-493
Strawberry	Pg3glc	97-250
Blackberry	Cy3glc	1010
Raspberry	Cy3glc; Cy3(6rhaglc)	171-1030
Blood Orange	Cy3glc; Cy3(6malglc)	3
Litchi	Cy3(6rhaglc)	48-117
Tamarillo	Cy3(6rhaglc); Dp3(6rhaglc); Pg3(6rhaglc)	7818
Grapes	Cy3glc; Dp3glc; Mv3glc; Mv3(6acglc); Mv3(6pcumglc); Pn3glc; Pt3glc	113
Red Onions	Cy3glc; Cy3(3glcglc); Cy3(6malglc); Cy3(6mal3glcglc)	49
Black carrot	Cy3(2xylgal); cy3(2xyl6glcgal); Cy3(2xyl6(6singlc));	4-1799
Red Lettuce	Cy3(6malglc)	0.7-4
Red cabbage	Cy3,5,diglc; Cy3(2glcglc)5glc; Cy3(2(2singlc)5glc)	199
Purple Sweet Potato	Pn3((6hbaglc)(6cafglc)5glc;Pn3(6hbaglcglc)5glc; Pn3((6ferglc)(6cafglc))5glc; Cy3((6hbaglc)(6cafglc))5glc	180-1407
Purple Potato	Cy3(6(4cumrha)glc)5glc; Dp3(6(4cumrha)glc)5glc; Mv3(6(4cumrha)glc)5glc;	3-1382
Red Wine	Cy3glc; Dp3glc; Mv3glc; Mv3(6acglc); Mv3(6pcumglc); Pn3glc; Pt3glc	240-350
Port Wine	Cy3glc; Dp3glc; Mv3glc; Mv3(6acglc); Mv3(6pcumglc); Pn3glc; Pt3glc	140-1110

As referred above, the reported anthocyanin content in plants depend on several intrinsic an extrinsic factors that consequently result in the huge variety of anthocyanins among foods.

Both the qualitative and quantitative are under the control of complex interactions between genotype, environmental factors and agricultural practice. Once anthocyanins are synthesized under a complex regulation of multiple genes, the content of these compounds has been used to identify species of plants [24]. Environmental factors and

agricultural practice, including light/UV irradiation, temperature, water availability/irrigation, and mineral nutrition, have for a long time been known to influence the biosynthesis and accumulation of these compounds [50]. Light, for example, is assumed to be one of the most important stimulators for anthocyanin production. During red coloration of lettuce leaves after UV-B irradiation, some genes were shown to be upregulated [51].

There are large variations in anthocyanin intake depending on the region or country, season and dietary habits, this latter particularly related to the consumption of red fruits and wine. The first estimation of the average intake of anthocyanins on a daily basis was performed by Kühnau in 1976. It was estimated that the daily intake of anthocyanins in the United States of America (USA) was situated in the range of 180 to 215 mg/ person (being the higher consumption during the summer) [52]. More recently, a screening for anthocyanins in more than 100 common foods in the USA, estimated a daily intake lower than initially reported (12.5 mg/ person) [53]. Other studies reported similar lower numbers on anthocyanin intake in the United Kingdom [54, 55]. In the other hand, the Finnish people is estimated to consume anthocyanidins in amounts such as 47 mg/ day [56]. This phenomenom has been explained by the high berry intake (an average of 52 g/ day) among Finnish population [57]. Mediterranean countries are among the best consumers of anthocyanins, and this fact may be explained by the cultural intake of wine in this region that accounts for an average of 46% of the total anthocyanin intake [58].

The estimation of the intakes is often problematic due to the difference in the techniques used and the more or less susceptibility to degradation of the anthocyanins we are dealing that complicates identification and quantification. Despite these issues, the more recent studies estimate an average intake on the order of ten miligrams per person, per day.

Toxicity should also be a parameter of attention, and in what concerns anthocyanins, they have straight A. Studies reported anthocyanins as non-toxic for humans [23]. Anthocyanins are authorized as natural food colorants in the European Union (E-163), Japan and USA. The daily recommended dose for an adult person was established in 2.5 mg/ kg of body weight [47].

3.4. ANTHOCYANINS AS BIOACTIVE COMPOUNDS… BIOLOGICAL PROPERTIES

Anthocyanins are now stated as bioactive compounds, consequence of the several evidences over the years on their effects has therapeutic agents. A panoply of biological activities has been shown. Anthocyanins act as antioxidants [59] and have anti-inflammatory and anti-cancer properties [60, 61]. They can also act against diabetes [62], neurodegenerative [63] and cardiovascular diseases [22]. Improvement of vision is another reported health effect for these compounds [64]. Some mechanistic studies in order to understand these properties were performed and suggested the induction of apoptosis in cancer cells through the activation of several factors [65-67].

All animals need O_2 for producing energy at the mitochondrial level. The use of oxygen to generate energy has the consequence of creating free radicals due to the production of ATP. There are many types of free radicals and non-radical reactive species present in living systems, however, reactive oxygen species (ROS) and reactive nitrogen species (RNS) are the primary reactive species in the human body. These compounds exert essential roles in cells at maintaining the redox balance, which is considered to be a fundamental parameter for aerobic life. If the balance shifts in favour of the oxidants, then an oxidative stress state is established. Oxidation is responsible for a series of mechanisms associated to degenerative diseases such as cancer and cardiovascular diseases [68]. Excess of ROS and RNS can damage cellular lipids, proteins or DNA affecting their normal functions. The implication of oxidative stress in chronic and degenerative diseases suggest that antioxidants are necessary to protect cellular components and maintain the normal functions of cells. The term antioxidant was initially defined by Halliwel and Guteridge [69] as *“any substance that when present at low concentrations compared with those of an oxidized substrate significantly delays or prevents oxidation of the substrate”*. With a deeper and broader knowledge of the true meaning of antioxidants the definition was later defined by Halliwell as *“a molecule that protects a biological target against oxidative damage”* [70].
Reports of epidemiological studies suggested that the intake of high quantities of flavonoids is related to a lower incidence of chronic diseases, and this may be, at least in part, linked to their antioxidant characteristics [71]. Therefore, and as an important group of flavonoids, anthocyanins have long been considered as strong dietary antioxidants [72].

The early studies focused on the direct free radical scavenging effects of anthocyanins and reported in some cases better activities than well-known antioxidants such as butylated hydroxytoluene or α-tocopherol [73].

Several chemical-based assays for evaluating the antioxidant capacity of dietary bioactives have been developed, but the lack of consistency found in these techniques has prompted the development of cell-based assays to evaluate their protective effects. The main advantage of using this cell-based assays in the diversity of cell types and stressors that can be used to effectively assess the antioxidant properties of the compounds [74].

Several studies have been carried out using cellular models to evaluated the antioxidative properties of anthocyanins. Studies in caco-2 cells suggested the involvement of anthocyanins in the inhibition of peroxyl-radical induced apoptosis [75]. Pre-treatment of fibroblast cells with Cyanidin-3-*O*-glucoside inhibited proapoptotic processes initiated by the oxidation of lysosome membranes [76]. Antioxidant activities were also found in HepG2, MCF-7 and MKN-28 cells, from hepatocarcinoma, breast and gastric cancer respectively [77-79].

As previously referred, anthocyanins highly depend on pH, therefore, the studies conducted in cell lines are usually performed at neutral pH values. This is consistent with the existence of less stable forms of anthocyanins such as chalcones [80]. And in fact, cyanidin glycosides from tart cherries were found to be spontaneously degraded at pH 7 [81]. Thus, in these type of studies anthocyanins, depending on the type, may degrade.

Another important factor to have in consideration is that a simple one-to-one extrapolation from in vitro to in vivo studies cannot be done. As Berger and co-workers stated: *"What happens in a Petri dish or in preclinical assays may not happen in people"* [82]. Hence, in vivo studies are essential to better understand the role of anthocyanins in health. The reports available are mainly based on the measurement of biomarkers in biological fluids. It was observed an increase in the overall plasma antioxidant capacity after the consumption of a single meal of about 200 g of blueberries [53, 83]. Another study reported a similar response in plasma after the consumption of 1.2 g of anthocyanins from the same source [84]. Black currant anthocyanins intake also resulted in the increase on the antioxidant plasma activity [85]. In rats, the oral treatment with *Hibiscus* anthocyanins lowered the levels of alanine and aspartate aminotransferase, enzyme markers of liver damage [86].

Also in rats, the oral administration of grape anthocyanins reduced the oxidative state promoted by the previous application of an oxidant chemical [87].

Anthocyanins in cancer…

Specific research in some diseases, such as cancer has been performed.

The studies on the cancer-preventive effects of anthocyanins, including results from in vitro cell culture and in vivo animal models, have been well documented. The latter research on this issue indicates that anthocyanins can act as anti-carcinogenic in several key points of the disease. The development of cancer in humans is such a complex process involving thousands of mechanisms at the same time that the success of a inhibitory agent depends on its ability to overcome this complex network.

Chronic inflammation is often a harbinger of a tumour. The abnormal overexpression and secretion of inflammatory factors are critical to tumorigenesis. It is reported that anthocyanins can control the expression and secretion of inflammatory factors by inhibiting the transcription factor NF-κB, through multiple pathways to exert their anti-inflammatory function [88, 89]. A large number of malignant cells undergo mitosis, are poorly differentiated and anthocyanins can induce terminal differentiation of tumour cells and block tumorigenesis [90].

Anthocyanins can act on Ras-ERK and PI3K/Akt pathways by decreasing the expression of AP-1 and thus inhibit cellular transformation [91]. Hou and co-workers found that delphinidin-3-*O*-glucoside, cyanidin-3-*O*-glucoside and petunidin-3-*O*-glucoside could inhibit the transformation of mouse skin cell line JB6P+ induced by TPA [91, 92].It was also found that delphinidin-3-*O*-glucoside could bind with Raf1 or MEK1 in an ATP-non-competitive way to inhibit the expression of AP-1 and NF-κB in $JB6P^{+}$ cells treated with TPA and further inhibit the expression of COX-2 and the production of PGE_2 [93].

Anthocyanins, especially malvidin-3-*O*-glucoside, could inhibit the activity of PDE and the hydrolysis of cAMP effectively in human colon cancer HT29 cells and thus inhibit the MAPK signalling pathway [94]

Chang and co-workers found that delphinidin-3-*O*-glucoside could activate p38-FasL and the pro-apoptosis protein Bid pathway, thereby inducing the apoptosis of HL-60 cells in a time-dependent and dose-dependent manner [95].

Anthocyanins extracted from purple potato could induce mitochondria to release endonuclease G and apoptosis-inducing factor through the JNK pathway to trigger

caspase-independent apoptosis of prostate cancer LNCaP and PC-3 cell lines [96, 97]. Many other studies are available reporting actions of anthocyanins in other stages of cancers. The efficacy of anthocyanins will depend on their pattern of substitution and the type of cancer. Figure 8 shows a suggested molecular mechanism for the action of anthocyanins in cancer.

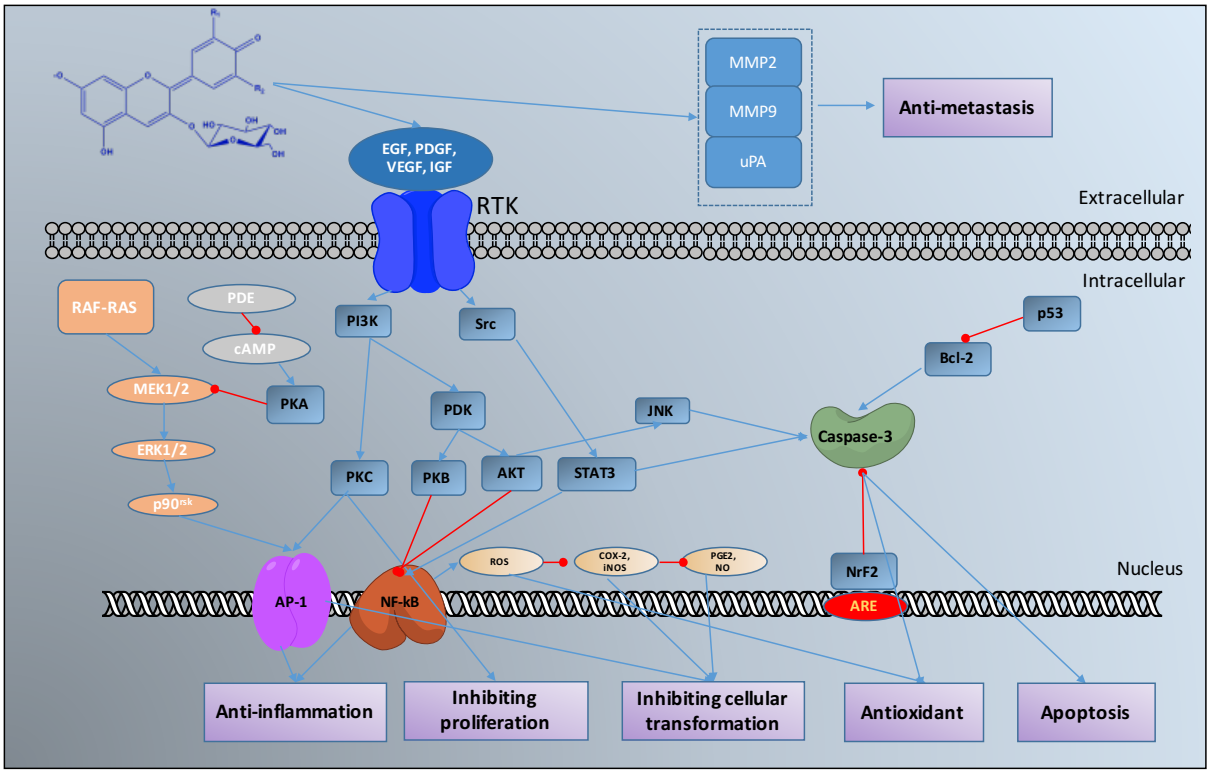

Figure 8. The main potential molecular mechanism of the anti-tumour effect of anthocyanins in vitro. Cancer cell growth might be inhibited by anthocyanins through targeting RTKs (e.g. EGFR, PDGFR and VEGF/VEGFR) and acting on the Ras-MAPK and PI3K/Akt signal cascade pathway. Inflammation might also be inhibited by anthocyanins through acting on the PI3K/Akt and NF-κB pathway to suppress the expression of COX-2 and iNOS and prevent cancer by regulating the expression of phase II antioxidant enzymes to achieve antioxidation through the Nrf2/ARE signalling system. During cancer initiation, anthocyanins might prevent malignant transformation by targeting the MAPK pathway and AP-1 factor and by inhibiting RTK activity. During cancer development, anthocyanins can induce apoptosis of cancer cells by activating caspases, mediated by ROS and JNK/p38-MAPK. In addition, anthocyanins might exert their anti-metastatic activities by targeting the VEGF signalling pathway and extracellular matrix degradation (via MMP2, MMP9, uPA). Partially adapted from [98].

Although a broad database about the biological activities of anthocyanins is well established, much more remains unknown. Anthocyanins have such complex biochemistry that we may never be able to establish a full comprehension of the bioactivities of these compounds.

4. BIOAVAILABILITY OF ANTHOCYANINS

4.1. GENERAL CONCEPTS OF PHARMACOKINETICS

For a bioactive compound that is not injected in our body to exert its health-benefit effects, it must be absorbed by the body upon intake becoming bioavailable.

Bioavailability is defined as the fraction of unchanged drug reaching the systemic circulation following administration by any route. By definition, the closest to the systemic circulation a drug is delivered, the higher will be it bioavailability, thus, intravenous administration of drugs has 100% of bioavailability. For a drug administered orally, on the other, the bioavailability will be always less than 100% for two reasons- incomplete extent of absorption and first-pass elimination. Other routes of administration exist, such as the parental routes (intramuscular and subcutaneous), inhalation, transdermal and rectal, each one of them with advantages and disadvantages. Natural compounds such as anthocyanins are consumed on a normal diet, hence, it is easy comprehensible that their bioavailability will never be complete.

The quantity of drug administered, reflects the dose and may be important for the efficacy of absorption. Absorption is the transference of a drug/compound from the site of administration to bloodstream, therefore, depending on the dose, the compound may never reach the systemic circulation. However, when a compound, or a fraction of it, crosses the gut barrier, it is said to become bioavailable. Absorption is in fact a primary focus in drug development and medicinal chemistry [99].

Bioavailability understanding slightly differs from a pharmacological and a nutritional point of view. Nutritionally speaking, the well-defined standards associated with the pharmaceutical industry cannot apply to nutrients and dietary ingredients, because utilization and absorption is a function of the nutritional status and physiological state of the subject, resulting in high inter-individual variation. Therefore, bioavailability for dietary supplements, where the route of administration is nearly always oral, can be simply defined as the proportion of the administered substance capable of being absorbed and available for use or storage [100].

Several processes occur that determines the bioavailability of a compound. For instance, in some cases, specific locals in the organism have the ability to store the compounds when the concentrations in plasma are too high, release them in the bloodstream in a controlled movement targeting the tissues of action. This process is defined as distribution.

The biotransformation of the compounds can also occur at the target tissues, where they can be submitted to enzymatic action and be degraded and transformed in other compounds.

Finally, the compounds must be excreted, normally through the excretory system. Elimination includes all the processes that are responsible for reducing the levels of bioavailable intact compounds, hence, enzymatic action and excretion are part of this process.

Obviously, these processes involve the crossing of barriers formed by cells, that divide and define the physiological environments and organs. Thus, the ability of the compounds to cross these obstacles, is crucial to their bioavailability. Several mechanisms are present to be used by compounds. The membrane transport can either occur by passive transport or active transport. Also, specialized transport mediated such as endo and exocytosis may occur.

Passive diffusion/transport is a spontaneous phenomenon exclusive of smaller molecules, usually lipophilic and non-ionic, that cross the membrane accordingly to a concentration gradient that is driven by the tendency of the system to grow in entropy. No energy input is needed for this kind of transportation.

On the other hand, active transport involves to spend of energy by two reasons: the transport against a concentration gradient, the transport of molecules mediated by specific transporters. In this latter case (the main one by which food nutrients may be actively transported), the transport can involve one or more transporters for influx and efflux of the compounds. Uniport, symport or antiport are the processes used by the transporters. These transport systems are usually specific and saturable. Figure 9 shows a general diagram of the biokinetcis of a compound.

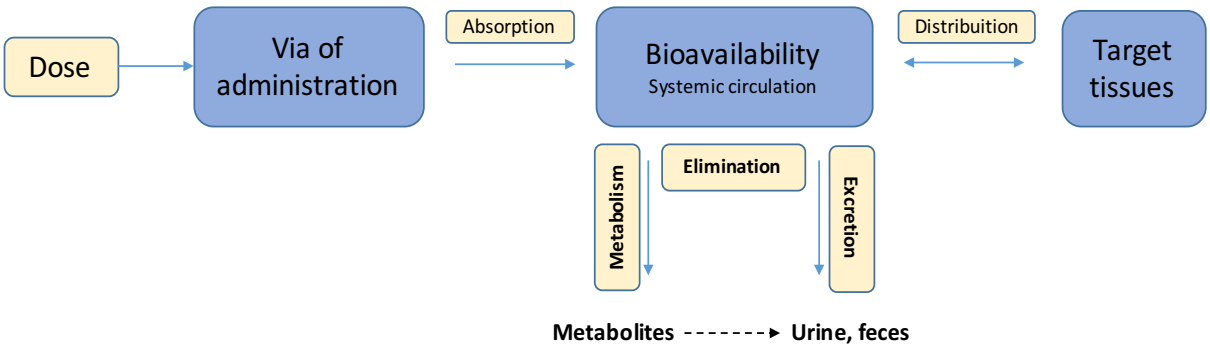

Figure 9. Diagram of a compound biokinetics.

Many factors influence the bioavailability of the compounds, particularly the ones administered by oral via. The physical-chemical characteristics such as size, solubility tendency or acidity constants can determine the ability of a compound to cross a membrane by one or another method, or even not cross at all.

Polyphenols, and in particular flavonoids (such as anthocyanins), are consumed orally as part of a normal diet, therefore, these and other factors related not only with the compound itself can define their bioavailability.

Food matrix, technological processing, chelating agents, storage time, and interactions of food components with the bioactives can improve or diminish their absorption rate. Fat, proteins and lecithin, for instance, are related to a positive effect on the absorption of compounds, while fibers normally inhibit the absorption.

The factors related to the host play, probably, the most important role in bioactives absorption.

The characteristics of the gastro-intestinal tract can influence the rate at the xenobiotics are absorbed. The presence of other foods, the pH, digestive enzymes, bile acids, microflora and overall permeability have impact on the target compounds.

In the stomach, the time of emptying dictates more or less contact with the gastric barrier. The intestinal transit time also defines more or less time of contact. These factors are crucial for a higher or smaller absorption once, to be transported nutrients need a proximity interaction with the barriers.

In the case of flavonoids, food matrix plays a pivotal role in the absorption of these class of compounds. Ethanol, for instance, can influence positively the absorption of anthocyanins at the intestinal level [101]. However, at the gastric level, a more recent study reported no significant differences between the presence or absence of ethanol [102]. These discrepancies may be due to several factors such as pH or phenotypic differences between the models used for the studies.

The frequency of consume in also an important factor. As referred before, under conditions of regular intake, even low amounts of antioxidants can significantly increase concentrations both at plasma and cellular levels an exert their effects.

Studies at both intestinal and gastric barriers with anthocyanins, showed that a chronic exposure of the cell models to red wine anthocyanins increased their absorption [102, 103]. Thus, the recommendation of the WHO about consuming fruits and vegetables every day as a healthy way of life is corroborated.

Other factors such as age and gender can induce differences that, as previously referred

will change the final bioavailability of the same compound, in an individual interaction between the food and the uniqueness of each human being. Figure 10 summarizes some of the extrinsic and intrinsic factors influencing bioavailability.

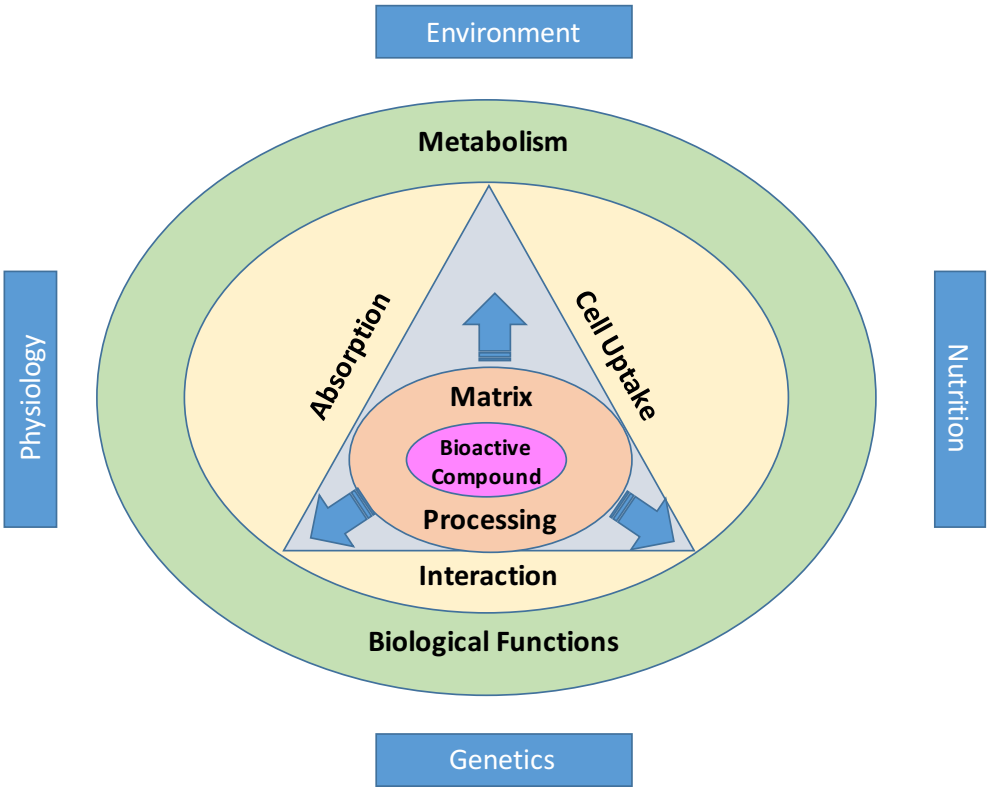

Figure 10. Relationship between factors affecting bioavailability of bioactive compounds in foods. Adapted from [104].

4.2. STATE OF THE ART ON ANTHOCYANINS BIOAVAILABILITY

Besides all the progress reached by the scientific community at increasing the range of knowledge about the biochemistry of anthocyanins, a lot is yet to discover, namely, with regard to the bioavailability of these compounds.

Since the 90's, the bioavailability of anthocyanins has been assayed in both animals and humans [105, 106]. More recently, several cell models started to be used, to have more clues on the potential mechanisms of absorption at the gastro-intestinal level [103, 107, 108]. Developing a mechanistic understanding on bioavailability and how to take advantage of it is one of the key aspects of functional foods.

Nowadays, we know that anthocyanins have a complex metabolism after ingestion and are considered to be less absorbed when compared to other classes of polyphenols. And

although, as we shall see, many questions can be partially answered, a lot remain to be fully comprehended in order to have a correct assessment on this issue, such as: which anthocyanins are more efficiently absorbed? Are anthocyanins absorbed only at main gastrointestinal organs or the absorption starts immediately at oral cavity? Does this absorption have a higher or low rate? Which cell mechanisms are involved in these processes? Which type of anthocyanins are more resistant to the metabolizing processes? Are the metabolites formed after enzymatic action or pH degradation an upgrade or a downgrade in the biological potential of anthocyanins?

Animal and human studies…

The digestive system of animals, is inevitably different from that of humans, however, studies with animals are essential to get clues on several science fields. The bioavailability of anthocyanins in animal models has been widely reported.
The observations from the animal studies allowed to get some interesting conclusions about the absorption of these compounds.

- They appear to be rapidly absorbed.
- Native anthocyanins are detected in urine and plasma
- Specific metabolites of anthocyanins appear in urine

In rats, anthocyanins were detected in the circulatory system after 0.25h-2h of dosing. The anthocyanin concentrations in the plasma reached a peak of about 3 μg/mL after 15 minutes and then rapidly declined within 2h following a single oral administration of bilberries [105]. Another study used an intubation technique to directly deliver isolated anthocyanins (Cyanidin-3-*O*-glucoside 320mg/ Kg of body weight) into the stomach of rats and the compounds were detected intact in plasma after 15 min, also this anthocyanin was detected after oral administration after 30 min of intake [109, 110]. This rapid absorption suggest that stomach is, an important local for the uptake of anthocyanins, and in fact, it was suggested that anthocyanins are absorbed at both stomach an intestine and bind to proteins in these tissues [111].
Urinary excretion is normally used to assess the bioavailability of compounds. The advantage of using urine analysis is that, as an end-product “reservoir” of the metabolism, is ideal to investigate the overall metabolism of a compound by a specific organism. In rats, after the oral administration of three isolated anthocyanins (delphinidin-3-*O*-rutinoside, cyanidin-3-*O*-rutinoside and cyanidin-3-*O*-glucoside) from black currant,

anthocyanins were found in blood after 30 min and were excreted in the urine with no detection of possible degradation products [112]. The previous cited studies also detected intact anthocyanins in human urine.

However, it is known that degradation of anthocyanins occur, and more recent studies reported the presence of anthocyanin-derived metabolites in urine and plasma of rats, pigs and rabbits. When rats were dosed with 100 mg of delphinidin-3-*O*-glucoside/ Kg of body weight, the maximum concentration in the plasma was reached within 15 minutes and the methylated metabolites reached a maximum plasma concentration after 1h [113]. Additionally, it was suggested that these metabolites were produced in the liver, rather than in the intestinal flora, evidencing an absorption of intact anthocyanins and posterior metabolization [114, 115]. Glucuronidated and methylated anthocyanin-derived metabolites were also reported to be the major types of metabolites present in the urine of pigs after oral administration [116]. Furthermore, the type of aglycone and sugar moiety in the anthocyanin was reported to influence the absorption rates and metabolism in pigs [117]. A study investigated the different parts of the small intestine and reported the presence of metabolites and also intact anthocyanins in the jejunum of rats [118]. Table 4 summarizes the works using animals to investigate anthocyanins bioavailability.

Table 4. Biokinetic studies of anthocyanins in animals.

Species	Anthocyanin Source	Dose (per kg Body Weight)[a]	C_{max}[b]	T_{max}(h)[c]	Urinary Excretion (%)[d]	Reference
Rat	Bilberry	400 mg	2-3 μg/mL	0.25		[105]
Rat	Elderberry Black currant	360 mg	3.80 μmol/L	0.25		[109]
Rat	Purple corn	400 mg	0.31 μmol/L	0.5		[110]
Rat	Black currant	359 mg Cy3glc	0.84 μmol/L	0.5		[112]
		476 mg Cy3rut	0.85 μmol/L	0.5		
		489 mg Dp3rut	0.58 μmol/L	2.0		
Rabbit	Black currant	117 mg	780 ng/mol	0.5	0.035 (4h)	[119]
		164 mg	100 ng/mol	0.25	0.009 (4h)	
		53 mg	450 ng/mol	0.5	0.023 (4h)	
Rat	Black currant	100 mg Dp3lgc	0.4 μmol/L	0.25		[113]

Pig	Marionberry	74 mg	0.103 μmol/L	1	0.088 (24h)	[116]
Rat	Purple black rice	100 mg Cy3glc			0.005 (4h)	[115]
Rat	Black currant	100 mg Cy3glc	0.18 μmol/L	0.25		[114]
Rat	Black currant		0.36 μmol/L	3	0.190 (24h)	[118]
Pig	Chokeberry Black currant Elderberry	229 μmol 140 μmol 228 μmol			0.096 (24h) 0.067 (24h) 0.131 (24h)	[117]
Pig	Black currant	100 mg	0.09 μg/mL	2-4		[120]
Pig	Raspberry	50 mg			0.073 (4h)	[53]

[a] total anthocyanins, if not stated otherwise

[b] maximal plasma concentration

[c] Time to reach C_{max}.

[d] % of intake

Although animal studies are often used and give very useful clues about bioavailability of compounds, studies with humans are necessary to confirm that the knowledge obtained with animals can be transferred and applied in people. There are numerous studies that show conclusively that in humans, anthocyanins are absorbed from the digestive tract, transit in the circulatory system, and are excreted in the urine.

Black currant anthocyanins were directly absorbed and detected in the blood and in the urine as intact forms [112]. Similar results were found for anthocyanins from boysenberry and blueberry [121]. More recently, the intact glycosides and their metabolites have been detected in the urine after the consumption of plum anthocyanins [122]. After the ingestion of red wine containing 68 mg of malvidin-3-*O*-glucoside/ 500 mL, or red grape juice containing 117 mg of the same anthocyanin/ 500 mL, malvidin-3-*O*-glucoside was found in plasma (20 min after intake of red wine and 180 min after intake of red juice) and urine of volunteers. Neither aglycons nor glucuronide or sulfate conjugates were found in the plasma or urine samples, indicating that this anthocyanin may be absorbed in the glucosylated form with no further significant metabolism [123]. However, when

anthocyanins from boysenberry were consumed, the intact cyanidin-based anthocyanins were detected in the urine together with several methylated and glucuronide metabolites derived from the original anthocyanins [124]. After the consumption of strawberry anthocyanins, conjugated metabolites with glucuronide and sulfate groups are excreted in the urine, accounting for more than 80% of the total excreted amount [125].

Similar results were found for cyanidin-3-*O*-glucoside from blackberry [126]. Also, when cyanidin-3-*O*-glucoside from plum was consumed, the monoglucuronide and methylated metabolites accounted for 20% and 42%, respectively, of the total detected anthocyanins in the urine of the volunteers [122]. These studies are indicative of a clear metabolization of the anthocyanins, but this process seems to depend on the type of anthocyanin consumed.

Compared with other polyphenols, the portion of the total anthocyanins that can be accounted by urinary excretion is low and is often lower than 0.1%. Although one of the first human studies in anthocyanins bioavailability reported an excretion of 5% over a 12h period following an intake of red wine anthocyanins, subsequent studies reported much lower rates. A study with black currant juice reported that the urinary excretion of the intake of 153 mg of anthocyanins/ 200 mL was only 0.02% to 0.05% of the oral dose administered [127]. In a study with boysenberry concentrate (345 mg of anthocyanin), black currant concentrate (189 mg of anthocyanin) and blueberry extract (439 mg of anthocyanin), the urinary excretion accounted for 0.01-0.06% of the total consumed over a 7h period after ingestion [121]. Malvidin glycosides from red grapes and red wine were reported to appear in urine in an extent between 0.18% and 0.23% of the ingested dose [128]. Pelargonidin-3-*O*-glucoside from strawberries, was excreted in urine with an extent of 1.80% [125]. In contrast, the urinary excretion of blackberry anthocyanins (mainly cyanidin-3-*O*-glucoside) was of only 0.16% [126]. Hence, the studies concerning urine analysis suggest that anthocyanins (or it conjugates) are excreted in a very low amount of the oral administered dose. In comparison, many other polyphenols may be excreted to the extent of 2-5% and a few achieve over 10% [129]. Anthocyanin concentrations achieved in plasma are usually in the range of dozens or hundreds of nanomolar, while other polyphenols can range in the micromolar [18].

These results may be explained in two ways: either the absorption of anthocyanins from the gastrointestinal tract is much slower than other polyphenols, or their absorption rate is comparable, but they disappear from the bloodstream very fast. The latter explanation could be consistent with the unusually rapid clearance of anthocyanins and their

metabolites through the renal system or by rapid disappearance arising from chemical instability. Also, this may suggest that anthocyanins are quickly directed to interacting with different tissues and cellular components and react with other molecules, altering completely their structure. And in fact, studies using $^{13}C_5$-labeled cyanidin-3-O-glucoside reported a recovery of 32% in feces and 5.4% in urine of anthocyanins or metabolization products from the oral dose [130, 131].

The consensus, for now, is that anthocyanins appear to be absorbed at the gastrointestinal tract, as fast as other polyphenols, or even faster as they appear to be among the few polyphenol classes that are absorbed from the stomach [102, 132, 133]. This phenomenon may be linked to the much greater stability of anthocyanins under acidic conditions, as found in the stomach. Potentially, anthocyanins in the plasma may transiently reach concentrations comparable with other polyphenols, but as the clearance of anthocyanins from the bloodstream appears to be rapid, the overall amount observed could be underestimated. Table 5 summarizes some studies of the biokinetics of anthocyanins from different sources in humans.

Table 5. Biokinetic studies of anthocyanins in humans.

Anthocyanin Source	Anthocyanin Dose (total intake)[a]	C_{max}[b]	T_{max}(h)[c]	Urinary Excretion (%)[d]	Reference
Red Wine (300 mL)	218 mg			5.10 (12h)	[106]
Elderberry extract (25 g)	360 mg	100 ng/mL	0.5		[134]
Black currant	236 mg	0.120 μmol/L	1.25-1.75	0.11 (8h)	[112]
Elderberry juice	180 mg	35 ng/mL	1		[135]
Black currant juice (200 mL)	153 mg			0.02-0.05 (5h)	[127]
Red Wine (500 mL)	68 mg Mv3glc	0.0014 μmol/L	0.8	0.02 (6h)	[123]
Dealcoholized red wine	56 mg Mv3glc	0.0017 μmol/L	1.5	0.02 (6h)	[123]
Red grape juice	117 mg Mv3glc	0.0028 μmol/L	2.0	0.02 (6h)	[123]
Elderberry (11g)	1.9 g			0.003-0.012 (6h)	[136]

Blueberry powder (100g)	1.2 g	0.029 μmol/L	4		[84]
Elderberry extract (12 g)	720 mg	0.097 μmol/L	1.2	0.06 (24h)	[137]
Elderberry extract (12 g)	720 mg			0,08 (4h)	[138]
Blueberry (189 g)	690 mg			0.004 (6h)	[138]
Red wine (400 mL)	180 mg	43 ng/mL	1.5	0.23 (7h)	[128]
Red grape juice (400 mL)	284 mg	100 ng/mL	0.5	0.18 (7h)	[128]
Black currant juice	1.24 g	53 ng/mL	0.75	0.07 (4h)	[119]
	0.72 g	16 ng/mL	0.75	0.05 (4h)	
	0.75 g	32 ng/mL	1.5	0.05 (4h)	
Black currant concentrate (300 mL)	189 mg			0.06 (7h)	[121]
Boysenberry concentrate (300 mL)	345 mg			0.03 (7h)	[121]
Blueberry extract (300 mL)	439 mg			0.02 (7h)	[121]
Strawberries (200 g)	76 mg			1.80 (24h)	[125]
Chokeberry extract (7.1 g)	721 mg	0.096 μmol/L	2.8	0.15 (24h)	[139]
Blackberries (200 g)	431 mg			0.16 (24h)	[126]
Strawberries (200 g)	222 μmoL Pg3glc			0.75 (without cream)	[140]
	13 μmol Pg3rut			1.00 (with cream)	
	6.2 μmol Cy3glu				
Strawberries (300 g)	Fresh 9.57 mg			0.9	[141]
	Stored 7.19 mg			0.8	
Cranberries	95 mg	4.64 nmol/L	3	0.79 (3h)	[142]
Blueberries	650 mg	138 nmol/L	1.5	1.2 (48h)	[143]

[a] **total anthocyanins, if not stated otherwise**

[b] **maximal plasma concentration**

[c] **Time to reach C_{max}.**

[d] **% of intake**

Is anthocyanins bioavailability really that low?

Although the *in vivo* studies reported an overall low bioavailability of the anthocyanins, the fact is that the majority of the studies have in account mainly the intact anthocyanins and the main metabolites (the phase II conjugated metabolites that will be further accounted in this introduction).

A very recent review by Kay et al. [144] stated that, if one has in account the low molecular weight phenolic and aromatic ring-fission catabolites, the bioavailability of the anthocyanins is considerably higher.

Upon food consumption, the components experience a lot of different conditions that may lead to intramolecular modifications. Cyanidin-3-O-glucoside administered to rats exhibited a half-life in the intestinal lumen of 2 h [111]. In vitro degradation studies on cyanidin and its glucosides at a physiological pH value revealed that after 4 h, 57% of the glucoside and 96% of the aglycone had degraded [145]. *In vivo*, glucosides are the only polyphenols that are extensively hydrolyzed by intestinal glycosidases [129]. Since anthocyanidins are substantially less stable than anthocyanins at physiological pH [145], it appears likely that the glycosylated forms may be rapidly degraded after intestinal deglycosylation and therefore are much less absorbed or metabolized. Glycosides resistant to deglycosylation, such as the commonly occurring rutinosides, should have a higher probability of being absorbed intact. In the absence of digestive glycosidase enzymes, there was no preferential degradation of glucosides relative to their glycosides [146]. These studies suggest that only anthocyanins that are not deglycosylated are significantly absorbed. Nevertheless, upon absorption, anthocyanins can suffer different intracellular metabolizing processes. Phase I involves reactions of oxidation, hydrolysis and hydration, while phase II form the famous conjugated metabolites that are reported in the majority of the works about anthocyanin bioavailability. The phase II metabolism involves reactions of sulfonation, glucoronidation, acylation and methylation, occurring more intensively than phase I, mainly at the liver and intestine [147].

The extent to which anthocyanins are subjected to phase I metabolism is not known, however, several flavonoids can act as substrates for some cytochrome P450 isoforms. Phase II reactions create larger moieties when reactive hydroxyl groups on anthocyanins become conjugated to methyl, glucuronic acid, or sulfate groups [147].

In general, glucuronidated anthocyanins predominate in human plasma and peak approximately 1 to 3 h post-ingestion, depending on ingested dose, anthocyanin type,

food matrix and coexisting nutrients [125, 126, 148-150]. Sulfonated and glucuronidated metabolites of Cyanidin-3-*O*-glucoside were identified in human urine after the consumption of strawberries and blackberries [126, 132].

Gut microbiota can also account for a significant alteration of anthocyanins. In vivo trials with lean and diet-induced obese mice with healthy and disrupted gut microbiota revealed that cyanidin-type anthocyanins were much more sensitive to gut microbial degradation than delphinidins [151]. When the gut microbiota was disrupted (due to the administration of antibiotics), administration of anthocyanins to the animals failed to curb body weight gain or improve glucose metabolism. But without antibiotic, the resulting anthocyanin metabolites (especially delphinidin-derived) were clearly protective against obesity and associated insulin resistance. In other studies, to evaluate the cardiovascular potential of anthocyanins, it was found that the gut-derived breakdown products (such as protocatechuic acid-4-sulfate or ferulic acid) induced the reduction of inflammatory cytokines, whereas lower concentrations of the parent anthocyanins (cyanidin-3-O-glucoside), suppressed the cytokines functions [152].

All these reports suggest that anthocyanins can undergo a series of transformations that are benefic to their bioavailability and consequently bioactivity. In fact, the majority of the absorbed anthocyanins are present as lower molecular weight products of chemical and microbial degradation [130, 131] (Figure 11). For instance, in a study where 9 volunteers consumed 300 g of raspberry berries containing 292 μmol of anthocyanins, a total of 16 compounds derived from the parent anthocyanins catabolization were identified in the urine collected 48h post-ingestion [153] (Table 6).

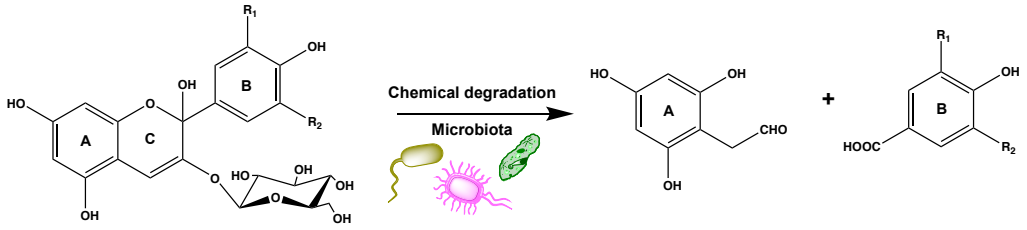

Anthocyanin	Phenolic Acid
Cy3glc	Protocatechuic acid
Pn3glc	Vanillic acid
Pg3glc	4-hydroxybenzoic acid
Mv3glc	Syringic acid
Dp3glc	Gallic acid
Pt3glc	Dihydroxy-3-methoxybenzoic acid

Figure 11. Degradation pathways of anthocyanins to phenolic compounds. Adapted from [154, 155].

Table 6. Compounds excreted in urine in increased amount 0-48 h after ingestion of 300 g of raspberries containing 292 μmol of anthocyanins. Adapted from [153].

Compounds	**Baseline (μmol)**	**Increased 0-48h excretion after raspberry intake (μmol)**
Caffeic acid-3'-sulfate	traces	1.0±0.1
Dihydrocaffeic acid-3'-sulfate	Traces	1.1±0.3
Ferulic acid	1.8±0.3	5.9±2.1
Ferulic acid-4'-sulfate	1.6±0.2	6.5±2.6
Isoferulic acid-4'-sulfate	Traces	0.5±0.2
Ferulic acid-4'-O-glucuronide	0.7±0.1	1.8±0.5
Isoferulic acid-3-'-O-glucuronide	0.3±0.1	1.0±0.4
Total hydroxycinnamic acids	4.4±0.6	17.8±5.3
3'-4'-dihydroxyphenylatic acid	0.4±0.2	2.9±1.3
3'-methoxy-4'-hydroxyphenylatic acid	n.d.	0.2±0.2
Total phenylatic acids	0.4±0.2	3.1±1.7
4-hydroxybenzoic acid	n.d.	6.4±1.7
3,4-dihydroxybenzoic acid (protocatechuic acid)	n.d.	Traces
3-methoxy-4-hydroxybenzoic acid (vanillic acid)	n.d.	Traces
4-dihydroxybenzoic acid-3-sulfate	0.1±0.0	0.3±0.1
3-hydroxybenzoic acid-4-sulfate	0.1±0.0	0.2±0.1
Total benzoic acid derivatives	0.2±0.0	6.9±5.0
4'-hydroxyhippuric acid	7.0±2.1	16.1±1.9
Total phenolic derivatives	12.0±2.3	43.9±8.0

In another study raspberry anthocyanins were incubated in vitro with human fecal slurries and a significant number of low molecular weight metabolites were also found [156]. The study found that the first step of degradation included the cleavage of the sugar moiety with subsequent degradation of cyanidin, resulting in accumulation of metabolites such as catechol or pyrogallol. Figure 12 shows the proposed pathways for the conversion of cyanidin-based anthocyanins.

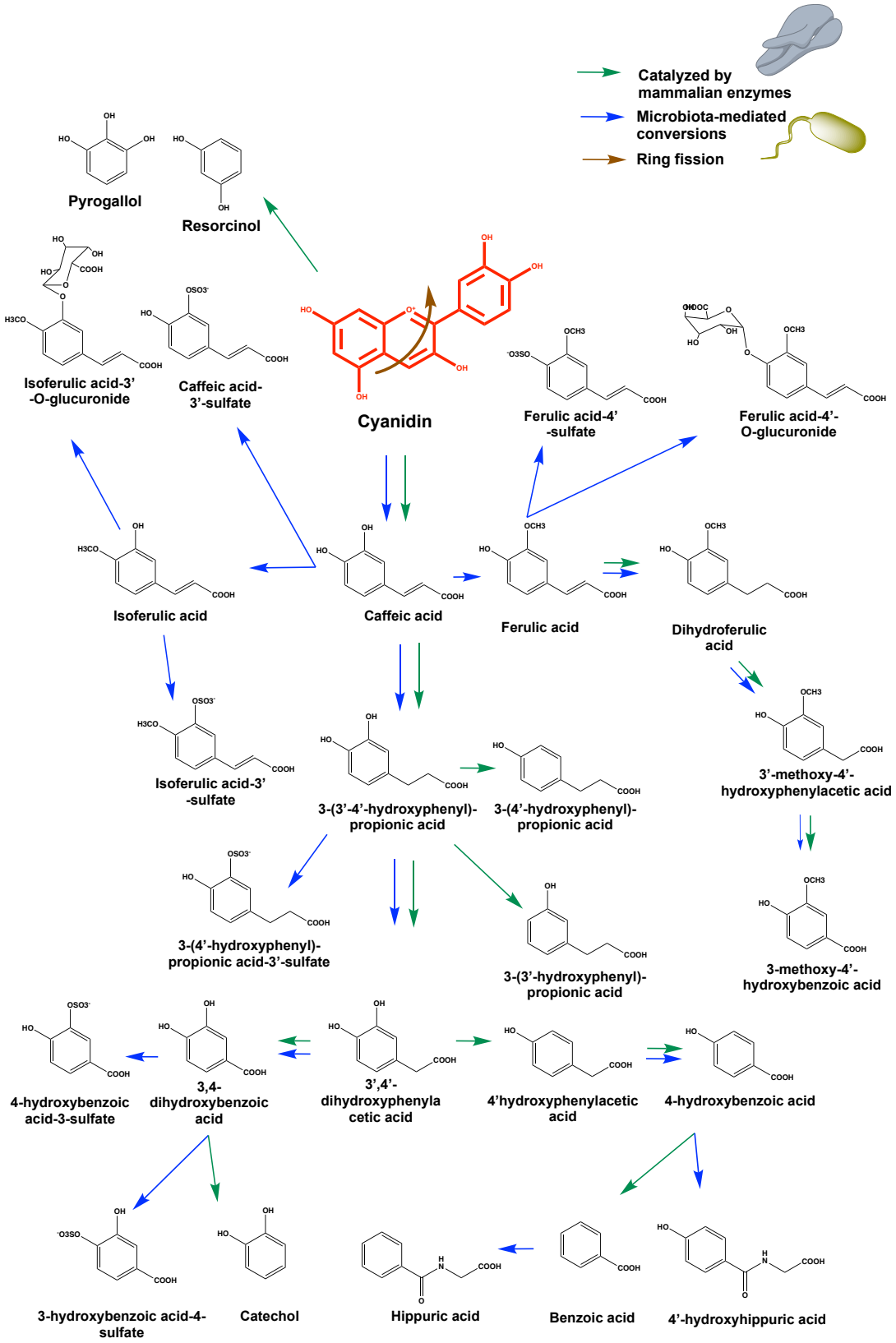

Figure 12. Proposed pathways for the conversion of cyanidin-based anthocyanins to phenolic acids and related compounds based on urinary excretion in feeds with red raspberries and in vitro fecal incubations [153, 156]. Adapted from [144].

It is clear from the conjugation of these results (only a symbolic representation of the total studies) and all the other publications, that anthocyanins bioavailability is extremely complex and many factors account for it. The metabolites seem to have crucial roles in the overall bioavailability of anthocyanins and can be formed at different stages. Also, the structure of the anthocyanin is important in defining the final fate of the compound.

In vitro studies… a powerful weapon to assess bioavailability?

In the previous section, some conclusions managed to answer some of the initial questions, at least, partially. Animal and human studies, are, undoubtedly, essential to understand the biokinetic parameters underlying the bioavailability of compounds. However, some answers cannot be answered using only this type of studies. Knowing the mechanisms involved on the absorption processes is as important as knowing which metabolites are formed after the absorption of anthocyanins.

In vitro studies, became, over the years, powerful resources to study biochemical processes in cells in order to comprehend the actions of bioactives. In the case of bioavailability of anthocyanins, several studies resorted to the use of these techniques to better understand how they are absorbed at the gastrointestinal level. And in fact, many of the previously reported *in vivo* studies demonstrated the presence of intact anthocyanins. Thus, it makes sense to evaluate their absorption in the parent structure.

The intestine is one of the main absorption sites of nutrients, and intestinal barrier cell models have been widely used to study bioavailability of compounds. The case of anthocyanins is well reported.

It was verified that the structural differences on the anthocyanins influenced they transport efficiency, although this transport was low [157]. After incubation of blueberry anthocyanins with caco-2 cells for 120 min, 3-4% of the total amount were absorbed by the cells [157]. In another study, anthocyanins from a black current extract were not found in any serosal solution after 80 min on incubation with caco-2 cells [158]. On the other hand, anthocyanins from açaí pulp registered a transport efficiency between 0.5% and 5% after 120 min [159]. The differences in key substituents in similar anthocyanins were also evaluated. Malvidin-3-O-glucoside transport efficiency was higher than compared to the dimer of catechin and malvidin-3-*O*-glucoside [160]. The diglucoside anthocyanins from grape/ blueberry extracts were not transported in quantifiable concentrations while the monoglucosides transport were between 0.005% and 0.06% [148].

As previously discussed, anthocyanins undergo a series of different transformations depending on pH. These assays, intend to mimic as much as possible the in vivo conditions. Thus, the working pH is usually neutral, which may explain the low transport rates observed. In fact, a study on Cyanidin-3-*O*-glucoside [145] showed that there was no significant difference between the Caco-2 cell and cell free incubations in terms of the losses of Cyanidin-3-*O*-glucoside and the appearance of degradation products. These findings suggest that the loss of anthocyanins may be the result of spontaneous chemical breakdown rather than Caco-2 cell induced enzymatic deglycosylation followed by chemical degradation.

The mechanism of anthocyanin absorption at the intestinal level is not yet fully known, however, it has been proposed that anthocyanins can interfere with the transporters responsible for their own transport. It has been described and accepted that GLUT2 is present on the apical side and can be gathered to the membrane in the presence of a large amount of glucose, therefore becoming the main transporter responsible for glucose uptake [103, 161]. It was found that GLUT2 expression assessed by RT-PCR was increased in Caco-2 cells pre-treated with red grape skin anthocyanins, by comparison with controls, indicating that chronic consumption of anthocyanins could be favorable for their own bioavailability. In addition, the tested red grape skin anthocyanins interfered with glucose uptake resulting in an inhibitory effect (about 60% decrease) [103]. Similarly, Pn-3-Glu from strawberry extract was able to influence glucose uptake into the cells and transport to the basolateral side by inhibiting activities of the glucose transporters [162]. Another study also confirmed that exposure to anthocyanin rich berry extracts derived from blueberry, bilberry, cranberry, elderberry, raspberry seeds and strawberry significantly reduce SGLT1 and GLUT2 expressions [163]. Inhibition studies conducted using the pharmacological agents, phloridzin, an inhibitor of SGLT1, or phloretin, an inhibitor of GLUT2, revealed that the absorption of Cy-3-Glu was significantly inhibited in the presence of these agents [163]. These evidences suggest that transporters involved in the uptake of glycosides are also responsible for the transport of anthocyanins at the intestinal level. Also, it corroborates the importance of using different methods other than in vivo, to access the fully comprehension of bioavailability.

However, intestine is not the only local that seems to be responsible for the uptake of anthocyanins.

Anthocyanin gastric absorption… Myth or a new reality?

Several in vivo studies, suggested the implication of the stomach in the absorption of anthocyanins, mainly due to the early appearance of these compounds in plasma of animals and humans upon oral administration. However, for a long time, the gastric cavity was ignored as a major site of absorption of anthocyanins, and the biochemical studies about transport mechanisms were massively focus on the intestine.

The evidences from in vivo studies, clearly suggest that intact anthocyanins are better absorbed than the respective aglycons. pH influences the integrity of anthocyanins, and at the gastric cavity, anthocyanins are more suitable to have higher stability when compared with other gastrointestinal tract organs due to the presence of an acidic environment (Figure 13). Thus, and accordingly to the reported knowledge, a more efficient absorption of anthocyanins should occur in stomach rather than in the intestine. In fact, several studies using animal models and cell models such as MKN-28 cells reported higher transport efficiencies of anthocyanins, than those reported for the transport studies in intestine. Anthocyanin glycosides were quickly and efficiently absorbed in the stomach (approximately 25%). However, their absorption varied greatly according to the anthocyanin structure and they were rapidly excreted into bile as intact and metabolized forms [132]. The absorption of red orange anthocyanins was studied in both rat stomach and intestine using in situ models [155]. A high proportion (about 20%) of red orange anthocyanins was absorbed from the stomach and no anthocyanin metabolite was observed in the stomach after 30 min of incubation. Recent studies with red wine anthocyanins reported transport efficiencies after 180 min of 5-8% for the whole extract and about 10% for isolated anthocyanins [102, 108].

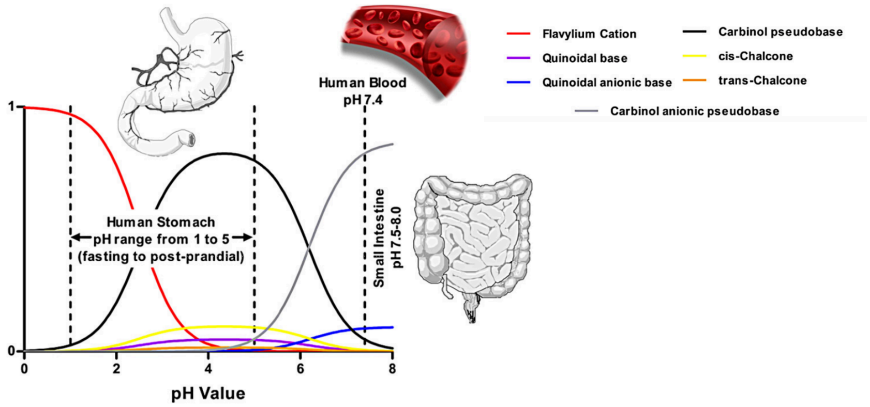

Figure 13. Schematic representation of the molar fraction of anthocyanin equilibrium form according to the gastrointestinal tract pH [133].

The mechanism through which anthocyanins may be transported at the gastric level as been assessed.

Anthocyanins showed a significant interaction with bilitranslocase, expressed in the gastric epithelial [107, 164] However, it should be noted that those in vitro assays performed were conducted at pH 8.0, which is far from the gastric conditions here no quinoidal forms could be detected. Other transporter candidates may include GLUT1, OAT2, SMCT1 and SMCT2, since the expression of these transporters has already been detected in stomach tissue [165, 166]. And in fact, a recent study reported a competitive interaction between glucose and red wine anthocyanins for the transport in MKN-28 cells [102]. High amounts of glucose decreased the transport efficiency of anthocyanins. However, this inhibition was never complete, suggesting that other mechanisms of transport may be involved. Glucose transporters GLUT1 and GLUT3 were shown to be expressed in MKN-28 cells and implied has being involved in the transport of red wine anthocyanins [102]. This was corroborated by computational biochemical studies [102].

Altogether, these results suggest that stomach may have much more impact on the bioavailability of anthocyanins than previously perceived and surely deserves deep attention to fulfil the knowledge on this matter.

Figure 14 shows the hypothetic pathways of anthocyanins overall metabolism.

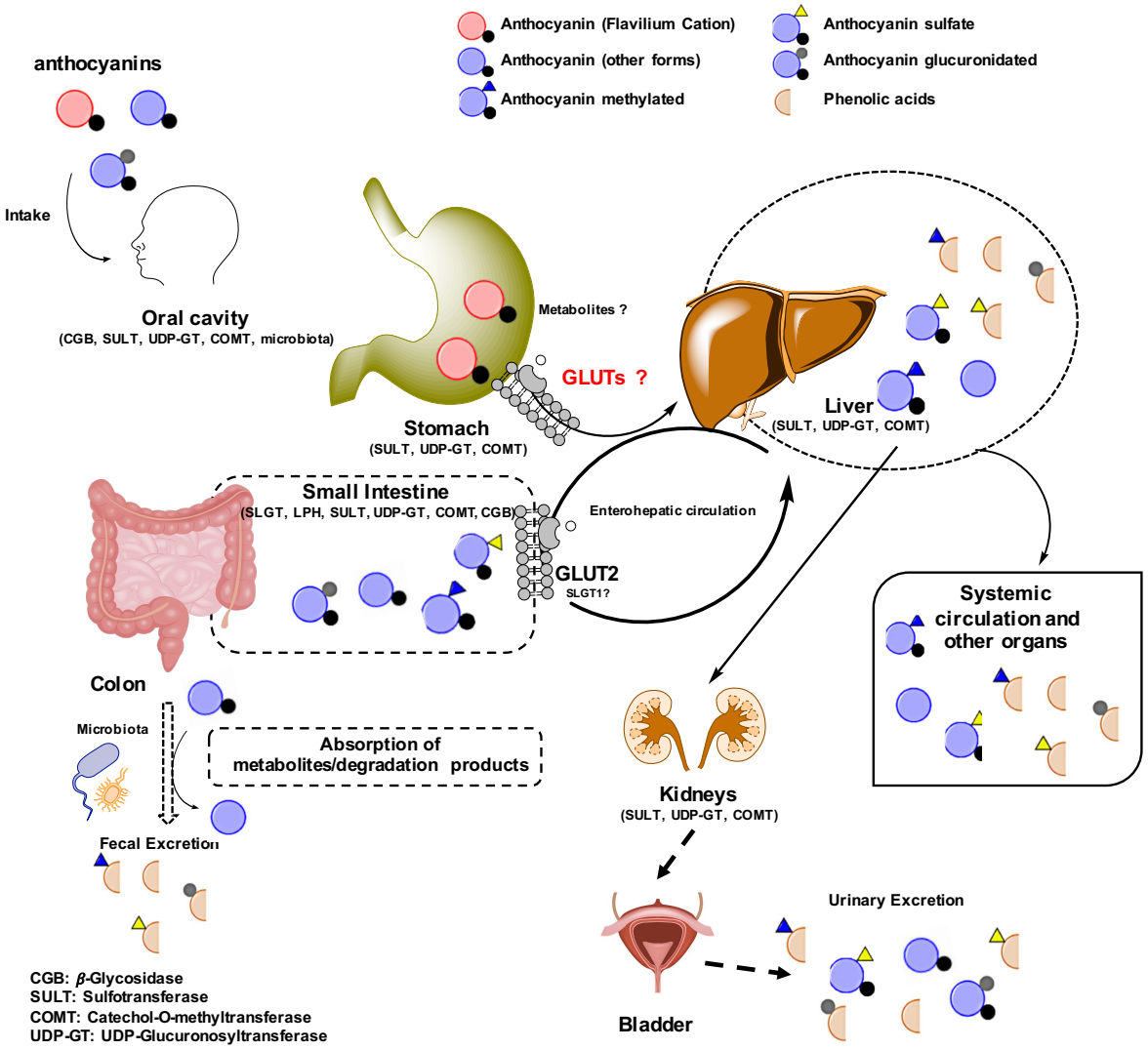

Figure 14. Pathways of anthocyanins absorption, distribution, metabolism and excretion, as proposed by Fernandes et al. [133]. Adapted and updated.

OBJECTIVES

The knowledge on how anthocyanins are absorbed and become bioavailable at the gastrointestinal level is essential to understand their health-benefit effects. The complexity anthocyanins chemistry and biochemistry deserves special attention, therefore the aim of this work was to characterize the bioavailability of anthocyanins at the gastrointestinal level, using different *in vitro* techniques.
Thus, this work has as main objectives:

- The physical and chemical characterization of anthocyanins from Purple-Fleshed Sweet Potato
- Understanding the behavior of these compounds at the gastric and intestinal cavities.
- Unveiling the molecular mechanism of absorption of anthocyanins at the gastric level.
- Using different sources of anthocyanins and other nutraceuticals to evaluate the absorption and bioactive properties in different cell lines

The present work is organized in two main parts.

Part I is divided in 3 chapters and includes the physical and chemical characterization of acylated anthocyanins extracted from Purple-Fleshed Sweet Potato and deals with the biochemical aspects about the absorption and bioavailability of these anthocyanins.
Part II is divided in 2 chapters. On the first chapter the study of the bioactivities using MCF-7 breast cancer cells and bioavailability using MKN-28 gastric cancer cells of red wine anthocyanins and derivatives was directed for the differences between the compounds formed during red wine ageing.
The second chapter shows the study of the main natural bioactive compounds present in *Gardenia Jasminoides Ellis*, a flower widely used in food industry in China and approved by the Chinese Pharmacopoeia for use in traditional Chinese medicine.

PART I

PHYSICAL, CHEMICAL AND BIOLOGICAL STUDIES OF ACYLATED ANTHOCYANINS

Part I of the present PhD dissertation is organized in three Chapters and presents the work developed in the University of Porto and in the New University of Lisbon. The first chapter includes the physical and chemical characterization of acylated anthocyanins extracted from Purple-Fleshed Sweet Potato, that will be used in further chapters. Chapters II and III deals with the biochemical aspects about the bioavailability of these anthocyanins. Chapter II is focused in whole anthocyanin extracts transephitelial transport at the gastrointestinal tract, while Chapter III is focused in individual anthocyanins for molecular mechanistic studies about their transport in gastric cells.

CHAPTER I

PHYSICAL AND CHEMICAL CHARACTERIZATION OF TWO PURPLE-FLESHED SWEET POTATO ANTHOCYANINS

Synopsis

The objective of the work developed in this chapter was to characterize the anthocyanins from Purple-Fleshed Sweet Potato.

The anthocyanins were extracted and the content analysed by HPLC-DAD and LC-MS. The results showed that Purple-Sweet Potato extract was rich in Peonidin and Cyanidin derivatives with multiple glucosylations and acylations. Two of the anthocyanins were isolated and their structure characterized by the analysis of LC-MS fragmentation patterns and by one and two-dimensional NMR analysis. The anthocyanins were identified as being *Peonidin-3-(6'-hydroxybenzoyl)-sophoroside-5-glucoside* and *Peonidin-3-(6'-hydroxybenzoyl-6''-caffeoyl)-sophoroside-5-glucoside*. Furthermore, the acid-base network of these two acylated anthocyanins was evaluated by means of *pH jump* techniques. Equilibrium and kinetic constants were determined, and overall these anthocyanins demonstrated a higher capacity in retaining the red and blue colors at acidic and basic pH values, suggesting a higher resistance to pH variations than the parent anthocyanin, Peonidin-3-*O*-glucoside. The presence of acylation groups seems to determine this particular characteristic. The fluorescence properties of these two anthocyanins were evaluated. Overall, the species present at higher pH values (from neutral to slightly basic) showed the most interesting fluorescence characteristics for both anthocyanins. An optimum $\lambda_{ex}/\lambda_{em}$ pair was set at λ_{ex} 610 nm/ λ_{em} 640 nm.

This chapter resulted in the following paper: ***Oliveira, H.,*** *Basílio, N., Pina, F., de Freitas, V., Mateus, N., Fernandes, I., "Physical and Chemical Properties of Anthocyanins from Purple-fleshed Sweet Potato", Submitted for publication.*

1. INTRODUCTION

Anthocyanins are amazing molecules and are among the most interesting and studied compounds within the class of flavonoids.

These compounds are normally present in the diet as a consequence of the growing intake of red fruits and vegetables. More than 700 different anthocyanins have been reported [27]. Chemically, anthocyanins are glycosylated, polyhydroxy or polymethoxy derivatives of a 2-phenyl benzopyrylium moiety and are usually represented by their flavylium cation. The different chemical structures of anthocyanins arise from the position and number of hydroxyl groups on the molecule, the degree of methylation, the nature and number of sugar moieties attached to the aglycone, and the position of the attachment, as well as the nature and number of aliphatic or aromatic acids attached to the sugars [167]. Different plants and food sources present different types of anthocyanins.

Among the healthy foods, Purple-Fleshed Sweet Potatoes (PFSP) are characterized by an intense purple color, due to the presence of high amounts of anthocyanin [168, 169]. Large research on the nutraceutical properties of PFSP has been done, and indicated that the extracted anthocyanins exhibited biological activities as strong radical scavengers and antimutagenic [169]. The cultivars of these species have been growing to meet the demand in health food markets, not only in Asian countries but also worldwide. Therefore, they are utilized in a variety of processed commercial products. This fact consequently led to the production of different varieties of PFSP with different contents of anthocyanins [170].

Differing from anthocyanins found normally in berries and grapes, PFSP anthocyanins primarily exist as poly-acylated and poly-glycosylated structures derived from Peonidin and Cyanidin [171]. Acylation with various phenolic acids makes PFSP anthocyanins unique and also provides some advantages in pH and heat resistances, light sensitivity, and overall stability [168], as anthocyanins are known to be reactive compounds that have their stability affected by oxygen, heat, light, pH and enzymes [24]. The (bio)chemistry of these compounds, responsible for the red and blue colors of food-stuffs they are part of, is very complex when compared to other flavonoids. Among the external phenomena affecting anthocyanins stability, pH may be the one with the most impact. In aqueous and hydro-alcoholic solutions at different pH values, anthocyanins undergo a series of modifications that originate different structural forms, with distinct physical and chemical

properties, in a dynamic equilibrium. The general mechanism of these transformations (using a PFSP anthocyanin structure as example) is presented in Figure 15.

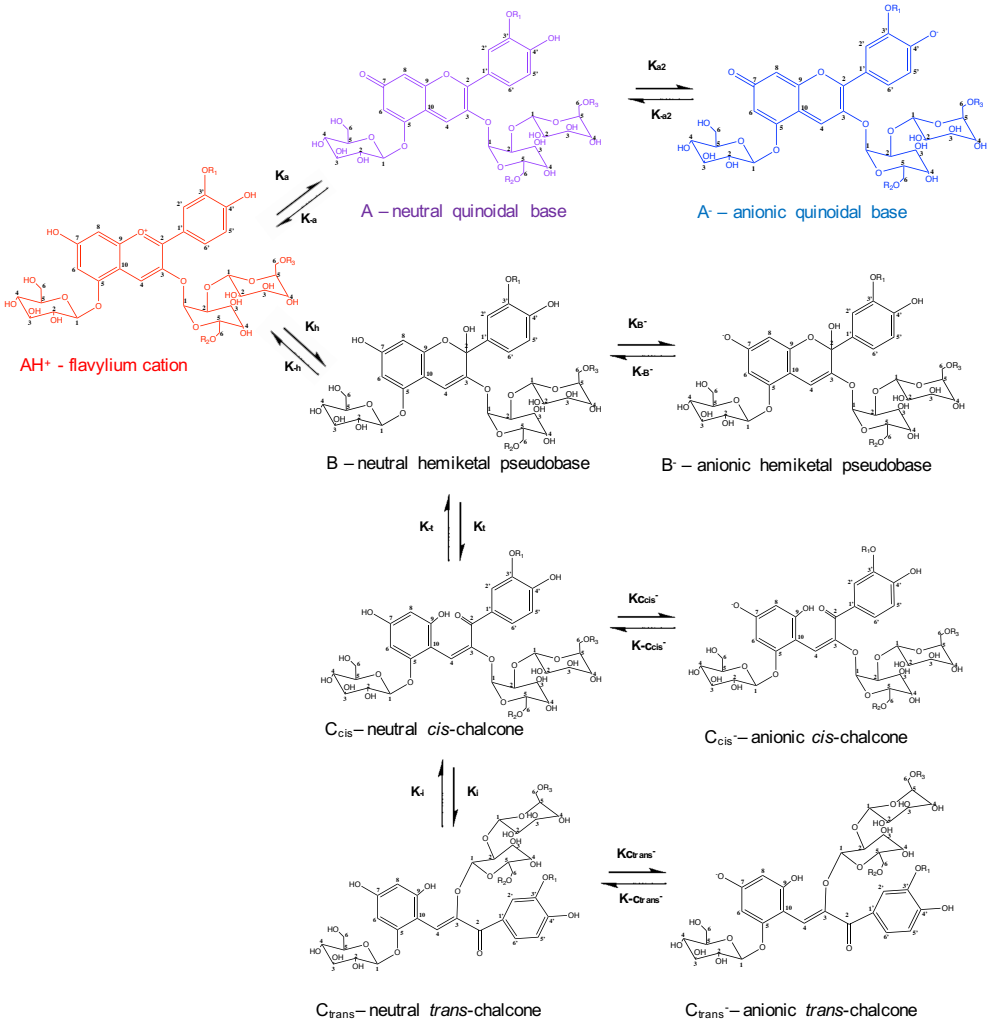

Figure 15. Proposed general equilibrium reactions for PFSP anthocyanins type. For peonidin-derived R_1 is *OCH_3*. R_2 and R_3 can be *H* or acyl groups (usually cinnamic or hydroxybenzoic acids).

At pH < 1, the dominant form of anthocyanins is the flavylium cation (*AH^+*), with a red color. By increasing pH, the flavylium cation donates a proton to give origin to a neutral quinoidal base (*A*), with a blue color and simultaneously a slower hydration process in which the flavylium cation receives a hydroxyl ion from water (generally at C2) to give rise to a neutral hemiketal pseudo-base (*B*). The hemiketal then establishes in sub-seconds an equilibrium with a ring-opening process at the pyran ring, tautomerizing to give the *cis*-chalcone (*C_{cis}*). This form will isomerize (much slower) to further give appearance to the

trans-chalcone (C_{trans}). At even higher pH values, the different forms tend to suffer a deprotonation to originate the respective anionic forms.

These phenomena are of significance when considering the preparation of foods, products shelf-life and the absorption of anthocyanins at the gastro-intestinal tract. During these processes, anthocyanins are exposed to different pH and temperature environments, which will lead to changes on their structure, and, therefore, on their bioactivities. Thus, the understanding of their physical and chemical network is essential.

One of the ways to study the structural conversion network is through relaxation methods: to a system in equilibrium instantaneous perturbations are applied (temperature, pressure or pH, normally designated by t*emperature jumps*, *pressure jumps* or *pH jumps*) that turn the system into a metastatic equilibrium. From that point, the system will evolve for a new equilibrium allowing the monitoring of several characteristics (UV-Vis spectra, ^{1}H-NMR spectra, etc.) that give the necessary data for establish the thermodynamic and kinetic equilibria [172].

The theory of the kinetic and thermodynamic of anthocyanins and related compounds multistates is firmly established in the acidic medium [173, 174] in particular after the contributions of Brouillard and Dubois [175] as well as McClelland [176], this last author working in synthetic flavylium compounds. A breakthrough on the comprehension of the anthocyanin multistate was given by Brouillard and Dubois, who have shown that the quinoidal base, in moderately acidic conditions, does not hydrate [175].

Several studies on this field have been published, using mainly *pH jumps* techniques and reporting the parameters of these equilibria for different monoglucoside and diglucoside anthocyanins [177, 178]. The most complete study with polyacylated anthocyanins was published by Dangles [179] and very recently, a work about the acid-base thermodynamic and kinetic equilibria of high molecular weight anthocyanins from Heavenly Blue flowers was also published [180]. However, no studies in PFSP anthocyanins on this issue are known. It is crucial to have the knowledge on these parameters in order to better comprehend all the reported properties of these amazing compounds as they are particular to each anthocyanin, and this fact may be crucial for defining a better or a worse anthocyanin for specific applications.

Thus, the study of the thermodynamic and kinetic parameters by means of *pH jumps* will be one of the main focus of this chapter.

Besides these characterizations that allow us to know the complex network of rearrangements that anthocyanins have, other interesting properties such as fluorescence

can be studied. Compounds displaying light-emitting properties can be very advantageous in several science fields.

Some anthocyanins show measurable fluorescence, but information on this topic in the literature is scarce. The study of Drabent and coworkers [181, 182] with red cabbage extracts, containing mainly cyanidin derivates, has shown that the colorless compounds present in these extracts have fluorescence, and that this emission is pH dependent. The fluorescence emission of anthocyanins has usually been investigated using excitation in the visible region and near UV, that is, at excitation wavelength, λ_{ex} > 270 nm. Low fluorescent quantum yield, especially of colored forms of anthocyanins, is one of the reasons why it is rarely studied [181-184].

The fluorescence techniques are highly sensitive and nondestructive. These techniques are useful tools for nondestructive monitoring of anthocyanin compounds [185]. Therefore, the fluorescence properties of PFSP anthocyanins were investigated due to their unique structure and intramolecular rearrangements that may result in interesting light characteristics and may be applied in biological studies, as we shall further see.

2. MATERIALS AND METHODS

2.1. Purple-Fleshed Sweet Potato Anthocyanins Extraction

Extraction of anthocyanins from Purple-Fleshed Sweet Potato (PFSP) was performed accordingly to previously described procedures [186]. PFSP was obtained in a local market (*Supercor*, *El Corte Inglés*), and the origin of production was Portugal.

PFSP was cut in slices and the anthocyanins were extracted in a solution of 70 % ethanol with ultra-sound assistance for 1h at room temperature. After that, the obtained extract was submitted to a centrifugation process at 2,800 x *g* for 15 min with the objective of remove insoluble materials like fibers and starch.

The resulting supernatant was filtered and phenolic acids were removed with a liquid-liquid extraction procedure (ethyl acetate/water, 1:1) and the resulting extract was applied on a Amberlite XAD-7HP column resin. This is a non-ionic macroreticular resin usually made of a polystyrene-divinylbenzene copolymer matrix that adsorbs and releases ionic species through hydrophobic and polar interactions; usually under isocratic conditions.

Acidified water was used to remove proteins, sugars and other interfering materials and acidified methanol to recover anthocyanins.

The enriched anthocyanin fraction was then applied on a reverse phase silica C-18 column to remove any remaining sugars.

The extract was freeze-dried and stored at -18º C until use for the next steps.

2.2. Isolation and Purification of two Anthocyanins from Purple-Fleshed Sweet Potato

Peonidin-3-(6'-hydroxybenzoyl)-sophoroside-5-glucoside and Peonidin-3-(6'-hydroxybenzoyl-6''-caffeoyl)-sophoroside-5-glucoside were isolated from Purple-Fleshed Sweet Potato using two preparative HPLC.

The first one, a Dionex Ultimate 3000, equipped with binary pump, an autosampler, a UV-Vis variable wavelength detector and an automated fraction collecter (Thermo Scientific). The stationary phase was composed by a µBondapak® C18 10µm pore size, 125Å, 100 x 25 mm i.d. PrepPak® Cartridge (Waters) column that allowed to obtain a high amount of isolated fractions with the anthocyanins of interest. The solvents were: A – $HCOOH/H_2O$

(1:9) and B – HCOOH/MeOH/H_2O (1:3:6). The method of elution was as follows: from 0 to 70 min solvent B increased from 20% to 85%; from 71 to 80 min solvent B was 100% and from 81 to 90 min the initial conditions were re-established. All the sequence was carried out at a flow rate of 7.5 mL/min. The detection occurred at 520 nm. The automated fraction collector was set for a collection by peak and a maximum of 5 mL was determined for each tube. In the end, the tubes corresponding to the same peak were mixed together. The second preparative HPLC allowed a high purification of the compounds of interest. The system was composed by a liquid chromatographer from ELITE LaChrom composed by a quaternary pump L-2130 and UV-Vis detector L-2420. The stationary phase utilized was a 250 x 4.6 mm i.d. reversed-phase C18 column (Merck, Darmstadt, Germany). Detection was carried out at 520 nm. The solvents were A - HCOOH/H_2O (1:9) and B - HCOOH/CH_3CN/H_2O (1:3:6). The gradient consisted of 20–52.5 % B for 35 minutes at a flow rate of 1.0 mL/min. The column was washed with 100 % B for 15 minutes and then stabilized at the initial conditions for another 15 minutes.

2.3. HPLC-DAD analysis

The HPLC analysis were used to monitor the processes of purification. For that, all the analysis was performed on Dionex Ultimate 3000 (Thermo Scientific; USA) equipped with a 250 x 4.6 mm i.d. reversed-phase C18 column (Merck, Darmstadt, Germany). Detection was carried out at 520 nm using a diode array detector (DAD). The solvents were (A) H_2O/HCOOH (9:1) and (B) H_2O/HCOOH/CH_3CN (6:1:3). The gradient consisted of 20–52.5 % B for 35 minutes at a flow rate of 1.0 mL/min. The column was washed with 100 % B for 15 minutes and then stabilized at the initial conditions for another 15 minutes.

2.4. LC-DAD/ESI-MS analysis

LC-DAD/ESI-MS analysis was done on a Finnigan Surveyor series liquid chromatograph, equipped with a Thermo Finnigan (Hypersil Gold) reversed-phase column (150 mm × 4.6 mm, 5 µm, C18) at 25 °C. The samples were analyzed using the same solvents, gradients, injection volume and flow rate referred above for the HPLC analysis. Double-online detection was done by a photodiode spectrophotometer and mass spectrometry. The mass detector was a Finnigan LCQ DECA XP MAX (Finnigan Corp., San Jose, Calif., USA) quadrupole ion trap equipped with an atmospheric pressure

ionization (API) source, using an electrospray ionization (ESI) interface. The vaporizer and the capillary voltages were 5 kV and 4 V, respectively. The capillary temperature was set at 325 °C. Nitrogen was used both as sheath and auxiliary gas at flow rates of 90 and 25, respectively (in arbitrary units). Spectra were recorded in positive ion mode between *m*/*z* 250 and 1500.

2.5. NMR analysis

The NMR spectrums of the purified anthocyanins were obtained with a Bruker Avance III 600 HD spectrometer (Bruker, Massachusetts, US), operating with a frequency of 600.13 MHz for ^{1}H and 150.90 MHz for ^{13}C, equipped with a 5 mm CPPBBO BB-^{1}H/^{19}F/D Z-GRD CryoProbe Prodigy and pulse gradient units capable of producing magnetic field pulsed gradients in the z direction of 50 G/cm. The measurements were performed with standard Bruker pulse sequences at 300 K (or, for structural purposes, 278 K). All ^{1}H chemical shifts are given with respect to tetramethylsilyl propionate (TSP; Sigma-Aldrich), which was used as an internal reference.
The experiments were performed at 30º C in MeOD/TFA (9.9:0.1).
4.6 mg of Peonidin-3-(6'-hydroxybenzoyl)-sophoroside-5-glucoside and 5.1 mg of Peonidin-3-(6'-hydroxybenzoyl-6''-caffeoyl)-sophoroside-5-glucoside were dissolved in 150 µL of MeOD/TFA solution. The use of TFA ensured a stabilization of the flavylium cation form for both anthocyanins. All the spectrum were calibrated and monodimensional (1H, 13C) plus bidimensional (COSY, HSQC and HMBC) experiences were performed.

2.6. Acid-Base Network of Purple-Fleshed Sweet Potato Anthocyanins

The thermodynamic and kinetic parameters of PFSP Anthocyanins were evaluated by UV−visible spectroscopy and direct pH jumps experiments.

2.6.1. UV−Visible Spectroscopy

The pH titration of PFSP Anthocyanins was performed by UV−visible spectroscopy using the pH jump technique from pH = 1 to higher pH values depending on the experiment.

For that, stock solutions of 1×10^{-4}M of each anthocyanin were prepared in 0.1 M HCl. Then to a plastic 10 × 10 mm cuvette were added 500 µL of a 0.1 M NaOH solution and 500 µL of a Theorell and Stenhagen universal buffer solution adjusted to the desired pH value. At the end, 500 µL of the stock solutions equilibrated at pH 1.0 (flavylium cation form) were added to the cuvette. The absorption spectra of the different solutions were obtained after approximately 60 min (pseudoequilibrium acidity constant, pK^a) after the pH jump (from pH 1.0 to the pH of the universal buffer solution) in a Varian-Cary 100 Bio spectrophotometer. The UV−visible spectra of the same solutions were also obtained after equilibration in the dark (equilibrium acidity constant, pK′a). The pH values of all solutions were measured in a Radiometer Copenhagen PHM240 pH/ion meter. The pH meter was calibrated with pH 4, 7, and 9 buffer solutions. The fittings for pK^a and pK′a determination were carried out using the Solver program from Microsoft Excel.

2.6.2. Stopped-Flow

Direct and reverse pH jumps experiments were conducted in an Applied Photophysics SX20 stopped-flow spectrophotometer provided with a PDA.1/UV photodiode array detector with a minimum scan time of 0.65 ms and a wavelength range of 200 to 735 nm. For direct pH jump, an equilibrated stock solution of the compounds at pH 1 were placed in one syringe whereas the buffer and base needed to raise the pH to the desired final pH were put in another syringe. Upon mixing, the concentration of the compounds was diluted by a factor of 2. For reverse pH jump, an equilibrated solution of the pigments in the universal buffer at pH ~ 5 was placed in a first syringe, and in a second syringe was placed an acidic solution (HCl, 0.2 M) to obtain the final pH ~ 1. For both pH jumps, direct and reverse, a small volume of the sample was recovered after the mixture to confirm the pH of the solution. The fittings for the determination of the thermodynamic and kinetic parameters were carried out using the program solver from Microsoft Excel.

2.7. Fluorescence Spectroscopy analysis

The fluorescence properties of the two PFSP anthocyanins were evaluated with a spectrofluorometer FluoroMax®-4 (HORIBA Scientific) in a QS High Precision Cell made of quartz SUPRASIL with a length path of 3 x 3 mm (Hellma Analytics). All the solutions were used in dilutions to match an absorbance of about 0.1 in the 510-530 nm spectral

region. All fluorescence spectra were corrected for the spectral response of the spectrofluorometer emission and excitation units.

Both anthocyanins were analysed at different pH values (from 1 to 11) at a concentration of 25 μM.

For all the experiments both the front and exit entrance slits consisted of a 5 nm bandpass. The grating parameters were: density 1200 (ex/em); blaze 330 (ex) and 500 (em).

For the different experiments, specific range of wavelengths were used for excitation and emission, and are expressed in the results section. Both excitation and emission spectrum were recorded for each anthocyanin at different pH values.

3. RESULTS

3.1. Structural characterization of PFSP anthocyanins

In order to have a full characterization of the two compounds isolated from PFSP extract using preparative HPLC techniques, different approaches were utilized. The chromatographic profile of the isolated compounds is present in Figure 16. The peak purities were 97% for peak 1 (that will be called Pn3HBsoph5glc for now) and 93% for peak 2 (that will be called Pn3HBCsoph5glc for now).

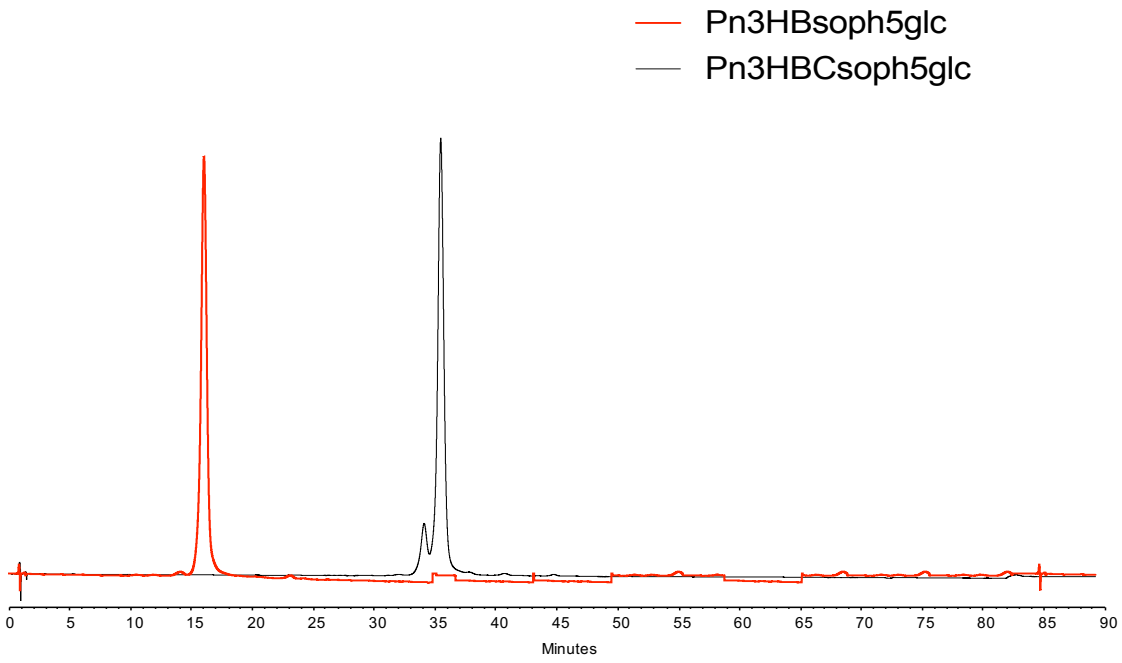

Figure 16. Chromatographic profile of the isolated compounds from Purple-Fleshed Sweet Potato monitored at 520 nm.

3.1.1. LC-DAD-ESI/MS-MS analysis

The LC-MS technique was used to have a fragmentation pattern of the two pigments and compare with the information available on the literature [168, 187, 188].

First, the full extract was characterized at 520 nm and the chromatographic profile was as shown in Figure 17. All the main anthocyanins present were identified based on their fragmentation patterns (Table 7).

A total of 11 anthocyanins were identified and quantified by HPLC coupled with an ESI/MS-MS detector. The Electrospray ionization (ESI) is a technique used in mass spectrometry that is based in the production of ions using an electrospray. This technique promotes a lower degree of fragmentation allowing the molecular ion to be always observed. However, it is necessary to couple this technique with tandem mass spectrometry (MS-MS) in order to get a fragmentation pattern for the molecular ion.

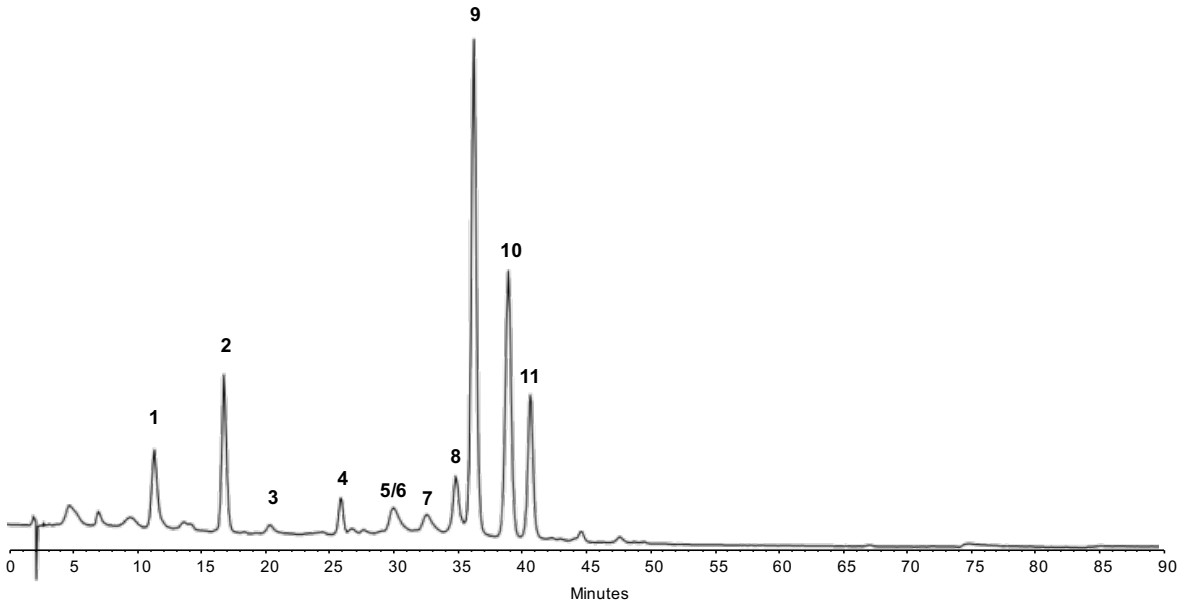

Figure 17. Chromatographic profile of Purple-Fleshed Sweet Potato anthocyanins at 520 nm analyzed by HPLC-DAD.

The fragmentations spectra of the identified anthocyanins were compatible with Peonidin or Cyanidin derivatives, acylated with caffeic, ferulic, and/or *p*-hydrobenzoic acids. The pattern of glycosylation of these compounds were similar, having a sophoroside group at C3 carbon and a glucose at C5.

Table 7. HPLC-DAD-ESI/MS-MS identification of the main anthocyanins present in Purple-Fleshed Sweet Potato extract at 520 nm.

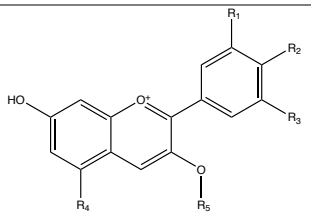

Purple-Fleshed Sweet Potato

peak	R_1	R_2	R_3	R_4	R_5	MS	MS^2/MS^3	$\lambda_{máx}$
1	OH	OH	H	O-Glc	6'-*p*-hydroxybenzoil-sophoroside	893.20	730.90; 449.02; 287.22	517
2	OCH_3	OH	H	O-Glc	6'-*p*-hydroxybenzoil-sophoroside	907.20	744.80; 462.87; 301.13	520
3	OH	OH	H	O-Glc	6'-feruloyl-sophoroside	949.20	786.87; 448.87; 287.20	520
4	OCH_3	OH	H	O-Glc	6'-feruloyl-sophoroside	963.27	800.80; 462.93; 301.20	520
5	OH	OH	H	O-Glc	6'-caffeoyl-sophoroside	935.07	772.87; 448.93; 287.27	526
6	OH	OH	H	O-Glc	6'-*p*-hydroxybenzoil -6''-caffeoyl-sophoroside	1055.20	892.85; 448.98; 287.09	526
7	OCH_3	OH	H	O-Glc	6'-caffeoyl-sophoroside	949.07	786.87; 462.93; 301.13	523
8	OCH_3	OH	H	O-Glc	6'-caffeoyl-6''-caffeoyl-sophoroside	1111.07	949.97; 448.88; 301.13	526
9	OCH_3	OH	H	O-Glc	6'-*p*-hydroxybenzoil -6''-caffeoyl-sophoroside	1069.13	906.87; 463.00; 301.13	526
10	OCH_3	OH	H	O-Glc	6'-caffeoyl-6''-feruloyl-sophoroside	1125.20	963.00; 462.93; 301.13	529
11	OCH_3	OH	H	O-Glc	6'-*p*-hydroxybenzoil -6''-feruloyl-sophoroside	1083.20	920.93; 463.87; 301.21	526

Two anthocyanins were isolated by preparative HPLC and the corresponding fragmentations were analysed in detail. For the first anthocyanin (compound 2) the molecular ion was identified as presenting a charge/mass reason (m/z) of 907. All the experiments were performed at low pH, to ensure that anthocyanins were stabilized in their flavilium cation form (see section 3.2. of the present Chapter for more details). This way, and once all the mass spectra were obtained in the positive mode, the molecular ion m/z corresponds to the molar mass of the compound or fragment. The main fragmentation of the molecular ion corresponds to the loss of a glucose unit (162 a.m.u.) originating an ion with m/z = 745. Other main fragment present in the MS^2 and MS^3 spectra is corresponding to the loss of the glucose at C5 and the *p*-hydroxybenzoic acid and one glucose at C3, originating an ion with m/z = 463. This ion is compatible with the molar mass of Peonidin-3-*O*-glucoside. Finally, the last main fragment corresponds to an ion of m/z = 301, which is compatible to the molar mass of the aglycone moiety of this anthocyanin, Peonidin. Thus, the compound was identified as being Peonidin-3-(6'-*p*-

hydroxybenzoyl)-sophoroside-5-glucoside (Pn3HBsoph5glc), with a molar mass of 907.65 g.mol^{-1}

The second anthocyanin isolated (compound 9), showed a molecular ion of m/z = 1069, corresponding to a molar mass of 1069.77 g.mol^{-1}. The main fragment of the molecular ion for this anthocyanin was an ion with m/z = 907. This fragment m/z is compatible with the structure of Pn3HBsoph5glc, and in fact, the loss a caffeic acid unit (162 a.m.u) match this m/z. However, the loss of a glucose unit (162 a.m.u) also matches, and looking for the fragmentation pattern of Pn3HBsoph5glc, this seems to be the most likely fragment to be formed with a m/z = 907. The other main fragments originated in the MS^2 and MS^3 spectra were compatible with the molar mass of Peonidin-3-O-glucoside and Peonidin, such as in the case of Pn3HBsoph5glc.

The compound was identified as being Peonidin-3-(6'-*p*-hydroxybenzoyl-6''-caffeoyl)-sophoroside-5-glucoside (Pn3HBCsoph5glc).

For all the other anthocyanins the fragmentation patterns were similar: first the loss of a glucose unit at the C5 carbon, second the loss of the acyl groups and the second glucose unit of the sophoroside group at C3 carbon and finally the loss of the last glucose at C3 to originate the corresponding aglycone.

The results of the LC-MS analysis suggest, then, the fragmentation the PFSP anthocyanins follow a concerted pattern, such as the one suggested in Figure 18 for Pn3HBsoph5glc and Pn3HBCsoph5glc.

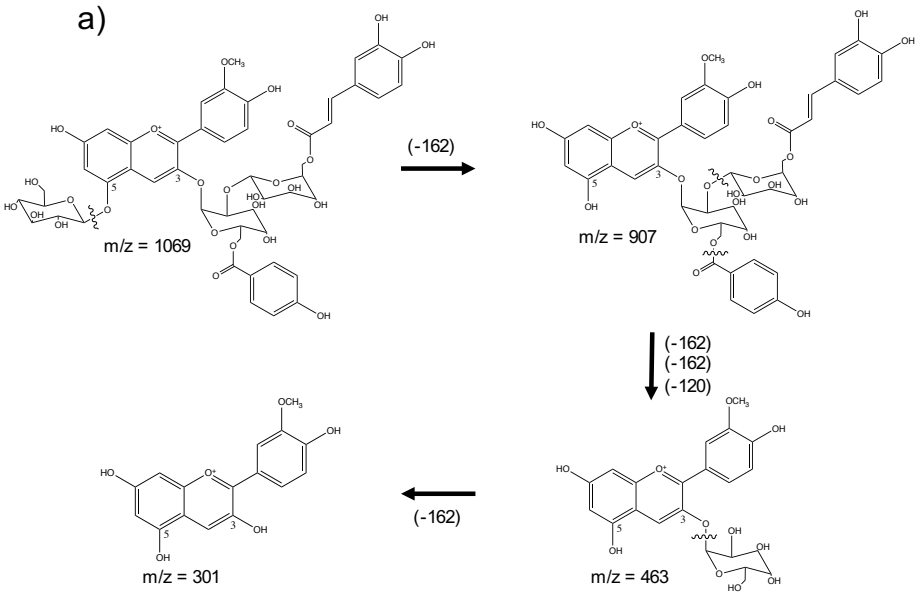

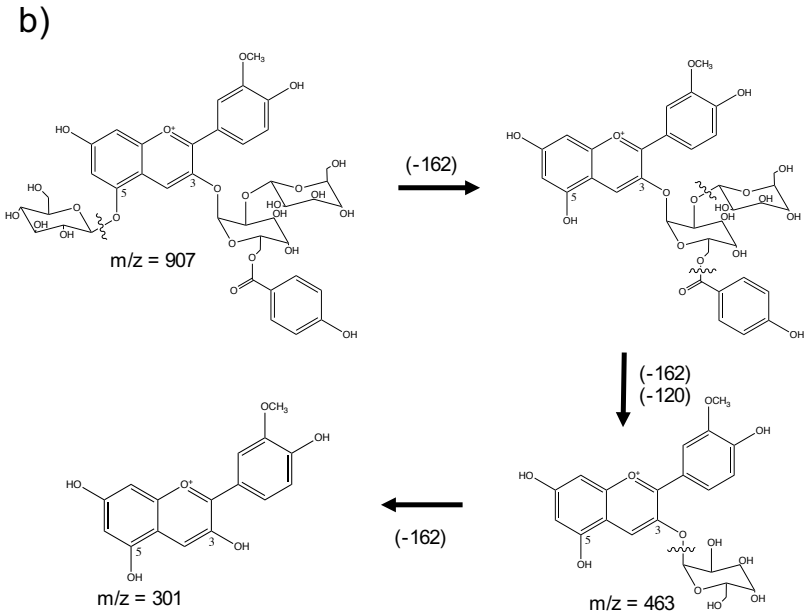

Figure 18. Proposed mechanism of fragmentation of a) m/z = 1069 Pn3HBCsoph5glc and b) m/z = 907 Pn3HBsoph5glc.

3.1.2. NMR spectroscopy analysis

Although the analysis of the mass spectra suggested that the isolated peaks were classified as being Peonidin-3-(6'-*p*-hydroxybenzoyl)-sophoroside-5-glucoside and Peonidin-3-(6'-*p*-hydroxybenzoyl-6''-caffeoyl)-sophoroside-5-glucoside, this attribution was based in the information present in the literature. To ensure that the attribution was correctly done, NMR analysis were performed. These techniques allow to obtain unique spectra for each molecule, thus obtaining detailed information about the structure of the molecules as it works based on the intramolecular changes of the magnetic fields of each atom.

Due to the possible presence of impurities in the samples, or even precipitation phenomena during the experiments, it was not possible to fully attribute all the protons and carbons in the compounds.

3.1.2.1. Peonidin-3-(6'-p-hydroxybenzoyl)-sophoroside-5-glucoside

The ^{1}HNMR spectrum of Pn3HBsoph5glc can be found in Figure 19. To attribute the signs to the respective protons and carbons in the molecule structure, a traditional nomenclature

was used: the flavanic aromatic rings were classified as A and B (benzene rings) and C (furan ring). The glucoses linked at the pyran ring were classified as glucose A and B (being A the directly linked to B) and the glucose linked to ring A was classified as glucose C. The acyl group was classified by the own name.

Table 8 shows the attribution of protons and carbons and the correlations found in the bi-dimensional analysis (HMBC and HSQC) for Pn3HBsoph5glc.

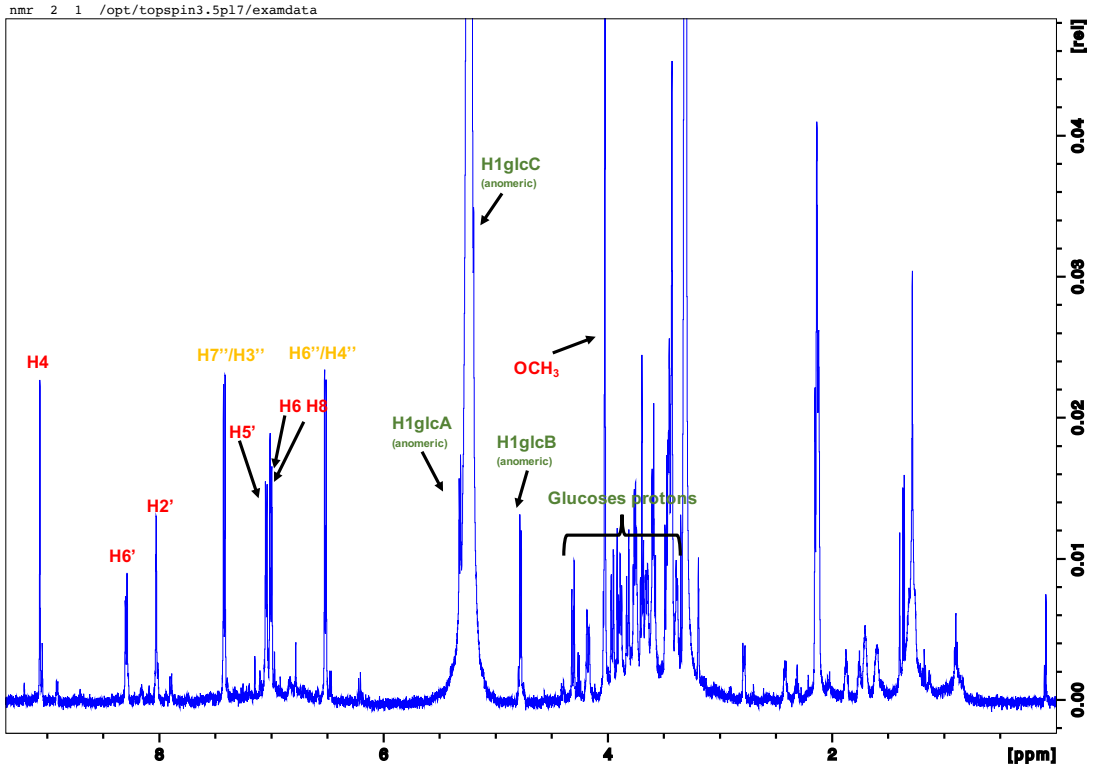

Figure 19. ^{1}HNMR spectrum for Pn3HBsoph5glc with the respective proton attributions.

The attribution started with the flavanic core. A total of 7 proton signals were determined to belong to this aromatic core. The highest chemical shift value (δ), corresponding to the most unprotected proton (δ = 9.06 ppm), should be attributed to a proton in the proximity of very electronegative atoms such as oxygens, thus this signal was attributed to the proton of C4 carbon (H4). The signal of C6' carbon (H6') appeared at 8.29 ppm as a duplet with *J* = 1.59 Hz, this may be the result of the conjugated double bounds between C6' and the oxygen of the C ring. This signal was followed by the signal attributed to C2' (H2') at δ = 8.03 ppm (duplet, *J* = 1.58 Hz). C5' carbon (H5') signal appeared at δ = 7.04 ppm (duplet, *J* = 9.76 Hz). C6 and C8 carbons (H6 and H8) signals appeared at δ = 7.01 and

6.99 ppm (duplets, *J* = 1.59 Hz and J = 1.58 Hz). The attributions were based on the electronegativity of the surroundings of each proton. The fact that C6 and C8, for example have very similar δ and *J* values, suggests that their surroundings have the same electronegative characteristics. Thus, one can assume that they are positioned near one or more oxygen atoms, most probably in a *orto*- position relative to that atoms.

Table 8. NMR attributions (^{1}H and ^{13}C) of Peonidin-3-(6'-*p*-hydroxybenzoyl)-sophoroside-5-glucoside, and the respective HSQC and HMBC correlations.

Moiety	Pos.	δ ^{1}H (ppm)	*J*, Hz	δ ^{13}C (ppm)	HSQC correlations	HMBC correlations
Flavanic Core	C2			165.5	-	H4
	C3			145.5	-	-
	C4	9.06	s	139.5	H4	C5; C2
	C5			156.7	-	H6
	C6	7.01	d (1.59)	105.3	H6	C8; C10; C5; C9
	C7			169.9	-	H8
	C8	6.99	d (1.58)	97.4	H8	C6; C7
	C9			156.9	-	H6
	C10			113.2	-	H6
	C1'			121.0	-	-
	C2'	8.03	d (1.58)	114.7	H2'	C6'; C4'; C2; C3'
	C3'			149.9	-	H2'; H5'; OCH_3
	C4'			156.9	-	-
	C5'	7.04	d (9.76)	117.4	H5'	C1'; C3'
	C6'	8.29	d (9.28)	130.1	H6'	C2'; C4'; C2
	OCH_3	4.02	s	56.9	OCH_3	C3'
p-hydroxybenzoyl	C1''			167.7	-	H3''; H7''
	C2''			121.5	-	H4''; H6''
	C3''	7.42	d (8.30)	132.2	H3''	C7''; C5''; C1''
	C4''	6.52	d (8.30)	115.7	H4''	C6'';C2''; C5''
	C5''			163.3	-	H3''; H7''; H4''; H6''
	C6''	6.52	d (8.30)	115.7	H6''	C6'';C2''; C5''
	C7''	7.42	d (8.30)	132.2	H7''	C3''; C5''; C1''
Glucose A	C1	5.32	d (7.80)	104.2	H1	C3
	C2	3.88	t (7.81)	83.3	H2	H1B;C3A
	C3	3.74	d (9.76)	77.6	H3	-
	C4	3.42	m ?	71.3	H4	C5A
	C5	3.47	d (9.28)	70.8	H5	-
	C6	4.31 4.17	d (13.78) dd (14.08;8.55)	64.3	H6	C4A; C1''
Glucose B	C1	4.78	d (7.32)	105.8	H1	H2A
	C2	3.39	d (8.30)	76.0	H2	C4B
	C3	3.43	m ?	75.5	H3	C5B
	C4	3.38	d (9.76)	77.9	H4	C1B
	C5	3.43	m ?	71.2	H5	-
	C6	3.82 3.65	d (12.70) d (12.53)	62.3	H6	-
Glucose C	C1	5.20	d (7.42)	102.5	H1	C5
	C2	3.69	t (9.28)	74.6	H2	C4C,C1C
	C3	3.59	t (7.32)	78.6	H3	C2C
	C4	3.43	m ?	77.8	H4	-
	C5	3.45	d (7.42)	78.8	H5	C3C
	C6	3.96 3.76	dd (13.78; 10.15) d (13.67)	62.4	H6	C4C

The most protected protons of the flavanic core belong to the $-OCH_3$ substituent. This signal appeared as a singlet at δ = 4.02 ppm due to the fact that the 3 protons linked to the carbon are equivalents.

The 2D NMR homonuclear correlation spectroscopy (COSY) experiments allows the identification of spins that are coupled to each other ($^2J_{H-H}$). This is then translated in a correlation of each frequency (proton signal) with the one belonging to the neighbour proton.

COSY experiments show a correlation between C5' and C6', confirming they are coupled. No more information was obtained for the flavanic core from COSY experiments, suggesting that all the other protons are not coupled with each other.

The next 2D NMR experiment used was the heteronuclear single-quantum correlation spectroscopy (HSQC) that allows the detection of correlations between nuclei of two different types which are separated by one bond ($^2J_{C-H}$). Thus, it is possible through this technique to correlate the δ values of ^{13}CNMR with the ^{1}HNMR δ values, and to know the carbon connected to each proton.

From the HSQC spectrum, it was possible to attribute the δ values of each carbon connected to the identified protons in the flavanic core. Therefore, the δ values were attributed as follows: C4 with δ = 139.5 ppm; C6 with δ = 105.3 ppm; C8 with δ = 97.4 ppm; C2' with δ = 114.7 ppm; C5' with δ = 117.4 ppm; C6' with δ = 130.1 ppm and OCH_3 carbon with δ = 56.9 ppm.

The ^{13}CNMR spectrum was coupled with attached proton test (APT) that allowed to distinguish CH_2 signals from CH and CH_3. The APT experiment yields methine (CH) and methyl (CH_3) signals positive and quaternary (C) and methylene (CH_2) signals negative.

Thus, from the spectra one can conclude that all the carbons attached to protons on the flavanic core are either CH or CH_3 being the latter only possible for the OCH_3 once this core is constituted of aromatic rings.

At this point, the information about the structure of the flavanic core is insufficient to determine the entire core.

The heteronuclear multiple-bond correlation spectroscopy (HMBC) 2D NMR analysis detects heteronuclear correlations over longer ranges of about 1-4 bonds $^{2-5}J_{C-H}$, meaning in practical terms that one can correlate protons and carbons that are not coupled with each other. This tool is very useful to provide a full structural characterization of a molecule, which without it, is often not possible.

The HBMC spectra showed several correlations for the aromatic protons.

The positions C2, C5, C7, C9 and C10 were confirmed due to the correlations found. Although the signals can appear up to $^{5}J_{C-H}$, the method was optimized for $^{3}J_{C-H}$. Thus, C2 appear with δ = 165.5 ppm, confirmed for the correlation by HMBC with the proton of C4 (δ ^{1}H = 9.06 ppm). The proton of the carbon C8 shows a coupling with a signal at δ = 169.9 ppm that was attributed to C7. Proton H6 coupled in the HMBC with a signal at δ = 113.2 ppm which was attributed to C10. Proton H6 also coupled with a carbon with two more unknown signals, δ = 156.7 ppm and δ = 156.9 ppm, which were attributed to C5 and C9, respectively.

Other correlations are visible and allowed to confirm the positions of the previous attributions by COSY and HSQC. However, the assignment of C3, C1' and C4' was not possible due to the inexistence of correlations in HMBC spectrum.

All this information allowed to confirm the existence of a core of Peonidin.

The next assignments were to the acyl group.

Two signals of the ^{1}HNMR were attributed to this group. The integration of the signals revealed the presence of two protons in each, suggesting the presence of equivalent hydrogens. Therefore, C3'' and C7'' (H3'' and H5'') were attributed to the signals with δ ^{1}H = 7.42 ppm (duplet, *J* = 8.30 Hz) while C4'' and C6'' (H4'' and H6'') were attributed to the signals at δ ^{1}H = 6.52 ppm (duplet, *J* = 8.30 Hz), this attribution was based on the theoretical position of the protons relative to the carboxylic moiety of the acyl group. The near the protons are, the more unprotected will be, resulting on a higher chemical shift.

Thus, the HSQC allowed to assign the respective δ ^{13}C values for the carbons. C3'' and C7'' with δ ^{13}C = 132.2 ppm while C4'' and C6'' with δ ^{13}C = 115.7 ppm.

COSY spectrum showed coupling between these protons. Due to the position of chemical shifts, one can conclude that these protons are in an aromatic ring structure, and having the acyl structure in mind, the only possible coupling shown in COSY is between the protons of C3'' and C4'' and the protons of C6'' and C7'' that are coupled with each other ($^{2}J_{H-H}$).

The remain unknown signals were easily attributed by HMBC spectrum analysis. The spectrum showed coupling between the odd protons and δ ^{13}C values of 163.3 ppm and 167.7 ppm. From these high chemical shifts one can confirm the positions of C1'' attributed with δ ^{13}C = 167.7 ppm (consistent with a carboxylic moiety) and C5'' with δ ^{13}C = 163.3 ppm. Furthermore, the even protons are too far from C1'' and the coupling that appears on HMBC is with δ ^{13}C = 163.3 ppm, confirming that this is C5'' carbon. Also, these protons couple with a δ ^{13}C = 121.5 ppm, that was attributed to C2''.

Hence, the structure of the acyl group was confirmed as being a hydroxybenzoic acid.

For the glucoses attribution, the inverse approach was utilized.

To understand which anomeric carbon belongs to the respective glucose, couplings on HMBC were analysed. Glucose ^{1}HNMR spectrum is well known and present some characteristics that can help on the identification of protons and therefore the carbons. Anomeric protons inherit two different characteristics due to their local environment: chemical shift due to shielding from the external magnetic field and *J*-coupling (J_{H-H}) from protons on the adjacent carbon (C2). The additional shielding of the oxygen shifts the anomeric protons down field from the rest of the non- exchanging protons allowing us to resolve them from the others, which occur between 3 and 4 ppm. Thus, the chemical shift of these protons is further downfield between 4.5 and 5.5 ppm. The second distinguishing characteristic is the spin-spin coupling (J_{H-H}). Non-equivalent protons on the adjacent carbon (C2) will couple to the anomeric proton creating a doublet. In glucose the α anomer has a dihedral angle of 60 degrees and a coupling constant of about 2.7 Hz, while the β anomer has an angle of 180 degrees and a coupling constant of about 7.2 Hz [189].

The proton at δ ^{1}H = 5.31 ppm (duplet, *J* = 7.80 Hz) shows a correlation in HMBC with the carbon at δ ^{13}C = 145.5 ppm. This carbon was not yet attributed; however, some assumptions can be made: the chemical shift is too high to be a carbon of a glucose moiety; all the carbon of the acyl group are attributed; thus, this carbon must be from the flavanic core. In the flavanic core, 3 carbons are not attributed, and considering the structure of peonidin, only one option is possible. Therefore, the signal at δ ^{13}C = 145.5 ppm was attributed to C3 carbon. This means that the proton at δ ^{1}H = 5.31 ppm belongs to C1 of glucose A of the sophoroside moiety, that is linked in the C3 position. Furthermore, the coupling constant of this proton (*J* = 7.80 Hz) indicates a β conformation [190, 191]. From HSQC, the signal of the corresponding carbon was attributed: δ ^{13}C = 104.1 ppm.

The proton at δ ^{1}H = 5.31 ppm (duplet, *J* = 7.42 Hz) showed a correlation in HMBC spectrum with a signal at δ ^{13}C = 156.7 ppm. This signal was previously attributed to C5, confirming that this proton corresponds to the anomeric carbon (C1) of glucose C, that is linked to the flavanic core trough a *O*-C5 bond. Once again, the coupling constant of this proton (*J* = 7.42 Hz) indicates a β conformation.

Another anomeric proton is visible at δ ^{1}H = 4.78 ppm (duplet, *J* = 7.32 Hz). This should be the proton corresponding to the anomeric carbon (C1) of glucose B, once is the only one left for attribution. From HSQC spectrum, it was possible to attribute the signal of C1

glucose B as being δ ^{13}C = 105.8 ppm. A correlation with a signal at δ ^{13}C = 83.3 ppm in the HMBC spectrum. This δ value is consistent with a carbon in a glucose moiety. In order to confirm the attribution of this signal, COSY and HSQC together with HMBC spectra were used, beginning with each anomeric proton and with a sequential analysis of the couplings, the remain protons and carbons of each glucose were successfully assigned. These assignments can be observed in Table 8. Therefore, the signal at δ ^{13}C = 83.3 ppm was attributed to C2 of glucose A, confirming a bound between glucose A and B, to form the sophoroside moiety. Once again, the coupling constant of this proton (J = 7.32 Hz) indicates a β conformation for glucose B, suggesting a β (1-2) linkage between the two glucoses.

At this point of the analysis, it is confirmed that the structure is formed by a peonidin with a glucose at C5 and a sophoroside moiety at C3. However, the linkage position of the acyl group (hydroxybenzoic acid) is not yet known.

Several approaches can be used, but in this case, the HMBC spectrum was analysed to search correlations for the protons of the C6 carbons of each glucose, once it is the most common place of acylation in anthocyanins. The linkage may occur at the hydroxybenzoic acid level either in the carboxylic or in the hydroxyl moieties. Thus, the correlations were particularly focused on C1'' and C5'' δ ^{13}C signals. The HMBC showed a correlation ($^{3}J_{C\text{-}H}$) at δ ^{1}H = 4.31 ppm with δ ^{13}C = 167.7 ppm. The assignments attributed this proton signal to one of the C6 protons of glucose A, thereby confirming the link of the acyl group at glucose A of the sophoroside group. Furthermore, the signal at δ ^{13}C = 167.7 ppm corresponds to the C1'' carbon, revealing that this linkage is through the carboxylic moiety. All the HMBC interactions and the proposed structure can be found in Figure 20. Also, the spectra files of each analysis can be found in Attachment I.

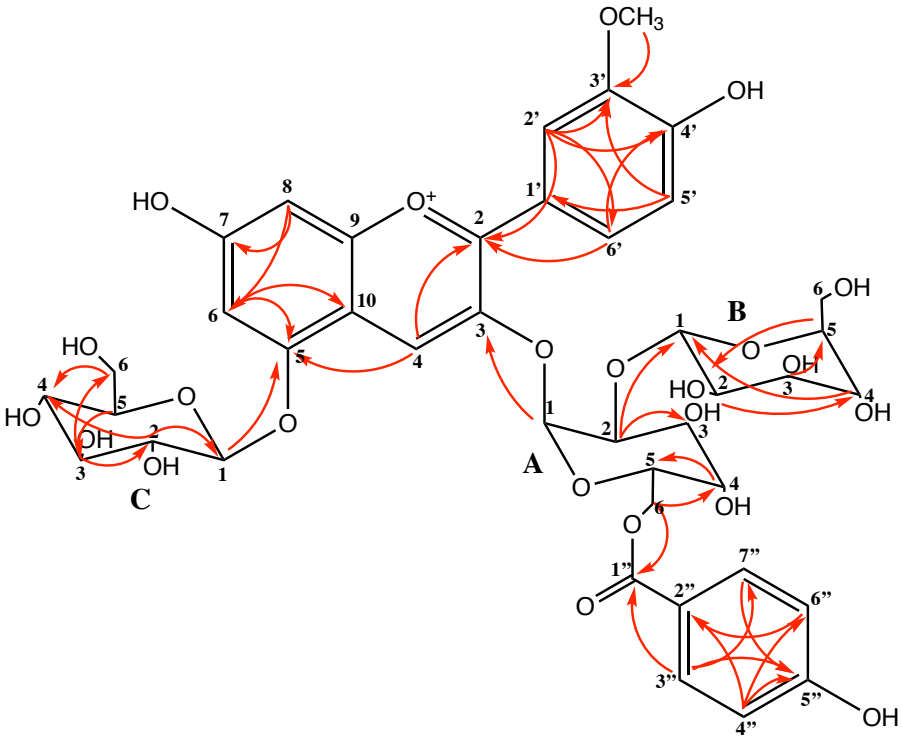

Figure 20. Structure of Peonidin-3-(6'-*p*-hydroxybenzoyl)-sophoroside-5-glucoside, and HMBC correlations represented by the red arrows.

3.1.2.2. Peonidin-3-(6'-p-hydroxybenzoyl-6''-caffeoyl)-sophoroside-5-glucoside

The ^{1}HNMR spectrum of Pn3HBCsoph5glc can be found in Figure 21. The attribution of the protons and carbons to the respective signals, was based on the previous assignments made for Pn3HBsoph5glc. In fact, the overlap of both ^{1}HNMR spectra, show similar chemical shifts, revealing similar structures. Five additional signals appear in Pn3HBCsoph5glc ^{1}HNMR spectrum, corresponding to the additional acyl group present in the structure (Figure 22).

The nomenclature followed the same system as in Pn3HBsoph5glc: the flavanic aromatic rings were classified as A and B (benzene rings) and C (furan ring). The glucoses linked at the furan ring were classified as glucose A and B (being A the directly linked) and the glucose linked to ring A was classified as glucose C. The acyl groups were classified by the own name.

Table 9 shows the attribution of protons and carbons and the correlations found in the bi-dimensional analysis (HMBC and HSQC) for Pn3HBCsoph5glc.

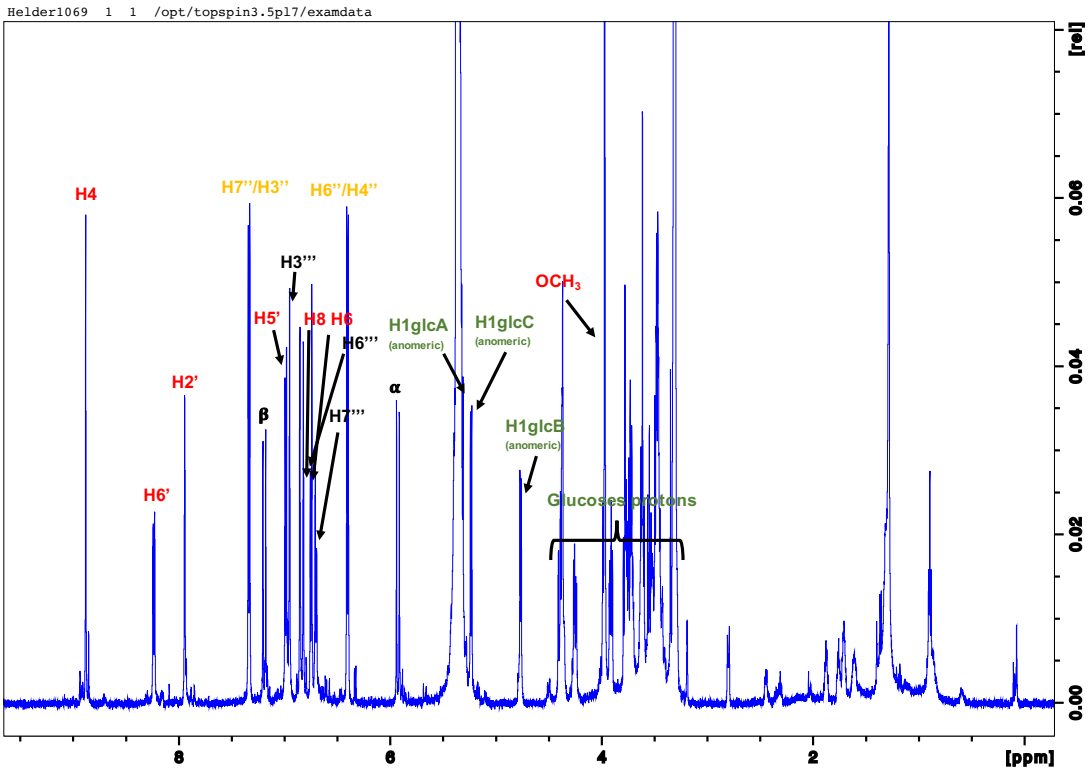

Figure 21. . [1]HNMR spectrum for Pn3HBsoph5glc with the respective proton attributions.

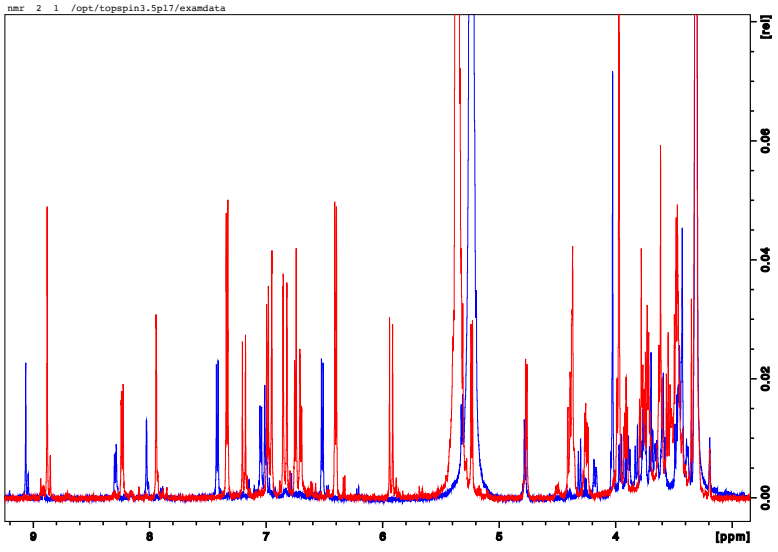

Figure 22. Overlap of the [1]HNMR spectra of Pn3HBsoph5glc (blue) and Pn3HBCsoph5glc (red). Five additional signals are present in the red spectrum, in the aromatic rings range.

Table 9. NMR attributions (^{1}H and ^{13}C) of Peonidin-3-(6'-*p*-hydroxybenzoyl-6''-caffeoyl)-sophoroside-5-glucoside, and the respective HSQC and HMBC correlations.

Moiety	Pos.	δ ^{1}H (ppm)	*J*, Hz	δ ^{13}C (ppm)	HSQC correlations	HMBC correlations
Flavanic Core	C2			163.3	-	H4; H2'; H6'
	C3			144.3	-	H1A; H4
	C4	8.88	s	138.44	H4	C2; C3; C5
	C5			155.5	-	H4
	C6	6.75	d (8.10)	104.2	H6	C10; H8
	C7			170.3	-	-
	C8	6.82		96.4	H8	C6; C5
	C9			157.2	-	-
	C10			126.0	-	H6
	C1'			119.3	-	-
	C2'	7.94	d (1.93)	113.47	H2'	C2; C3'; C4'
	C3'			148.3	-	H2'; H5'; OCH_3
	C4'			157.3	-	H2'; H6'
	C5'	6.99	d (8.76)	116.3	H5'	C3'
	C6'	8.23	dd (1.96;8.54)	128.73	H6'	C4'
	OCH_3	3.97	s	55.5	OCH_3	C3'
p-hydroxybenzoyl	C1''			166.0	-	H6A; H3''
	C2''			120.5	-	H4''; H6''
	C3''	7.33	d (8.66)	130.76	H3''	C5''; C7''; C1''; C6''
	C4''	6.40	d (8.66)	114.6	H4''	C2''; C6''; C5''; C3''
	C5''			162.0	-	H3''; H4''; H7''
	C6''	6.40	d (8.66)	114.6	H6''	C2''; C4''; C3''
	C7''	7.33	d (8.66)	130.76	H7''	C5''; C3''; C4''
caffeoyl	C1'''			168.7	-	H6B
	C2'''			113.9	-	Hβ; H7'''
	C3'''	6.95	d (1.74)	104.5	H3'''	Cα
	C4'''			148.6	-	-
	C5'''			148.5	-	H6'''
	C6'''	6.85	d (1.8)	113.8	H6'''	-
	C7'''	6.70	dd (1.5;8.3)	121.8	H7'''	H6''', C2'''
	Cα	7.19	d (15.77)	112.9	Hα	H3'''
	Cβ	5.93	d (15.77)	145.68	Hβ	C2'''
Glucose A	C1	5.33	d (7.10)	103.1	H1	C3; C3A; H4A
	C2	3.92	t (8.12)	82.5	H2	C3; H1B
	C3	3.72	d (8.78)	74.6	H3	C1B; H2A
	C4	3.79	m ?	75.8	H4	C3A; C1A
	C5	3.56	m ?	69.9	H5	C3A, H6A
	C6	4.27 4.43	d (13.57) dd (13.07;9.48)	62.6	H6	C5A; C1''
Glucose B	C1	4.78	d (6.87)	104.9	H1	C2A; H3A
	C2	3.48	m ?	76.2	H2	C4B; H5B
	C3	n.a	n.a	n.a	n.a.	-
	C4	3.46	m ?	74.5	H4	H2B; H6B
	C5	3.54	m ?	74.1	H5	C2B
	C6	4.39 3.73	m ? m ?	62.3	H6	C4B; C1'''
Glucose C	C1	5.25	d (7.70)	101.1	H1	C5; C3C
	C2	3.74	t (8.97)	73.2	H2	-
	C3	3.48	m ?	78.6	H3	C6C; H4C
	C4	3.49	m ?	69.9	H4	C3C, H6C
	C5	3.63	d (8.88)	76.9	H5	-
	C6	3.99 3.78	s ? d (8.54)	61.1	H6	C4C; H3C

The eleven signals present in the aromatic zone, characteristic from Peonidin core and *p*-hydroxybenzoyl were attributed as follows: proton signal of C4 (H4) at δ ^{1}H = 8.88 ppm (singlet); proton of C6 (H6) at δ ^{1}H = 6.75 ppm (duplet, *J* = 1.63 Hz); proton of C8 (H8) at δ ^{1}H = 6.82 ppm (duplet, *J* = 1.63 Hz); proton of C2' (H2') at δ ^{1}H = 7.94 ppm (duplet, *J* = 1.93 Hz); proton of C5' (H5') at δ ^{1}H = 6.99 ppm (duplet, *J* = 8.76 Hz); proton of C6' (H6') at δ ^{1}H = 8.23 ppm (double duplet, *J* = 1.96 and 8.54 Hz). For the *p*-hydroxybenzoyl moiety the signals were attributed as follows: protons of C3'' (H3'') and C7'' at δ ^{1}H = 7.33 ppm (duplet, *J* = 8.66 Hz); protons of C4'' (H4'') and C6'' (H6'') at δ ^{1}H = 6.40 ppm (duplet, *J* = 8.66 Hz). The HSQC analysis allowed to assign the respective chemical shift of the ^{13}CNMR spectrum (δ ^{13}C) to the carbons (Table 9), and the HMBC correlations permitted to assemble these blocks.

The five additional signals in the ^{1}HNMR signals were attributed to the other acyl group (caffeic acid) accordingly to the electronegative environment of each carbon. Therefore, the protons in the aromatic ring were attributed to the following signs: C3''' (H3''') to the signal at δ ^{1}H = 6.95 ppm (duplet, *J* = 1.80 Hz); C6''' (H6''') to the signal at δ ^{1}H = 6.85 ppm (duplet, *J* = 1.74 Hz) and C7''' to the signal at δ ^{1}H = 6.70 ppm (double duplet, *J* = 1.5 and 8.3 Hz). One can see that both δ ^{1}H and *J* values are very similar for the protons of C3''' and C6'''. This fact is easy understandable due to their position on the aromatic ring, being both *orto*- and *para*- relatively to the hydroxyl groups. The last two signals have *J* values typical from a double bound in a *trans*- conformation (*J* = 15.77 Hz), thus they should be α and β carbons of caffeic acid structure. Due to the proximity to the carboxylic group, the signal at δ ^{1}H = 7.19 ppm (duplet, *J* = 15.77 Hz) was attributed to carbon α and the signal at δ ^{1}H = 5.93 ppm (duplet, *J* = 15.77 Hz) was attributed to carbon β.

The HMBC correlations allowed the attribution of the anomeric protons of each glucose. The signal at δ ^{1}H = 5.33 ppm (duplet, *J* = 7.10 Hz) coupled with a signal at δ ^{13}C = 144.3 ppm (carbon C3), thus, it was assigned to the anomeric carbon of glucose A (C1) linked to the flavanic core at C3.

Glucose C anomeric carbon (C1) was assigned to the signal at δ ^{1}H = 5.25 ppm (duplet, *J* = 7.70 Hz), once it showed a correlation with carbon C5 (δ ^{13}C = 155.5 ppm) and the last anomeric carbon (C1) was attributed to glucose B, δ ^{1}H = 4.78 ppm (duplet, *J* = 6.87 Hz). Once again the coupling constants suggest a β conformation for the three glucoses. The additional correlations were analysed and the protons and carbons were attributed to the respective signals with exception of glucose B C3, that did not show any signals or

correlations, however, the assemble of each glucose was fully completed. Just as in the case of Pn3HBsoph5glc the correlation in HMBC of the signal δ ^{1}H = 4.78 ppm (H1 glucose B) with the signal δ ^{13}C = 82.5 ppm (C2 glucose A), is compatible with the existence of a bound between glucose A and B forming the sophoroside moiety through a β 1-2 linkage. The C6 protons and carbons of each glucose were attributed as follows: glucose A - δ ^{1}H = 4.27 and 4.43 ppm (duplet, *J* = 13.57 Hz and double duplet, *J* = 9.48 and 13.07), δ ^{13}C = 62.6 ppm; glucose B - δ ^{1}H = 4.39 and 3.73 ppm (multiple, multiple), δ ^{13}C = 62.3 ppm; glucose C - δ ^{1}H = 3.99 and 3.78 ppm (singlet and duplet, *J* = 8.54 Hz), δ ^{13}C = 61.1 ppm. At this point the structure is assembled at Peonidin and glucoses levels, however information is lacking about the position of each acyl group.

The ^{13}CNMR-APT spectrum shows two chemical shifts (δ ^{13}C) consistent with the existence of carboxylic moieties. This carboxylic functional groups belong to the acyl structures, and once the carbon at δ ^{13}C = 166.0 ppm was attributed to C1'' of *p*-hydroxybenzoyl moiety (due to the existence of a correlation between this signal and the signal of C3'' (δ ^{1}H = 7.33 ppm)), it was easy to assigned the C1''' carbon of the caffeoyl substituent (δ ^{13}C = 168.7 ppm).

Finally, HMBC showed correlations between C1'' and H6 from glucose A, and correlations between C1''' and H6 from glucose B, confirming the final structure of this compound has being acylated at glucose A with a hydroxybenzoic acid and at glucose B with a caffeic acid, both through the C6-OH of each glucose. All the HMBC interactions and the proposed structure can be found in Figure 23. Also, the spectra files of each analysis can be found in Attachment II.

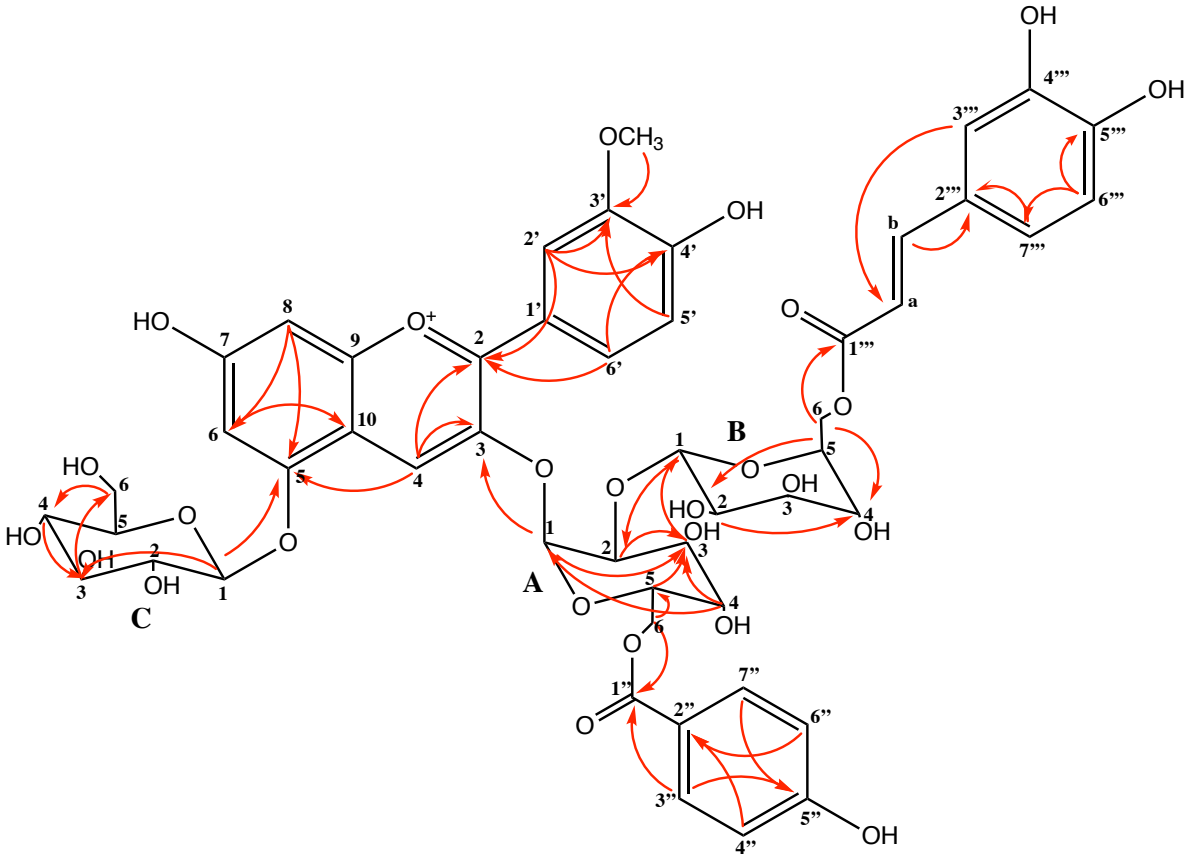

Figure 23. Structure of Peonidin-3-(6'-*p*-hydroxybenzoyl-6''-caffeoyl)-sophoroside-5-glucoside, and HMBC correlations represented by the red arrows.

3.2. Acid-Base Network of Purple-Fleshed Sweet Potato Anthocyanins

To better understand the results, some theoretical knowledge about the mathematical interpretation of the multi-state chemistry of flavylium compounds (such as anthocyanins) is necessary. For that, several theoretical statements are presented prior to the results. These information is not present on the Introduction section for a better flow in thesis organization and interpretation.

The determination of thermodynamic and kinetic constants is essential to understand the chemical equilibria that are typical from anthocyanins in solution.

As mentioned in Introduction, the structural transformations of natural and synthetic flavylium salts in acid and slightly acidic aqueous solutions can be distinguish at the equilibrium. The five species present are: (i) the flavylium cation, AH^+; (ii) the quinoidal base, *A*, obtained from the former by a proton transfer; (iii) the hemiketal, *B*, formed from

flavylium cation by a hydration reaction; (iv) the *cis*-chalcone, C_{cis}, obtained from the hemiketal through a tautomeric process; and (v) the *trans*-chalcone, C_{trans} resulting from the isomerization of the *cis*-chalcone.

In this section, the use of techniques such as *pH jumps* were used. These techniques refer to the perturbation of a system through the sudden modification of the pH value in solutions thermodynamically equilibrated. *Reverse* and *direct pH jumps* can be applied, if the objective is to reduce or increase the initial pH value, respectively.
The equilibria presented in Introduction for anthocyanins can be described by the following set of equations:
For acidic to moderately acidic pH values (1 < pH < 5), it follows:

$$AH^+ + H_2O \rightleftharpoons A + H_3O^+$$

Equation 1. Proton transfer reaction (K_a)

$$AH^+ + H_2O \rightleftharpoons B + H_3O^+$$

Equation 2. Hydration reaction (K_h)

$$B \rightleftharpoons C_{cis}$$

Equation 3. Tautomerization reaction (K_t)

$$C_{cis} \rightleftharpoons C_{trans}$$

Equation 4. Isomerization reaction (K_i)

For moderately acidic to moderately basic pH values (5 < pH <8), comes that:

$$AH^+ + H_2O \rightleftharpoons A^- + H_3O^+$$

Equation 5. Proton transfer reaction (K_{a2})

$$B + H_2O \rightleftharpoons B^- + H_3O^+$$

Equation 6. Proton transfer reaction (K_B^-)

$$C_{cis} + H_2O \rightleftharpoons {C_{cis}}^- + H_3O^+$$

Equation 7. Proton transfer reaction (K_{Ccis}^-)

$$C_{trans} + H_2O \rightleftharpoons {C_{trans}}^- + H_3O^+$$

Equation 8. Proton transfer reaction (K_{Ctrans}^{-})

A system at the thermodynamic equilibrium, represents a situation that starting from AH^+ as the predominant species, is achieved in a timescale ranging from a few minutes to days [80, 176, 192], depending on the substituents of the flavylium.

As previously shown [193], the molar fraction distribution of the acidic form can be obtained from:

$$\alpha' = \frac{[AH^+]}{C_0} = \frac{[H^+]}{[H^+] + K'_a}$$

Equation 9. Mathematical relationship between the molar fraction of AH^+ and the apparent acidic constant (K'_a)

Where K'_a is given by eqn. 10 and C_0 by eqn. 11.

$$K'_a = K_a + K_h(1 + K_t) + K_h K_t K_i$$

Equation 10. Mathematical relation between K'_a and the other equilibrium constants.

$$C_0 = [AH^+] + [A] + [B] + [C_{cis}] + [C_{trans}]$$

Equation 11. Representation of C_0 conjugating all the species present in equilibrium.

Inspection of eqn. 9 shows that its mathematical form is analogous to the molar fraction of a single acid-base equilibrium, therefore, each set of equations (1-4 and 5-8) can be simplified and described by one global equation.
For the more acidic pH values the equation can be defined as follows:

$$AH^+ + H_2O \rightleftharpoons CB + H_3O^+$$

Equation 12. Simplified acid-base equilibrium reaction for the flavylium cation at acidic pH values (K'_a)

The term *CB* comes for *Conjugated Base* and describe all the species with origin in the flavylium cation (AH^+). It concentration can be mathematically described by the sum of the concentrations of the respective involved species:

$$[CB] = [A] + [B] + [C_{cis}] + [C_{trans}]$$

Equation 13. Correlation between the concentration of conjugated base and the several anthocyanin forms present in equilibrium with the flavylium cation.

And the respective molar fraction can be given by:

$$\frac{[A]+[B]+[C_{cis}]+[C_{trans}]}{C_0}=\beta'=\frac{K'_a}{[H^+]+K'_a}=1-\alpha'$$

Equation 14. Correlation between the molar fraction of CB and the apparent acidic constant (K'_a)

For the set of equations of the reactions occurring at higher pH values, the logic is the same, and so, an apparent equilibrium constant can also be defined:

$$K''_a=\frac{K_{a2}K_a+K_B{-}K_{-h}+K_{C_{cis}}{-}K_{-t}K_{-h}+K_{C_{trans}}{-}K_{-h}K_{-i}K_{-t}}{K'_a}$$

Equation 15. Correlation between the apparent equilibrium constant and the other equilibrium constants for the species at higher pH values.

The molar fraction α', defined by eqn. 9, can be plotted against the different pH values of the experiments to give a sigmoid curve, analogous to a titration process. Thus, the apparent equilibrium constant can be obtained by spectrophotometric measurement (with or without *stopped flow* resources) [193]. The expression is given by:

$$Abs=A+A_0\frac{10^{(pK'_a-pH)}}{1+10^{(pK'_a-pH)}}$$

Equation 16. Expression for the fitting of the experimental values for determining K'_a.

where *A*bs is the pH-dependent absorbance (at any wavelength, but preferably at the absorption maximum of flavylium), *A,* the absorbance at the same wavelength, measured at a pH value sufficiently low to obtain exclusively flavylium cation, and A_0, the absorbance at a pH value high enough to have CB as the sole species present in solution.
For the determination of the equilibrium constants for the different species, the individual expressions of the molar fractions of each component of CB can be calculated using:

$$\frac{[A]}{C_0}=\frac{K_a}{K'_a}\beta';\ \frac{[B]}{C_0}=\frac{K_h}{K'_a}\beta';\ \frac{[C_{cis}]}{C_0}=\frac{K_hK_t}{K'_a}\beta';\ \frac{[C_{trans}]}{C_0}=\frac{K_hK_tK_i}{K'_a}\beta'$$

Equation 17. Expressions for the determination of the equilibrium constants of the species in equilibrium.

According to eqn. 17, calculation of the several equilibrium constants is thus reduced to the determination of the molar fraction distributions of each component of CB (at any pH value, but preferably when $\beta' = 1$) provided that K'_a is already known from eqn. 9 and 16.

As pointed out by Brouillard [41] in the case of natural anthocyanins and some synthetic flavylium salts, more than one hydroxyl substituent is available to form the quinoidal bases. In this case eqn. 1 must be written in more than one acid-base equilibrium. However, this situation does not introduce any additional problem to the calculation approach once the contribution of each hydroxyl group can be written as a single equation, where K_a will be the sum of the different hydroxyl K_a's (as the case of the expression for CB).
This "global" acidity constant can be then calculated from the set of eqn. 17, by performing *pH jumps* from pH < 1 to a value where pH $\gg$ pK_a.
At this pH the flavylium cation is totally converted into quinoidal base and the hydration process is generally slow enough to be followed by a conventional spectrophotometer. In addition, the absorption spectrum of quinoidal base is red shifted (batochromism) in comparison with those of the other species. This circumstance permits choice of a wavelength for which the quinoidal base is the sole absorbing species and, therefore, the absorbance taken immediately after the pH jump (i.e. after the proton transfer) A'_0, corresponds to the maximum of the concentration of this species.
At the end of the kinetic process (final equilibrium) the absorbance of the quinoidal base indicates its final concentration A'_1. The ratio A'_1/A'_0 is equal to the molar fraction distribution of the quinoidal base at the final equilibrium (when $\beta' = 1$).
The systematic use of *pH* and *temperature jumps* to study flavylium compounds (such as anthocyanins), still is the simplest technique to elucidate the kinetics of transformations of these compounds. In general, the compounds are stored at pH < 1 and pH jumps are carried out from this pH to higher values. Otherwise the system can be equilibrated at pH > 1 and concentrated acid added in order to obtain the back reaction that forms flavylium cation.
From the equilibrium reactions previously described, the proton-transfer reactions represent the first process that occurs upon a pH jump from pH < 1 to higher values is the transfer of a proton to water. This reaction is known to have velocities much faster than hydration, tautomerization and isomerization reactions and for this reason, conventional spectrophotometry, including stopped-flow analysis, is useless. This does not allow the determination of the rate constants, however if one have in account the following

considerations, it is possible to determine the equilibrium constants: the stopped-flow technique allows to make a spectrophotometric monitoring 10 ms after the mixture of the solutions (pH variation); the hydration reaction (of kinetics from subseconds to seconds), after 10 ms only occurred in the range of about 0.005% [172]; the proton-transfer reaction has already reached the equilibrium; the spectra registered at the beginning of the spectrophotometric monitoring reflect the equilibrium (in the proton-shift reactions) between AH^+, A and A^-, accordingly to the final values of the *pH jumps*.

To determine the remaining equilibrium constants (hydration and tautomerization) and to confirm the acidity constant, an apparent pseudo-equilibrium constant $K^{\wedge}_a$ can be used, whe isomerization is considerably slower than the other reactions. Three main processes with very different timescales can generally be observed for these natural compounds: (i) Proton transfer is the fastest and occurs in the microsecond timescale. (ii) Hydration (including tautomerization) takes place on a timescale from subseconds to several minutes (if pH is not much higher than pK_a). (iii) Isomerization occurs in, hours. Also, anthocyanins exhibit a high *cis-trans* isomerization barrier [173].
These flavylium multistates possessing a high *cis-trans* isomerization barrier have a great advantage once it allows to use $K^{\wedge}_a$ considering an intermediate (pseudo-equilibrium) state for which is possible to calculate pseudo-equilibrium constants. Generally, this state is considered at the end of the hydration/tautomerization reaction (once tautomerization is much more rapid than hydration). Thus, this constant can be determined despising the isomerization equilibrium.

$$K^{\wedge}_a = K_a + K_h(1 + K_t)$$

Equation 18. Definition of apparent pseudo-equilibrium constant ($K^{\wedge}_a$)

It has been demonstrated that α' can be related with the molar fractions of anthocyanins in equilibrium (eqn. 9 and eqn.17). In the case of the pseudo-equilibrium one can also determine an experimental $\alpha^{\wedge}$ value and the respective molar fractions. In the case of this study, the experimental $\alpha^{\wedge}$ value was obtained through *reverse pH jumps* with stopped-flow.

The correlation between the experimental $\alpha^{\wedge}$ and the molar fractions is demonstrated by the following set of equations:

$$\alpha\hat{} = \frac{[AH^+]}{C\hat{}_0} = \frac{[H^+]}{[H^+] + K\hat{}_a};\ \frac{[A]}{C\hat{}_0} = \frac{K_a}{K\hat{}_a}\beta\hat{};\ \frac{[B]}{C\hat{}_0} = \frac{K_h}{K\hat{}_a}\beta\hat{};$$

$$\frac{[C_{cis}]}{C\hat{}_0} = \frac{K_h K_t}{K\hat{}_a}\beta\hat{};\ \beta\hat{} = 1 - \alpha\hat{} = \frac{K\hat{}_a}{[H^+] + K\hat{}_a}$$

Equation 19. Relations between the pseudo-equilibrium constants and the molar fractions of the species present.

On the basis of the arguments presented above, the kinetic equations that account for the second intermediate state (pseudo-equilibrium attained prior to the *cis-trans* isomerization when the tautomerism is much more rapid than hydration) can be simplified to the following:

$$A + H^+ \underset{k_a}{\overset{k_{-a}[H^+]}{\rightleftharpoons}} AH^+ \underset{k_{-h}[H^+]}{\overset{k_h}{\rightleftharpoons}} (C_{cis} + B) + H^+$$

These processes can be conveniently studied by means of *pH jumps*. One must have in mind that the addition of buffers can give rise to large changes in the rates of the reactions, thus in this work the concentration of buffer was reduced to the minimum value necessary to consider the pH constant during the reactions.

This is very advantageous because it simplifies the resolution of the differential equations that result from the above reactional expression.

$$k_1 = k_a + k_{-a}[H^+]$$

$$k_2 = \frac{[H^+]}{[H^+] + K_a} k_h + \frac{k_{-h}[H^+]}{(1 + K_t)}$$

Equation 20. Expressions for the determination of the proton-transfer and hydration (plus tautomerization) kinetic constants, k_1 and k_2.

Where k_1 and k_2 are, respectively, the rate constants for the proton transfer and hydration plus tautomerization processes.

The pH dependence of eqn. 20 for the determination of hydration constant (k_2) can be simplified in two extreme cases:

(i) when $[H^+] \gg K_a$ the observed relaxation constant depends linearly on $[H^+]$

$$k_2 = k_h + (1 + K_t)k_{-h}[H^+]$$

Equation 21. Simplified expression for the determination of hydration (plus tautomerization) kinetic constant, when $[H^+] \gg K_a$.

(ii) when $[H^+] \ll K_a$ the contribution of the reverse reaction is very low the expression comes as

$$k_2 = \frac{k_h}{K_a}[H^+]$$

Equation 22. Simplified expression for the determination of hydration (plus tautomerization) kinetic constant, when $[H^+] \ll K_a$.

With these theoretical statements, the results can now be presented and easily understood.

Each anthocyanin will be presented in separate, just as in the case of the NMR analysis.

3.2.1. Peonidin-3-(6'-p-hydroxybenzoyl)-sophoroside-5-glucoside

Figure 24 shows the initial spectra obtained immediately after the mixture (< 10 ms) for the pH jumps from pH = 1 to higher pH values (from 1.30 to 10.06 with increments of about 0.5) using the stopped-flow technique. The observed variations in this time scale are assigned to the acid-base equilibria between AH^+, A and A^-. Considering the absorbance at 508 nm as a measure of AH^+ concentration and the absorbance at 600 nm as a measure of the anthocyanin quinoidal forms (A and A^-), one can graphically draw it values as a function of pH (Figure 25). Considering two consecutive deprotonation processes, one can apply a function $f(x) = Aobs(508nm) = \frac{[H^+]^2}{[H^+]^2+K_{a1}[H^+]+K_{a1}K_{a2}} A1(508nm) + \frac{K_{a1}[H^+]}{[H^+]^2+K_{a1}[H^+]+K_{a1}K_{a2}} A2(508nm) + \frac{K_{a1}K_{a2}}{[H^+]^2+K_{a1}[H^+]+K_{a1}K_{a2}} A3(508nm)$ for the values at 508 nm or $g(x) = Aobs(600nm) = \frac{[H^+]^2}{[H^+]^2+K_{a1}[H^+]+K_{a1}K_{a2}} A1(600nm) + \frac{K_{a1}[H^+]}{[H^+]^2+K_{a1}[H^+]+K_{a1}K_{a2}} A2(600nm) + \frac{K_{a1}K_{a2}}{[H^+]^2+K_{a1}[H^+]+K_{a1}K_{a2}} A3(600nm)$ for the values at 600 nm and adjust them (making a *fitting*) to the experimental values and thus determining pK_{a1} and pK_{a2} [193, 194]. The data was fitted to afford the pK_{a1} = 4.1 for the neutralization of the flavylium cation to give the quinoidal base (A) and pK_{a2} = 7.5 for the ionization of A to give A^-.

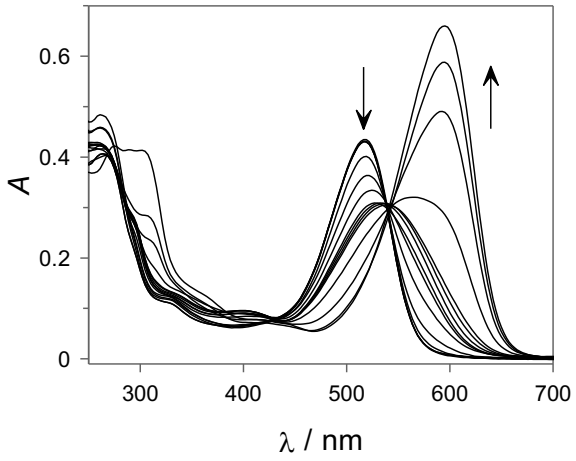

Figure 24. UV-Vis spectral variations observed for compound (6.4×10^{-5} M) immediately (10 ms) after a direct pH jump from pH = 1 to higher pH values.

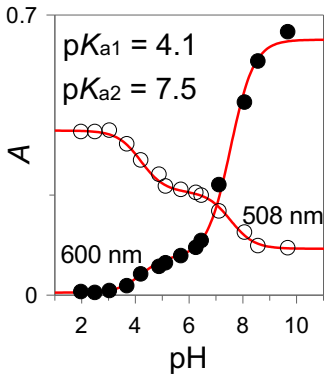

Figure 25. Absorbance values for 508 and 600 nm as a function of pH obtained by the *pH jumps* monitored by stopped-flow and respective *fittings*.

Knowing the values of the acidity constants, it is possible to determine the molar fractions (α or $\chi_{[AH^+]}$) for each equilibrium forms (Figure 26). Considering eqns 1 and 5, and the respective equilibrium constants, one can verify that the molar fractions of AH^+, A and A^- are given by the following expressions:

$$\chi_{[AH^+]} = \frac{[H^+]^2}{[H^+]^2 + K_{a1}[H^+] + K_{a1}K_{a2}};\ \chi_{[A]} = \frac{K_{a1}[H^+]}{[H^+]^2 + K_{a1}[H^+] + K_{a1}K_{a2}};\ \chi_{[A^-]} = \frac{K_{a1}K_{a2}}{[H^+]^2 + K_{a1}[H^+] + K_{a1}K_{a2}}$$

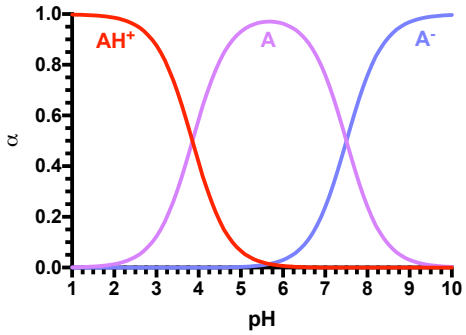

Figure 26. Molar fractions (α) of AH^+, *A* and A^-, determined from the fittings, for Pn3HBsoph5glc.

While the formation of the quinoidal base and ionized quinoidal base is very fast and cannot be monitored by the stopped flow technique, the hydration of the flavylium to give the hemiketal (*B*) and *cis*-chalcone (C_{cis}) occurs in the millisecond to seconds time scale, depending on the pH, and can be readily monitored. Figure 27 shows, as an example, the time-dependent UV-Vis spectroscopic variations observed after a direct pH-jump from pH = 1 to pH = 5.13.

At slightly acidic pH values the kinetics follow a pseudo-first order rate law that accounts for the rate-limiting hydration of the flavylium cation to give *B* followed by a faster, and therefore kinetically silent, ring-opening tautomerization of *B* to give C_{cis}.

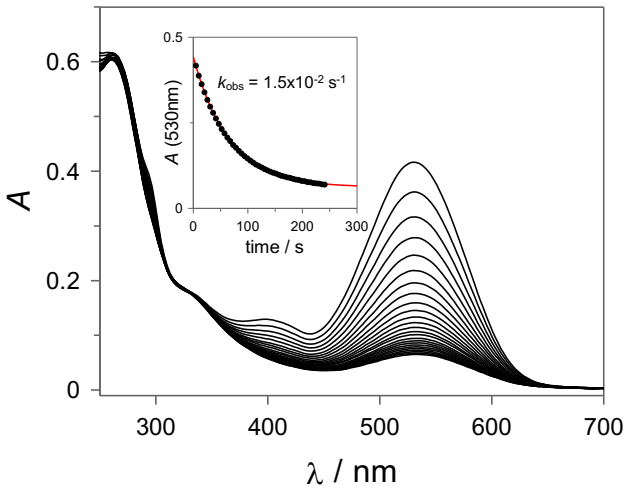

Figure 27. Time depend spectral changes observed after a direct pH jump from pH = 1 to pH = 5.13 monitored by UV-Vis spectroscopy. The *fitting* for the calculation of k_{obs} is also represented.

Representing the UV-Vis spectra of the compound at different pH values and after waiting enough time for the hydration and tautomerization reactions to reach the equilibrium allows the determination of the $pK^{\wedge}_a$ = 2.75 (Figure 28) corresponding to the pseudo-

equilibrium stablished between the flavylium cation and a conjugate base $CB^{\wedge}$ that is defined as $[CB^{\wedge}] = [A] + [B] + [C_{cis}]$. The relative mole fraction of B and Cc at the pseudo-equilibrium can be readily obtained from reverse pH-jump experiments as described above (Figure 29). The pre-exponential factor of the faster kinetic process (dehydration of *B*) is proportional to the mole fraction of *B* and the slowest one proportional to C_{cis}. Thus the ratio between these two pre-exponential factors is $K_t = [C_{cis}] / [B]$.

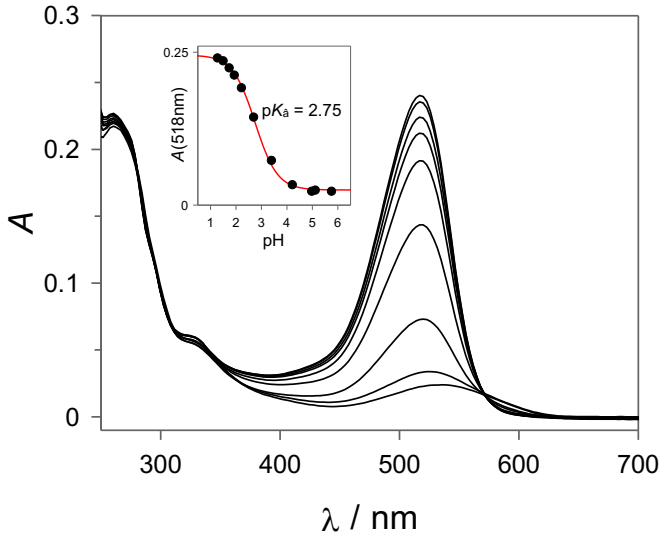

Figure 28. pH-dependent UV-Vis spectral variations observed for compound (3.35×10^{-5} M) at the pseudo-equilibrium.

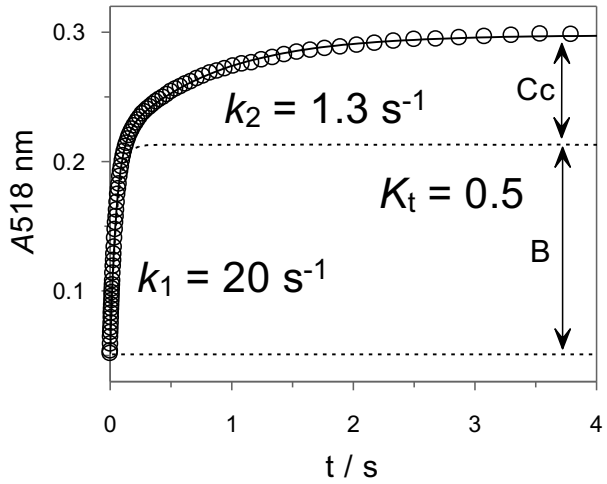

Figure 29. Kinetic trace observed for the regeneration of the flavylium cation after a reverse pH-jump from pH = 4.8 to pH = 0.94.

After the equilibration of A, B and Cc with AH^+, through a direct pH jump, a final process can take place in a much longer time scale due to the isomerization of Cc to give the *trans*-chalcone. This process can be monitored by following the absorbance variations at ca.

330-360 nm as in Figure 30. After storing the solutions used for the determination of the $pK^{\wedge}_a$ in dark to allow final equilibration (ca. 48 hours for the present compound), a pK'_a of 2.69 was determined (Figure 31).

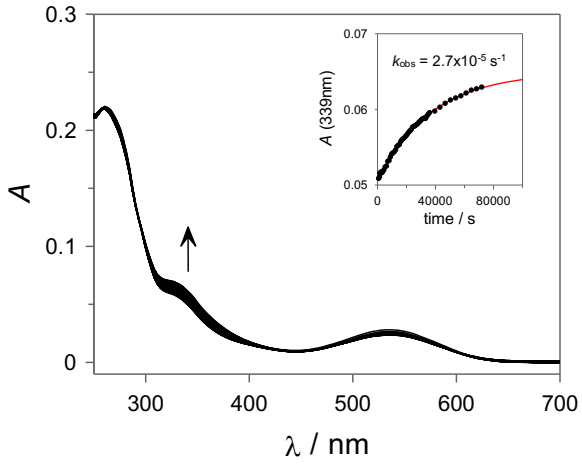

Figure 30. UV-Vis spectral variations observed for compound (3.35x10^{-5} M) after a direct pH jump from pH = 1 to pH = 5.12 followed during enough time to monitor the slow isomerization process

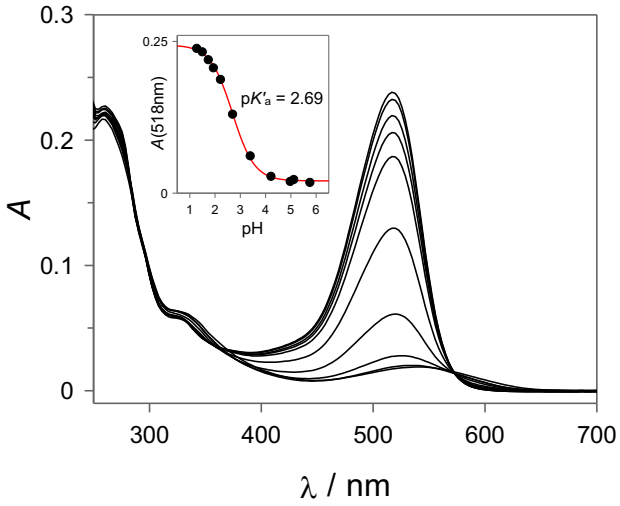

Figure 31. pH-dependent UV-Vis spectral variations observed for compound (3.35x10^{-5} M) at the equilibrium.

The small difference between $pK^{\wedge}_a$ and the pK'_a is compatible with a small fraction (13%) of Ct at the equilibrium.

This can be verified from a reversed pH jump of an equilibrated solution at pH 4.98 to pH = 0.86, Figure 32, followed in longer time scale (because the A, B, and Cc are converted in AH^+ in a time scale of seconds). A value of 12% was obtained for the Ct in good agreement with the value estimated from the p$K^{\wedge}_a$ and the pK'_a data.

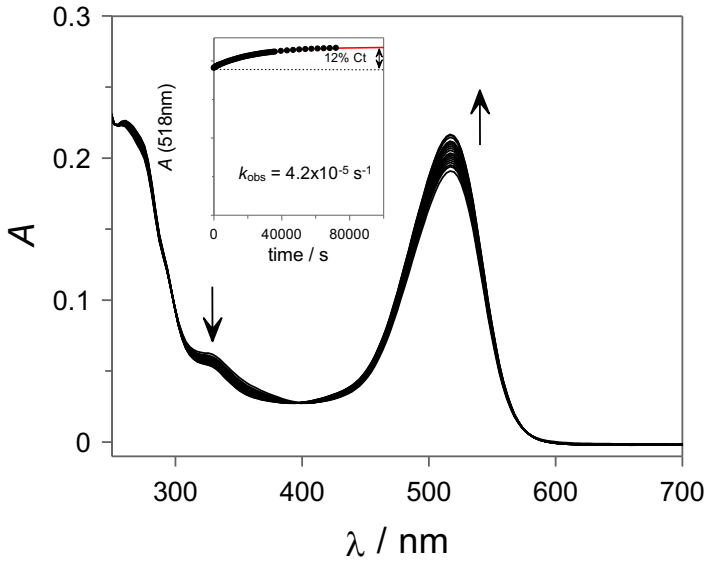

Figure 32. Regeneration of the flavylium cation after a reverse pH-jump from pH = 4.98 to pH = 0.86. In the time scale of the experiment the spectral variations correspond to the conversion of Ct at the equilibrium into flavylium cation.

The observed rate constants obtained from direct pH jumps to reach the pseudo-equilibrium are represented Figure 33. This kinetic data can be fitted with equation 23 to obtain the hydration kinetic parameters k_h and k_{-h}. During the fitting procedure K_t and K_a were kept constant and equal to the values previously determined, which allow the determination of the following values for k_h = 0.215 $s^{-1}$and k_{-h} = 170 $s^{-1}M^{-1}$ which leads to K_h = 1.26x10^{-3} M^{-1}. Also K_i was calculated with this values and using the molar fractions.

$$k_{obs} = \frac{[H^+]}{[H^+] + K_a} k_h + \frac{[H^+]}{1 + K_t} k_{-h}$$

Equation 23. Expression for the determination of k_h and k_{-h} (same as equation 20).

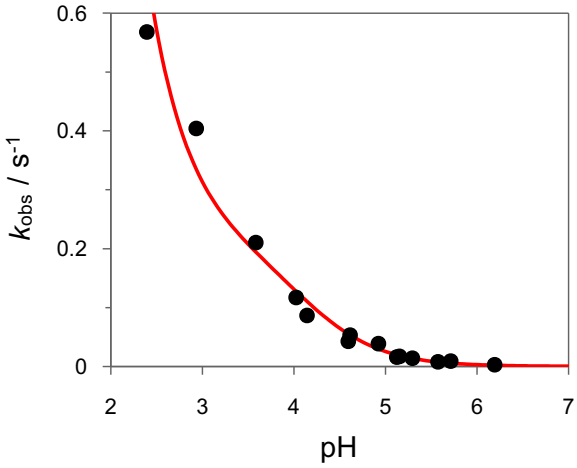

Figure 33. Observed rate constants to reach the pseudo-equilibrium obtained after direct pH jumps from pH 1 to higher pH values.

Figure 34 shows the spectral evolution after a direct pH jump (from pH 1 to 7.35) for a long time. One can see that the loss of absorbance at 585 nm is very slow, with a k_{obs} = 1.7x10^{-4} s^{-1}.

The calculated constants are summarized in Table 10.

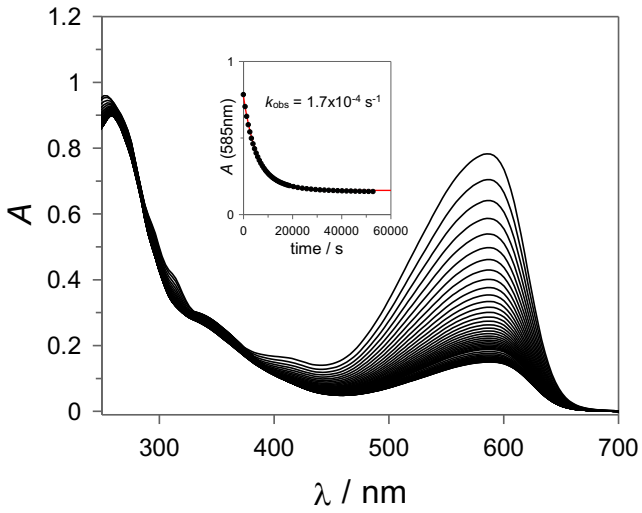

Figure 34. Time depend spectral changes observed for compound Pn3HBsoph5glc after a direct pH jump from pH = 1 to pH = 7.35 monitored by UV-Vis spectroscopy.

Table 10. Calculated constants for Peonidin-3-(6'-p-hydroxybenzoyl)-sophoroside-5-glucoside

Constants	pK'_a	p$K^{\wedge}_a$	pK_{a1}	pK_{a2}	K_t	K_h (M^{-1})	K_i	k_h (s^{-1})	k_{-h}($M^{-1}s^{-1}$)
Pn3HBsoph5glc	**2.69**	**2.75**	**4.1±0.1**	**7.5±0.1**	**0.5**	**1.26×10^{-3}**	**0.42**	**0.22**	**170**

3.2.2. Peonidin-3-(6'-p-hydroxybenzoyl-6''-caffeoyl)-sophoroside-5-glucoside

The same procedures were applied to this anthocyanin with the objective to compare with Pn3HBsoph5glc.

Figure 35 shows shows the initial spectra obtained immediately after the mixture for the pH jumps from pH = 1 to higher pH values (from 1.18 to 10.07 with increments of about 0.5) using the stopped-flow technique. The data was fitted as in Pn3HBsoph5glc to afford the pK_{a1} = 4.2 for the neutralization of the flavylium cation to give the quinoidal base (*A*) and pK_{a2} = 7.8 for the ionization of *A* to give A^-. The fitting is also demonstrated in Figure 35.

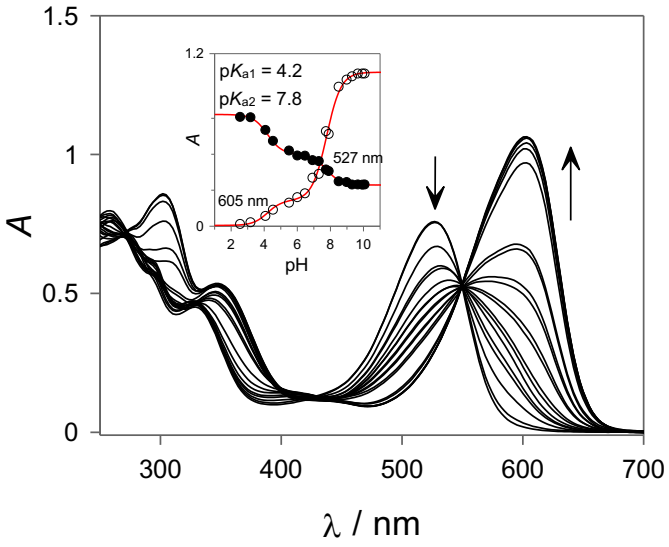

Figure 35. UV-Vis spectral variations observed for compound 1069 (6.83×10^{-5} M) immediately (10 ms) after a direct pH jump from pH = 1 to higher pH values and absorbance values for 527 and 605 nm as a function of pH obtained by the *pH jumps* monitored by stopped-flow and respective *fittings*.

The molar fractions for the proton-transfer equilibrium were obtained and represented in Figure 36. Figure 37a shows, as an example, the time-dependent UV-Vis spectroscopic variations observed after a direct pH-jump from pH = 1 to pH = 5.8, for the posterior calculation of $pK^{\wedge}_a$ represented in Figure 37b, corresponding to the pseudo-equilibrium stablished between the flavylium cation and a conjugate base $CB^{\wedge}$ that is defined as $[CB^{\wedge}] = [A] + [B] + [C_{cis}]$.

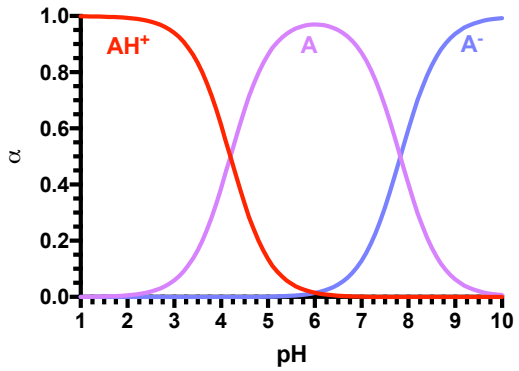

Figure 36. Molar fractions (α) of AH^+, *A* and A^-, determined from the fittings, for Pn3HBCsoph5glc.

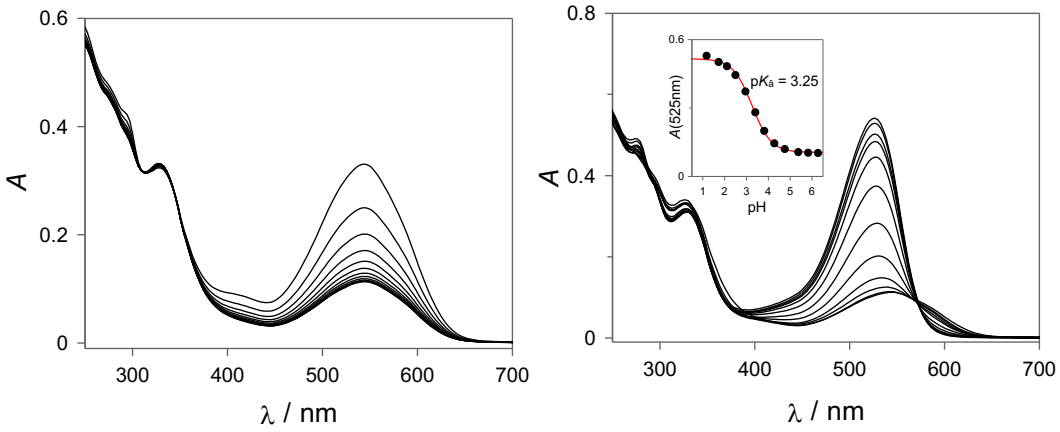

Figure 37. (a) -on the left- Time depend spectral changes observed after a direct pH jump from pH = 1 to pH = 5.8 monitored by UV-Vis spectroscopy. (b) –on the right- pH-dependent UV-Vis spectral variations observed for compound 1069 ($3.33x10^{-5}$ M) at the pseudo-equilibrium.

K_t was calculated from the molar fractions of *B* and C_{cis}, obtained from the *reverse pH jumps*, as in the case of Pn3HBsoph5glc, using the ratio $K_t = [C_{cis}] / [B]$ (Figure 38).

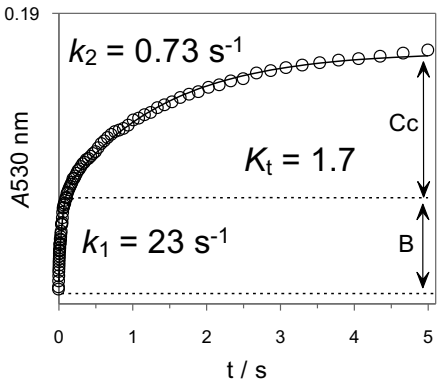

Figure 38. Kinetic trace observed for the regeneration of the flavylium cation after a reverse pH-jump from pH = 5.8 to pH = 1.2.

After storing the solutions used for the determination of the $pK^{\wedge}_a$ in dark to allow final equilibration (48 hours for the present compound, just as in the case of Pn3HBsoph5glc), a pK'_a of 3.15 was determined (Figure 39).

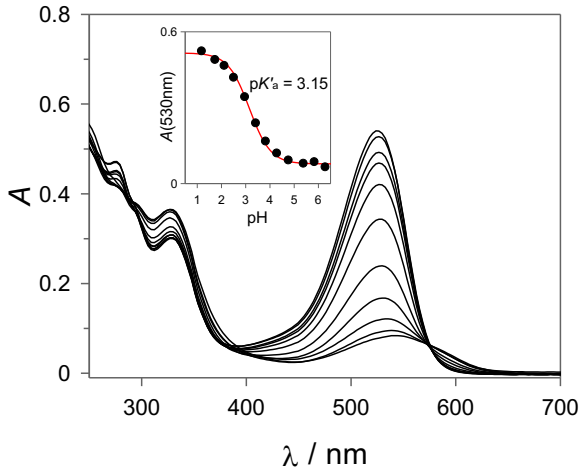

Figure 39. pH-dependent UV-Vis spectral variations observed for compound (3.33×10^{-5} M) at the equilibrium.

The process of isomerization cis-trans was monitored by following the absorbance variations at 330-360 nm and is present in Figure 40. Once again, the small difference between $pK^{\wedge}_a$ and the pK'_a is compatible with a small fraction (11%) of Ct at the equilibrium. This can be verified from a reversed pH jump of an equilibrated solution at pH 5.41 to pH = 0.61, Figure 40, followed in longer time scale (because the A, B, and Cc are converted in AH^+ in a time scale of seconds). A value of 13% was obtained for the Ct in good agreement with the value estimated from the p$K^{\wedge}_a$ and the pK'_a data.

From the fitting of the values of the observed rate constants to reach the pseudo-equilibrium (Figure 41), using the derived equation 23, it was possible to calculate following values for $k_h = 0.05\ s^{-1}$ and $k_{-h} = 330\ s^{-1}M^{-1}$ which leads to $K_h = 1.5 \times 10^{-4}\ M^{-1}$.

Table 11 shows the kinetic parameters determined for Peonidin-3-(6'-hydroxybenzoyl-6''-caffeoyl)-sophoroside-5-glucoside.

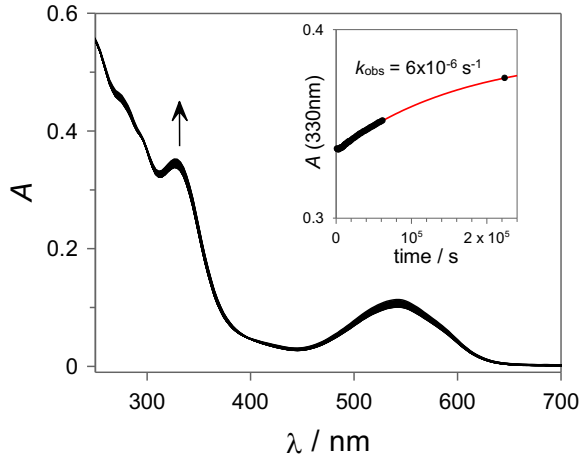

Figure 40. UV-Vis spectral variations observed for compound (3.33x10^{-5} M) after a direct pH jump from pH = 5.41 to pH = 0.61 followed during enough time to monitor the slow isomerization process.

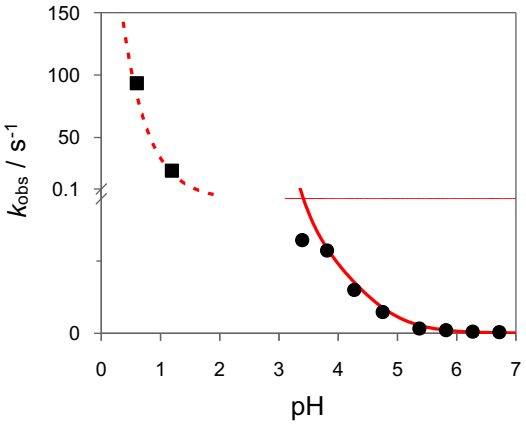

Figure 41. Observed rate constants to reach the pseudo-equilibrium obtained after direct pH jumps from pH 1 to higher pH values (circles) and after reverse pH jumps from pseudo-equilibrated solutions (pH = 5.8) to more acidic conditions (black circles, faster process see Figure 36).

Table 11. Calculated constants for Peonidin-3-(6'-p-hydroxybenzoyl-6''-caffeoyl)-sophoroside-5-glucoside

Constants	pK'_a	p$K\hat{}_a$	pK_{a1}	pK_{a2}	K_t	K_h (M^{-1})	K_i	k_h (s^{-1})	k_{-h}(M^{-1}s^{-1})
Pn3HBCsoph5glc	**3.15**	**3.25**	**4.2±0.1**	**7.8±0.1**	**1.7**	**1.5×10^{-4}**	**0.56**	**0.05**	**330**

As in the case of Pn3HBsoph5glc, the spectral evolution after a direct pH jump (from pH 1 to 7.35) for a long time was observed (Figure 42). The calculated k_{obs} was 1.2x10^{-4} s^{-1}.

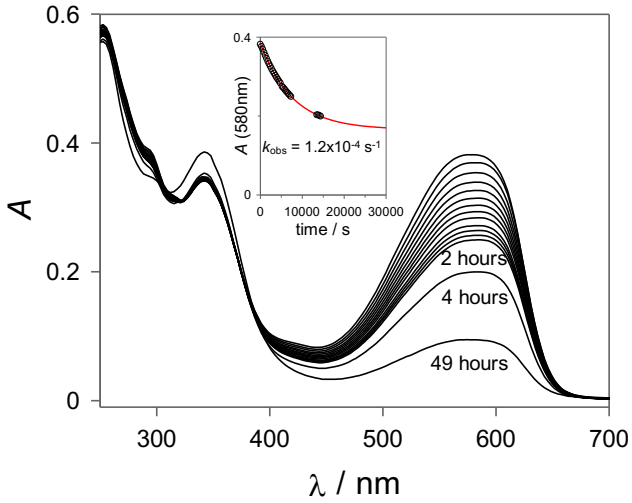

Figure 42. Time depend spectral changes observed for compound Pn3HBCsoph5glc after a direct pH jump from pH = 1 to pH = 7.35 monitored by UV-Vis spectroscopy.

Figure 43 shows the evolution of the colour at the different pH values after a long period of time, for Pn3HBCsoph5glc, as an example. Similar results were observed for Pn3HBsoph5glc.

One can see a loss of of the purple and blue colour (typical from *A* and A^- species) for higher pH values.

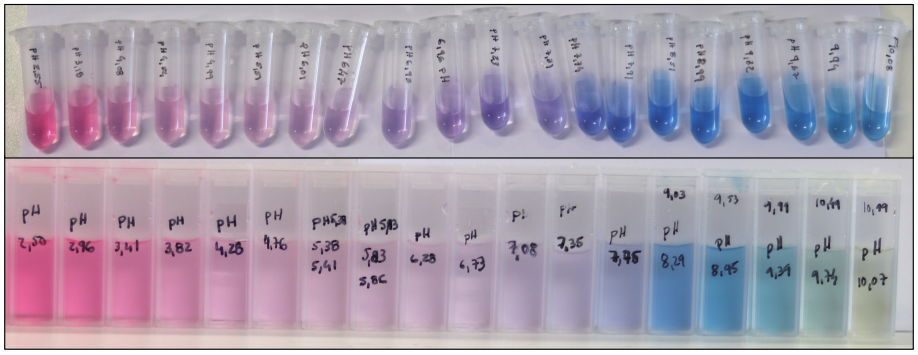

Figure 43. Color characteristics at each pH for Pn3HBCsoph5glc. At the top are represented the colors few seconds after the pH jumps mixtures and at the bottom the colors after 3 days. pH values from 2.50 to 10.08 are represented. The pictures are from different preparations but with the same concentration of pigment.

Looking to the stopped-flow experiments and inspecting the molar fractions of the several anthocyanin forms allows to choose the *pH jumps* spectra in which the final pH just have one specie (or predominantly one specie): under pH 2.0 (mainly AH^+) and above pH 8.0 (mainly A^-). This way, is possible to know the spectra in the visible region of the forms AH^+

e A^-. Choosing an adequate pH value (e.g. 6), one can obtain, by mathematical decomposition, the spectrum of *A*. For that, to the spectrum of pH 6, the spectra from AH^+ and A^- are subtracted multiplied by the respective molar fractions and the value is divided by the molar fraction of *A*.

The result is patent on Figure 44, for both anthocyanins. This result will be important for the next section as we shall see.

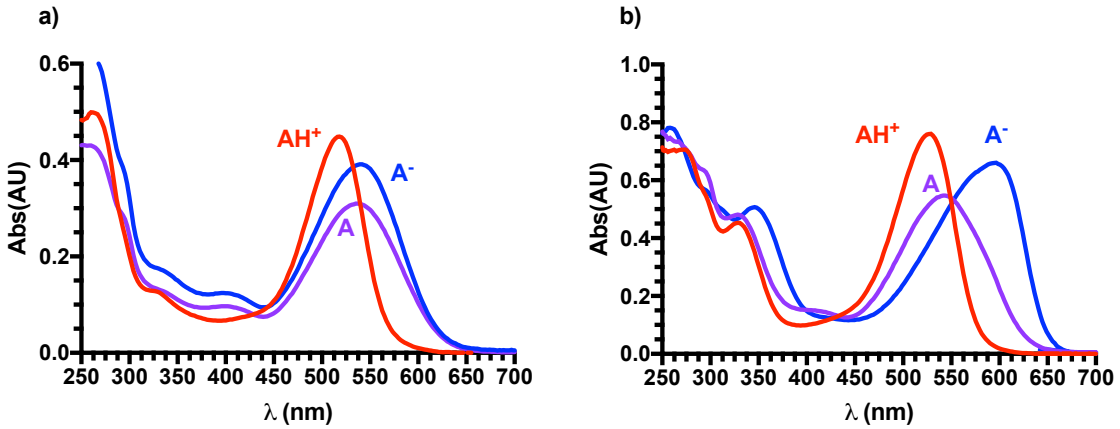

Figure 44. Spectra on the visible region of AH^+, *A* and A^-, for a) Pn3HBsoph5glc and b) Pn3HBCsoph5glc.

The molar distributions of AH^+, *A*, A^-, *B*, C_{cis} and C_{trans} were calculated for Pn3HBCsoph5glc. This was achieved by the derivation of the expressions for the calculation of the proton-transfer molar fractions (see above). However, for that, the value of pK''_a was necessary. This was achieved through a fitting of the spectra absorbance at the equilibrium for a wavelength of 610 nm as function of pH values. This allowed to achieve a pK''_a value of 8.6. The fitting and pK''_a determination was only possible for Pn3HBCsoph5glc, so the molar distributions of Pn3HBsoph5glc are not presented.

Considering eqn. 24 and Table 12, one can then calculate the molar distributions presented in Figure 45.

$$\chi_{[Z]} = \frac{n}{[H^+]^2 + K'_a[H^+] + K'_a K''_a}$$

Equation 24. Demonstrative equation for the definition of the molar fractions of anthocyanin forms at the equilibrium. n is detailed in table 12 for each form.

Table 12. Expressions for n, for the calculations of the molar fractions in equilibrium using the general expression in equation 24.

Z (equilibrium form)	n
AH^+	$[H^+]^2$
A	$K_{a1}[H^+]$
A^-	$K_{a1}K_{a2}$
B	$K_h[H^+]$
C_{cis}	$K_hK_t[H^+]$
C_{trans}	$K_hK_tK_i[H^+]$

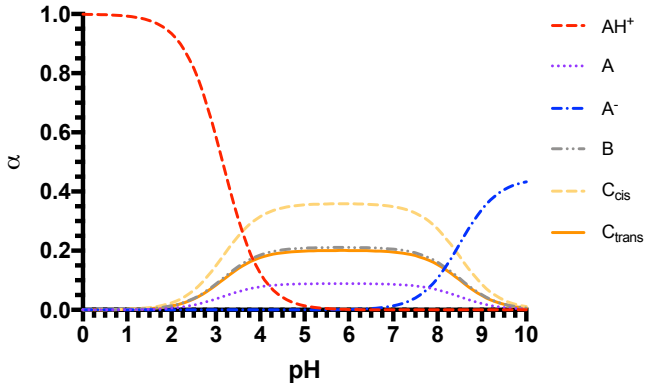

Figure 45. Representation of the molar fractions of the equilibrium forms of Pn3HBCsoph5glc.

3.3. Fluorescence Properties of Purple-Fleshed Sweet Potato Anthocyanins

The fluorescence properties of Pn3HBsoph5glc and Pn3HBCsoph5glc were evaluated. Fluorescence excitation spectra is intrinsically related to the absorbance spectra of the species, thus and accordingly to the previous spectra traced for AH^+, *A* and A^- species (Figure 44), the anthocyanins at pH 1, pH 5 and pH 8 were excited under an λ_{ex} wavelength corresponding to the maximum of absorbance of each species spectrum, and the corresponding emission spectrum was obtained. It is important to note that the solutions were not equilibrated, being the analysis made few seconds after the mixture to reach the final pH. Therefore, the equilibrium AH^+, *A*, A^- was selected as best suited to comparison. Pn3HBsoph5glc was excited at λ_{ex} = 522, 549 and 550 nm for pH 1, 5 and 8, respectively, while Pn3HBCsoph5glc was excited at λ_{ex} = 528, 545 and 605 nm for pH 1, 5 and 8. Figure 46 shows the emissions spectra for both anthocyanins.

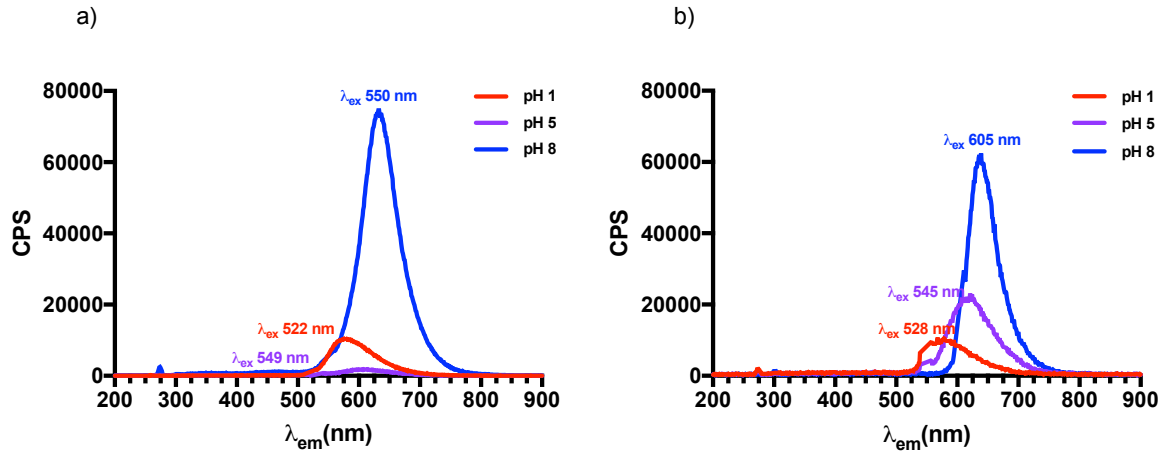

Figure 46. Emission spectra of a) Pn3HBsoph5glc and b) Pn3HBCsoph5glc at pH 1, pH 5 and pH 8. The λ_{ex} wavelengths were based on the maxima absorbance of the corresponding UV-Vis spectra presented in Figure 44. Both anthocyanins were tested at a concentration of 25 x 10^{-5} M to ensure an absorbance lower than 0.1.

The results show that the increase of the pH values of the anthocyanin solutions results, first, a delocalization of λ_{ex} wavelengths to higher values (accordant with the red shift mentioned in the previous section for the maxima absorbance), and second, in an increment of the fluorescence intensity (translated in higher CPS counts) with a concomitant bathochromic effect for λ_{em} maxima, as in the case of λ_{ex}. These observations are similar to both anthocyanins, although it is more evident in the case of Pn3HBsoph5glc. For pH 1, Pn3HBsoph5glc showed a λ_{em} maximum at 586 nm, while for pH 5 the λ_{em} maximum was at 602 nm and for pH 8 the λ_{em} maximum was at 631 nm. On the other hand, Pn3HBCsoph5glc showed λ_{em} maxima at 589 nm, 622 nm and 641 nm for pH 1, pH 5 and pH 8, respectively.

This suggest a slight bathochromic effect for Pn3HBCsoph5glc when compared to Pn3HBsoph5glc.

When looking to the intensity of each peak, one can see that Pn3HBsoph5glc reached intensities of 10128, 1904 and 74956 CPS for pH 1, pH 5 and pH 8 at the λ_{em} maxima, respectively, while Pn3HBCsoph5glc reached intensities at the λ_{em} maxima of 10501, 22555 and 62420 CPS, for pH 1, pH 5 and pH 8.

At pH 1, the intensities are similar, however at pH 8 Pn3HBsoph5glc seems to have better fluorescence. The most evident difference, though, lies on pH 5. For Pn3HBsoph5glc the intensity of the peak is almost residual when compared to the other λ_{em} maxima, while in Pn3HBCsoph5glc the peak at pH 5 is even higher than that for pH 1.

Once the species in solution at pH 8 showed the better fluorescence properties, the next experiments were performed having in account the $\lambda_{ex}/\lambda_{em}$ pair used for this solution.
Solutions of both anthocyanins were prepared at a range of pH values (from 1 to 11) and the excitation and emission spectra were traced.
For the excitation spectra of Pn3HBsoph5glc, a maximum λ_{em} wavelength of 630 nm was used and for the emission spectra, a maximum λ_{ex} wavelength of 550 nm. For the excitation spectra of Pn3HBCsoph5glc, a maximum λ_{em} wavelength of 640 nm was used and for the emission spectra, a maximum λ_{ex} wavelength of 610 nm.
Figure 47 shows the excitation and emission spectra of Pn3HBsoph5glc. Both λ_{ex} and λ_{em} intensity increases with the increase of the pH, at the maximum observed for the higher pH values. It is interesting, however, to notice that for the species at acidic pH, a different λ_{ex} maximum is observed (λ_{ex} 517 nm). It decreases with the increase of pH to give place to the new maximum at higher wavelengths (λ_{ex} 592 nm). One can notice that the intensity reaches it maximum value at pH 9 and then decreases for higher pH values. In what accounts for λ_{em}, only one peak is clearly visible (λ_{em} 640 nm). Similarly to λ_{ex} intensity, it reaches a maximum value at pH 9.
The complete spectrum from 400 to 800 nm is presented in Figure 48.

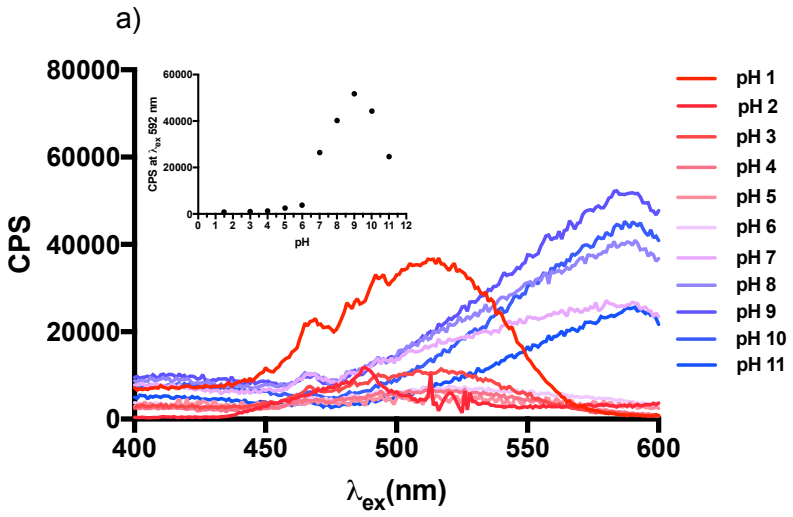

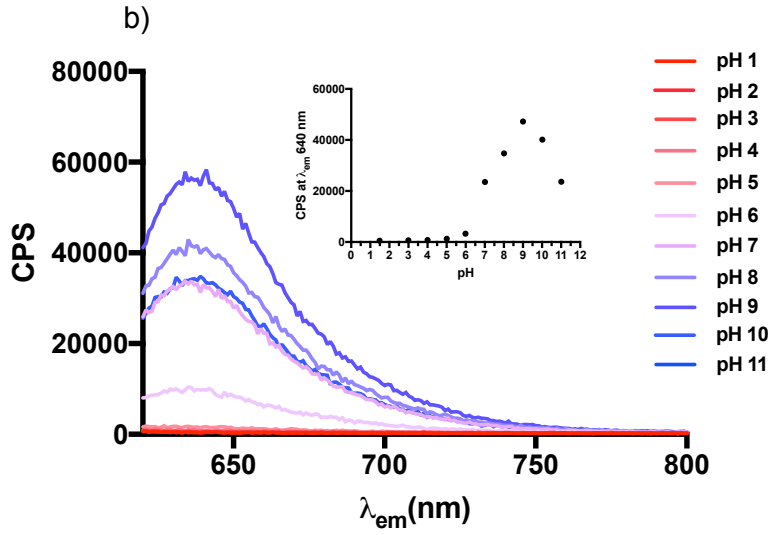

Figure 47. Excitation (a) and Emission (b) spectra of Pn3HBsoph5glc. The maximum CPS counts for each pH spectrum is also represented. For excitation these values are corresponding to an λ_{ex} of 592 nm and for emission to an λ_{em} of 640 nm.

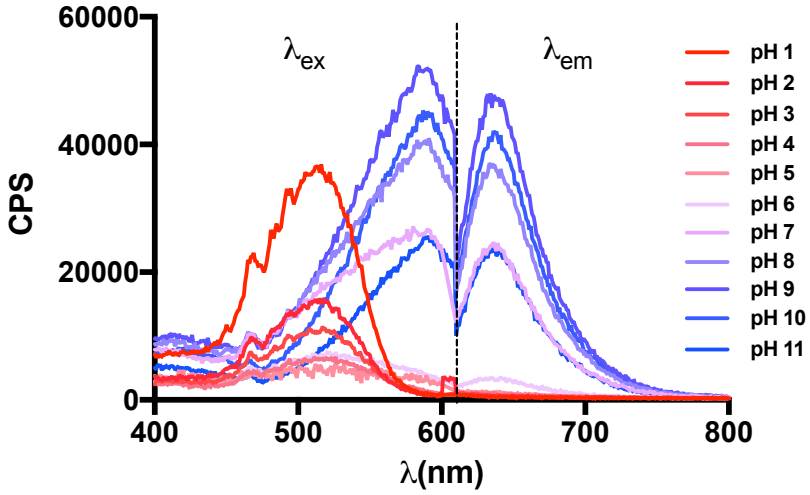

Figure 48. Complete *ex/em* spectrum for Pn3HBsoph5glc.

From Figure 48, one can see that the most interesting fluorescence properties are for pH values located between pH 7 and pH 11, with an optimum $\lambda_{ex}/\lambda_{em}$ of 592/640 nm.

In what accounts for Pn3HBCsoph5glc, the excitation and emission spectra presented an evident maximum for λ_{ex} and λ_{em} at only one specific wavelength (Figure 49). However, for λ_{ex}, at acidic pH values, a less evident peak appears (λ_{ex} 525 nm), such as in Pn3HBsoph5glc, but not as obvious. The peaks of λ_{ex} and λ_{em} were 599 nm and 645 nm, respectively. Figure 49 also shows the intensity of fluorescence at the different pH values

for the λ_{ex} and λ_{em} maxima. As in Pn3HBsoph5glc, the peaks reach their maximum at pH 9.

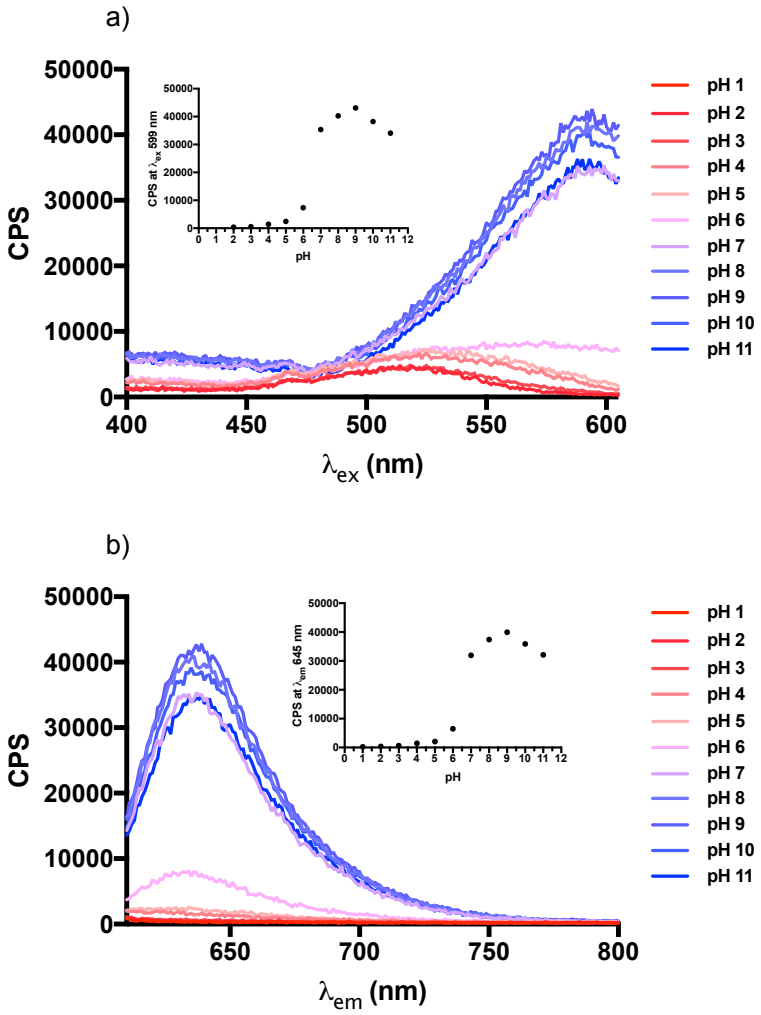

Figure 49. Excitation (a) and Emission (b) spectra of Pn3HBCsoph5glc. The maximum CPS counts for each pH spectrum is also represented, for excitation these values are corresponding to an λ_{ex} of 599 nm and for emission to an λ_{em} of 645 nm.

For Pn3BCsoph5glc, the most interesting fluorescence properties are for pH values located between pH 7 and pH 11, with an optimum $\lambda_{ex}/\lambda_{em}$ of 599/645 nm (Figure 50). Therefore, the results show similar fluorescence properties for both anthocyanins, especially at higher pH values. Having this in account, a global $\lambda_{ex}/\lambda_{em}$ pair for the studies in the next chapters was set at λ_{ex} 610 nm/ λ_{em} 640 nm.

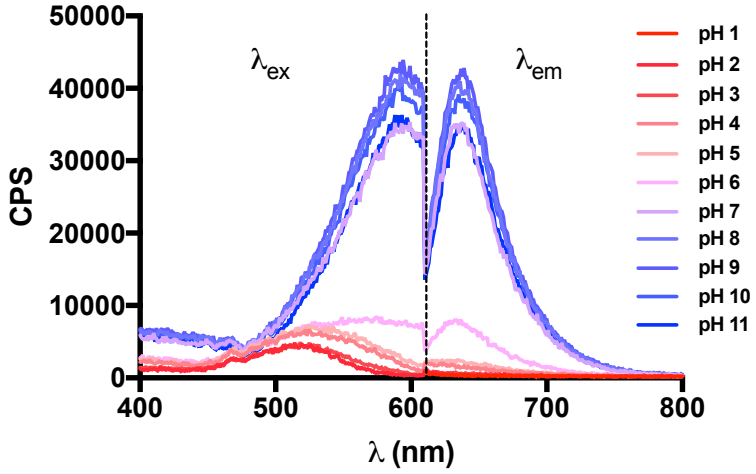

Figure 50. Complete *ex/em* spectrum for Pn3HBCsoph5glc.

4. DISCUSSION AND CONCLUSION

Anthocyanin-rich foods are, nowadays, at the center of nutrition and food science attentions. It is now clear, that anthocyanins are much more than just natural food colorants. They are present in several food sources, such as Purple Sweet Potato widely used at Asian countries, in the food industry.

The chromatographic analysis of the extract obtained from Purple-Fleshed Sweet Potato, revealed the presence of acylated anthocyanins derived from Peonidin and Cyanidin. These anthocyanins also had the particularity of being di-glucosilated at C3 and C5. In fact, potatoes are roots, and not fruits. Among all research on anthocyanin, the several reports over the years show that more complex anthocyanins are generally present in flowers and vegetables and the simple ones in fruits [24] .

Two anthocyanins from the extract were isolated, Peonidin-3-(6'-hydroxybenzoyl)-sophoroside-5-glucoside and Peonidin-3-(6'-hydroxybenzoyl-6''-caffeoyl)-sophoroside-5-glucoside. The LC-MS analysis suggested a standardized mechanism of fragmentation that involves bound break at the glucose moieties. These glucose moieties, in nature, help to increase the stability of the aglycone and the water stability. Therefore, the results can indirectly show the most vulnerable points of these compounds. From a nutritional point of view this is very important, and in fact, studies show that anthocyanins are hydrolyzed in the gut to anthocyanidins, either by gut flora or intestinal enzymes [154].

The NMR analysis further confirmed the structure of these two compounds. The signals revealed the key bounds necessary for confirmation: glucoses and acyl groups position. Therefore, the compounds are constituted by a sophoroside moiety at C3 with a single or a double acylation and by a glucoside at C5, both derived from Peonidin. Pn3HBCsoph5glc has an extra caffeic acid at the sophoroside group, while Pn3HBsoph5glc presents only the acylation with hydroxybenzoic acid.

Stability is a very important and challenging element when considering the impact of anthocyanins in areas as different as color industry or human metabolism. The common anthocyanins are known to present an instability in the presence of light, oxygen, most pH values and other physical and chemical parameters. Their stability is known to be highly linked to the distribution of the secondary forms of the anthocyanidin moiety, that are dependent on the pH [37, 42, 195].

A good way to understand how specific anthocyanins modulate themselves to achieve different structures, is to study the acid-base network of these compounds. Thus, the

knowledge about the thermodynamic and kinetic properties can give us very important clues about them.

The results revealed interesting differences between both anthocyanins. First, comparing the apparent acidity constants at equilibrium and pseudo-equilibrium, one can see that for pseudo-equilibrium they are higher. This is easy explained by inherent loss of color resulting from the equilibrium establishment. At the pseudo-equilibrium the color of the solution will be inevitable higher, thus resulting in a higher value for $pK\hat{}_a$. Pn3HBsoph5glc showed a lower value, when compared to Pn3HBCsoph5glc for the apparent acidity constants. This suggests that Pn3HBCsoph5glc has a higher capacity of red color maintenance for a broader range of pH values. This can be interesting for technological applications.

Looking at pK_{a1} and pK_{a2}, they are very similar for both. The network of the secondary structures is highly dependent on pH and in this case both anthocyanins seem to have similar molar fraction distribution, in terms of key pH values for structural change for the proton-transfer phenomena, and this can be seen in Figures 26 and 36. However, this does not mean that the molar fractions of the other species are the same, neither that the stability is the same.

The most interesting results lie on the remaining constants, representative of the other several chemical processes involved in these networks of structural changes: hydration, tautomerization and isomerization.

Beginning with hydration, one can see the kinetic parameters for the direct reaction (k_h) are about 4 times higher for Pn3HBsoph5glc, while the parameters for the reverse reaction (k_{-h}), are about 2 times higher for Pn3HBCsoph5glc. This results in a higher hydration constant for Pn3HBsoph5glc. Therefore, Pn3HBCsoph5glc is less susceptible to hydration than Pn3HBsoph5glc, which is in accordance with a maintenance of the red color for a broader range of pH values.

This difference may be due to the presence of the extra acyl group in the sophoroside moiety. Additional intramolecular arrangements may occur that can lead to a better shielding effect on the oxygen of the pyran ring.

Although it was only possible to calculate the molar fractions at the equilibrium for Pn3HBCsoph5glc, due to the impossibility of calculating pK''_a for Pn3HBsoph5glc, the tautomerization constant can give us some good clues about this. Once, K_t depends on the amounts of B and C_{cis}, one can predict which species will be present in higher amount after hydration reaches the maximum extension.

Therefore, if K_t is higher than 1, tautomerization is much faster than hydration, leading to a C_{cis} as the main form present. On the other hand, for K_t values lowerr than 1, hydration prevails and the amount of C_{cis} will be lower than *B*. Here, the results clearly show that the presence of the extra acyl group (the only difference between the two compounds), promotes the opening of the pyran ring.

The isomerization constants are similar and low, and in fact the results demonstrated that the amount of C_{trans} at the equilibrium was very low.

Now, comparing these results with previous results published for the precursor anthocyanin *Peonidin-3-O-glucoside* [178], one can find clear differences on thermodynamic and kinetic parameters.

Table 13 shows that parameters previously determined for *Peonidin-3-O-glucoside*.

Table 13. Reported constants for Peonidin-3-*O*-glucoside as stated in [178].

Constants	pK'_a	p$K\hat{}_a$	pK_{a1}	pK_{a2}	K_t	K_h (M^{-1})	K_i	k_h (s^{-1})	k_{-h}($M^{-1}s^{-1}$)
Pn3glc	**2.4**	**-**	**3.6±0.1**	**-**	**0.26**	**4.9×10^{-3}**	**-**	**0.19**	**39**

Overall, we can see that the thermodynamic constants, suggest higher delocalization of the equilibrium towards the hydration phenomena. Furthermore, the tautomerization constant suggest that C_{cis} amount is higher in the acylated anthocyanins, which may be the result of the acylation, as previously referred.

The fact that the acidity constants are higher and the hydration constant is lower in the PFSP anthocyanin, this can lead to a higher resistance due to less formation of the hemiketal forms. In fact, some authors defend that the hydration of anthocyanins is the most critical step for these compounds to experience degradation [24]. Also, several reports suggest that anthocyanins with acyl groups are relatively stable in neutral or weakly acidic aqueous solutions [38-40, 42, 196-198]. The intramolecular arrangements may be at the origin of this increased stability. The association between the anthocyanidin and the aromatic acyl groups possibly makes it difficult for a water molecule to attack the position 2 of the C ring (pyran ring) keeping the anthocyanidins in their stable forms (flavylium cations or quinoidal forms).

Making use of fluorescence properties of these compounds (when they have it) can be very advantageous in several science fields.

To evaluate the fluorescence characteristics of PFSP anthocyanins, the UV-Vis absorption spectra were used as a model to excite the anthocyanins. The results

suggested that overall, the forms present at higher pH values (mainly anionic charged forms) have the most interesting fluorescence properties. Almost 20 years ago, a study stated that anthocyanins presented several λ_{ex} and consequently different λ_{em} [181]. As it known, the fluorescence of compounds in solutions takes place from the lowest energetic equilibrium to the excited state S_1 and the fluorescence spectrum is shifted towards longer wavelength with respect to the $S_0 \rightarrow S_1$ absorption spectrum. In solutions containing one light-emitting compound, the fluorescence spectrum presents one band that does not depend on the wavelength of λ_{ex}, with respect to position. However, if exciting a solution at different λ_{ex} produces different λ_{em} in distinct spectral regions, this is indicative of the presence of several species in solution that have fluorescence characteristics. In compounds such as anthocyanins, this is very important to have in mind, once their structure is highly dependent on pH. Thus, using a range of pH values is essential when studying physical and chemical properties of anthocyanins.

Despite the fact that this approach is important, the separation of particular species within a solution is extremely hard for several reasons [199]. Overlapping of fluorescence spectra and common regions of excitation, are the most common phenomena presented as responsible for these difficulties.

All of these reasons led to the choice of using, at a first approach, 3 different λ_{ex} wavelengths, that allowed to visualize a higher fluorescence intensity for the species at the highest pH tested.

The results also suggest that the presence of the extra acyl group in Pn3HBCsoph5glc inhibits somehow the molecule to emit under the λ_{ex} used as in the case of Pn3HBsoph5glc. On the other hand, both Figure 46 and Figures 49 and 50, show that Pn3HBCsoph5glc has better fluorescence properties in the neutral to basic pH range. If we relate these findings with the results from the acid-base studies, a possible explanation may arise. Pn3HBCsoph5glc molar fraction distribution in equilibrium, revealed C_{cis} and B/B^- as the main anthocyanin form in this range of pH values. The fact that hydration is slow, gives rise to more colored species. Therefore, we can infer that the opening of the C ring to form *cis*-chalcone promotes more efficient light-emitting properties. In fact, the first reports about anthocyanins fluorescence, as supplementary method for the acid-base network studies, reported that chalcone species present fluorescence [184, 199]. However, the main responsible should be the quinoidal bases, once the excitation is out of the range of the chalcone absorbance.

The emission spectra of a young table red wine and a 3-year-old Port red wine, under excitation at 500 nm, produced fluorescence peaks of 595 nm and 625 nm, respectively, at acid pH values [185]. Red cabbage anthocyanins, showed peaks of absorption at 520 nm when excited at 410 nm in slightly acidic conditions [181]. Therefore, different anthocyanins will have different fluorescence characteristics, which can justify the fact that the results of this study differ from the previous.

Nevertheless, it is shown here that anthocyanins from PFSP (in particular Pn3HBsoph5glc and Pn3HBCsoph5glc), have clear fluorescence properties, and especially at higher pH values. This is extremely interesting and useful in biological researches using anthocyanins, and once this thesis main focus is the biochemistry of anthocyanins bioavailability, further studies will be performed on the next chapters making use of these findings. Although this study was performed with two isolated anthocyanins, further studies will be performed with the entire anthocyanin-rich extract, so, and as Pn3HBCsoph5glc is the main anthocyanin present in PFSP extract, a global $\lambda_{ex}/\lambda_{em}$ of 610/640 nm was defined as we shall see further.

CHAPTER II

IN VITRO GASTROINTESTINAL BIOAVAILABILITY OF ACYLATED ANTHOCYANINS FROM PURPLE-FLESHED SWEET POTATO

Synopsis

An extract from Purple-Fleshed Sweet Potato were used to evaluate some parameters on the bioavailability of the anthocyanins at the gastro-intestinal tract. Simulated oral, gastric and intestinal digestions were performed, for Purple-Fleshed Sweet Potato anthocyanins and for Red Wine anthocyanins, for comparison. Overall, the results suggest that anthocyanins are degraded only at the intestinal level. Also, Purple-Fleshed Sweet Potato anthocyanins showed higher resistance to digestions when compared to Red Wine anthocyanins.

The antiproliferative properties of the anthocyanins in Purple-Fleshed Sweet Potato were evaluated and no significant differences were found among the compounds tested. Therefore, the transepithelial transport of Purple-Fleshed Sweet Potato anthocyanins was assayed using two different cell lines, MKN-28 (gastric cavity) and Caco-2 (intestinal cavity). The effect of food matrix on the transport efficiency of these anthocyanins was also evaluated. At last, the intracellular localization of these anthocyanins was assayed, making use of the fluorescence characteristics determined in Chapter I. It was possible to see that anthocyanins localize inside cells, mainly accumulated in specific regions of both MKN-28 and Caco-2 cells.

This chapter resulted in the following paper: ***Oliveira, H.,*** *Perez-Gregório, R., de Freitas, V., Mateus, N., Fernandes, I. (2018) "Comparison of the in vitro gastrointestinal bioavailability of acylated and non-acylated anthocyanins: Purple-Fleshed Sweet Potato vs Red Wine.", Food Chemistry accepted manuscript, DOI: 10.1016/j.foodchem.2018.09.159*

1. INTRODUCTION

There has been a growing interest in vegetables and fruit consumption. People are becoming more aware of the potential health benefits of such foods, mainly due to their nutritional values. These contain bioactive compounds, such as phenolics, anthocyanins, carotenoids, and ascorbic acid, among others [200]. From the different groups, anthocyanins represent the main water soluble class of polyphenolic compounds responsible for the reddish to bluish colours of foods [36] and are associated with several health benefit properties . Anthocyanins are present in several fruits and vegetables such as grapes, berries, red cabbage, apples, radishes, and others [26]. From the different foods, Purple Fleshed Sweet Potato (PFSP) represents an interesting source of anthocyanins, due to the growing consumption of this root. In the past years, sweet potato cultivars with deep purple flesh were developed in Japan, Korea, New Zealand, and other countries to meet a growing demand in the health food markets [201]. Conversely to the anthocyanins commonly found in berries, PFSP anthocyanins primarily exist as di- or tri-glycosylated acyl forms mainly derived from cyanidin and peonidin anthocyanidins [186]. The acylation pattern with different phenolic acids makes PFSP anthocyanins unique and also provides advantages concerning pH, heat and light resistance, giving them an overall higher stability [186, 202]. Also, from a bio-nutritional perspective, these compounds have been associated to antioxidant and anti-proliferative activities [169]. Biological activities of specific acyl groups are still under evaluation; however, it is believed that additional free phenolic hydroxyl groups may raise bio-functionality of anthocyanins [186]. Thus, it becomes quite clear that acylated anthocyanins may be interesting targets as natural health therapeutics.

Although health benefits of compounds are always extensively studied, many authors still overlook a crucial point: their bioavailability. The effectiveness of the bioactivities of every compound highly depends on their bioavailability properties [203]. Anthocyanins are no exception and their bioavailability was usually considered low, with less than 1% being recovered after ingestion [18]. More recently, it has been shown that anthocyanins bioavailability may have been underestimated over the years, by only evaluating one site of absorption and by only searching the native forms [144]. Also, from a nutritional perspective, the food matrix environment will highly influence the rates of absorption of

the compounds and their bioavailability [204]. Thus, prior to their bioactive properties, one should assay and understand their bioavailability.

Therefore, the aim of this study was to evaluate the bioavailability of acylated anthocyanins from Purple Fleshed Sweet Potato. For that, the stability of these anthocyanins during gastrointestinal simulated digestions was evaluated and compared to the one observed for less complex anthocyanins from Red Wine. Also, the kinetics of absorption of these anthocyanins were evaluated on two cell models from the gastrointestinal tract, MKN-28 (stomach) and caco-2 (intestine) cells. Furthermore, the effects of food matrix components present in purple fleshed sweet potato (glucose, starch and proteins) on the absorption of the PFSP anthocyanins were assayed on both gastric and intestinal cell models.

2. MATERIALS AND METHODS

2.1. Anthocyanin Extraction and Characterization

Extraction of anthocyanins from Purple-Fleshed Sweet Potato (PFSP) was performed accordingly to previously described procedures [186] and in accordance with section 2.1. of Chapter I.

PFSP was cut in slices and the anthocyanins were extracted in 70 % ethanol with ultra-sound assistance for 1h. The obtained extract was centrifuged at 2,800 x *g* for 15 min to remove insoluble materials like fibers and starch. The resulting supernatant was filtered and phenolic acids were removed with LLE extraction (ethyl acetate/water, 1:1). The resulting extract was applied on a Amberlite XAD-7HP column resin. This is a non-ionic macroreticular resin usually made of a polystyrene-divinylbenzene copolymer matrix that adsorbs and releases ionic species through hydrophobic and polar interactions; usually under isocratic conditions.

Acidified water was used to remove proteins, sugars and other interfering materials and acidified methanol to recover anthocyanins.

The enriched anthocyanin fraction was then applied on a reverse phase silica C-18 column to remove any remaining sugars. The extract was freeze-dried and stored at -18º C until use.

Grape skin anthocyanins (*Vitis vinifera*) were used as a control comparison group throughout the study.

Anthocyanins were extracted with an aqueous solution of methanol (1:1) acidified with HCl, for 2 days at room temperature. The grape anthocyanin extract was filtered in a 50 µm nylon membrane and then purified by TSK Toyopearl gel column (250 x 16 mm i.d.) chromatography according to the procedure described previously [205]. Briefly, the column was initially eluted with water to remove sugars and other phenolic compounds present in the extract. Then, with a solution of acidified methanol, all the anthocyanins present in the grape extract were eluted and freeze-dried.

All the concentrations used during the study for Purple-Fleshed Sweet Potato extracts were based on a molar mass of 1041.49 g. mol^{-1} and for Red Wine extract on a molar mass of 500 g. mol^{-1}. The values were calculated according to the relative amount of each major anthocyanin identified by HPLC-MS-MS in each extract.

Peonidin-3-glucoside was isolated by preparative HPLC from the Red wine extract while Peonidin-3-(6'-hydroxybenzoyl)-sophoroside-5-glucoside and Peonidin-3-(6'-hydroxybenzoyl-6''-caffeoyl)-sophoroside-5-glucoside were isolated by the same method from Purple-Fleshed Sweet Potato.

2.2. Protein Extraction and Characterization

1 g of Purple Sweet Potato (PSP) or Purple-Fleshed Sweet Potato (PFSP) powder was dissolved in 40 mL of water and submitted to stirring for 10 min. The solution was centrifuged at 2800 x *g* for 10 min for starch elimination. The supernatant was collected and addition of ammonium sulphate was performed for protein precipitation. The saturated solution was centrifuged at 10000 x *g* for 15 min at 4ºC. The pellet was collected, suspended in water and submitted to dialysis (membrane cut-off 3.5 kDa). The dialysed sample was then freeze-dried. 1 g of dialysed extract was dissolved in 40 mL of water and the addition of 10 g of polyvinylpolypyrrolidone (PVPP) was performed. The sample was centrifuged for 15 min at 10000 x *g* and the supernatant was collected and freeze-dried. The sample was freeze-dried. Proteins were further purified by ion-exchange chromatography in DEAE-Sephadex A50 column. Equilibration was achieved using Tris.HCl 50 mM pH 8.0, and elution was performed with Tris.HCl 50 mM pH 5.0.

PFSP protein fraction was dried in a SpeedVac and dissolved in 25 µL of x electrophoresis sample buffer (50 mM Tris-HCl, pH 6.8, 12% v/v glycerol, 4% SDS, 2.5% v/v β-mercaptoethanol, and 0.01% bromophenol blue) and heated at 60 ºC for 1 h with shaking. The samples were then analysed by SDS-PAGE, using 15% acrylamide resolving gel. The stacking gel was 6% acrilamide. The cathode buffer was 0.1 M Tris and 0.1% SDS, and the anode buffer was 0.2 M Tris-HCl, pH 8.9. Electrophoresis was performed on a Bio-Rad MiniProtean Cell electrophoresis apparatus (Bio-Rad). After electrophoresis, the gels were stained with Imperial Protein Stain, a Coomassie R-250 dye-based reagent. The staining with Imperial Protein Stain was done according to the supplier's instructions. The discoloration step was done by washing the gels with water until the bands were visible. Molecular weights were estimated by comparison with the migration rates of standard proteins.

Tryptic digestion of the excised bands was performed according to the literature [206] and the resulting peptides were analysed by nano-LC-MS. After electrophoresis, the bands of

interest were excised from the gel and transferred to a rack. The gel pieces were washed twice with 25 mM ammonium bicarbonate/50% ACN, one time with 100% ACN, and after the washes, the gel pieces were dried in a SpeedVac (Thermo Savant). Twenty microliters of 10 µg/mL trypsin in 50 mM ammonium bicarbonate was added to the dried residue, and the samples were incubated overnight at 37 ºC. After the incubation, the extraction of tryptic peptides was performed by the addition of 10% formic acid/50% ACN three times, followed by lyophylization in a SpeedVac (Thermo Savant). Tryptic peptides were resuspended in 10 µL of a 50% ACN/0.1% formic acid solution.

The digested tryptic peptides were sequenced after chromatographic separation by tandem mass spectrometry. Chromatographic separation was performed into a UHPLC Dionex Ultimate TM 3000 RS LC nano system coupled to a LTQ-XL Orbitrap mass spectrometer equipped with an EASY-nano spray source (Thermo Scientific). The system was controlled by Chromeleon (UHPLC) and Xcalibur (LTQ-XL) software. The EASY-spray PepMap C18 (15 cm x 75 µm ID) 3 um 100 A (Thermo Scientific) was used in the LC separation process. A binary solvent mixture was used for the analysis; solvent A consisted of 0.2 % (v/v) formic acid (FA) aqueous solution, and solvent B was 0.2 % (v/v) FA in acetonitrile. The linear gradient for LC-MS/MS analysis ranged for 10 to 30 % B over 80 min followed by 55%B at 90min and the subsequent clean step at 0.3 µL/min. The injection volume was performed to achieve a final protein concentration of 2 µg into the system. LTQ operation parameters were set as follows: capillary temperature 250 ºC, source voltage 1.9 kV and tube lens 100 V.

Tandem mass spectrometry was carried out by data dependent acquisition mode (DDA) inducing the fragmentation of the three most intense multicharged peaks with a dynamic exclusion of 60 s and using isotope data dependence. Mass resolution was fixed at 60000 and it the monoisotopic precursor option was selected. The CID energy used was 35 V.

2.3. Simulated Gastrointestinal Digestions

For saliva interactions, the procedure was performed as previously described [207]. Whole saliva was collected from healthy non-smoking volunteers at 2 p.m. after at least 1 h without food or beverage ingestion. Then, it was treated with 10 % TFA solution (final concentration 0.1 %) and centrifuged at 8000 x *g* for 5 min. This study was conducted according to the Declaration of Helsinki and was approved by the Ethics Committee of Medical School of University of Porto (EK84032011). The HPLC profile of the whole saliva

was analyzed and in accordance with previous work [207]. After collection of saliva a mixture of 1:1 with anthocyanin extracts with or without matrix components was prepared. The reaction time was 10 min, followed by a centrifugation at 8000 x *g* for 5 min.

Simulated gastric and intestinal digestions procedures were in accordance with an international consensus with some modifications [208]. For gastric simulated digestions, 2 mL of anthocyanin extract with or without matrix components was mixed with 1.5 mL of simulated gastric fluid (SGF) electrolyte stock solution (as prepared in [208]): 320 μL porcine pepsin stock solution of 25 000 $U.mL^{-1}$ made up in SGF electrolyte stock solution pepsin from porcine gastric mucosa 674 $U.mg^{-1}$ protein, Sigma), 1 μL of 0.3 M $CaCl_2$, 40 μL of 1 M HCl to reach pH 3.0 and 139 μL of water. The digestion time was 3 h at 37ºC with regular pH checking and adjustment. For simulated intestinal digestions, 2 mL of the previous simulated gastric digestions were mixed with 1.1 mL of simulated intestinal fluid (SIF) electrolyte stock solution (as prepared in [208]), 500 μL of a pancreatin solution 800 $U.mL^{-1}$ made up in SIF electrolyte stock solution based on trypsin activity (pancreatin from porcine pancreas, Sigma), 4 μL of 0.3 M $CaCl_2$, 15 μL of 1 M NaOH to reach pH 7.0 and 381 μL of water.

All the controls were made in water to match the respective dilutions. Matrix components solutions were done as follows: for purple fleshed sweet potato samples starch at 6.0 $mg.mL^{-1}$, glucose at 60 mM and Purple fleshed Sweet Potato protein extract at 50 μM (of Sporamin B equivalents) were added. For red wine samples: 60 mM of glucose and 12% of ethanol were added. The samples were acidified with HCl 6 M to a final concentration of 1 % and frozen at -18 ºC until HPLC analysis.

2.4. Cell Cultures

All the cell manipulations were performed in a biological chamber with vertical laminar flux and graded level 2A of biosafety (ADS Laminaire).

Human cancer cell line from stomach, MKN-28, was gently given by Professor Celso Reis from IPATIMUP (Porto, Portugal) being initially acquired to *Cell Bank, Riken BioResource Center* (JCRB0253). It was grown as monolayers and maintained at 37 °C in an atmosphere of 5% CO_2 and 90 % relative humidity. For routine maintenance, cells were cultured in 22.1 cm^2 tissue culture dishes as monolayers and maintained in RPMI 1640 AQmedia (Sigma, Germany), supplemented with 10 % fetal bovine serum (FBS)

(Biowhittaker, Lonza, Belgium) and 1 % of antibiotic/antimycotic solution (100 units/mL of penicillin, 100 mg/mL of streptomycin, and 0.25 mg/mL of amphotericin B) (Sigma).
Human cancer cell line from intestine, Caco-2, was acquired to American Type Culture Collection (ATCC37-HTB). They were grown and harvested in the same conditions and maintained in MEME (*Minimum Essential Medium Eagle*) (Sigma-aldrich, Germany), supplemented with 15 % fetal bovine serum (FBS) (Biowhittaker, Lonza, Belgium) and 1 % of antibiotic/antimycotic solution (100 units/mL of penicilin, 100 mg/mL of streptomycin, and 0.25 mg/mL of amphotericin B) (Sigma Aldrich, Spain). Cells were maintained in exponential growth and for this purpose a subculture was performed with harvested cells by trypsinization (0.25 %, w/v, trypsin−$EDTA_4$−Na) once a week.
For maintenance of cellular division, after removal of culture medium, the cells were washed with Phosphate Buffer Saline (PBS), and detached from the culture flask with 0.25 %, w/v, trypsin−$EDTA_4$−Na. After that, a dilution (1:3) was performed and the cells were seeded in new culture flasks with 21 cm^2 of growing area (Corning Costar).

2.5. Antiproliferative Experiments - Sulforhodamine B assay

Solutions of 200 mM of PFSP extract (based on the malor mass of 1041.49 g. mol^{-1}) and each compound were prepared in water. These stock solutions were conserved at -18ºC, allowing to obtain a uniform sampling in the various tests performed. Before each experiment the stock solutions were heated to room temperature and sonicated for 5 minutes in order to obtain an optimum solubilisation of the compounds.
Before each experiment the appropriate dilutions of the samples were performed. The effect of the compounds on the growth of each human cancer cell line was evaluated accordingly to the adopted method by NCI (Bethesda, USA), in the program *"In vitro Anticancer Drug Discovery Screen"*. It is a micromethod that utilizes 96-well plates and evaluates the effect compounds on exponential growing cells after a continue exposition of 48h, through the quantification of the cellular protein content with the protein dye Sulforhodamine B (SRB).
This method allows the simultaneous evaluation of two compounds in three cell lines, however in this case, only one line at a time was used. In Figure 51, a schematic representation of the plate distribution of the compounds on the different concentrations is presented.

Briefly, each cell line was seeded in the 96-well plates (100 µL/well) at a density that ensured an exponential growth ($1.5\times10^5\ viable\ cells/mL$), in complete culture medium and incubated for 24h at 37ºC prior to the addition of the compounds. It was tested a concentration range for each compound (100 µL/well), which were prepared by serial dilutions (1:2) in complete culture medium. In each experiment the compounds were tested with 6 replicates. Columns 6 and 7 worked as growth controls for each cell line. For each experimental plate, an identical plate was prepared and named T0 (time 0), that allowed the determination of the protein content at the time of compounds addition. T0 plate was fixed at the time of compounds addition with a solution of 50% tricloroacetic acid (TCA) for 60 minutes at 4ºC. After 48h of exposure to the compounds, the cells were fixed with the solution of 50 % TCA at 4ºC followed by a washing step with water. After totally dried, the cells were stained with a SRB solution (0.4% in 1% of glacial acetic acid) (50 µL/well) for 30 minutes, at room temperature. The excess of SRB was removed by washing the plates with a solution of 1% acetic acid. The SRB was then solubilized with Tris-HCl buffer (1 M in water, pH 8.0) (100 µL/well). Finally, the plates absorbance was read at 492 nm with a plate spectrophotometer (Bio-tex Instruments Inc., Powerwave XS, USA).

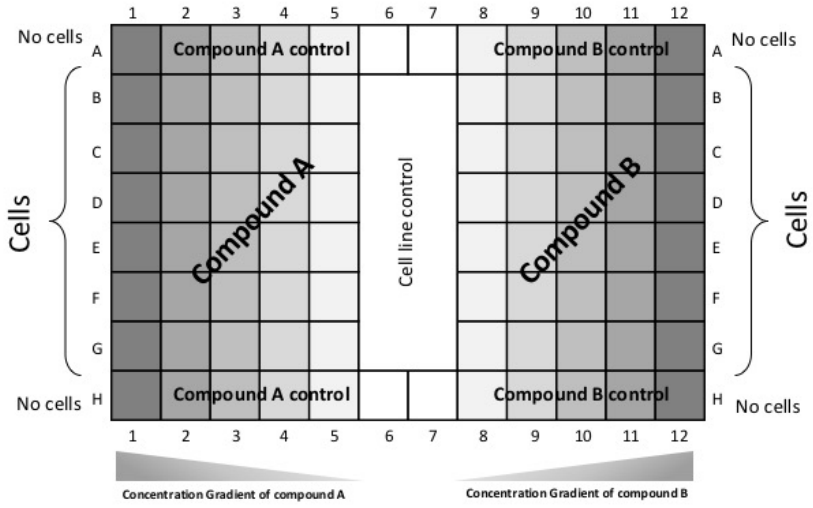

Figure 51. Schematic representation of the 96-well plate showing the distribution of the cell lines and the 5 sequenced concentrations of compounds A and B. Also, the controls of cell lines (no exposition to compounds) and the controls of the compounds (no cells) are represented.

2.6. Transport Experiments

MKN-28 and Caco-2 cells were plated on 12-well *Transwell*® polycarbonate permeable inserts, 12 mm diameter, 0.4 µm pore size tissue culture inserts (Corning Costar, Corning, NY) at 75 % confluence (Figure 52). Cells were cultured during 7 days (MKN-28) or 21 days (Caco-2) at 37 °C in an atmosphere of 5 % CO_2 and the medium was changed every two days.

The resistance across the monolayer was measured using MILLICELL-ERS epithelial voltammeter (Millipore Co., Bedford, MA) with "chopstick" electrodes. Filter-grown cells were adapted to 37 ºC temperature to allow for more standardized TEER measurements. The TEER was measured before the experiments to monitor cell layer confluence and the integrity of the tight junctions. The TEER of the cell layers was calculated according to the equation:

$$TEER(\Omega.cm^2) = R\ x\ A$$

Where *R* is the resistance measured and *A* is the surface area of filter (1.12 cm^2). Experiments were conducted only in MKN-28 cell monolayers that showed a TEER > 150 $\Omega.cm^2$, and in Caco-2 cell monolayers that showed a TEER > 250 $\Omega.cm^2$ (determined at 37 ºC).

In transport experiments Hanks medium (HBSS) at pH 7.4 was the main component of the basolateral medium. A pH of 5.0 was obtained by adding solid 2-(N-morpholino) ethane sulphonic acid (MES) to give a concentration of 25 mM and then adjusting the pH with 5 M HCl. The pH values of the above solutions were stable in the absence of cells.

Transepithelial transport experiments were performed using a similar procedure from the one described elsewhere [209].

After the grown of cells (7 or 21 days) to reach a monolayer, the medium was removed and cells were washed with HBSS: pH 7.4 at the basolateral side and with HBSS pH 5.0 or 7.4 (MKN-28 or caco-2, respectively) at the apical side. For caco-2 cells, 24h prior to the experiments, the medium was replaced by fresh medium without foetal bovine serum (FBS).

The anthocyanin solutions prepared in HBSS pH 5.0 or pH 7.4 at different concentrations were added to the apical side of the cells and HBSS containing 2 % FBS free of polyphenols was added to the basolateral compartment. Transepithelial transport was

followed as a function of time, at 37 ºC. Samples were taken from the basolateral side and replaced by fresh medium at 30', 60' 120' minutes for caco-2 cells and 30', 60' 120' and 180' minutes for MKN-28 cells. The samples (150 µL) were acidified with HCl 6 M to a final concentration of 1 % and frozen at -18 ºC until HPLC analysis.

The transport efficiency was calculated accordingly to the following equation:

$$Transport\ Efficiency\ (\%) = \frac{Basolateral\ concentration\ at\ a\ given\ time}{Apical\ concentration\ at\ time\ 0} \times 100$$

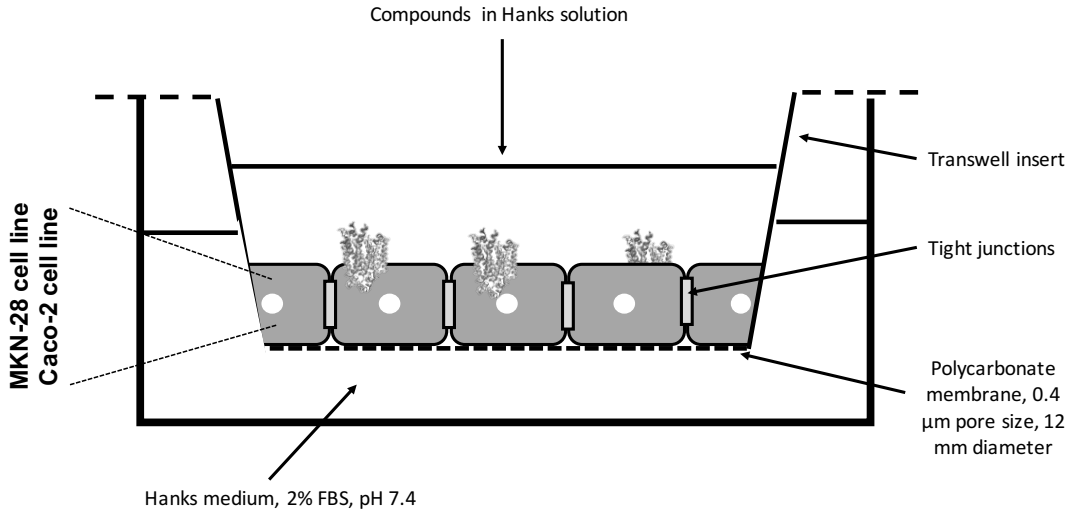

Figure 52. Schematic representation of a Transwell well of a 12-well plate containing an insert with a polycarbonate membrane, 0.4 µm of pore size, 12 mm diameter, showing the localization of cells monolayer. Also, the apical and basolateral sides are represented containing the respective mediums.

2.7. Laser Confocal Scanning Microscopy experiments

For the imaging experiments, MKN-28 and Caco-2 cells were maintained in culture, and grown as monolayers and maintained at 37 °C in an atmosphere of 5% CO_2 and 90 % relative humidity. When the cells were ready to subculture, they were washed with Phosphate Buffer Saline (PBS), and detached from the culture flask with 0.25 %, w/v, trypsin−$EDTA_4$−Na. After that, a dilution (1:20) was performed and the cells were seeded in 35 mm glass-bottom dishes divided in 4 chambers (µ-Dish 35 mm Quad – Ibidi, Germany) suitable for microscopy analysis. 500 µL of cells suspension was added to each chamber.

After 24 hours, the complete medium was removed and the attached cells were washed 3 times with Hanks pH 7.4 and the PFSP extracts were applied. The extracts were diluted in Hanks solution at a final concentration of 100 μM and 250 μL were added to each chamber. The incubation time with each cell line was 3 hours. After that, the cells were washed in PBS 3x and membrane fluorescent stain diluted in PBS was applied: CellMask™ Green Plasma Membrane Stain at a final concentration of 2,5 μg. mL^{-2} (50 μL were added to each chamber). The cells were incubated with the stain for 5 minutes and then washed 3 times with PBS. Hanks solution pH 7.4 was added to each chamber (250 μL) and the live cells were observed with a Leica TCS SP5 II (Leica Microsystems, Germany) laser confocal scanning microscope for study the intracellular localization of the anthocyanins. The ex/em pairs of CellMask™ Green Plasma Membrane Stain and PFSP anthocyanins were 525/535 nm and 610/640 nm, respectively. For that, the following lasers were used on the capture of images: Diode 405nm; Ar 458, 476, 488, 496, 514 nm; DPSS561 561nm; HeNe 633nm. The objective was a HC PL APO CS 40x /1.10 CORR Water and the software used to obtain the images was the LAS AF (Leica Microsystems, Germany). The post treatment of the images was performed with Fiji (ImageJ) software. All the images, controls and experiments, for both cell lines, were treated with the same colour, brightness and contrast parameters. The channel corresponding to the bright field was removed from the final image. The green channel was treated with the following seetings: B&C – minimum 0; maximum 169. The red channel was treated as follows: B&C – minimum 0; maximum 107.

2.8. HPLC analysis

HPLC analysis of anthocyanins was performed on Dionex Ultimate 3000 (Thermo Scientific; USA) equipped with a 250 x 4.6 mm i.d. reversed-phase C18 column (Merck, Darmstadt, Germany). Detection was carried out at 520 nm using a diode array detector (DAD). The solvents were (A) H_2O/HCOOH (9:1) and (B) H_2O/HCOOH/CH_3CN (6:1:3). The gradient consisted of 20–52.5 % B for 35 minutes at a flow rate of 1.0 mL/min. The column was washed with 100 % B for 15 minutes and then stabilized at the initial conditions for another 15 minutes.

LC-DAD/ESI-MS analysis was done on a Finnigan Surveyor series liquid chromatograph, equipped with a Thermo Finnigan (Hypersil Gold) reversed-phase column (150 mm × 4.6 mm, 5 μm, C18) at 25 °C. The samples were analyzed using the same solvents, gradients, injection volume and flow rate referred above for the HPLC analysis.

Double-online detection was done by a photodiode spectrophotometer and mass spectrometry. The mass detector was a Finnigan LCQ DECA XP MAX (Finnigan Corp., San Jose, Calif., USA) quadrupole ion trap equipped with an atmospheric pressure ionization (API) source, using an electrospray ionization (ESI) interface. The vaporizer and the capillary voltages were 5 kV and 4 V, respectively. The capillary temperature was set at 325 °C. Nitrogen was used both as sheath and auxiliary gas at flow rates of 90 and 25, respectively (in arbitrary units). Spectra were recorded in positive ion mode between *m*/*z* 250 and 1500.

2.9. Statistical Analysis

One-way ANOVA with comparisons between all groups for SRB experiments and Two-way ANOVA with Bonferroni's multiple comparisons test for transepithelial transport were performed using GraphPad Prism version 7.00 for Windows/MacOS, GraphPad Software, San Diego California USA, www.graphpad.com. *p<0.05; **p<0.01, **p<0.001

3. RESULTS

3.1. Characterization of Anthocyanins from Purple Fleshed Sweet Potato and Red Wine

As shown in Chapter 1, a total of 11 anthocyanins were identified and quantified by HPLC–MS/MS in the Purple Sweet Potato extract. All of them were Peonidin- or Cyanidin-3-sophoroside-5-glucoside derivatives, acylated with caffeic, ferulic, and/or *p*-hydrobenzoic acids (Table 14). The main peak was attributed to Peonidin-3-(6'-*p*-hydroxybenzoyl-6''-caffeoyl)-sophoroside-5-glucoside (*m*/z 1069, peak 9).

For the Red Wine extract, a total of 7 main anthocyanins were identified: 3-*O*-monoglucosides derivatives from delphinidin, cyanidin, petunidin, peonidin and malvidin and Malvidin-3-*O*-coumaroylglucoside and Malvidin-3-*O*-acetylglucoside.
The identification of anthocyanins was based on matching the fragment patterns to the mass spectrum database of anthocyanins collected from other published articles [210, 211].

Table 14. Identification of the major anthocyanins present in Purple-Fleshed Sweet Potato and Red Wine, by HPLC-MS-MS at 520 nm.

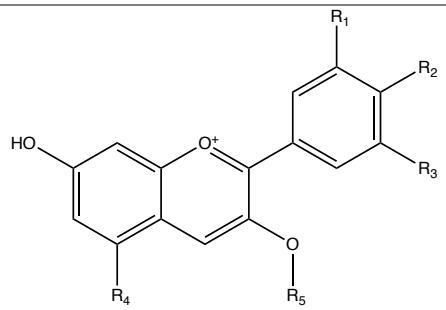

Purple-Fleshed Sweet Potato

peak	R_1	R_2	R_3	R_4	R_5	MS	MS^2	$\lambda_{máx}$
As in table 7.								

Red Wine

peak	R_1	R_2	R_3	R_4	R_5	MS	MS^2	$\lambda_{máx}$
12	OH	OH	OH	OH	Glc	465.06	303.17	524
13	OCH_3	OH	OH	OH	Glc	479.16	317.20	526
14	OCH_3	OH	H	OH	Glc	463.20	301.13	517
15	OCH_3	OH	OCH_3	OH	Glc	493.17	331.20	528
16	OCH_3	OH	OCH_3	OH	Acetyl-glucoside	535.20	331.20	529
17	OCH_3	OH	OCH_3	OH	Coumaroyl-glucoside	639.17	331.20	331

3.2. Simulated Gastrointestinal Digestions

The effect of the processes occurring during a normal digestion on anthocyanins stability after ingestion was evaluated. Anthocyanins extracts from both PFSP and red wine were used to test the stability behaviour of acyl substituents during gastrointestinal digestion. Furthermore, the effect of food matrix on anthocyanin stability was also evaluated. Several concentrations of extracts were tested, based on the probable amount of *in vivo* anthocyanins (from an average consumption of 200 g of PFSP and 200 mL of Red Wine) at a given time point (10 min for salivary phase, 180 min for gastric phase, 120 min for intestinal phase). Also, the added food components were based on the constitution of Purple Sweet Potatoes and Table Red Wines. The experiments followed the normal path of ingestion, digestion and excretion phases, so the samples of simulated gastric digestion were the resulting reactions of oral cavity interactions and the samples of simulated intestinal digestion were the resulting reactions of simulated gastric digestion.

Overall, the effect of saliva on the stability of both PFSP and wine anthocyanins extracts after 10 minutes of reaction was not significant. Both extracts, with or without matrix components added, did not suffer any significant reduction on HPLC areas when compared to the respective controls (Figure 53).

a)

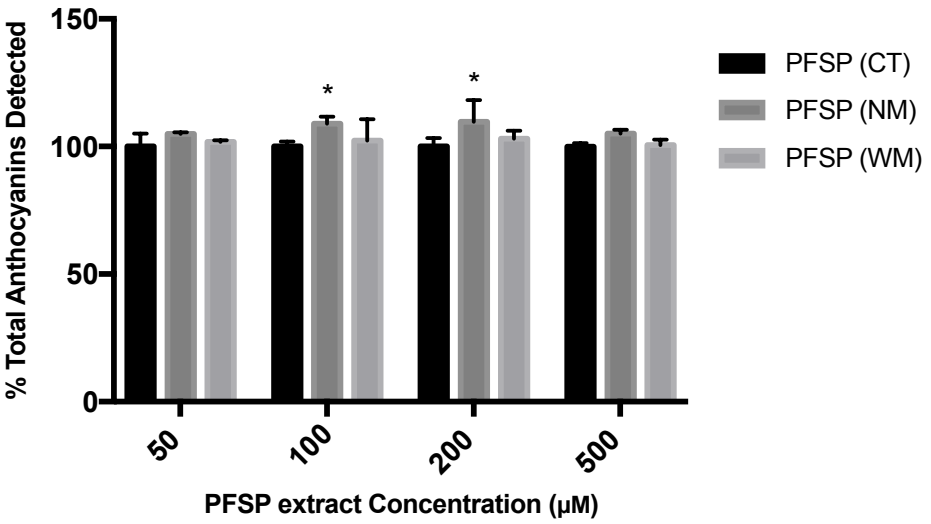

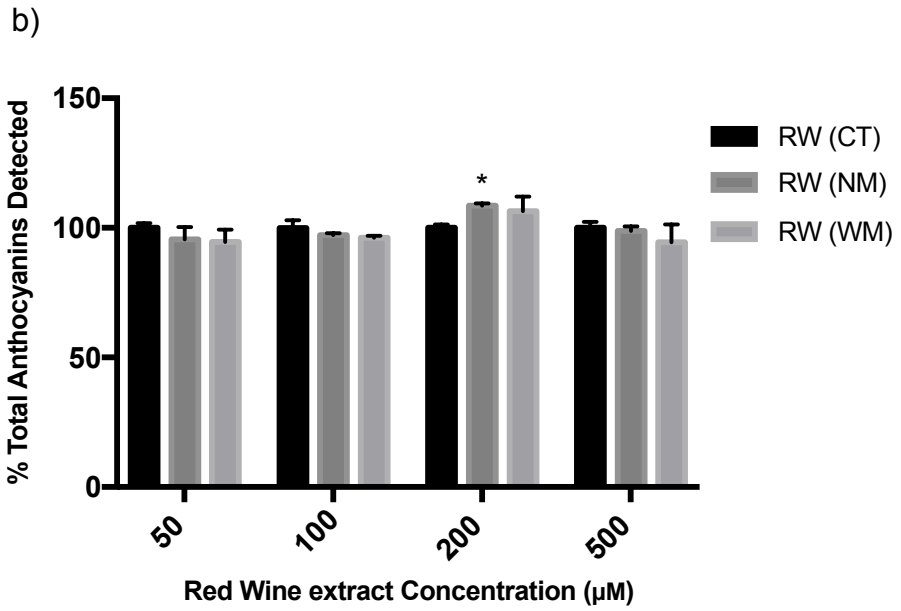

Figure 53. Detection of total anthocyanins from Purple Sweet Potato and Red Wine after interaction with human saliva. a) Purple Fleshed Sweet Potato extracts interactions with human saliva. PFSP (CT) – purple fleshed sweet potato extract control; PFSP (NM) – purple sweet potato extract subjected to saliva interaction without the addition of matrix components; PFSP (WM) – purple sweet potato extract subjected to saliva interaction with the addition of matrix components. b) Red wine extracts interactions with human saliva. RW (CT) – red wine extract control; RW (NM) –red wine extract subjected to saliva interaction without the addition of matrix components; RW (WM) – red wine extract subjected to saliva interaction with the addition of matrix components. Detection was performed with HPLC analysis at 520 nm. Results are presented as total anthocyanins detected (%) (mean ± SEM). Significantly different from control for the same concentration: ∗, $p < 0.05$.

However, it is possible to observe that for some concentrations, the amount of anthocyanin detected after the interaction with human saliva is higher than the control. This may be due to interactions between the salivary constituents and the anthocyanins, that promote the dissociation of self-aggregated anthocyanins, a phenomenon that often occurs at higher concentrations.

As in the case of the interactions at the oral cavity, simulated gastric digestion did not interfere with the overall stability of the PFSP anthocyanin extracts, as revealed by the amount of anthocyanins detected before and after gastric reactions (Figure 54a). In the case of red wine anthocyanin extracts, it seems to exist a pattern of reduction, but with no significant differences. This behaviour was not observed in the presence of food matrix components (Figure 54b).

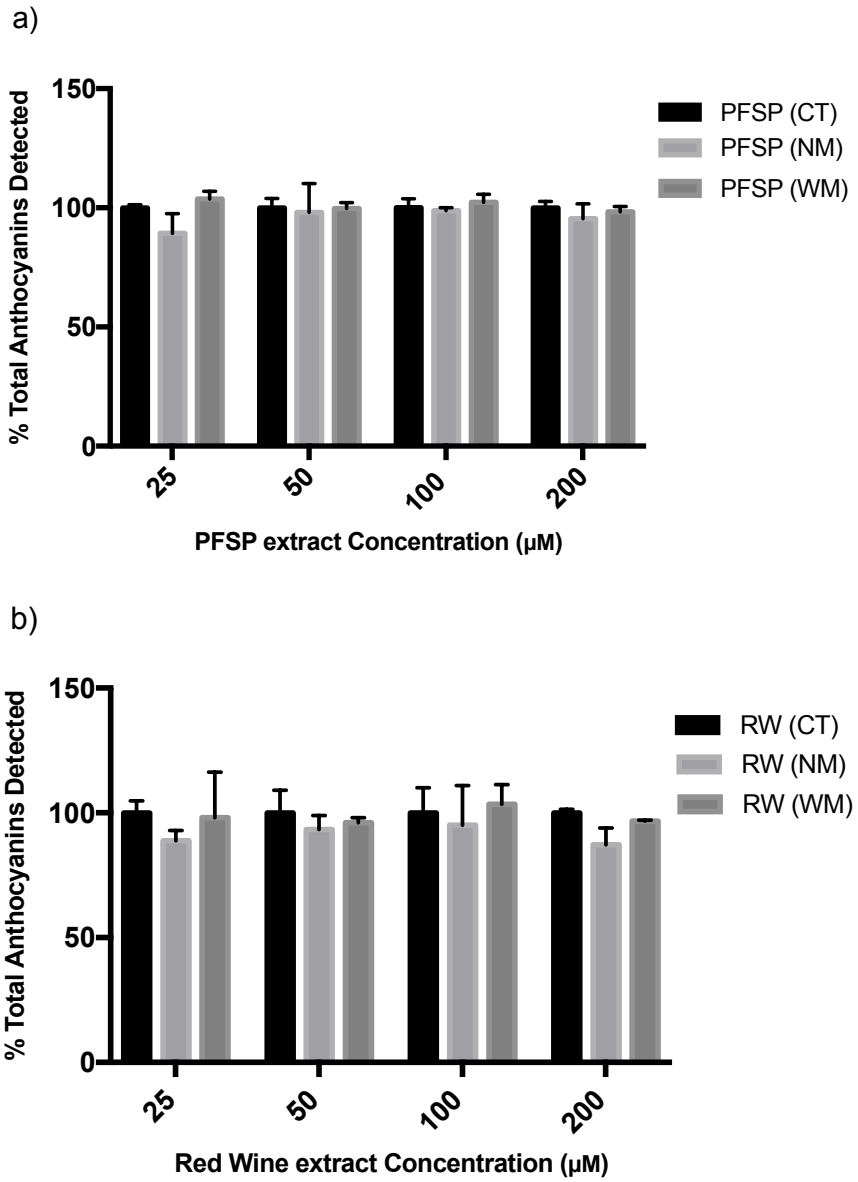

Figure 54. Detection of total anthocyanins from Purple Sweet Potato and Red Wine after a simulated gastric digestion (SGD). a) SGD of purple sweet potato extracts. PFSP (CT) – purple sweet potato extract control; PFSP (NM) – purple sweet potato extract subjected to digestion without the addition of matrix components; PFSP (WM) – purple sweet potato extract subjected to digestion with the addition of matrix components. b) SGD of Red wine. RW (CT) – red wine extract control; RW (NM) –red wine extract subjected to digestion without the addition of matrix components; RW (WM) –red wine extract subjected to digestion with the addition of matrix components. Detection was performed with HPLC analysis at 520 nm. Results are presented as total anthocyanins detected (%) (mean ± SEM). Significantly different from control for the same concentration: ∗, $p < 0.05$

Only at the intestinal level, a clear degradation of anthocyanins is observed for both samples. Reductions of 27-43 % in the case of PFSP extracts without matrix components and of 22-31 % in the case of PFSP extracts with added matrix components (Figure 55a). For wine extracts a similar behaviour was observed with reductions of 49-52 % in the case

of extracts without added matrix components and of 30-45 % in the case of extracts with added matrix (Figure 55b).

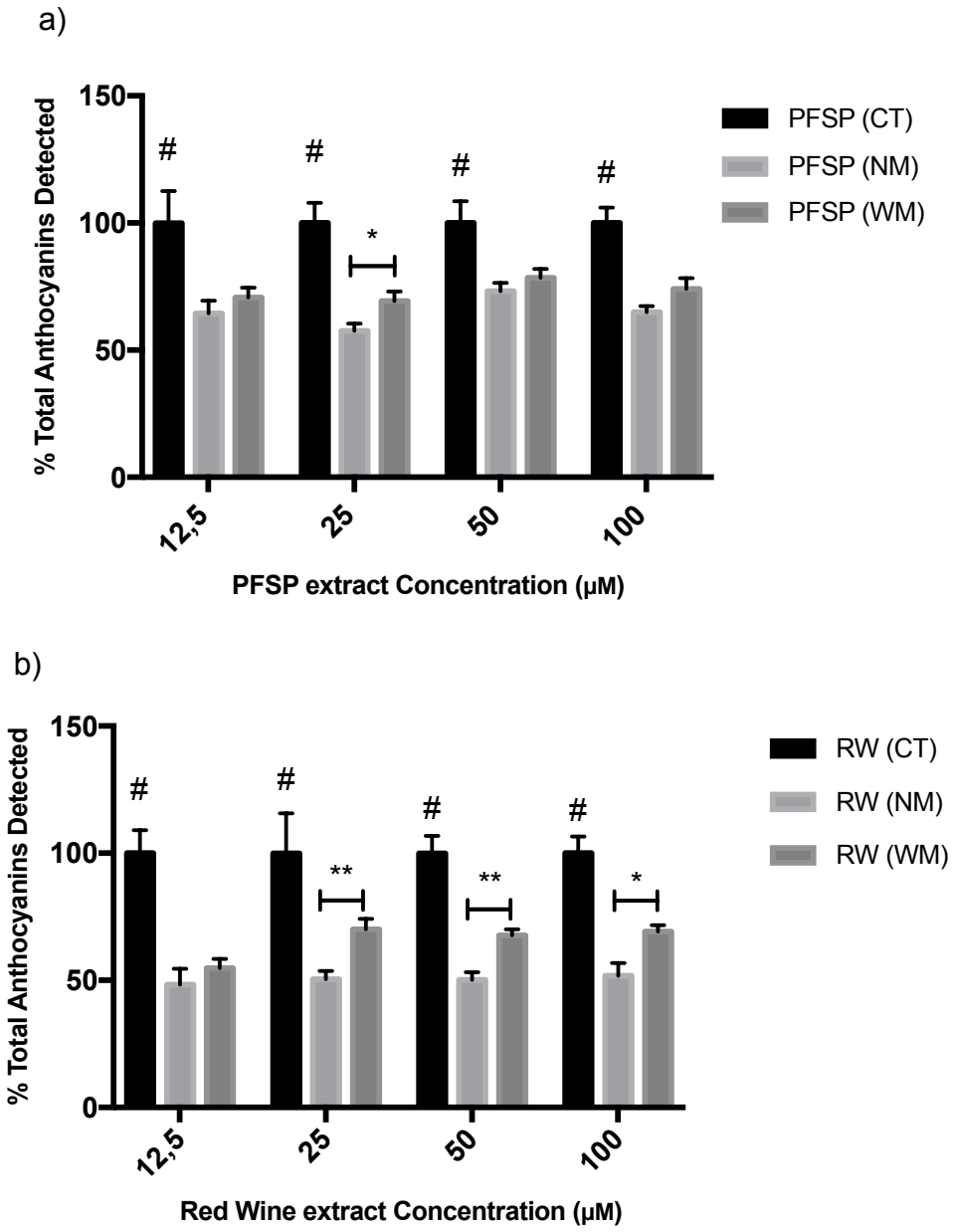

Figure 55. Detection of total anthocyanins from Purple Sweet Potato and Red Wine after a simulated intestinal digestion (SID). a) SID of purple sweet potato extracts. PFSP (CT) – purple sweet potato extract control; PFSP (NM) – purple sweet potato extract subjected to digestion without the addition of matrix components; PFSP (WM) – purple sweet potato extract subjected to digestion with the addition of matrix components. b) SID of Red wine. RW (CT) – red wine extract control; RW (NM) –red wine extract subjected to digestion without the addition of matrix components; RW (WM) –red wine extract subjected to digestion with the addition of matrix components. Detection was performed with HPLC analysis at 520 nm. Results are presented as total anthocyanins detected (%) (mean ± SEM). Significantly different from control for the same concentration: ∗, $p < 0.05$. Significantly different from both tests for the same concentration: #, $p < 0.001$.

3.3. Purple Sweet Potato Proteins Identification and Characterization

With the main objective of isolating the proteins from PFSP, in order to perform further studies focusing on the impact of the food matrix on the absorption of the anthocyanins, a proteomic study was performed with two types of potatoes: The Purple-fleshed Sweet Potato and the Purple Sweet Potato (PSP). The anthocyanin profile at 520 nm was the same for both species (Figure 56). The only difference was the localization of the pigments. While in PFSP the anthocyanins are in both peel and flesh, in PSP the anthocyanins are only located in the peel, making the latter a better source of proteins without anthocyanins in higher yields.

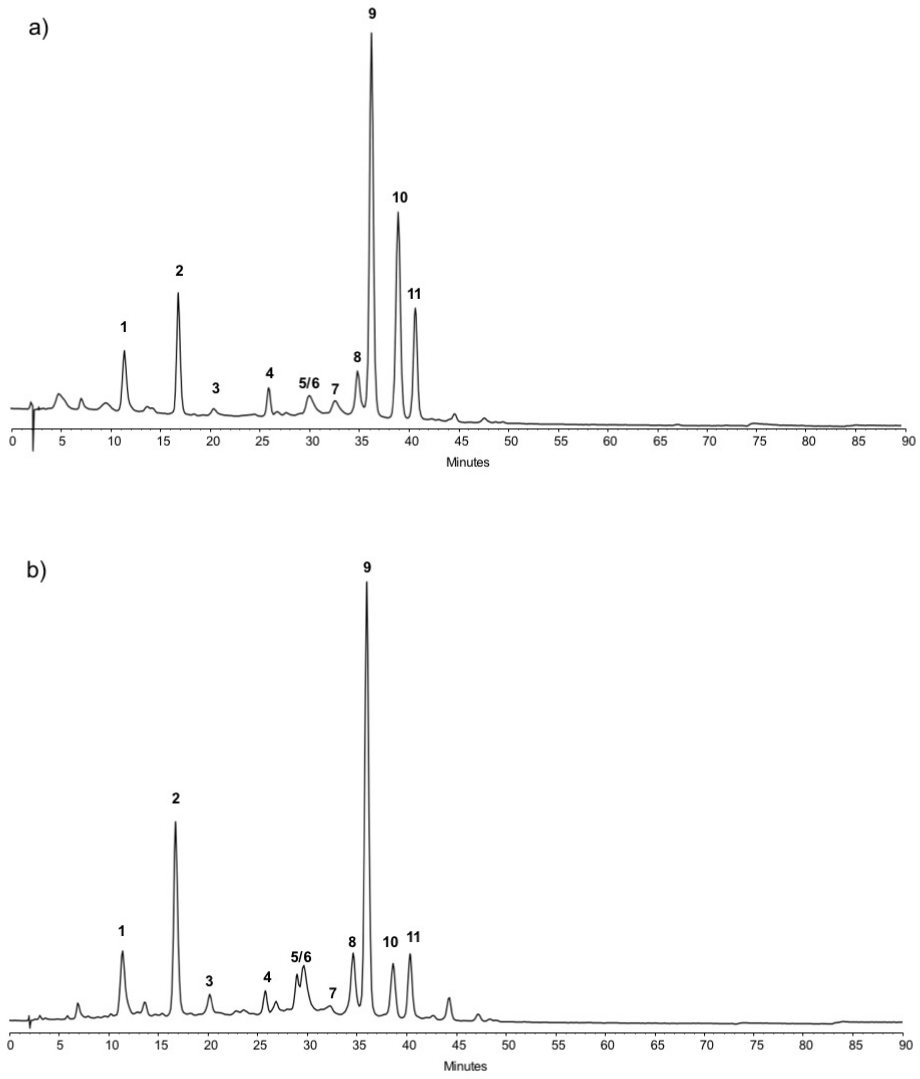

Figure 56. HPLC chromatograms of anthocyanins extracts at 520 nm; a) The extract of PFSP and b) the extract of PSP. A similar profile was found for both species of sweet potatoes and the major anthocyanins present in each

were identified as being the same. The numbers on the chromatograms are corresponding to the anthocyanins from Table 14 on the section 3.1 of the present chapter.

PFSP and PSP protein profile were characterized by SDS-PAGE and further identified by bottom-up proteomics (described in detail in the section 2.3 of the present chapter). No differences were detected in the protein profile of both varieties by SDS-PAGE (Figure 57). Four main protein bands were solved in gel electrophoresis after coomasie blue staining. According to the molecular weight markers, proteins molecular weight round the 100kDa, 50kDa, 25 KDa and 20KDa. Other minor bands were detected but in a much lower quantity. The identification was therefore focused on major bands.

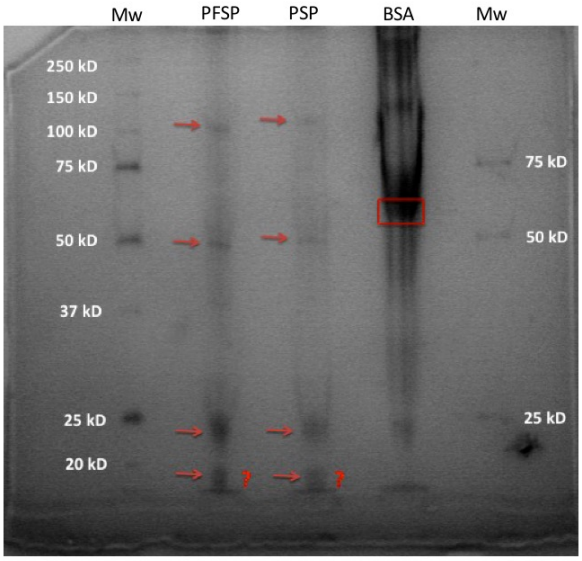

Figure 57. SDS-PAGE protein profile of Purple-Fleshed Sweet Potato and Purple Sweet Potato varieties. Mw - Molecular weight standards; PFSP – Purple-Fleshed Sweet Potato; PSP – Purple Sweet Potato; BSA – Bovine Serum Albumine.

After tryptic digestion, 100KDa band was identified as alpha-1,4 glucan phosphorylase L isozyme, the protein corresponded to the electrophoretic mobility of 50kDa was identified as Beta-amylase and finally, the most intense band, rounding the 25-20kDa was identified as being the Sporamin A and B (Table 15). For all proteins identified, the scores rounding the 105.9 to 208.9 with protein covers higher than 77%. The precursor ions +3 charged get scores higher than 5 and the peptides doubly charged obtained scores rounding 3. Little information was obtained from precursor ions with charges higher than 3 and the monocharged ions have not been into account. Overall, no differences were found in the

proteins identified from PSP or PFSP being the most abundant proteins the Sporamin A and B followed by Beta-amylase and alpha-1,4 glucan phosphorylase L isozyme.

Table 15. Identification of proteins present in Purple-Sweet Potato with the highest score.

Description	Score	Coverage	MW [kDa]
Sweet potato sporamin A OS=Ipomoea batatas PE=2 SV=1 - [Q40092_IPOBA]	208,91	87,21	24,0
Sporamin A OS=Ipomoea batatas PE=2 SV=1 - [SPOR1_IPOBA]	201,68	87,21	24,0
Sporamin A (Fragment) OS=Ipomoea batatas PE=2 SV=1 - [Q2Q581_IPOBA]	194,42	95,98	21,8
Beta-amylase OS=Ipomoea batatas GN=BMY1 PE=1 SV=4 - [AMYB_IPOBA]	156,10	94,99	56,0
Sporamin B OS=Ipomoea batatas GN=IBSPB6 PE=4 SV=1 - [J9TKA6_IPOBA]	133,11	87,04	24,0
Alpha-1,4 glucan phosphorylase L isozyme, chloroplastic/amyloplastic OS=Ipomoea batatas PE=2 SV=1 - [PHSL_IPOBA]	105,89	76,54	108,5

3.4. Antiproliferative Properties of Purple-Fleshed Sweet Potato Anthocyanins

Prior to the transport experiments, an evaluation of the antiproliferative effect of the PFSP extract was performed. Although the focus of the work is not directed for the bioactivity and cytotoxicity of the compounds, it was important to evaluate this parameter and although the following experiments were performed in different conditions, these informations were valuable to ensure that the procedures followed without compromising the cell barriers due to deleterious effects caused by the presence of PFSP anthocyanins. The approach used the technique currently used by the NCI (USA) for the search of compounds with antiproliferative activity and that is described in detail on the section 2.5. of the present chapter.

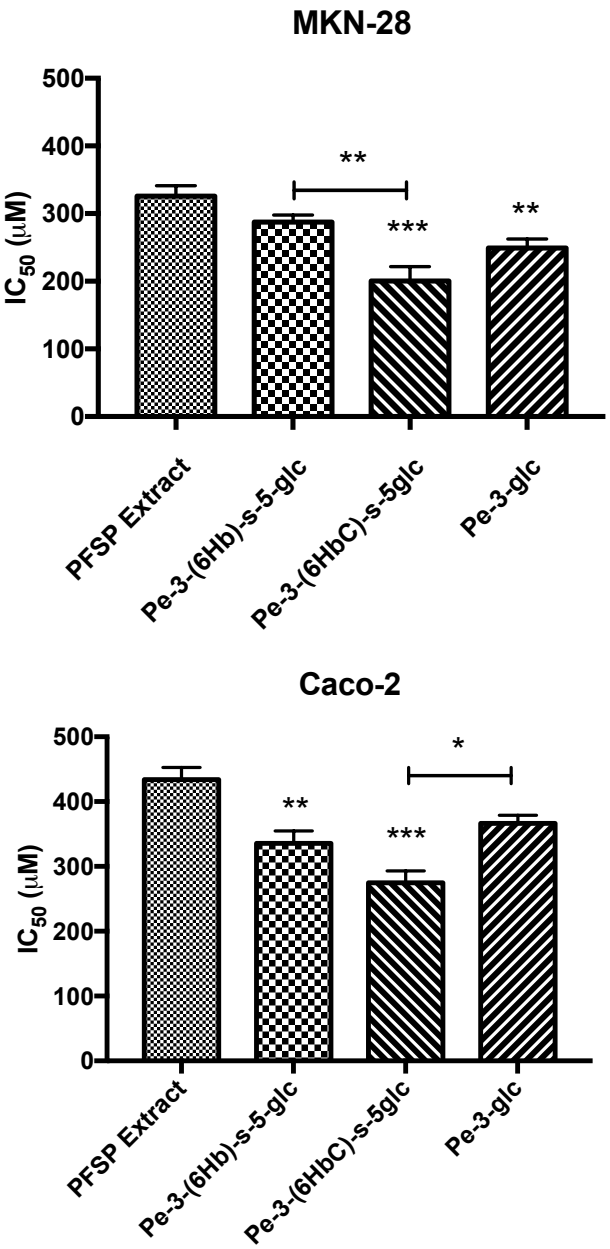

Figure 58. Anthocyanins effect on the proliferation of MKN-28 and caco-2 cells, evaluated by SRB method. Cells were treated with a range of concentrations (31.25 μM – 500 μM) for 48h. Results are presented as mean±SEM (n=6-12). Significantly different from PFSP extract, other indicated ∗, $p < 0.05$; **, $p<0.01$; ***, $p<0.001$.

For MKN-28 cells, it is possible to observe an IC_{50} value of 325.9 ± 15.49 μM for the PFSP extract, 287.8 ± 10.19 μM for the Peonidin-3-(6'-*p*-hyxdroxybenzoyl)-sophoroside-5-glucoside, 200.6 ± 21.14 μM for Peonidin-3-(6'-*p*-hyxdroxybenzoyl-6''-caffeoyl)-sophoroside-5-glucoside and 249.4 ± 13.39 μM for Peonidin-3-glucoside, meaning that these concentrations are the minimum necessary to stop the growth of 50% of the cells

population. So, it is clear that lower IC_{50} values can be translated into higher cytotoxicity for the cells.

For Caco-2 cells the values were as follows: 433.9 ± 18.81 μM for the PFSP extract, 335.6 ± 19.32 μM for the Peonidin-3-(6'-*p*-hyxdroxybenzoyl)-sophoroside-5-glucoside, 274.9 ± 18.31 μM for Peonidin-3-(6'-*p*-hyxdroxybenzoyl-6''-caffeoyl)-sophoroside-5-glucoside and 366.5 ± 12.37 μM for Peonidin-3-glucoside.

As it is possible to see by Figure 58 the results demonstrate a higher resistance to the antiproliferative effect of PFSP anthocyanins by caco-2 cells. This observation may be due to the differences between the metabolism of the two cell lines, giving a higher resistance to the intestinal cells when compared to the gastric ones.

A similar study was performed with two anthocyanins isolated for PFSP and the native anthocyanin, peonidin-3-glucoside, to have a comparison control.

Although the two anthocyanins will only be used in experiments of Chapter III, the results will be presented in conjugation with the ones of the extract.

From Figure 58, one can see that Peonidin-3-(6'-*p*-hyxdroxybenzoyl-6''-caffeoyl)-sophoroside-5-glucoside showed, for both cell lines, the lowest IC_{50} value.

From a statistical point of view, all the isolated compounds were significantly more cytotoxic than the PFSP extract. Also, in the case of MKN-28 cell line, significant differences were found between Peonidin-3-(6'-*p*-hyxdroxybenzoyl-6''-caffeoyl)-sophoroside-5-glucoside and Peonidin-3-(6'-*p*-hyxdroxybenzoyl)-sophoroside-5-glucoside, and in the case of caco-2 cell line, significant differences were found between Peonidin-3-(6'-*p*-hyxdroxybenzoyl-6''-caffeoyl)-sophoroside-5-glucoside and Peonidin-3-glucoside, reinforcing the status of Peonidin-3-(6'-*p*-hyxdroxybenzoyl-6''-caffeoyl)-sophoroside-5-glucoside as the most cytotoxic.

This may be explained by the structural differences, described in detail in Chapter I. The addition of the caffeic acid at the sophoroside moiety can possibly improve the reactivity of the anthocyanin due to the addition of more hydroxyl groups. Thus, the anthocyanin can interact more easily with different metabolic processes that leads to the ultimate death of the cells.

3.5. Kinetics Transport Experiments in the Gastrointestinal tract with Purple Fleshed Sweet Potato Anthocyanins

In order to evaluate the conditions of test and to optimize the methods, after seeding the cells on transwell plates (method explained in detail on section 2.6. of the present chapter) the transepithelial resistance was monitored (TEER).

The TEER values were followed during the growth of the cells every day at 37ºC: 7 days for MKN-28 cells and 21 days for caco-2 cells. Figure 59 shows the results. It is possible to see that after 5 days of progressive increase, the TEER values for MKN-28 cells reached a plateau, indicating the formation of tight junctions and a monolayer suitable for performing the transepithelial transport experiments.

These tight junctions separate the apical surface from the basolateral side to ensure the cellular polarity and the formation of a monolayer barrier. This way, the passage of solutes and water between the paracellular space is highly conditioned [212].

Similar results were observed for caco-2 cells; however, the plateau is reached after 15 days. The cells were left for 7 more days to allow the differentiation into enterocytes. The small decrease on the TEER values may be the result of this differentiation process.

The differences on the values for both cell lines are clear. The higher values for caco-2 may be, once more due to the morphological and metabolic differences of each cell line.

Given the results, all further experiments were performed with initial values of TEER higher than 150 $\Omega.cm^2$ in the case of MKN-28 cells and 250 $\Omega.cm^2$ in the case of caco-2 cells.

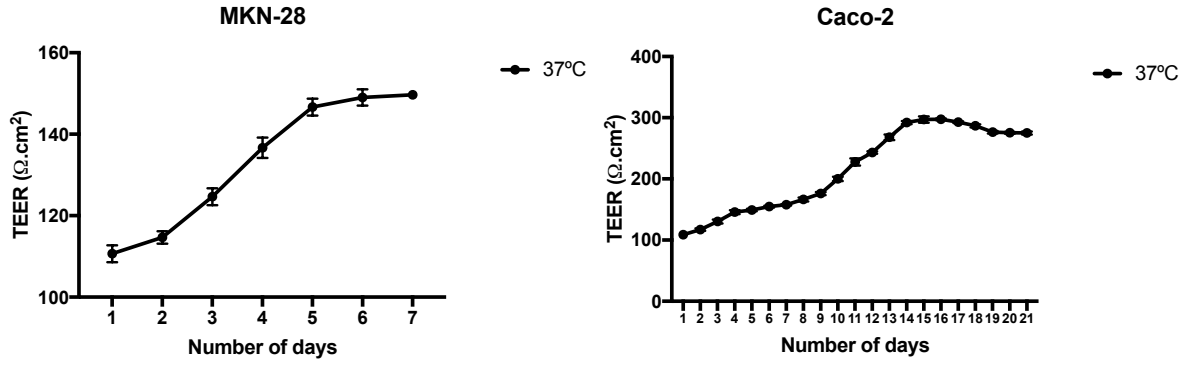

Figure 59. Transepithelial Electrical Resistance (TEER) measuraments along time, in MKN-28 and Caco-2 cells.

The TEER values were also evaluated during the experiments at the time points of aliquots collection. For all the concentrations tested, it was observed that the variations were slight for both cell lines (Figure 60). Only at 180 min for MKN-28 cells and 120 min for caco-2, a more pronounced variation occurs, evidencing higher values. This may be due to the design of the experiment itself. Some studies, demonstrated that the TEER values are dependent not only on the formation of the tight junctions and monolayers, but also on the medium used for the cells, and in some cases we can observe a decrease of about 40% on the values, by changing from a complete medium to a buffer medium such as Hanks [108, 213]. Thus, to ensure the minimum influence of the medium effect, all the measures during the 7 or 21 days were performed with fresh Hanks medium at the respective pH values for each cell line, however, in the latter case, the replacement of the medium was only possible at the end of the experiments (120 or 180 min), which may explain the higher values found.

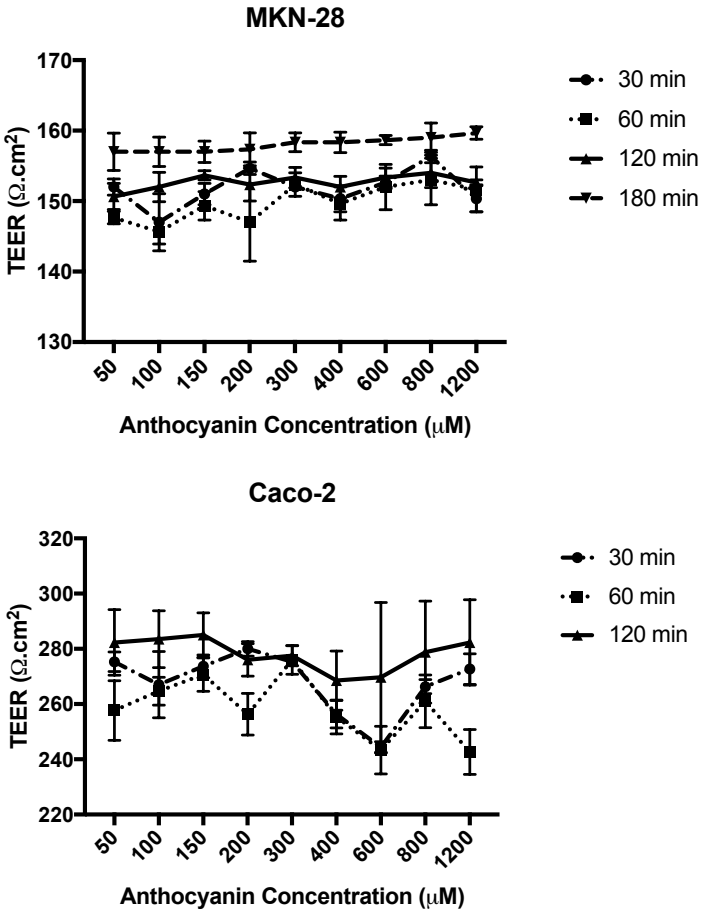

Figure 60. Transepithelial Electrical Resistance measuraments during transwell experiments for different concentrations of PFSP anthocyanins extract, in MKN-28 and Caco-2 cells.

Transport studies of anthocyanins at stomach and intestine level were performed based on previous established models for MKN-28 and Caco-2 cells, and accordingly to the TEER results [103, 209].

The anthocyanin extracts were applied on the apical side of the cells cultured on inserts of Transwell plates and the experiments were followed for 3 h (MKN-28 cell line) or 2 h (Caco-2 cell line), in order to mimic the time of the digestive processes at the stomach and at the intestine.

Overall, the transport of anthocyanins was time dependent and all the anthocyanins present on the apical side were detected at the basolateral side on both MKN-28 and Caco-2 cell lines (Figures 61-63).

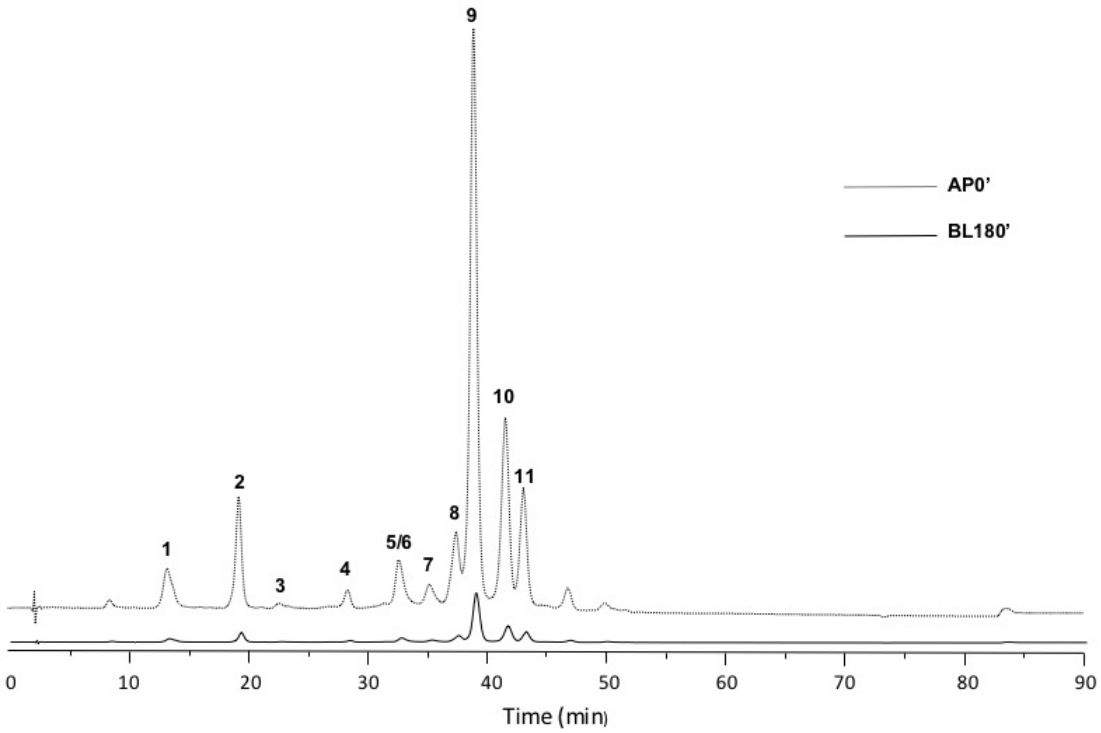

Figure 61. Representative HPLC chromatograms of PFSP extract at 520 nm for a transwell experiment in MKN-28 cells. The results are presented for the apical initial time of the transwell experiment (AP0') and for the final aliquot at 180 min from the basolateral side (BL180'). The initial anthocyanins were all detected after 180 min. The numbers on the chromatograms are corresponding to the anthocyanins from Table 14 on the section 3.1 of the present chapter.

In the gastric cell line MKN-28 the transport behaviour was time and concentration dependent for the first 120 min of the experiment. However, after 180 min the results revealed that a concentration dependence is not observable for the higher amounts tested. The basolateral higher concentration detected after 3 hours was 57.40 ± 1.78 μM (Figure 62).

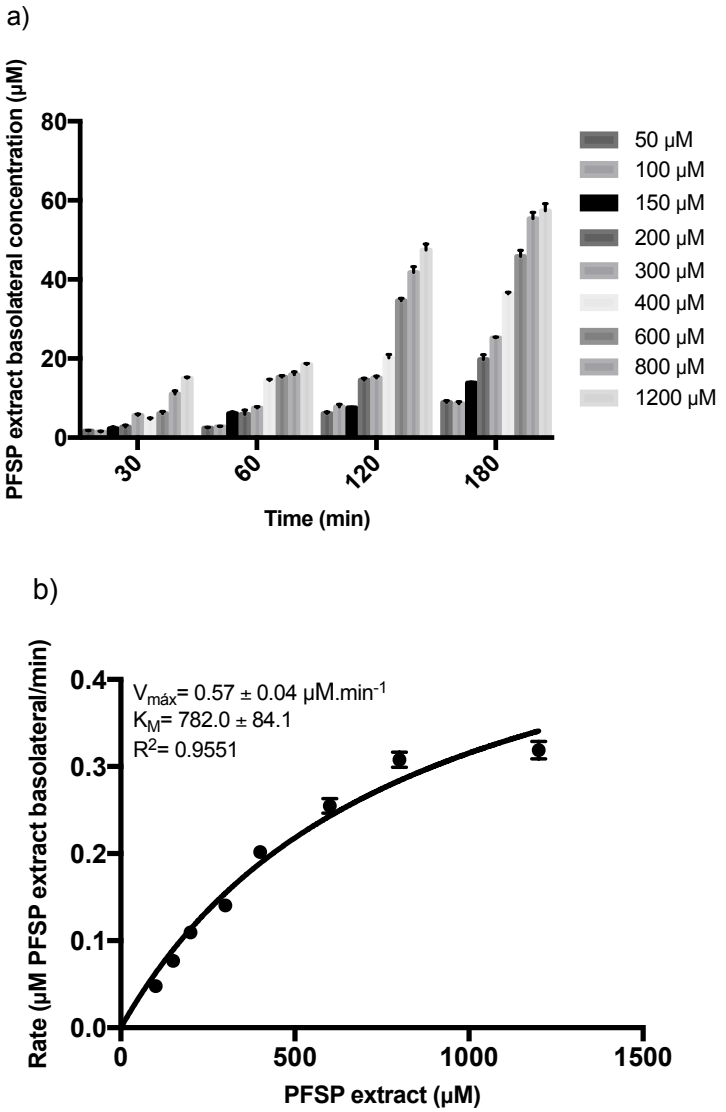

Figure 62. Transport experiments in MKN-28 cell line to determine Michaelis-Menten parameters. a) MKN-28 basolateral detection of purple-fleshed sweet potato anthocyanins at different time points for a range of initial concentrations (50 to 1200 µM). Results are presented as total amount detected on basolateral side after 30, 60, 120 and 180 min (mean±SEM) (n=6-10). b) MKN-28 Michaelis-Menten plot or fate of absorption as a function of purple-fleshed sweet potato extract concentration for 180 min time point. The kinetics parameters V_{max} and K_M were calculated by nonlinear regression analysis using GraphPad Prism 7.0® software. Detection was performed with HPLC analysis at 520 nm.

In the intestinal Caco-2 cell line the transport behaviour was time dependent during the 120 min of experiment, but this pattern was not observed, once again, for concentration dependence. During all experiment time points, the typical concentration dependence behaviour is not observable for the higher amounts tested. The basolateral higher concentration detected after 2 hours was 37.52 ±1.93 µM (Figure 63).

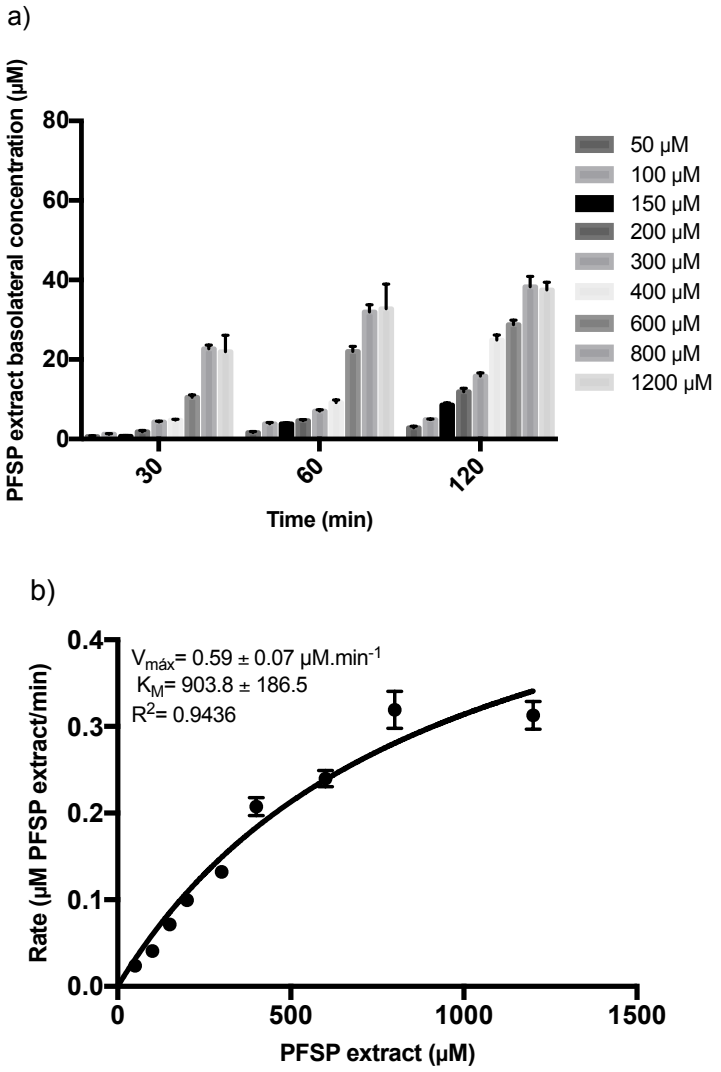

Figure 63. Transport experiments in Caco-2 cell line to determine Michaelis-Menten parameters. a) Caco-2 basolateral detection of purple-fleshed sweet potato anthocyanins at different time points for a range of initial concentrations (50 to 1200 µM). Results are presented as total amount detected on basolateral side after 30, 60 and 120 min (mean±SEM) (n=4-6). d) Caco-2 Michaelis-Menten plot or fate of absorption as a function of purple-fleshed sweet potato extract concentration for 120 min time point. The kinetics parameters V_{max} and K_M were calculated by nonlinear regression analysis using GraphPad Prism 7.0® software. Detection was performed with HPLC analysis at 520 nm.

Kinetic studies of PFSP extract transport in MKN-28 cells were conducted in the presence of a proton gradient (pH 5.0 apical/pH 7.4 basolateral). In Caco-2 cells there was no gradient present (pH 7.4 apical/pH 7.4 basolateral). These differences resulted from the experimental designs projected to mimic the *in vivo* physiological conditions of the fed state. For both cell lines a range from 50 to 1200 µM was applied, which was previously shown to not alter the integrity of each cell barrier used.

Once the behaviour presented by the transport of anthocyanins at the different concentrations across the gastric and intestinal barriers were similar to the one of a saturable transport, the model of enzyme-subtrate interactions described by Leonor Michaelis and Maud Menten in 1913 [214] was applied to understand the kinetics of transport process.

The typical hyperbolic Michaelis-Menten curves for the 3 h (MKN-28 cell line) and for the 2 h (Caco-2 cell line) are displayed in Figures 62b and 63b.

The kinetic parameters V_{max} and K_M calculated by nonlinear regression analysis were determined to be 0.57 ± 0.04 μM.min^{-1} and 782.0 ± 84.1 μM for MKN-28 cells, respectively. For Caco-2 cells, the same parameters were determined to be 0.59 ± 0.07 μM.min^{-1} and 903.8 ± 186.5 μM.

3.6. The effect of food matrix on anthocyanins transport across gastrointestinal barriers

The effect of starch, glucose and proteins, normal constituents of Purple-Fleshed Sweet Potato, on the transport efficacy of anthocyanins was tested on MKN-28 and Caco-2 cell lines. For both cell lines, the behaviour of transport efficiency was time dependent during the experimental time.

For MKN-28 cell line, no significant differences were found comparing the anthocyanin extract (AE) with AE plus the addition of starch, suggesting no effect on anthocyanins transport at a concentration of 6 mg. mL^{-1} of starch. Significant differences were found when adding 60 mM of glucose to AE ($p < 0.001$) and for PFSP initial extract (Figure 64).

Furthermore, the influence of proteins extracted from PFSP with a range from 12.5 μM to 100 μM (based on Sporamin equivalents) was assayed. For all concentrations tested, significant differences were found when comparing with AE ($p < 0.001$). It is possible to see a concentration dependent behaviour on the decrease of anthocyanins with the increase of protein concentration (Figure 64). The maximum efficiency transport of anthocyanins at 3 h was around 8 % for PFSP anthocyanin extract.

For Caco-2 cell line, a similar pattern was found. No significant differences when comparing the anthocyanin extract with the AE plus starch, suggesting no effect on anthocyanins transport at the tested concentration (Figure 64). Significant differences were found when adding 60 mM of glucose ($p < 0.001$). The same was observed for PFSP

extract. The influence of proteins extracted from PFSP with the same range as in MKN-28 cells was tested.

For all concentrations tested, significant differences were found when comparing against AE ($p<0.001$). As in stomach cells, it is possible to see a concentration dependent behaviour on the decrease of anthocyanins transport with the increase of protein amount (Figure 64). The maximum efficiency transport of anthocyanins at 3 h was around 5 % for PFSP anthocyanin extract.

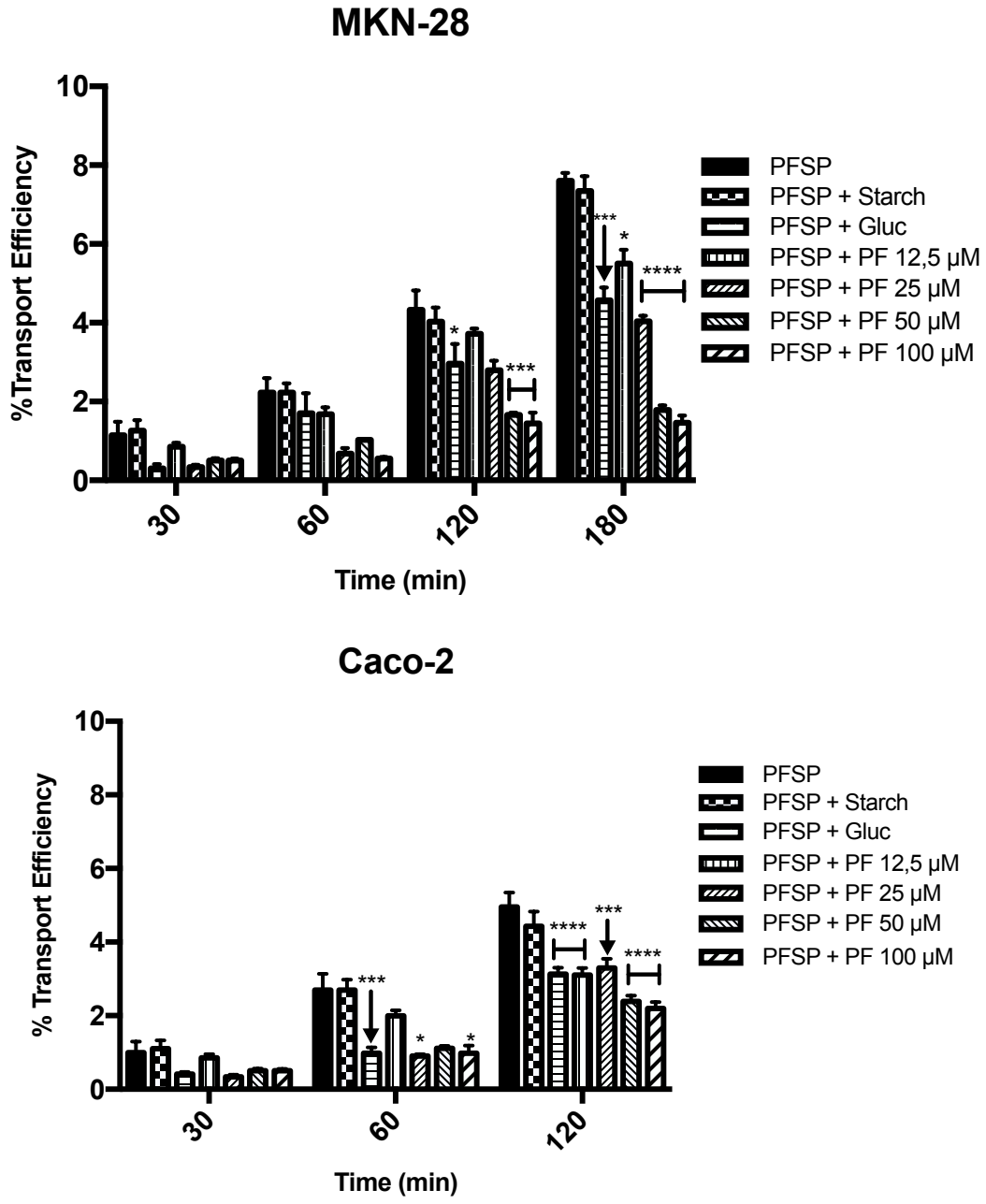

Figure 64. Effect of matrix components on transport efficiency of purple-fleshed sweet potato anthocyanins on MKN-28 and caco-2 cell lines. MKN-28 – transport efficiency studies were performed under a gradient (pH 5.0 apical/pH 7.4 basolateral). Results are presented as transport efficiency (%) after 30, 60, 120 and 180 min (mean±SEM). b) Caco-2 – transport efficiency studies were performed without gradient (pH5.0 apical/pH7.4 basolateral). Results are presented as transport efficiency (%) after 30, 60, 120 (mean±SEM) (n=12). Transport efficiency percentages were calculated as (compound concentrations at the basolateral side over time)/(compound concentrations at the apical side at 0 h) × 100. Significantly different from control for the same incubation time: ∗, $p < 0.05$; **, $p<0.01$; ***, $p<0.001$; ****, $p<0.0001$. PFSP - purple fleshed sweet potato anthocyanins 200 µM; Starch – starch 6.0 $mg.mL^{-1}$; Gluc – glucose 60 mM; PF – protein fraction from purple sweet potato.

3.7. Intracellular localization of PFSP anthocyanins on MKN-28 and caco-2 cells – Laser Scanning Confocal Microscopy

In Chapter I of Part I, the fluorescence properties of two anthocyanins from PFSP were evaluated. The results showed interesting characteristics that were further utilized to perform applied experiments with MKN-28 and caco-2 cells. The inner fluorescence of the pigments allowed us to evaluate their intracellular localization, in order to better understand all the transport processes and biological activities.

For having a better layout of the cells, a plasma membrane fluorescent marker was used. The plasma membrane is a convenient marker of cell boundaries and as such, a number of probes have been used for staining of the membrane, in this case we utilized the CellMask™ Green Plasma Membrane Stain that enables fast and uniform labeling of the plasma membrane in almost all cell types. This stain works rapidly and can be detected using a standard FITC filter set with any imaging instrument. Depending upon the cell type and experimental conditions, the plasma membrane staining will last for 60–90 minutes without detectable internalization, providing enough time for most live cell dynamic studies. Furthermore, this staining is resistant to fixation processes, although in this case with used non-fixed cells. The ex/em pair of this marker was 522/535 nm which ensured no interference with the anthocyanins pair (ex/em 610/640 nm). Like this, fluorescence images were obtained with two distinct colours; green for plasma membrane and red for anthocyanins (Figure 65).

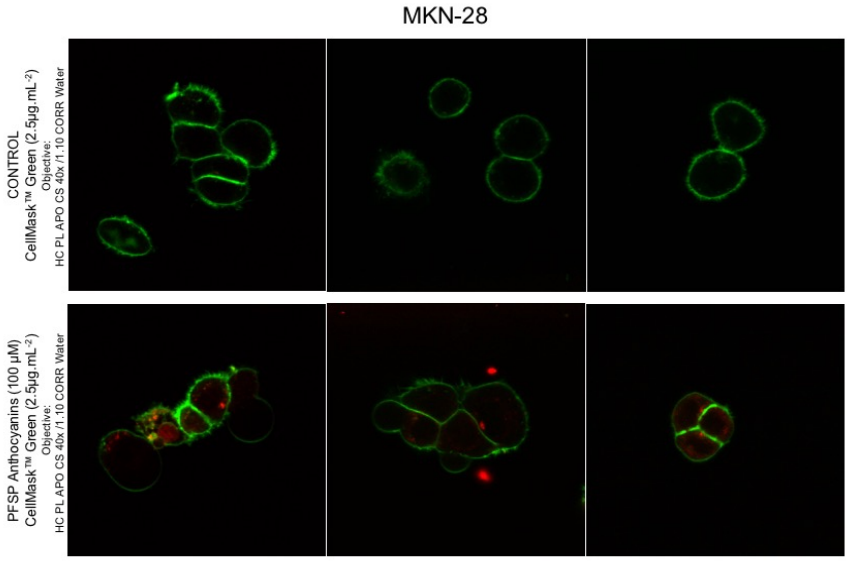

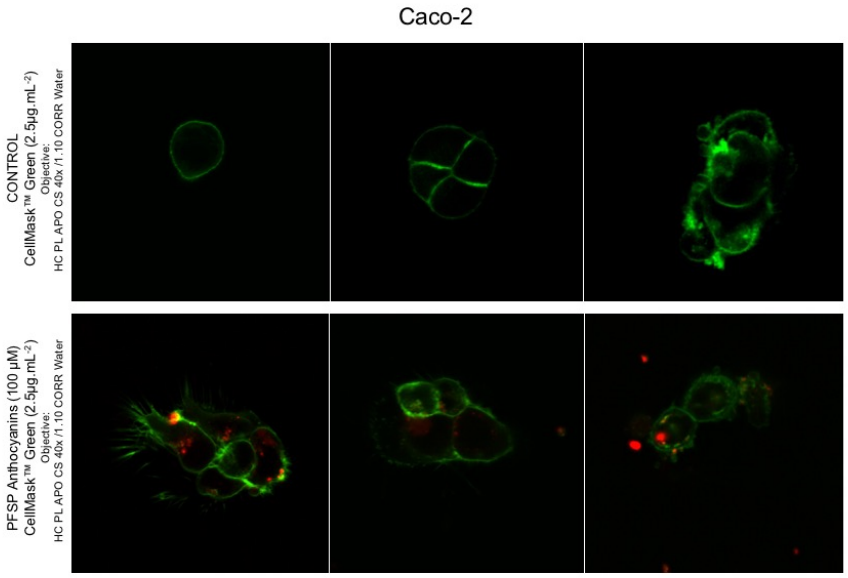

Figure 65. Live-cell imaging of the intracellular localization of PFSP anthocyanins in MKN-28 and caco-2 cells by Laser Confocal Scanning Microscopy analysis. Selected optical planes from MKN-28 cells and caco-2 where green stains for the plasma membrane; red stains for the PFSP anthocyanins. Cells were treated with anthocyanins for 3 hours, and then stained with CellMask™ Green for 5 min before the microscope analysis. The lasers used on the analysis were: Diode 405nm; Ar 458, 476, 488, 496, 514 nm; DPSS561 561nm; HeNe 633nm. All the images were collected at 40x magnitude with a HC PL APO CS 40x/1.10 CORR Water. The ex/em pairs of CellMask™ Green Plasma Membrane Stain and PFSP anthocyanins were 522/535 nm and 610/640 nm, respectively. All the images were treated the same way on brightness and contrast parameters. All the RGB values were kept the same. To the composite of each image was removed the channel corresponding to the bright field.

The distribution of the anthocyanins in the selected optical planes for both cell lines is clearly uneven as they appear accumulated in specific areas of the cells.

All the anthocyanins detected (red coloration) were confirmed to be inside the cells through a progressive layer analysis of each image.

Analysing the specific localization, the results shows that anthocyanins are mainly concentrated on the areas near the plasma membrane. This may be the result of a process of exocytosis, consequence of the incubation time of the cells with the extract. In fact, microscopic analysis revealed some regular and shaped anthocyanin filled bodies densely distributed that may be compatible with endo or exosomal vesicles, however the plasma membrane stain did not clearly highlight these organelles. Besides that, anthocyanins appear not only as concentrated spots but also as localized smudges, especially on MKN-28 cells.

4. DISCUSSION AND CONCLUSION

Anthocyanins have been described as a health-benefit group of polyphenol with well described biological properties such as anti-tumoral and anti-inflammatory, and antioxidant characteristics [215, 216]. These inherent biochemistry attributes have hampered the efforts to understand their health benefits. Biological *in vitro* assays are excellent tools to understand the mechanism of action of such pigments.

Despite the beneficial properties of anthocyanins, their effectiveness at preventing or treating health conditions depends on their bioavailability. Bioavailability is defined as the fraction of ingested nutrients or bioactive compounds that are digested, absorbed, and metabolized through normal pathways. Additionally, the concept of bio-accessibility can be defined as the fraction which is released from the food matrix into the gastrointestinal tract and becomes available for absorption.

Food digestion implies several phases and processes that leads to an optimal transformation of foods, for a proper absorption of the nutrients. These processes involve a wide range of pH variations, and the action of several enzymes along the way, resulting in a difficult environment for food constituents that often undergo several transformations, depending on their initial structure, and then, affecting their final absorption rates [217].

In this chapter, simulated digestions were performed to understand how these processes may affect the stability of ingested anthocyanins.

Upstream to gastrointestinal absorption, a variety of binding processes can take place, namely interaction with food proteins or with salivary proteins and digestive enzymes [198, 218].

The results suggested that anthocyanins from both red wine and PFSP are stable when interacting with human salivary constituents. Recent studies with saliva shows interesting interactions between tannins and salivary proteins, contributing to the astringency phenomenon of red wine and other beverages rich in polyphenols [219].

Besides that, the results show a higher amount of anthocyanins detected after the interaction with saliva, which, at a first glance, was not expected, once previous studies demonstrated an interaction between anthocyanins and salivary proteins [220]. However, this may be explained by the auto-association properties anthocyanins have [32], especially at higher concentrations. This phenomenon seems to be more pronounced in PFSP case, which may be explained by the higher complexity of their anthocyanins. Thus, the interaction with saliva seems to promote the disaggregation of anthocyanins enabling

them to be more available without compromising their stability.

When food matrix components were added, it was possible to see a stabilization of the amount of anthocyanins detected by HPLC-DAD when compared to control. These observations may be the result of natural interactions between anthocyanins and other compounds normally present in foods, in this case, from red wine and PFSP. The fact that the increase on the amount of anthocyanins detected after interaction with saliva is no longer observable, may be due to probable hindrance phenomenon that do not allow those interactions to occur.

At the gastric level, it was possible to notice a pattern of reduction after simulated gastric digestions. This tendency is more evident in the case of red wine anthocyanins. This may be due to the complexity of anthocyanins present in both extracts. Anthocyanins from Red wine are mainly C3 monoglucosides while anthocyanins from PFSP contain both glucosides and diglucosides moieties with acyl substituents resulting in high molecular weight pigments as it was identified by HPLC-MS-MS analysis. In fact, previous studies have confirmed that anthocyanin glycosylic acylation affects the *in vitro* and *in vivo* chemical stability of acylated anthocyanins [33, 221].

This gastric simulated digestion was performed in the presence of pepsin that is normally found in high amount in gastric juice. Also the pH of the solution was 3 to mimic the conditions of the stomach during a digestion. A recent study with similar simulated gastric conditions with blueberries anthocyanins demonstrated the same reduction tendency, although there were no significant differences, which is in accordance with the present findings [222]. Anthocyanins from blueberries are mainly monoglucosides such as in Red Wines. Nevertheless, the results suggest that in the tested conditions, gastric digestion did not affect the stability of anthocyanins in a significant way. In fact, some studies with other classes of polyphenols demonstrate that the gastric phase of digestion processes does not affect their overall stability [223].

The same study with blueberries anthocyanins showed a significant reduction of the overall anthocyanins amount detected after a simulated intestinal digestion [222]. The results present in this chapter also show a reduction of the total amount of anthocyanins detected after the simulation. The results also suggest a higher reduction in the red wine case, with overall reduction matching more than a half of the initial amount that reaches the intestinal cavity. Once more, the samples were yielded from the previous simulated gastric digestion, resulting in new dilutions and consequently reduced final concentrations. Intestine is known as the main metabolizing organ of the gastrointestinal tract. In our

simulated intestinal digestion, we used pancreatin, a mixture of the main enzymes that are present in the intestinal environment at pH 7. Anthocyanins at such high pH values are mainly present in their carbinol (anionic) pseudobase and quinoidal forms. These latter are not as stable as their flavylium form, and so are easily degraded [36]. These facts may explain the observed results.

The addition of matrix components, resulted in a lower reduction of anthocyanins after simulated digestions. This suggest that food matrix may somehow exert a protective effect against degradation of anthocyanins in the intestinal environment. These feature is more pronounced in red wine anthocyanins. This phenomenon, once more, may be due to the structure differences between red wine and purple fleshed sweet potato anthocyanins, which makes the first ones more vulnerable to the action of digestion components, and consequently the food matrix protective effect seems to be higher. A recent study comparing the effect of the presence of a food matrix with almonds suggested a significant effect on polyphenol bio-accessibility from almond skin in both the gastric and duodenal environments [224]. Also, it is suggested in the same study a potential interaction between the dietary fibers present in almond skin and polyphenols that may act as a barrier to prevent a total release of the phytochemicals during digestion processes.

A study with pomegranate anthocyanins verified the effect on co-digestion of different foodstuffs and food components with anthocyanins. It was verified a reduction on the losses at the intestinal level upon the co-digestion with food components such as glucose, fructose, starch and different proteins [225].

In another study with anthocyanins from grape pomace, the results after gastric and intestinal digestion showed that only in the intestine phase a decrease on the amount of recovered anthocyanins was significant, furthermore, the higher amount of recovered anthocyanins were obtained from an insoluble fraction (in some cases, all the anthocyanins were entirely recovered from the insoluble fraction), suggesting, once again, that food matrix may influence the action of digestion environments, protecting the anthocyanins from degradation [226].

All these findings are in accordance with our results.

Caco-2 cell line is widely used as a model for the assessment of bioavailability at the intestinal level. For a long time, the intestine was believed to be the only absorption site for anthocyanins, however, *in vivo* studies, demonstrated an early appearance of these flavonoids in plasma in their parent form. Such observations were not compatible with an exclusive intestinal absorption, suggesting the involvement of stomach in such procedures

[136, 227].

In fact, over the past few years, the absorption of anthocyanins at the stomach level has been gaining interest among the scientific community. *Transwell*® models with gastric cell lines have been created, such as the MKN-28 model developed by Fernandes I. *et al.* [209] and used during all the transepithelial experiments performed in this work. Thus, to have a full comprehension of the absorption of anthocyanins, one must evaluate both gastric and intestinal cavities. Concerning this study, only the native forms were evaluated, although it is widely known that anthocyanins derivatives are also present, mainly after enzymatic action at the intestinal level [126].

The studies reported on the literature on the gastric and intestinal bioavailability of anthocyanins were mainly done with the 3-monoglucosides, 3,5-diglucosides and 3-monoglucosides acylated forms [102, 103, 107]. However, to the best of our knowledge, no studies with highly complex acylated anthocyanins were performed regarding this issue. The results herein suggest an overall higher resistance of this type of anthocyanins to gastrointestinal simulated conditions, hence, PFSP anthocyanins were used to perform the absorption experiments.

In both cell lines, the transport was time dependent. For the higher concentrations, the amounts detected on the basolateral side were similar, suggesting the involvement of a saturable transport system. This observation is clear after 180 min for MKN-28, but for caco-2 cell line this tendency is observed during all the experimental time points. These differences suggest a more readily system of transport in caco-2 than in MKN-28, which may be due to the inner biological characteristics of each cell line. In fact, both cells are quite different, both morphologically and physiologically. Also, overall smaller amounts of anthocyanins were detected on caco-2 cell line comparing with gastric cells at the final point of both experiments. These may be due to the differences on the models used to mimic *in vivo* conditions. In the gastric model, apical pH values were set to 5, while in intestinal model the pH values were set to 7.4. This has consequences on the structure of the anthocyanins. At pH 5 carbinal pseudobases form will prevail, while at pH 7.4 carbinol (anionic) pseudobase and other charged quinoidal forms are the main structures present [36], which may influence the overall transport rates.

The kinetic parameters observed revealed a V_{max} similar for both cell lines. This observation suggest that the absorption rates may depend on the anthocyanins themselves rather than the cell barrier. However, K_M parameters are different, suggesting a higher affinity (lower value) between the transport system and the anthocyanins on the

MKN-28 cells comparing to the intestinal cells. This observation may explain the higher amounts detected on the basolateral side of gastric cells transepithelial transport experiments.

The effects of the addition of food matrix on anthocyanins uptake were also assayed. For both cell lines the results followed a similar pattern, although an overall higher transport efficiency was observed on MKN-28 cells. From the added food constituents only starch did not show an inhibition of anthocyanins transport.

Glucose was added at a 60 mM concentration value, as previously reported for anthocyanins from Red Wine [102]. The transport significantly decreased in both cell lines. Previous studies suggested the putative involvement of glucose transporters on the absorption of monoglucoside anthocyanins at both gastric and intestinal cell lines [102]. In fact, MKN-28 cells showed the presence of GLUT1 and GLUT3 [102] and caco-2 cells the presence of GLUT2 [103]. Our results are in accordance with the previous findings for monoglucoside anthocyanins, suggesting a similar absorption mechanism for these highly complex acylated anthocyanins. However, our results do not allow to conclude about the bio-accessibility trough C-5 free glucoside on these anthocyanins once cells may have functional enzymes such as esterases that have the ability to remove acyl groups and potentially allowing C-3 glucosides to become available to interact with such transporters. Nevertheless, other transport systems may be involved, once there is no full inhibition of transport, as previously described [102].

Furthermore, a protein gradient was applied to the anthocyanin extract.

The protein extract was isolated from both Purple-Fleshed Sweet Potato and Purple Sweet Potato, and it was identified as being mainly formed by proteins from the Sporamin family. In fact, several studies reported Sporamin proteins as the main proteins present in Sweet Potatoes, with values up to 80% of the total protein content [228, 229]. Sporamins are known as tripsin inhibitors, suggesting a high reactive behavior of these proteins [230]. Studies demonstrated activity as radical scavengers and glutathione-like peroxidase activity [231].

The results show a significant decrease of transport efficiency for every concentration used at the final experiment points for both cell lines, but not for the earlier time points, suggesting a time dependent interaction. In MKN-28, for the higher amounts of protein, the transport efficiency was below the passive transport value (2 % transport efficiency). This result is not compatible with an exclusive competitive inhibition but rather a decrease of the transport resulting from interactions between proteins and anthocyanins at the

apical side. In fact, studies have suggested that anthocyanins may interact with several types of proteins [211, 232]. Nevertheless, these latter observations certainly need more research, to understand the type of interactions involved.

Finally, by using the fluorescent properties of PFSP anthocyanins that were described in Chapter I, an imaging study was performed with the main objective of localize anthocyanins inside gastric and intestinal cells.

The analysis of the live-cells fluorescent images revealed that anthocyanins are unevenly distributed among cells. This can be correlated somehow with the results of transepithelial transport experiments. These results suggested that PFSP are transported across gastric and intestinal cells through saturable mechanisms that are time dependent. The fact that anthocyanins are concentrated near the plasma membrane of the cells after 3 hours of incubation may be related to this type of transportation, however, this can be only correlated with the smudges found, mainly on MKN-28 cells. Also, it was observed several amounts of anthocyanins concentrated in regular spherical shapes, that may be compatible with vesicles resulting from exocytosis processes (once the endocytosis at the 3h time point is highly unlikely to occur, in a higher yield than exocytosis processes). These results confirm an uptake of the anthocyanins by both MKN-28 and caco-2 cells. Furthermore, the particular distribution may be related to the position of specific organelles inside the cells, with which anthocyanins may interact to exert their biological activities. However, to confirm this theory, more studies are needed with the staining of specific organelles rather than just the plasma membrane.

As a conclusion, the overall results demonstrate the importance of assaying the bioavailability of these type of highly acylated anthocyanins. Altogether, they suggest similar absorption characteristics as normal anthocyanins but with higher resistance to gastro-intestinal digestion processes. It was also clear that food components such as glucose and proteins affected the transport efficiency of these anthocyanins, so one must attend to this issue when assessing anthocyanins bioavailability.

CHAPTER III

MOLECULAR MECHANISM OF TRANSPORT OF ANTHOCYANINS AT THE GASTRIC LEVEL: A NANO-APPROACH

Synopsis

In this chapter, a nano-approach to assess the mechanism of absorption of anthocyanins in MKN-28 cells was used.

The effect of temperature was evaluated and the results demonstrated a very significant reduction on the transport efficiency at 4ºC.

Gold nanoparticles were used to deliver anti-sense sequences to the target mRNAs selected for this work: GLUT1 and GLUT3.

Both gene silencing and the effect on the protein level were evaluated and the cells were seeded in Transwell plates and the nanoparticles were applied. Transpithelial transport studies were performed.

The results showed that transport efficiency of all the anthocyanins tested was reduced in the presence of both anti-GLUT1 and anti-GLUT3 nanoparticles. Efflux and organic transporters inhibition was also performed, and the results suggest that other transporters besides GLUTs may be involved in the absorption of anthocyanins at the gastric level. Computational biochemical studies were performed, in order to evaluate the interaction between the two anthocyanins isolated at Chapter I and a monoglucoside Peonidin-3-*O*-glucoside. Overall the results suggest that the structural complexity of these anthocyanins did not affect their binding to the transporters, corroborating the previous experimental results.

This chapter resulted in the follow paper: ***Oliveira, H.,*** *Roma-Rodrigues, C., Santos, A., Veigas, B., Brás, N., Faria, A., Calhau, C., de Freitas, V., Baptista, P. V., Mateus, N., Fernandes, A. R., Fernandes, I., (2018) "GLUT1 and GLUT3 involvement in anthocyanin gastric transport – Nanobased targeted approach", Submitted for publication.*

1. INTRODUCTION

Positive correlations have been established between the consumption of flavonoid-rich foods and health benefits, in different *in vitro* and animal studies, but also in several epidemiological studies [233, 234]. The beneficial effect of these foodstuffs has been attributed to the presence of polyphenolic compounds including anthocyanins. Although the consumption of anthocyanins may easily reach 200 mg/day, their bioavailability has been reported to be quite low (<1 %) [235]. Anthocyanins are poorly absorbed as genuine parent glycosides or detected in blood as metabolites [236, 237].

The bioavailability of these compounds cannot be addressed only from a simple nutritional perspective. These pigments have unique physical-chemical properties that affect their behaviour *in vivo*. The bioavailability of anthocyanins is the most difficult one to assess amongst all flavonoid compounds as a result of their occurrence under different structures in equilibrium depending on pH. In addition, biological samples are complex matrices making it hard to perform a clear chemical profile to properly identify and quantify bioactive molecules.

Anthocyanins are also very unstable at neutral pH and physiological temperature, and can interact with proteins or carbohydrates. Also, the bioavailable forms of anthocyanins *in vivo* are not exclusively the same that occur in food since they are also largely metabolized yielding several types of metabolites [236]. Considering *in vivo* conditions, anthocyanins are readily metabolized, degraded or excreted from the organism.

Due to their rapid appearance in plasma, the absorption of anthocyanins is also likely to occur at the gastric level, although the information on this topic is scarce [235]. Preliminary studies with a gastric cell barrier (MKN-28) model indicated that anthocyanins uptake involves a saturable transport but the absorption mechanism remains unknown [238]. Glucose transporters have been suggested as the main transporters involved in the absorption of these nutraceuticals [239].

To further elucidate the role of glucose transporters in the uptake mechanism of anthocyanins in this gastric cell barrier model, a nano-based approach was explored herein using gold nanoparticles (AuNPs) functionalized with specific antisense hairpins for *GLUT1* and *GLUT3* gene silencing.

AuNPs, due to their extraordinary physical-chemical properties (i.e. high surface-to-volume ratio, allowing surface modification with a plethora of molecules for specific targeting and reduced size allowing interaction with biomolecules in a one-to-one scale),

intrinsic chemical stability and apparent lack of toxicity, can be used as a vectorization tool to specifically and selectively silence gene expression, with greater efficiency over commercial available transfection agents like lipofectamine [240]. AuNPs have been used as vehicles to deliver silencing moieties (e.g. antisense oligonucleotides, siRNA) to silence genes involved in several cellular processes [241-245].

Four anthocyanins, with a glucose moiety at different positions were assayed in this study: Malvidin-3-*O*-glucoside (Mv3glc), Peonidin-3-*O*-glucoside (Pn3glc), Peonidin-3-(6'-hydroxybenzoyl)-sophoroside-5-glucoside (Pn3HBsoph5glc) and Peonidin-3-(6'-hydroxybenzoyl-6''-caffeoyl)-sophoroside-5-glucoside (Pn3HBCsoph5glc). This work aimed to apply novel and useful means yielding new data to comprehend how anthocyanins from different natural sources are absorbed using the *in vitro* human stomach cell model, MKN-28.

2. MATERIALS AND METHODS

2.1. Purification of anthocyanin from red fruits and vegetables

The extraction methodology was the same used on the experiments of Chapters I and II. Briefly, grape skin anthocyanins (*Vitis vinifera*) were extracted with an aqueous solution of methanol (1:1) acidified with HCl, for 2 days at room temperature. The *Vitis vinifera* grape anthocyanin extract was filtered in a 50 μm nylon membrane and then purified by TSK Toyopearl gel column (250 x 16 mm i.d.) chromatography according to the procedure described previously [205]. The extract was freeze-dried and stored at -18º C until use.
Purple fleshed sweet potatoes (PFSP) were cut in slices and anthocyanins were extracted in 70 % ethanol with ultra-sound assistance for 1 h. The obtained extract was centrifuged at 2,800 x *g* for 15 min to remove insoluble materials. The resulting supernatant was filtered and phenolic acids removed with Liquid-Liquid extraction (ethyl acetate/water, 1:1). The resulting extract was applied on a XAD-7HP column. Water was used to remove proteins, sugars and other interfering materials, and methanol used to recover anthocyanins. The enriched anthocyanin fraction was applied on a C-18 column to remove any remaining sugars. The extract was freeze-dried and stored at -18º C until use.
Further HPLC preparative chromatography of the total anthocyanin extracts was performed to obtain purified Mv3glc, Pn3glc, Pn3HBsoph5glc and Pn3HBCsoph5glc. The purity and structural characterization of the three pigments was confirmed by HPLC-DAD-MS and NMR.

2.2. HPLC analysis

HPLC analysis of anthocyanins was performed on Dionex Ultimate 3000 (Thermo Scientific; USA) equipped with a 250 x 4.6 mm i.d. reversed-phase C18 column (Merck, Darmstadt, Germany). Detection was carried out at 520 nm using a diode array detector (DAD). The solvents were (A) H_2O/HCOOH (9:1) and (B) H_2O/HCOOH/CH_3CN (6:1:3). The gradient consisted of 20–52.5 % B for 35 minutes at a flow rate of 1.0 mL/min. The column was washed with 100 % B for 15 minutes and then stabilized at the initial conditions for another 15 minutes.

2.3. Au-nanoconjugate Synthesis and Characterization

Synthesis of AuNPs with 14 nm of diameter was performed by the citrate reduction method [246] and functionalization as previously described (Conde et al, 2013). AuNPs were functionalized with poly(ethylene glycol) (PEG) modified with a thiol group (AuNP@PEG) to obtain a 30% of coverage. AuNP@PEG were subsequently functionalized with antisense thiolated oligonucleotides for each target gene: *GLUT1*/*SLC2A1* 5'-GCTATGACATGAGGCGACCCGTCAGCTTCATAGC-3' and *GLUT3*/*SLC2A3* 5'-TTTCGGATCTAATTCAAGTCTTCAAGCCGAAA-3' (palindromic sequence underlined) (AuNP@PEG@anti-*GLUT1* and AuNP@PEG@anti-*GLUT3*). Au-nanoconjugates were prepared at a 1:100 ratio (AuNP:oligonucleotide) and centrifuged at 14,000 x *g* for 40 minutes, the precipitate was washed three times with RNAse free water. The number of oligonucleotides bound to the surface of AuNPs was determined using Quant-iT Oligreen ssDNA reagent (ThermoFisher Scientific). The Au-nanoconjugates were stored at 4°C in the dark and characterized by UV-Vis spectroscopy, Transmission Electron Microscopy (TEM) and Dynamic Light Scattering (DLS).

2.4. Cell culture

The MKN-28 cells originating from human gastric epithelium were kindly provided from IPATIMUP (Porto, Portugal). Cells were maintained in RPMI medium (RPMI 1640 (LifeTechnologies) supplemented with 10 % (v/v) fetal bovine serum (FBS, LifeTechnologies), non-essential aminoacids (MEM, LifeTechnologies) and mixture of 100 U/mL Penicillin and 100 µg/mL Streptomycin (LifeTechnologies)), at 37 °C, 5 % (v/v) of CO_2 and 99 % (v/v) of relative humidity.

2.5. GLUT1 and GLUT3 silencing

MKN-28 cells ($2x10^5$) were initially seeded on 35 mm disks, and incubated for 24 h at 37 ºC, 5 % (v/v) CO_2 and 99 % (v/v) relative humidity to obtain a cell monolayer with 75 % confluence. Afterwards, the medium was replaced by fresh RPMI medium supplemented with AuNP@PEG@anti-*GLUT1* or AuNP@PEG@anti-*GLUT3* at an oligonucleotide concentration of 20 nM and 30 nM for 9 h, 12 h and 24 h. For control purposes, cells were challenged in parallel with 0.63 nM AuNP@PEG, corresponding to 20 nM of

oligonucleotide (AuNPs:oligonucleotide ratio = 1:30), or 0.75 nM AuNP@PEG, corresponding to 30 nM of oligonucleotide (AuNPs:oligonucleotide ratio = 1:40).

After cell detachment using TrypleExpress (LifeTechnologies), cells were pelleted by centrifugation at 500 x *g* for 5 min at room temperature, and total RNA extracted using SV Total RNA Isolation System (Promega) according to the manufacture's protocol. cDNA was synthetized from total RNA (100 ng) using NZY M-MuLV First-Strand cDNA Synthesis kit (NZYtech) according to manufacturer's instructions.

Expression of *GLUT1* and *GLUT3* was evaluated using the Kapa SYBR Fast qPCR Master Mix (KAPABIOSYSTEMS) with the following primers at a final concentration of 0.08 µM each: *GLUT1* forward (5'-CAATGCTGATGATGAACCTG-3') and *GLUT1* reverse (5' –GGGATGAAGATGATGCTCA-3'); *GLUT3* forward (5' –ATGGGGACACAGAAGGTCACC-3') and *GLUT3* reverse (5' –AGCCACCAGTGACAGCCAAC-3'). The RT-qPCR was performed in a Corbett Rotor-Gene 6000 thermal cycler (QIAGEN) with the following conditions, initial denaturation at 95 °C for 5 min and 30 cycles of 95 °C for 45 seconds, 62 °C for 25 seconds and 72 °C for 45 seconds. Expression data were analyzed by the Ct method ($2^{-\Delta\Delta Ct}$) [247] using *GAPDH* as a housekeeping gene [248] and cells treated with AuNP@PEG as control. The two most commonly used methods to analyze data from real-time, quantitative PCR experiments are absolute quantification and relative quantification. Absolute quantification determines the input copy number, usually by relating the PCR signal to a standard curve. Relative quantification relates the PCR signal of the target transcript in a treatment group to that of another sample such as an untreated control. The $2^{-\Delta\Delta C}{}_T$ method is a convenient way to analyze the relative changes in gene expression from real-time quantitative PCR experiments. Three independent biological replicates were performed for each condition and a significative gene silencing result was considered when $2^{-\Delta\Delta Ct} < 0.5$, and *p-value* < 0.05 (using t-test in GraphPad Prism vs 6.0 software).

2.6. Simultaneous silencing of both transporters

After identifying the best conditions for the effective silencing of *GLUT1* or *GLUT3,* the most suitable strategy for silencing both genes under the conditions required for transport studies was evaluated. MKN-28 cells were seeded in 24 well plates with a density of $1x10^5$ cells/mL in RPMI medium. Cells were incubated for 5 days at 37 ºC, 5 % (v/v) CO_2, 99 % (v/v) relative humidity, and the medium changed by fresh medium every two days. After

reach a uniform layer of cells covering the bottom of the well, cells were challenged with RPMI medium supplemented with 5.5 mM fructose (Merck KGaA, Darmstadt, Germany) and: a) 30 nM AuNP@PEG@anti-*GLUT1* (AuNP@GLUT1 condition), b) 20 nM AuNP@PEG@anti-*GLUT3* (AuNP@GLUT3 condition), c) 30 nM AuNP@PEG@anti-*GLUT1* + 20 nM AuNP@PEG@anti-*GLUT3* (AuNP@GLUT1+3 condition), d) 0.75 nM AuNP@PEG (AuNP@PEG1 condition, control of a)), e) 0.63 nM AuNP@PEG (AuNP@PEG3 condition, control of b)), or f) 1.38 nM AuNP@PEG (AuNP@PEG1+3 condition, control of c)). For control purposes, cells were also challenged with RPMI medium supplemented only with 5.5 mM fructose. After 24 h of incubation, cells were collected (24 h time point) or the medium replaced by fresh medium supplemented with the same concentration of nanoparticles as used before and collected after an additional 24 h of incubation (24h + 24 h time point). To collect cells, the medium was discarded, the cells were washed 3 times with Phosphate Buffer Saline (PBS), and scraped from the bottom in 500 µL PBS. After a 5 min centrifugation at 500 x *g*, pelleted cells were solubilized in lysis buffer [150 mM NaCl, 50 mM Tris-HCl, pH 8.0, 5 mM ethylenediaminetetraacetic acid (EDTA), 2 % (v/v) NP-40, 1 x Phosphatase inhibitor (PhosStop, Roche), 1 x Proteases inhibitors (complete Mini, Roche), 1 mM Phenylmethylsulfonyl fluoride (PMSF) and 0.1 % (w/v) 1,4-Dithiothreitol (DTT)] for protein extraction, or in PBS for *GLUT1* and *GLUT3* expression evaluation performed as described above.

2.7. Western Blot for GLUT1 and GLUT3 quantification

Pelleted cells solubilized in lysis buffer were incubated for at least 2 h, at – 80 ºC, and subjected to 5 cycles of 2 min and 30 sec of ultrasounds with 30 sec intervals on ice between each cycle. Total extracts were then centrifuged (750 x *g*, 5 min) and supernatant was transferred to a new clean tube. The total amount of protein of each sample was quantified using Pierce 660 nm protein assay kit (Thermo Scientific) according to the manufacturer instructions, and 10 µg protein was used for the Western-Blot analysis. Protein extracts were first separated in a Sodium Dodecyl Sulfate polyacrylamide gel electrophoresis (SDS-PAGE) using a 10 % (w/v) polyacrylamide gel with a 37.5:1 of acrylamide:bisacrylamide ratio (Merck Millipore) and then transferred onto a 0.45 µm PVDF membrane (GE Healthcare). After blocking membrane with 5 % (w/v) low fat milk in TBST (50 mM Tris-HCl, pH 7.5, 150 mM NaCl, 0.1 % (w/v) Tween-20), the blots were

incubated for 1 h with a 1:200.000 dilution of GLUT1 antibody [EPR3915] (ab115730, Abcam) or with a 1:15.000 dilution of GLUT3 antibody [EPR10508(N)] (ab191071, Abcam), washed 3 times for 5 min with TBST, incubated another 1 h with 1:2.000 dilution of anti-IgG rabbit HRP-linked antibody (ref. 7074, Cell Signalling), washed again 3 times (5 min) with TBST and treated with WesternBright ECL (Advansta, USA) for signal acquisition in a Hyperfilm ECL (GE Healthcare). After stripping (0.1 M glycine, 20 mM magnesium acetate, 50 mM KCl, pH 2.2) and washing 3 times for 5 min with TBST, the membranes were blocked with 5 % (w/v) low fat milk in TBST, incubated for 1 h with a 1:5.000 dilution of β-actin antibody (ref A5441, Sigma), washed 3 times for 5 min with TBST, incubated for 1 h with 1:3.000 dilution of anti-IgG mouse HRP-linked antibody (ref. 7076, Cell Signalling), washed 3 times for 5 min with TBST and treated with WesternBright ECL (Advansta, USA) for signal acquisition in a Hyperfilm ECL (GE Healthcare). The percentage of area of the protein band on each sample was measured using ImageJ2 software.

The percentage of GLUT1 or GLUT3 in each sample was calculated by normalizing to the internal control (β-actin) and the corresponding control (cells treated with AuNP@PEG).

2.8. Transport studies

Transepithelial transport experiments were performed using a similar procedure from the one described elsewhere [238] and in accordance with the methods performed in Chapter II. Briefly, MKN-28 cells grown on polycarbonate transwell permeable inserts, 12 mm diameter, 0.4 μm pore size (Corning Costar, Corning, NY) at 75 % confluence. Cells were cultured at 37 °C in an atmosphere of 5% CO_2 and the medium was changed every two days. At 7 days MKN-28 cells were fully confluent and differentiated, so the transport experiments were initiated at that time. Experiments were conducted only in MKN-28 cell monolayers that showed a TEER > 150 $\Omega.cm^2$ (determined at 37 ºC) measured using MILLICELL-ERS epithelial voltammeter (Millipore Co., Bedford, MA) with “chopstick” electrodes.

Before transport experiments and to further confirm that the addition of nanoconjugates did not affect cellular barrier integrity and cells toxicity, MKN-28 cells were seeded on 6.5 mm transwell inserts, 0.4 μm pore size, using 8W TransFilter Adapter of ECIS system (Applied Biophysics, Troy, NY, USA). Cells were grown to confluence and transepithelial electrical resistance (TEER) was continually measured.

To further confirm the silencing efficacy of the nanoconjugates at the protein level in the transwell plates, cells were gently detached from the transwell membrane with PBS, centrifuged (500 x *g* for 5 min) and solubilized in lysis buffer for Western-Blot procedure, as described above.

After this treatment, media was removed and cells were washed with Hanks' medium (HBSS), pH 7.4 at the basolateral side and with HBSS pH 5.0 at the apical side. Anthocyanin solution (500 μM) in HBSS pH 5.0 was added to the apical side of the cells and HBSS containing 2 % fetal bovine serum free of polyphenols was added to the basolateral compartment. Transepithelial transport was followed as a function of time, at 4ºC and 37 ºC. Samples were taken from the basolateral side and replaced by fresh medium. The samples (150 μL) were acidified with HCl 6 M to a final concentration of 1 % and frozen at -18 ºC until HPLC analysis.

2.9. Molecular Docking

The crystal structures of human glucose transporters GLUT1 (PDBID: 4PYP, at 3.2 Å of resolution) [249] and GLUT3 (PDBID: 4ZW9, at 1.5 Å of resolution [250] were used to build the two systems. The GLUT1 transporter is in an inward-facing conformation and it is bound to a glucose analogue (*n*-nonyl-β-D-glucopyranoside (β-NG)), while GLUT3 is bound to D-glucose in an outward-occluded conformation. All crystallographic water and ligand molecules were removed, and polar hydrogen atoms were added considering the protonation state of the residues at physiological pH. The structures of the three anthocyanins (Pn3glc, Pn3HBsoph5glc and Pn3HBCsoph5glc) were build using the GaussView software [251].

Ligand:protein docking calculations were performed with the VsLab software [252] that uses the AutoDock 4.2 software [253] to run the docking calculations and the VMD 1.9.2 program for visual inspection and analysis [254].

The grid maps were centered into the glucose unit and comprised 54x54x70 points of 0.375 Å spacing. The Lamarckian genetic algorithm was employed (population size of individuals: 150; maximum number of energy evaluations: $2.5x10^6$; and maximum number of generations: 27000). For all the calculations, 50 docking rounds were performed with step sizes of 2.0 Å for translations and with orientations and torsions of 5.0°. Kollman partial charges were assigned to all transporters' atoms. All docking conformations were clustered within 2.0 Å root-mean-square-deviations (RMSD) to prevent similar poses.

To validate the docking protocol, we employed our docking procedure for D-glucose, for which there was X-ray structural information considering both transporters (only the D-glucopyranoside atoms from the crystal GLUT1:sugar structure were considered). Figure 66 shows the superposition of both geometries (X-ray and top-ranked docking pose) for the two transporters. Considering the small RMSD values for the sugar heavy atoms, when comparing both the X-ray and top-ranked docking poses (2.4 Å and 2.6 Å, respectively), we deemed our docking procedure fit for describing the correct binding mode of D-glucose. Hence, they were used to evaluate the binding mode and affinities of the three phenolic compounds under evaluation. All docking poses were ranked by the binding energy values, and the protein-ligand complexes with the best energetic scores were taken as starting structures for the subsequent molecular dynamics (MD) simulations.

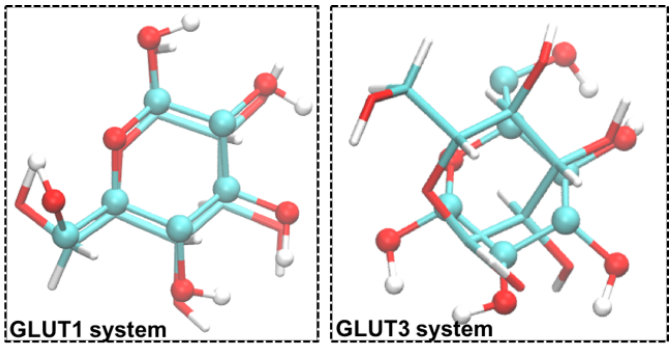

Figure 66. Superposition of the crystallographic molecules (D-glucopyranoside of D-NG and D-glucose for GLUT1 and GLUT3, respectively; depicted in licorice) with the top-ranked D-glucose docking pose (depicted in balls-and-sticks).

2.10. Molecular Dynamics (MD) simulations

Based on energetic and structural criteria, the most favorable binding pose from the previous docking protocol, and considering each distinct transporter: ligand complexes, was incorporated into a POPC bilayer system, with 80 POPC lipids per layer. A hydration level close to 50 water molecules per lipid, and an ionic concentration of 0.15 M of NaCl was employed. Both membrane:GLUT-transporter models were constructed with the CHARMM-GUI webserver [255]. Figure 67 illustrates the entire system used in the MD simulations for both GLUT1 and GLUT3 transporters.

The antechamber tool was used to parametrize the ligands, which were optimized with the HF/6-31G(d) level of theory by using the Gaussian 09 software [256]. The RESP algorithm [257] was used to calculate the atomic point charges to be employed in the MD simulations. The ff99SB [258], GAFF [259], and SLIPIDS [260] force fields were used to

characterize the proteins, the ligands and the membrane components, respectively. The TIP3P water model was employed. The starting geometry of each complex was minimized and equilibrated for 20 ns (with position restraints on protein atoms). Subsequently, the restraints were removed and each system was simulated for 100 ns. The SHAKE algorithm was applied to all bonds with hydrogen atoms [261], which allowed for a 2 fs time-step using the Verlet leapfrog algorithm. Temperature and pressure were set to 310 K and 1 atm with the Langevin thermostat [262] and the Berendsen barostat, respectively. Periodic boundary conditions were considered. A non-bonded cut-off value of 10 Å was used. Long-range electrostatic interactions were treated by a particle-mesh Ewald scheme [263]. All simulations were carried out using the PMEMD module, implemented in the AMBER 12.0 simulations package [264]. The results were analyzed with the CPPTRAJ tool [265], and simulations were visually inspected with the VMD 1.9.2 program [254].

The binding free energy values between the polyphenolic compounds and each GLUT transporter were determined using the Molecular Mechanics/Poisson Boltzmann Surface Area (MM/PBSA) approach [266]. 160 structures of each molecular complex were extracted over the last 80 ns of each MD simulation for analysis.

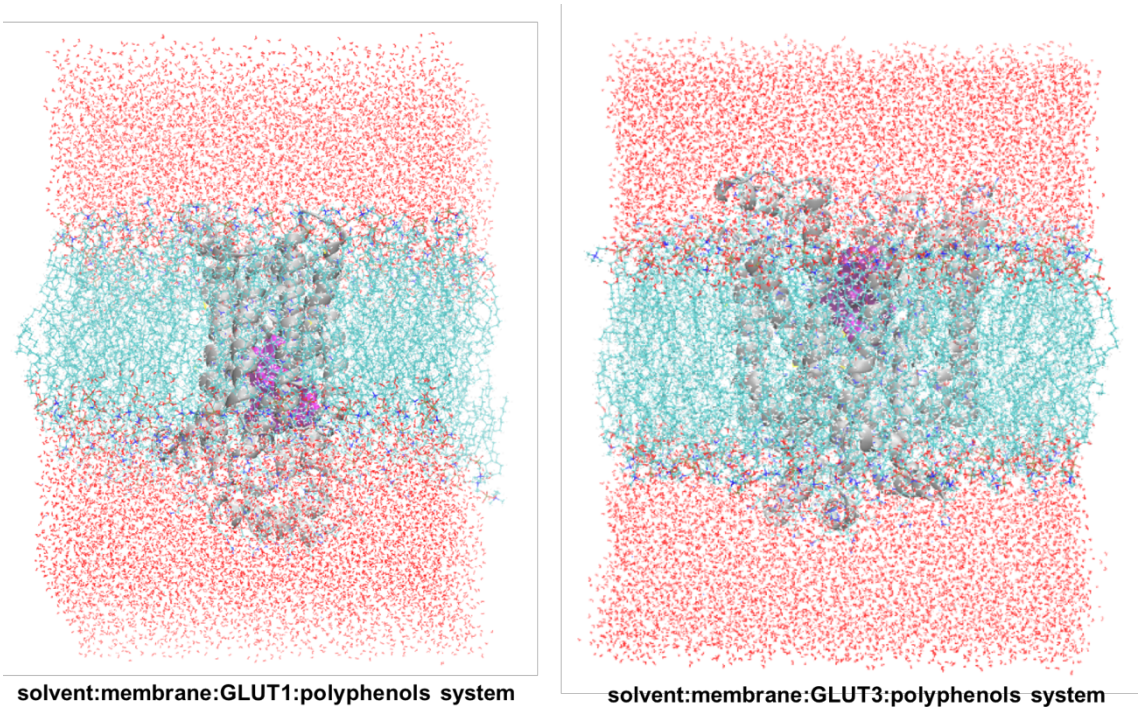

Figure 67. Representation of the entire systems used in the MD simulations for both GLUT1 and GLUT3 transporters. The glucose transporters are represented in cartoon and colored in gray, while the polyphenol compounds are represented as a purple surface. The bilayer atoms are depicted with sticks and colored by atom type, whilst the solvent molecules represented in lines and colored by atom type.

2.11. Statistical analysis

All data was expressed as mean ± SEM from at least three independent experiments. Two-way ANOVA with Bonferroni's multiple comparisons test and t-student test were performed using GraphPad Prism version 7.00 (GraphPad Software, San Diego California USA). Statistical significance was considered when $p < 0.05$.

3. RESULTS

3.1. Effect of temperature in the transport of anthocyanins through MKN-28 gastric barrier

Natural anthocyanins are glycosylated flavonoids. In this study Malvidin-3-*O*-glucoside (Mv3glc) and Peonidin-3-O-glucoside (Pn3glc) have a glucose moiety at the C3 position and purple fleshed sweet potato (PFSP) anthocyanins have a glucose moiety at the C5 position and two additional glucoses at C3.

The structures of the red wine anthocyanins Mv3glc and Pn3glc and the two main anthocyanins from PFSP Peonidin-3-(hydroxybenzoyl)-sophoroside-5-glucoside (Pn3HBsoph5glc) and Peonidin-3-(6'-hydroxybenzoyl-6''-caffeoyl)-sophoroside-5-glucoside (Pn3HBCsoph5glc) are presented in Figure 68.

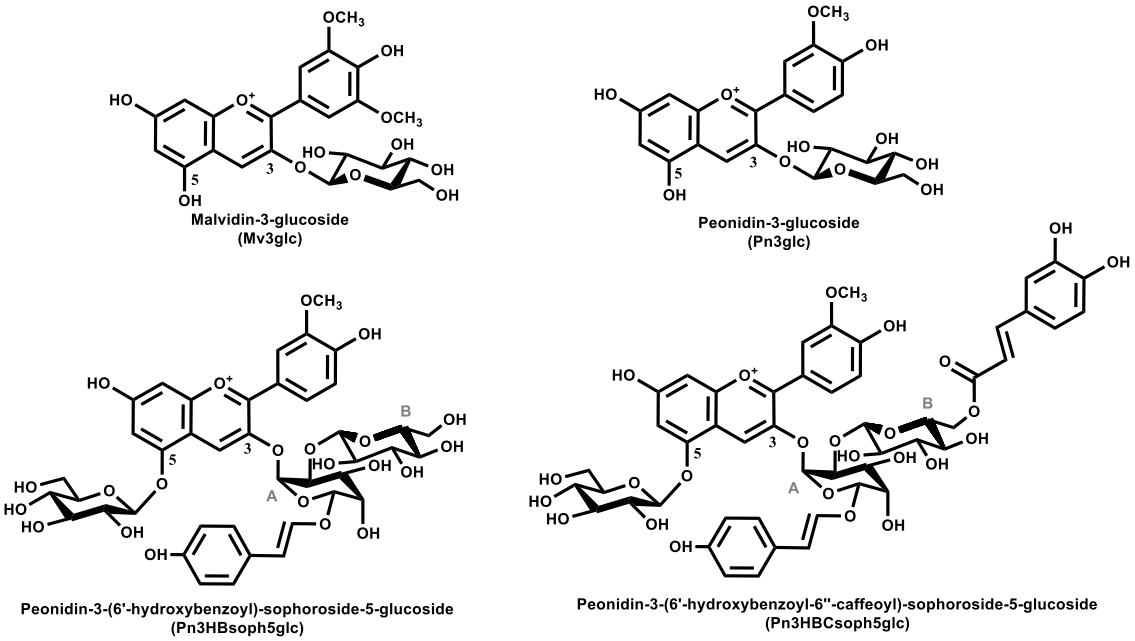

Figure 68. Chemical structures of the four anthocyanins assayed in the transepithelial transport studies.

In the case of anthocyanidins (anthocyanins lacking glucose) the hypothesis of transport by passive diffusion can be raised due to their higher hydrophobicity, but this hypothesis is not viable for anthocyanins due to the presence of the glucose moiety. It is highly unlikely for the glucose molecule to cross the cell membrane without a transporter system.

To demonstrate this, Mv3glc, Pn3glc and PFSP anthocyanins gastric transport was evaluated in MKN-28 cell barrier at 4 ºC and 37 ºC. The results obtained at 4 ºC showed that the paracellular transport efficiency is below 2 % (Figure 69). Therefore, these results demonstrate that anthocyanins were actively transported by MKN-28 cells. Since glucose transporters had already been suggested as the main transporters involved in the absorption of these pigments [239], the effect of their inhibition was further evaluated using a nano-based approach.

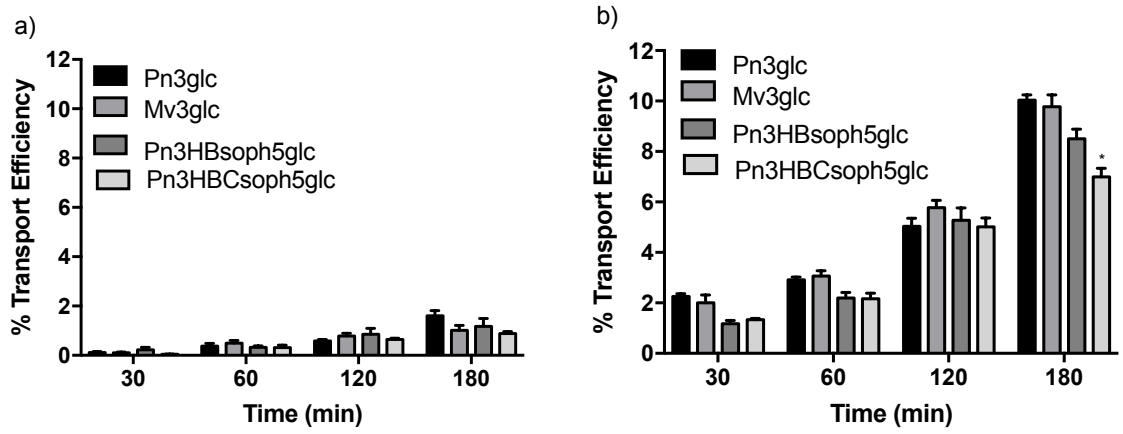

Figure 69. Transport efficiency of Pn3glc, Mv3glc, Pn3HBsoph5glc and Pn3HBCsoph5glc through MKN-28 barrier (Apical → Basolateral) at A) 4 ºC and B) 37 ºC. The experiments were conducted with apical pH 5.0 and basolateral pH 7.4. Results are presented as transport efficiency (%) (mean ± SEM). Transport efficiency percentages were calculated based on (compound concentrations at the basolateral side overtime)/(compound concentrations at the apical side at the zero hours)*100.

3.2. Gold nanoparticle synthesis and characterization

Stable AuNPs with an average diameter of 14 ± 1 nm (Figure 70) were synthesized and functionalized with a PEG spacer for increased stability and biocompatibility [242, 267]. These AuNP formulations represented the basic nanoparticle constructs for downstream functionalization with the respective antisense oligonucleotide sequences, targeting *GLUT1* and *GLUT3* mRNAs. In presence of the complementary sequence, the ssDNA hybridizes with the mRNA, forming a double stranded structure inhibiting the translation of mRNA into protein [268, 269].

The nanoconjugates were characterized by Transmission Electron Microscopy (TEM), UV-Vis spectroscopy, and Dynamic Light Scattering (DLS) (Figure 70). Data show an increase in the hydrodynamic radius after each step of functionalization with values of 19

nm for AuNPs, 21.5 nm for AuNP@PEG, and 31 nm for both AuNP@PEG@anti-*GLUT1* and AuNP@PEG@anti-*GLUT3*, indicating a successful functionalization. The antisense oligonucleotide coverage was determined by fluorescence-based assay with a final 1:40 and 1:30 AuNPs to oligonucleotide ratio for *GLUT1* and *GLUT3*, respectively.

	TEM (nm)	SPR Peak	DLS size(nm)
AuNPs	14 ± 1	520	19
AuNP@PEG	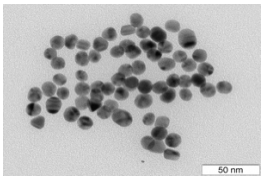	521	21.5
AuNP@PEG@anti-*GLUT1*		524	31
AuNP@PEG@anti-*GLUT3*		524	31

Figure 70. Characterization of gold nanoconjugates. Gold nanoparticles (AuNPs), AuNPs functionalized with 30 % PEG (AuNP@PEG) and AuNP@PEG functionalized with anti-GLUT1 (AuNP@PEG@anti-GLUT1) or anti-GLUT3 (AuNP@PEG@anti-GLUT3) through Transmission Electron Microscopy (TEM), Dynamic Light Scattering (DLS) and UV-Vis (Surface Plasmon Resonance, SPR peak).

3.3. GLUT1 and GLUT3 gene silencing and effect at the protein level

The most suitable conditions for *GLUT1* and *GLUT3* gene silencing (time and concentration of the silencing moieties) in the MKN-28 cell line were determined. A concentration of 30 nM of nanoconjugates induces a more noticeable down-regulation of *GLUT1*, while a concentration of 20 nM induces a higher down-regulation of *GLUT3* expression after 24 h of incubation (Figure 71).

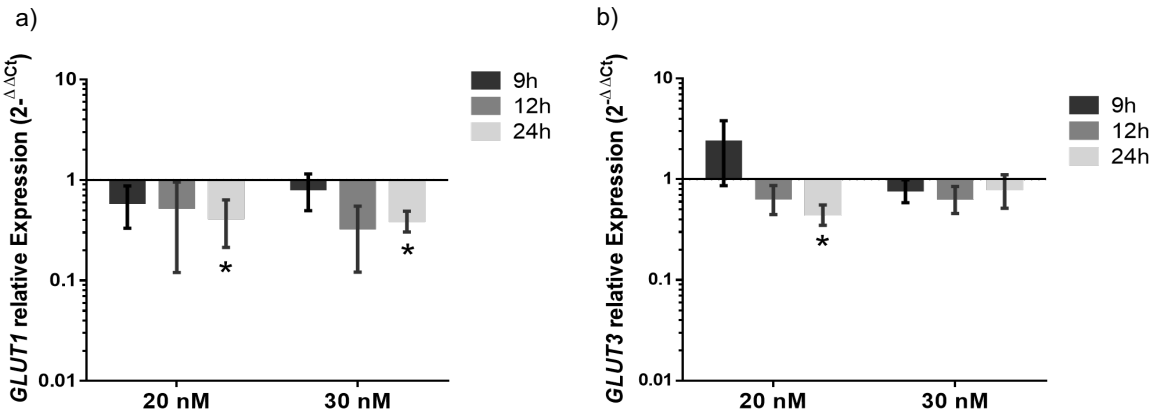

Figure 71. a) GLUT1 relative expression in MKN-28 cells incubated with 20 nM or 30 nM gold nanoparticles functionalized with 30 % PEG and anti-GLUT1 (AuNP@PEG@anti-GLUT1) for 9 h, 12 h and 24 h at 37 °C, 5 % (v/v) CO_2 and 99% (v/v) relative humidity. b) GLUT3 relative expression in MKN-28 cells incubated with 20 nM or 30 nM gold nanoparticles functionalized with 30 % PEG and anti-GLUT3 (AuNP@PEG@anti-GLUT3) for 9 h, 12 h and 24 h at 37 °C, 5 % (v/v) CO_2 and 99% (v/v) relative humidity. Gene expression variation is calculated via $2^{-\Delta\Delta Ct}$, using as reference GAPDH gene. Error bars represents SEM of at least three independent experiments. * p-value < 0.05 relative to relative expression at 9h incubation of corresponding sample.

Afterwards, the silencing efficacy of the nanoconjugates under the conditions required for transport studies was evaluated at the mRNA and protein levels. Figure 72 shows a decrease in the expression of *GLUT1* and *GLUT3* genes in the presence of all nanoconjugates (AuNP@GLUT1, AuNP@GLUT3 or AuNP@GLUT1+3) and for both time points (24 h or 24 h+24 h). However, the decrease of *GLUT1* expression was more pronounced in the presence of AuNP@GLUT1 and AuNP@GLUT1+3 nanoconjugates (compared to control (cells exposed to the same AuNP@PEG concentration)) (Figure 72A). Concerning *GLUT3* gene expression, the decrease was more pronounced in MKN-28 cells incubated with AuNP@GLUT3 and AuNP@GLUT1+3 nanoconjugates (compared to control) (Figure 72B). In this latter, the decrease of GLUT3 gene expression was more pronounced after 24 h + 24 h incubation period (Figure 72B).

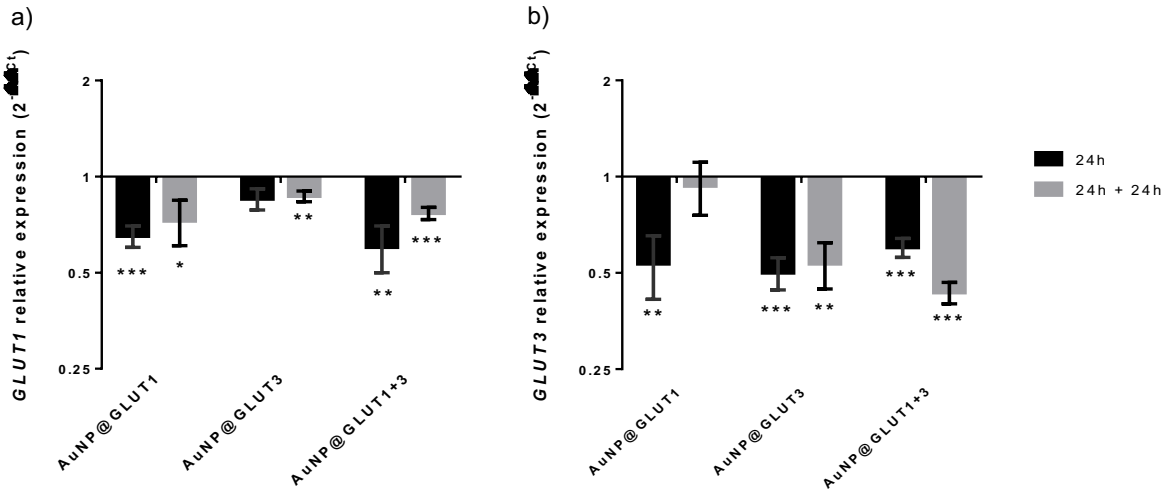

Figure 72. *GLUT1* (a) and *GLUT3* (b) relative expression in MKN-28 cells incubated for 24 h (black bars) or 24 h + 24 h (grey bars) with fresh RPMI medium supplemented with 5.5 mM fructose and 30 nM AuNP@GLUT1, 20 nM AuNP@GLUT3, or a mixture of AuNP@GLUT1+3. After 24 h cells were collected or incubated for an additional 24 h with fresh medium supplemented according to the first incubation. Gene expression was calculated through $2^{-\Delta\Delta Ct}$, using as internal reference *GAPDH* gene, and normalized to respective control samples consisting in MKN-28 cells treated with RPMI medium supplemented with 5.5 mM fructose and 0.75 nM AuNP@PEG (control of AuNP@GLUT1), 0.63 nM AuNP@PEG (control of AuNP@GLUT3), or 1.38 nM AuNP@PEG (control of AuNP@GLUT1+3), and collected at the same time point. Error bars represent the SEM of at least three independent experiments. * p-value < 0.5, ** p-value< 0.005, *** p-value < 0.0005.

Expression of GLUT1 protein further demonstrate the silencing efficacy at the gene expression level, where a decrease of expression at 24 h + 24 h was also observed in cells incubated with AuNP@GLUT1 and AuNP@GLUT1+3 nanoconjugates (decrease of 0.4 and 0.6-fold, respectively, compared to control) (Figure 73A and 73C). However, for the same incubation period, the amount of GLUT3 protein decreases slightly when cells were stimulated with the AuNP@GLUT1+3 nanoconjugate (Figure 73B and 73D). The only exception to this trend was a higher reduction at the protein level observed for the first 24 h incubation period with the AuNP@GLUT3 nanoconjugate.

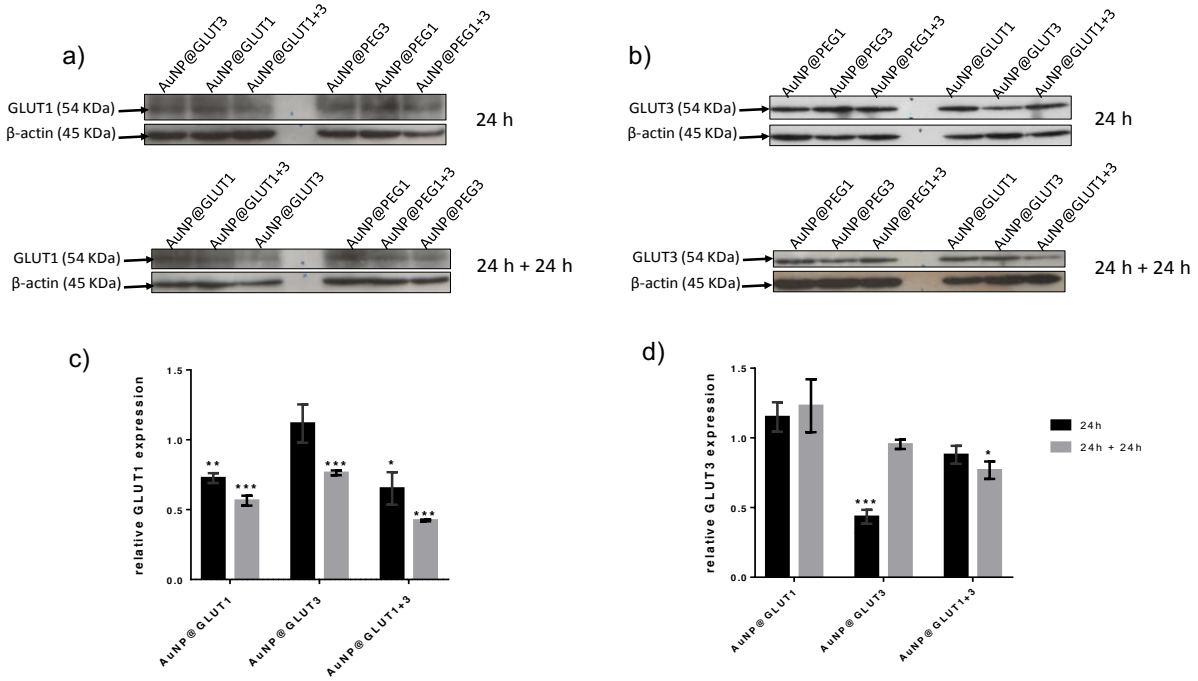

Figure 73. a) Western Blot analysis of GLUT1 and β-actin proteins; b) Western Blot analysis of GLUT3 and β-actin proteins. Represented Western Blots correspond to 10 µg total protein of MKN-28 cells grown on 24 well plates and incubated for 24 h with fresh RPMI medium supplemented with 5.5 mM fructose and 0.75 nM AuNP@PEG1, 0.63 nM AuNP@PEG3, 1.38 nM AuNP@PEG1+3, 30 nM AuNP@GLUT1, 20 nM AuNP@GLUT3, or a mixture of AuNP@GLUT1+3. After this 24 h period, cells were incubated for an additional 24 h with fresh medium supplemented according to the first incubation. c) GLUT1 relative intensity values normalized to corresponding intensity of β-actin protein and to the corresponding AuNP@PEG control sample. d) GLUT3 relative intensity values normalized to corresponding intensity of β-actin protein and to the corresponding AuNP@PEG control sample. Error bars represents SEM of at least three independent experiments. The grey line on the border of blots represent the place where images were cropped. Full length blot images can be found in Attachment III. * p-value < 0.5, ** p-value< 0.005, *** p-value < 0.0005.

To understand whether the GLUT1 and GLUT3 protein expression variation pattern could be translated to assays using transwell plates, MKN-28 cells were cultured in transwell plates, submitted to the same treatment as described above and analysed after 24 h + 24 h incubation. The incubation period (24 h + 24 h) was selected based on the higher reduction of both gene and protein expression for GLUT1 and GLUT3.

Under these conditions, a more pronounced decrease of both GLUT1 and GLUT3 proteins expression is observed in all analysed samples, and a 70 % decline of GLUT1 and GLUT3 expression in the presence of AuNP@GLUT1 and AuNP@GLUT3 nanoconjugates was observed (Figure 74). The decreased abundance of these proteins is consistent with the

inhibition of the *GLUT1* and *GLUT3* mRNA translation into proteins, suggesting an effective silencing mediated by AuNPs in the MKN-28 gastric barrier after 24 h + 24 h incubation and hence, further anthocyanins transport studies were performed in these conditions.

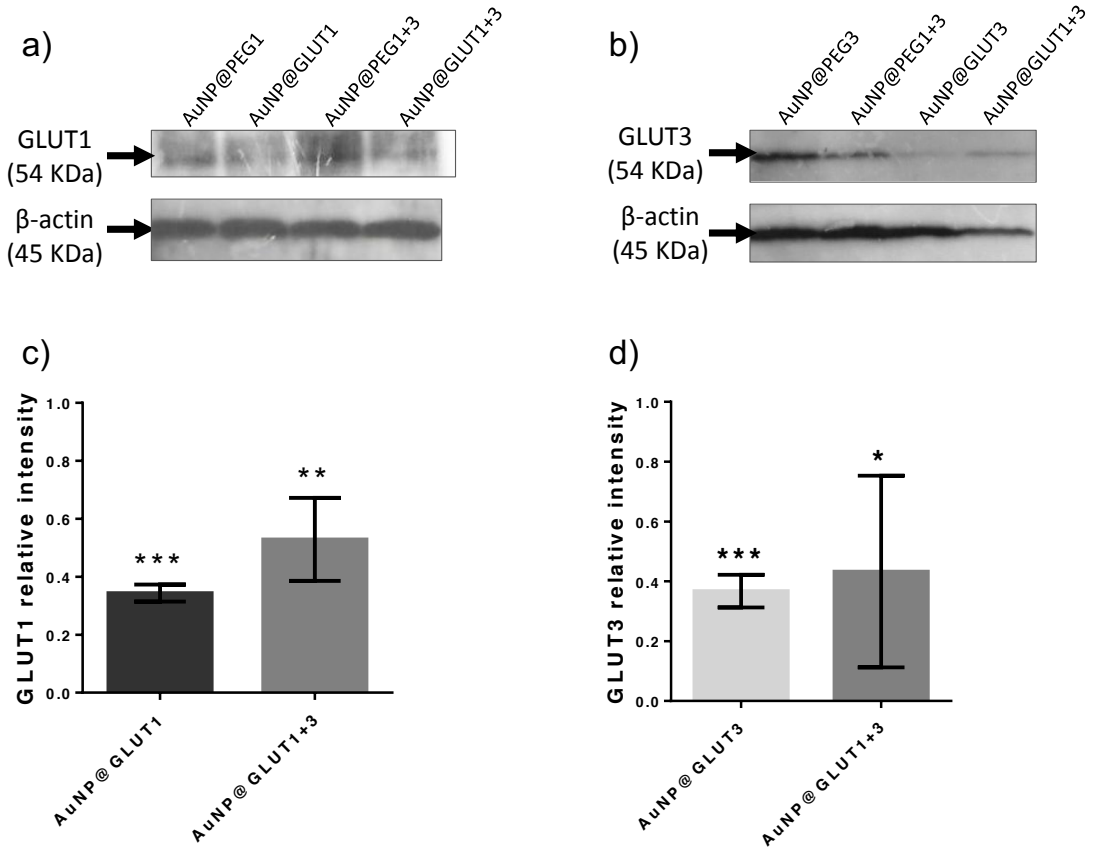

Figure 74. a) Western Blot analysis of GLUT1 and β-actin proteins; b) Western Blot analysis of GLUT3 and β-actin proteins. Represented Western Blots correspond to 10 μg total protein of MKN-28 cells grown on transwell plates and incubated for 24 h with fresh RPMI medium supplemented with 5.5 mM fructose and 0.75 nM AuNP@PEG1, 0.63 nM AuNP@PEG3, 1.38 nM AuNP@PEG1+3, 30 nM AuNP@GLUT1, 20 nM AuNP@GLUT3, or a mixture of AuNP@GLUT1+3. After this period of time, cells were incubated for an additional 24 h with fresh medium supplemented as previously. c) GLUT1 relative intensity values normalized to corresponding intensity of β-actin protein and to the corresponding AuNP@PEG control sample. d) GLUT3 relative intensity values normalized to corresponding intensity of β-actin protein and to the corresponding AuNP@PEG control sample. Error bars represents SEM of at least three independent experiments. The grey line on the border of blots represent the place where images were cropped. Full length blot images can be found in Attachment IV. * p-value < 0.5, ** p-value< 0.005, *** p-value < 0.0005.

3.4. Effect of glucose transporters inhibition on Mv3glc and PFSP anthocyanins transport

Mv3glc is the main anthocyanin present in red wine. Due to the similarity in the transport efficiencies between Mv3glc and Pn3glc and since both have a glucose moiety at the same position the following assays were performed only with Mv3glc and PFSP anthocyanins.

No toxicity and no barrier impairment was observed after incubation of MKN-28 cells for 24 h + 24 h in the presence of the nanoconjugates (Figure 75) which validates the nano-approach further applied.

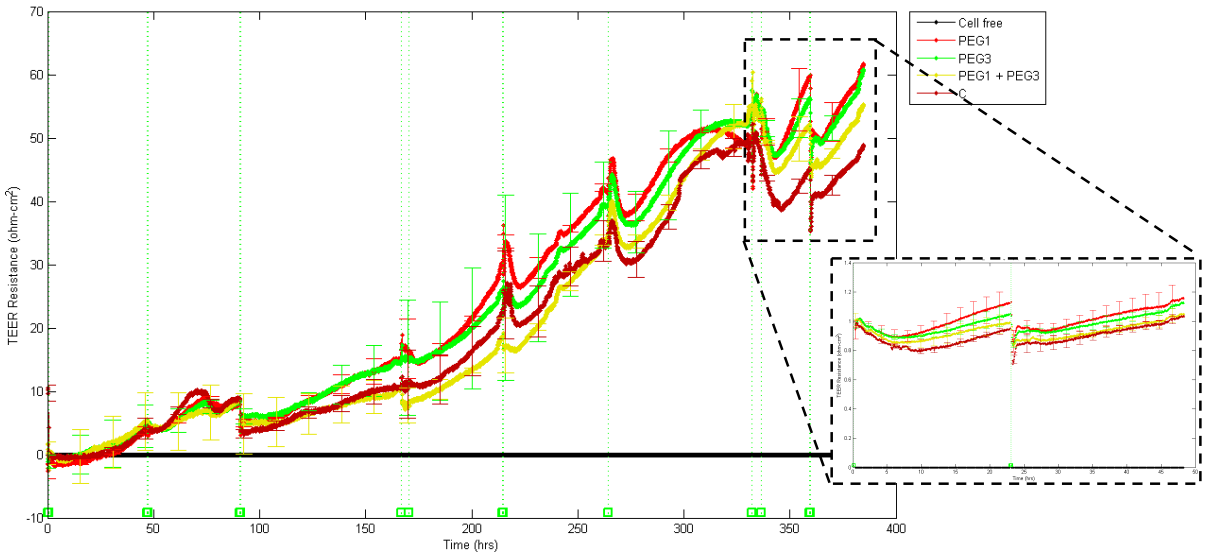

Figure 75. ECIS profile of MKN-28 cells during the incubation with gold nanoparticles for 24h+24h.

The transport of Mv3glc through the gastric cell barrier was evaluated after the incubation of MKN-28 cells for 24 h + 24 h in the presence of the nanoconjugates to induce the silencing of *GLUT1* and *GLUT3* genes. As observed in Figure 76A it is possible to conclude that both GLUT1 and GLUT3 transporters are involved in the uptake of Mv3glc, since a reduction of transport around 2 % was observed after 180 min in comparison with the respective control (AuNP@PEG). In addition, the inhibitory effect was much more pronounced and additive when both transporters were inhibited simultaneously (Figure 76B), suggesting a synergistic effect of GLUT1 and GLUT3 in mediating Mv3glc transport. Previous studies showed that *GLUT1* and *GLUT3* isoforms are present in MKN-28 gastric

cell line, being the latter the main one expressed [239]. The results highlight the implication of both isoforms, possibly due to the high homology degree between them.

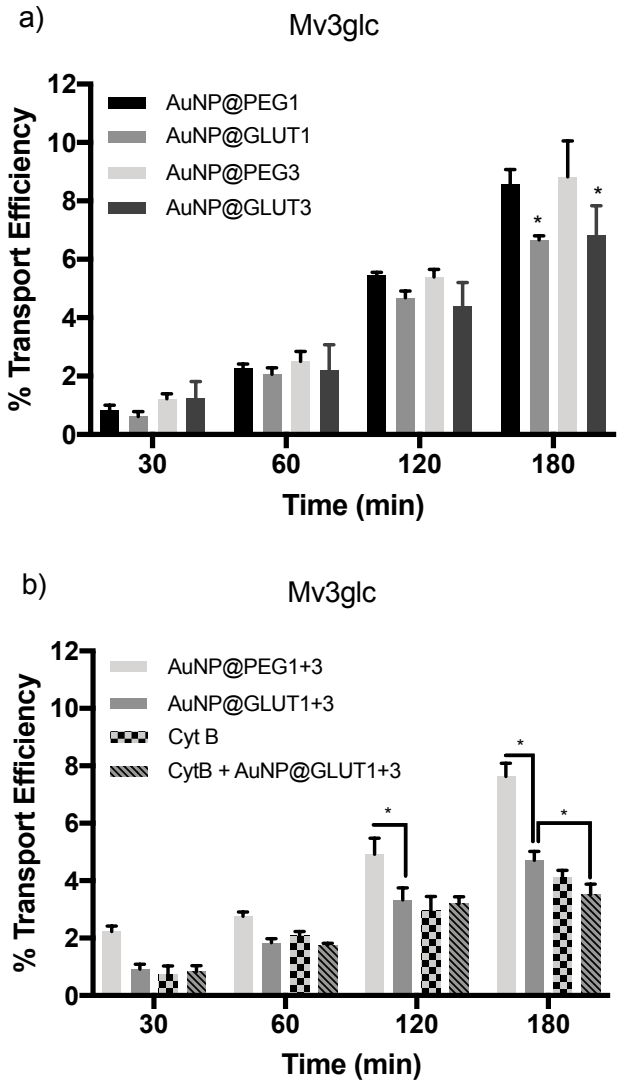

Figure 76. Transport efficiency of Mv3glc through MKN-28 barrier (Apical → Basolateral). The experiments were conducted with apical pH 5.0 and basolateral pH 7.4 in the presence of A) 30 nM AuNP@GLUT1, 20 nM AuNP@GLUT3, or 0.75 nM AuNP@PEG (control of AuNP@GLUT1) or 0.63 nM AuNP@PEG (control of AuNP@GLUT3), B) 1.38 nM AuNP@PEG (control of AuNP@GLUT1+3), a mixture of AuNP@GLUT1+3, Cythochalasin B (CytB, 50 μM) or a mixture of AuNP@GLUT1+3 and Cythochalasin B (50 μM). Significantly different from respective control *p<0.05.

The PFSP anthocyanins tested were transported through MKN-28 cell barrier with a kinetics that increased during incubation time, although the transport efficiency at 180 minutes (~7 - 8 %) was lower than the one observed for Mv3glc (~10 %). This difference

may result from the steric hindrance effect conferred by the additional sugar moieties and the esterification with the acyl groups at the C3 sophoroside moiety.

After treatment with AuNP@GLUT1 or AuNP@GLUT3, the two PSFP anthocyanins tested were less transported compared to the one observed for cells treated only with AuNP@PEG (Figure 77 and 78), revealing a similar trend to the one previously observed for Mv3glc (Figure 76). This reinforces the hypothesis of glucose implication in the absorption of these compounds, either at C3 or C5 position.

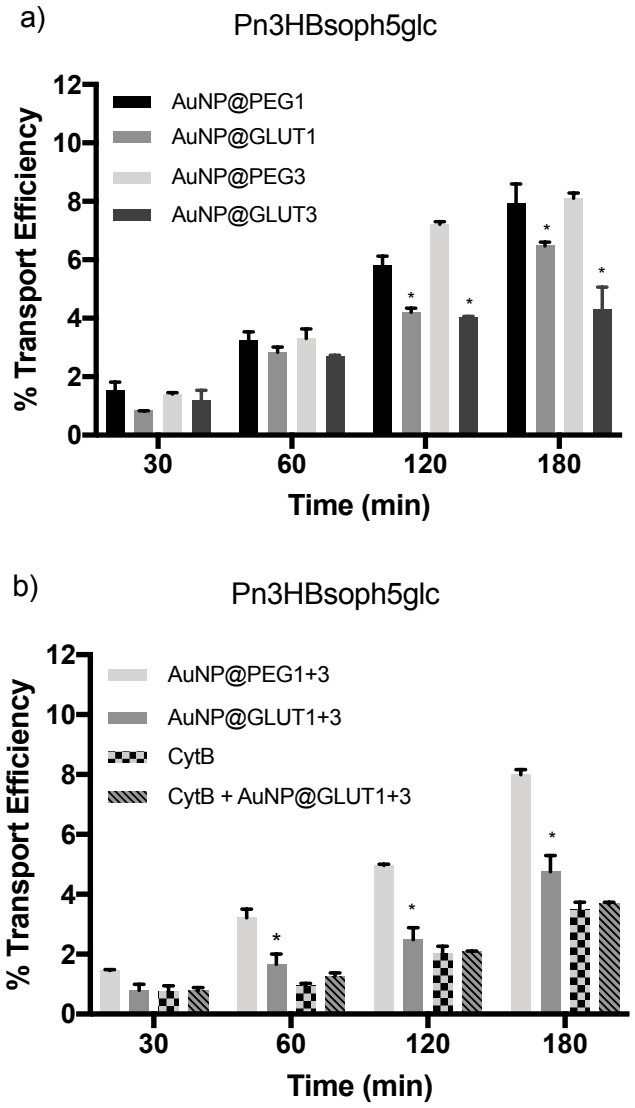

Figure 77. Transport efficiency of Pn3HBsoph5glc through MKN-28 barrier (Apical → Basolateral). The experiments were conducted with apical pH 5.0 and basolateral pH 7.4 in the presence of 30 nM AuNP@GLUT1, 20 nM AuNP@GLUT3, or 0.75 nM AuNP@PEG (control of AuNP@GLUT1) or 0.63 nM AuNP@PEG (control of AuNP@GLUT3), 1.38 nM AuNP@PEG (control of AuNP@GLUT1+3), a mixture of AuNP@GLUT1+3, Cythochalasin B (CytB, 50 μM) or a mixture of AuNP@GLUT1+3 and Cythochalasin B (50 μM). Significantly different from respective free oligonucleotide nanoparticle treatment * $p<0.05$

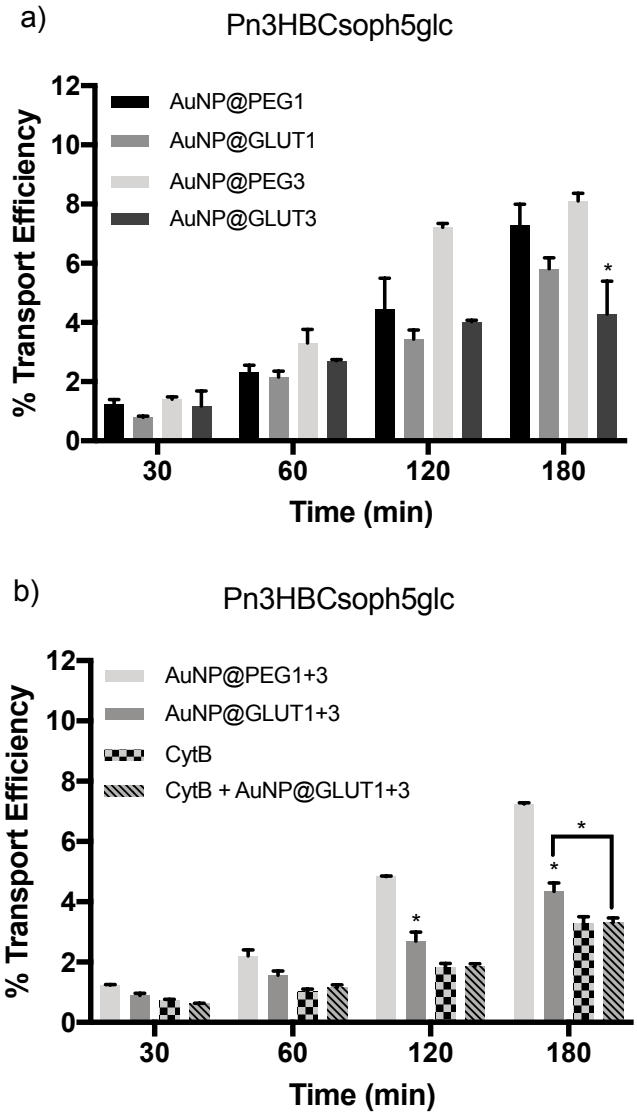

Figure 78. Transport efficiency of Pn3HBCsoph5glc through MKN-28 barrier (Apical → Basolateral). The experiments were conducted with apical pH 5.0 and basolateral pH 7.4 in the presence of 30 nM AuNP@GLUT1, 20 nM AuNP@GLUT3, or 0.75 nM AuNP@PEG (control of AuNP@GLUT1) or 0.63 nM AuNP@PEG (control of AuNP@GLUT3), 1.38 nM AuNP@PEG (control of AuNP@GLUT1+3), a mixture of AuNP@GLUT1+3, Cythochalasin B (CytB, 50 μM) or a mixture of AuNP@GLUT1+3 and Cythochalasin B (50 μM). Significantly different from respective free oligonucleotide nanoparticle treatment * $p<0.05$.

Since GLUT1 and GLUT3 are constitutively expressed at the cell apical membrane, part of the transport still observed after inhibition of the *de novo* synthesis by treatment with AuNP@GLUT1 and AuNP@GLUT3 may result from the implication of the constitutive fraction. Due to the absence of total reversion of transport efficiency to the levels observed at 4 ºC at the section 3.1 of the present Chapter (below 2 %), it was hypothesized that the constitutive glucose transporters could be the ones responsible for the transported anthocyanin to the basolateral side. This fact was confirmed by simultaneous addition of

cytochalasin B and AuNP@GLUT1+3. Since the inhibitory effect was higher in the presence of cytochalasin B, the constitutive transporters seem to have an implication for the net transport (Figures 76-78). Even in the presence of cytochalasin B, total reversion to the paracellular levels was not accomplished. Therefore, the possible contribution of other transporters to the amount transported to the basolateral side was assessed using other specific inhibitors.

3.5. Effect of organic transporters and efflux transporters inhibition

Additional studies were performed with Mv3glc using inhibitors of organic anion and cation transporters, since at pH 5.0 (pH of apical side) several anthocyanin forms may occur in equilibrium with other forms, including charged ones, such as quinoidal bases or flavylium cations [133] and also with efflux inhibitors.

Probenecid, an inhibitor of transmembrane organic anion transporters (OAT1) with expression in MKN-28 cell line [270] showed no effect on Mv3glc transport. In fact, at pH 5.0, a reduced amount of anionic species may be detected.

Atropin, an i*nhibitor of* organic cation *transporter* (*OCT1) and* verapamil known as a P-glycoprotein inhibitor, both expressed in MKN-28 cells [271, 272], were able to reduce the amount of Mv3glc detected in the basolateral side of the gastric barrier model. The first one may be related to the decrease of absorption of Mv3glc in the flavylium cation form and the latter with the inhibition of efflux transporters. As a consequence of efflux transporters inhibition, a cytosolic accumulation of Mv3glc may be indirectly inferred by the decrease in the amount observed in the basolateral side (Figure 79).

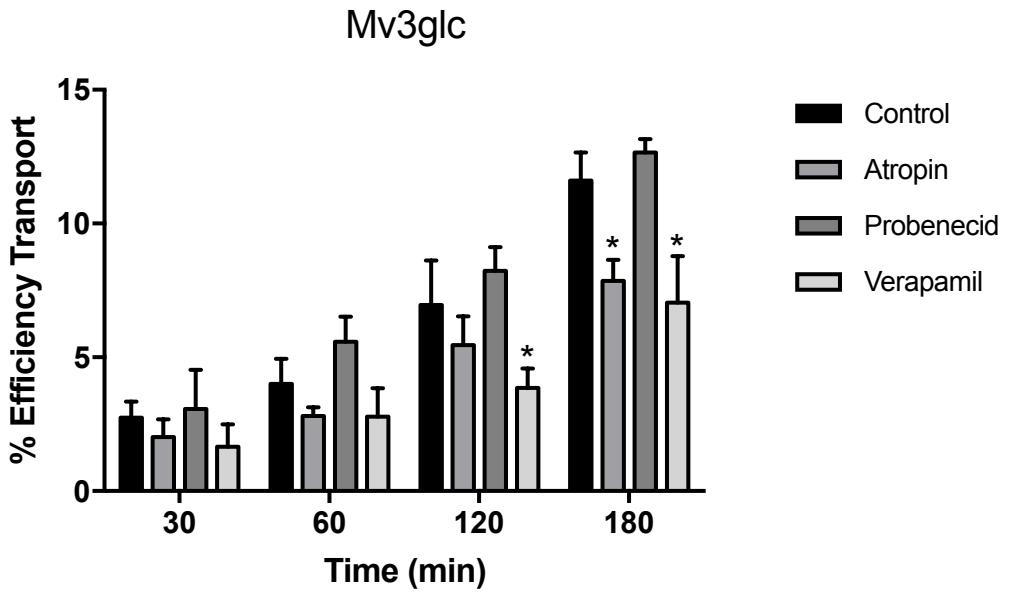

Figure 79. Transport efficiency of Mv3glc through MKN-28 barrier (Apical → Basolateral) in the presence of 50 μM of different inhibitors. The experiments were conducted with apical pH 5.0 and basolateral pH 7.4. Significantly different from control (AuNP@PEG) for the same incubation time * $p<0.05$.

3.6. Molecular Docking and Molecular Dynamics (MD) simulations

Due to the differences observed in the transport efficiency of the two PFSP anthocyanins compared with monoglucoside Pn3glc, different computational simulations were used to assess the implication of their complexity degree.

For that, the two PFSP anthocyanins were used with it precursor: Pn3glc, Pn3HBsoph5glc and Pn3HBCsoph5glc against both human GLUT1 and GLUT3 transporters, to perform molecular docking studies allied to molecular dynamics simulations. Once, as it was shown on Chapter I, the structure with higher prevalence at pH 5 (the pH value of the all the transepithelial transport experiments at the gastric level on the apical side) is the hemiketal neutral form, all the theoretical studies were performed with the anthocyanins in that form.

Table 16 shows the binding free energies for the top-two docking solutions of each complex. The energies and the binding mode of compounds Pn3HBsoph5glc and Pn3HBCsoph5glc are quite similar between the top-two docking solutions. For GLUT 1

the sophoroside moiety and the glucose at C5 seem to have a pivotal role on the interactions, while for GLUT 3 the hydroxybenzoyl group seems to have the main role. However, compound Pn3glc interacts with both GLUT receptors by its aromatic planar region (AC and B rings) or by the glucose unit (glc), which may be due to its small size. Considering the little difference of the binding free energy of the two docking solutions (S1 and S2) for all compounds (maximum difference of 1.4 kcal.mol^{-1}), only the first docking solutions were chosen to perform the MD simulations, in which each GLUT:ligand complex was simulated in a hydrated POPC bilayer model system.

Table 16. $\Delta G_{binding}$ values obtained for the three polyphenols docked into the GLUT1 and GLUT2 transporters. The groups that are inserted deeper into the GLUT channel were also indicated.

GLUT transporter	polyphenol	$\Delta G_{binding}$ / kcal.mol^{-1}	more buried groups
GLUT1	**Pn3glc: S1**	-12.2	AC and B
	Pn3glc: S2	-10.8	glc-C3
	Pn3HBsoph5glc: S1	-8.4	B and soph-C3
	Pn3HBsoph5glc: S2	-8.1	soph-C3
	Pn3HBCsoph5glc: S1	-14.2	AC and glc-C5
	Pn3HBCsoph5glc: S2	-13.8	glc-C5
GLUT3	**Pn3glc: S1**	-11.7	AC and B
	Pn3glc: S2	-10.7	glc-C3
	Pn3HBsoph5glc: S1	-13.4	glc-C5
	Pn3HBsoph5glc: S2	-13.0	hydroxybenzoyl and glc-C5
	Pn3HBCsoph5glc: S1	-11.2	hydroxybenzoyl
	Pn3HBCsoph5glc: S2	-10.9	hydroxybenzoyl

Figures 80 and 81 show the binding region of each GLUT1:polyphenol and GLUT3:polyphenol complex, respectively. Overall, it was observed that the polyphenols moieties that interact more deeply within both GLUT channels (first docking solution) are, mainly, the free glucoses and AC rings. The exceptions being Pn3HBCsoph5glc for GLUT3 docking and Pn3HBsoph5glc for GLUT1. This suggests that these groups may have a key role in the binding and translocation of these ligands through the two transporters. Interestingly, it was verified that the larger compounds (Pn3HBsoph5glc and Pn3HBCsoph5glc) showed frequent/stable intramolecular interactions, in which the phenolic rings establish π-π and CH-π stacking contacts. For example, compound Pn3HBCsoph5glc has three sets of intramolecular interactions when bound to both glucose transporters: i) the AC and glc-C5 rings establish a perpendicular π-π stacking

mode; ii) glc-C3 and hydroxybenzoyl rings interact through a perpendicular CH-π stacking; and iii) there is a parallel CH-π stacking of glc-glc-C3 and hydroxybenzoyl rings. In addition, the three sets of interactions maintain their overall orientation in both channels, where the first set of interactions is facing outwards and the last group of interactions is facing inward. These results suggest that the larger polyphenols should present a similar translocation mechanism. This agrees with the previous proposal for the anthocyanins crossing mechanism through human GLUT receptors [102].

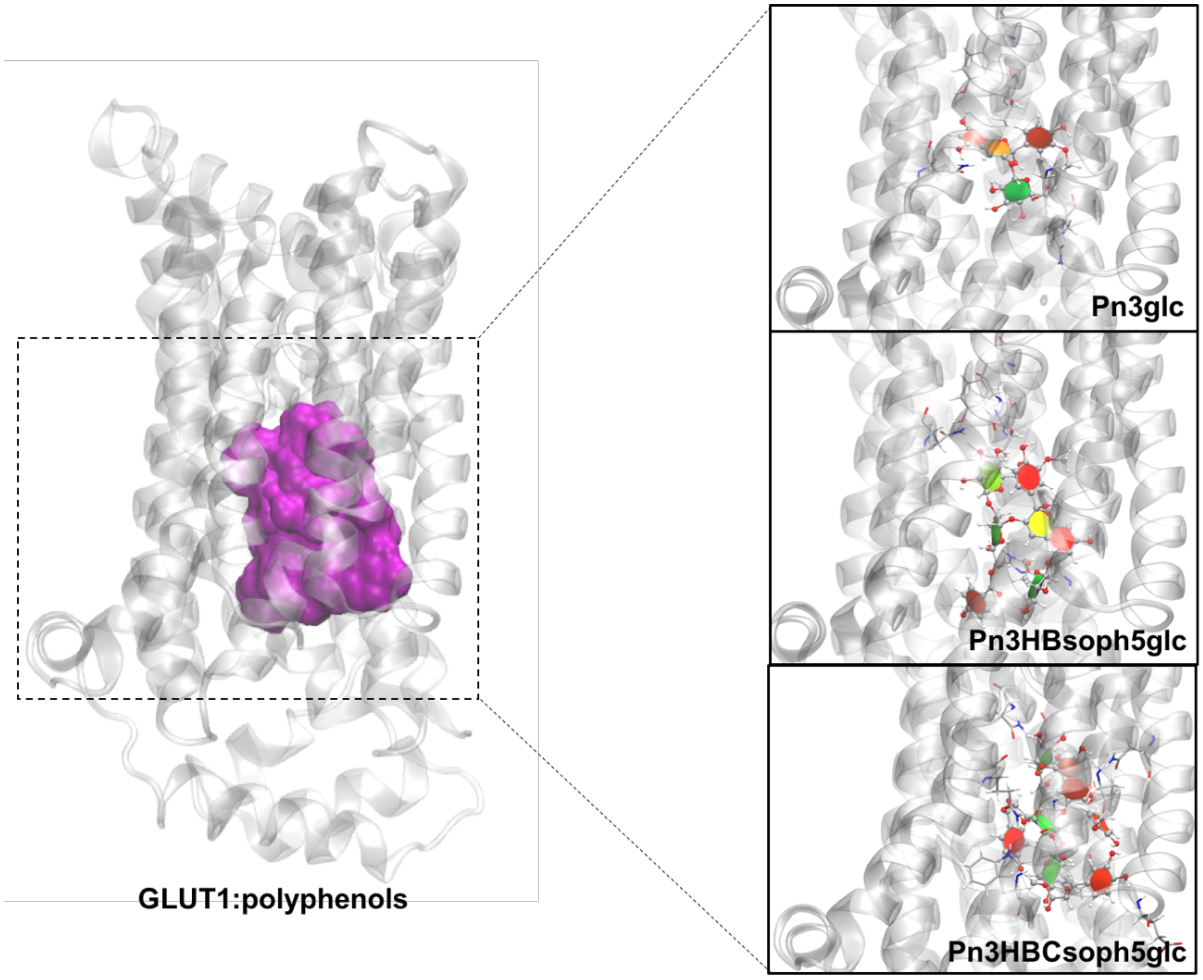

Figure 80. Representation of the optimized structure of each GLUT1:polyphenol complex. The main amino acids involved in the polyphenols' binding are also shown (depicted with sticks and colored by atom type). GLUT1 is represented in cartoon and colored in gray, while the polyphenol compounds are represented as ball-and-sticks and colored by atom type. Aromatic, non-aromatic saccharide, and non-aromatic non-saccharide rings of each polyphenol are colored in red, green and orange, respectively. The binding region of GLUT1 for all polyphenols is represented as a purple surface.

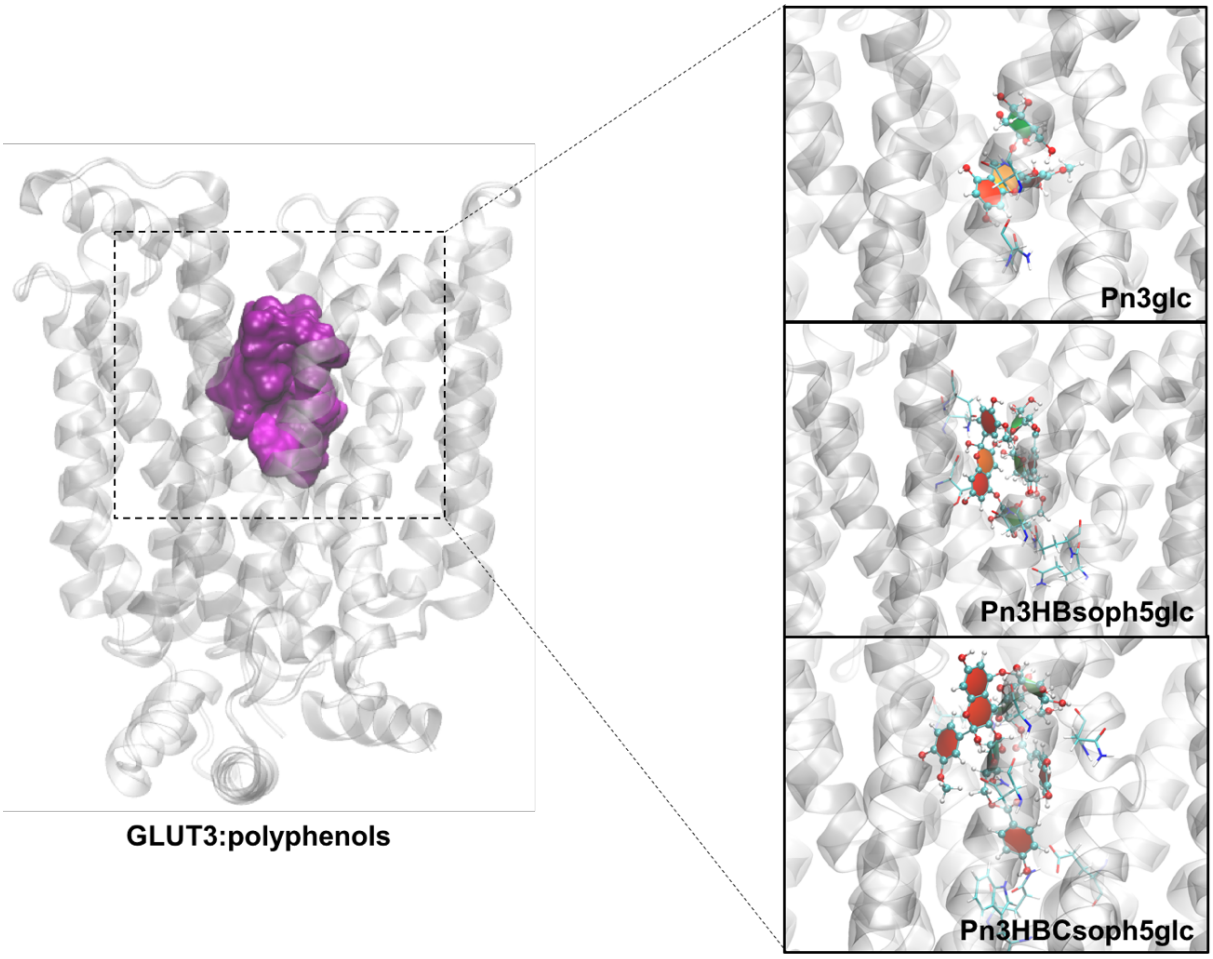

Figure 81. Representation of the optimized structure of each GLUT3:polyphenol complex. The main amino acids involved in the polyphenols' binding are also shown (depicted with sticks and colored by atom type). GLUT3 is represented in cartoon and colored in gray, while the polyphenol compounds are represented as ball-and-sticks and colored by atom type. Aromatic, non-aromatic saccharide, and non-aromatic non-saccharide rings of each polyphenol are colored in red, green and orange, respectively. The binding region of GLUT3 for all polyphenols is represented as a purple surface.

Table 17 summarizes the binding free energy and the RMSD values for the six GLUT:polyphenol systems. The average RMSD values for the protein backbone of the GLUT1 and GLUT3 transporters are quite small (*ca.* 3 and 2 Å, respectively), and they revealed that all simulations were equilibrated at approximately 20 ns. Hence, the last 80 ns of each MD simulation were used to: i) determine the protein:ligand binding free energies, ii) the structural information on the ligands interaction with the GLUT transporters, and iii) the number of water molecules. The analysis of the MD trajectories revealed that all polyphenols remained bound to the same GLUT region throughout the

entire simulations, suggesting the establishment of stable intermolecular interactions. At 80 ns of the GLUT1 simulation, the compound Pn3glc changed its conformation, where the B ring approximated the glucose unit, establishing an intramolecular CH-π interaction. This behaviour justified the higher RMSD value for this compound in GLUT1.

Table 17. $\Delta G_{binding}$ values obtained for the six GLUT:polyphenol systems along the MD simulations. The groups that are inserted deeper into the GLUT channel, the RMSD of protein backbone and ligand atoms as well as the number of water molecules around each polyphenol were also indicated.

system	$\Delta G_{binding}$ / kcal.mol^{-1}	more buried groups	RMSD receptor / Å	RMSD polyphenol / Å	no. water 0-3.5 Å
GLUT1:Pn3glc	-10.2	AC and B	3.07 ± 0.25	2.85 ± 0.63	14.38 ± 2.95
GLUT1: Pn3HBsoph5glc	-8.4	B and glc-glc-C3	3.07 ± 0.32	1.50 ± 0.17	29.88 ± 3.33
GLUT1:Pn3HBCsoph 5glc	-15.4	AC and glc-C5	3.09 ± 0.64	1.86 ± 0.20	27.23 ± 4.91
GLUT3:Pn3glc	-6.0	AC and B	2.24 ± 0.18	1.63 ± 0.47	17.91 ± 3.46
GLUT3: Pn3HBsoph5glc	-3.6	glc-C5	2.07 ± 0.13	1.90 ± 0.18	24.88 ± 3.50
GLUT3:Pn3HBCsoph 5glc	-16.1	hydroxybenzoyl	2.11 ± 0.17	1.43 ± 0.22	20.13 ± 2.84

Compounds Pn3glc and Pn3HBsoph5glc showed a higher affinity for GLUT1 than GLUT3, whilst the biggest compound (Pn3HBCsoph5glc) showed a similar affinity for both receptors (*ca.* -16 kcal.mol^{-1}). The order of the polyphenols binding affinity for both glucose transporters is Pn3HBCsoph5glc > Pn3glc > Pn3HBsoph5glc, which may be related with their different molecular size and/or their distinct solvation facilities. In fact, the order of the average number of water molecules within a radius of 3. 5 Å around the three polyphenols is Pn3HBsoph5glc>Pn3HBCsoph5glc>Pn3glc when bound to both glucose transporters (see Table 17). On the one hand, this indicates that compound Pn3HBsoph5glc is the one surrounded by more solvent molecules, which could justify its smaller binding free energy to the glucose transporters. On the other hand, this data also revealed that both GLUT binding channels were highly exposed to the solvent, which could facilitate the binding of these polyphenols due to their high water-soluble ability. Previous diffusion studies also described the water permeability through glucose transporters [273].

Table 18 displays structural information on both GLUT binding pockets, in particular the most frequent hydrogen bonds (H-bonds) established between the polyphenols and the amino acids of the transporters. These results indicate that the bigger compound (Pn3HBCsoph5glc) is the one that establishes the highest number of H-bonds with the proteins. Analyzing the contacts established with GLUT1, the hydroxyl groups of polyphenols interact mainly with the side chains of Thr30, His160, Gln161, Gln282, Asn288, Tyr292, Asn317, Glu329, Glu380, Trp388 and Asn413, as well as the carbonyl backbone group of Gly384. This suggests the importance of these residues for polyphenols binding, which could influence their translocation. This result is concurrent with previous mutagenesis studies in which the mutation of five of these residues (Gln161, Gln282, Asn288, Trp388 and Asn411) showed severely reduced transport activities and glucose uptake [274-276]. Other experimental and computational studies also pointed out Tyr292 and Glu380 as contributors to sugar translocation [249, 274].

In relation to GLUT3, the main residues involved in H-bonds with the polyphenols are Gln159, Gln170, Gln280, Gln281, Asn286, Glu378, Trp386 and Asn413. A previous crystallographic study suggested that six of these residues are relevant for sugar transport by this transporter. In particular, they propose that Asn286 contributes to the flexibility required for the structural shift from outward-open to outward-occluded conformations [250].

In all simulations, the major moieties of polyphenols involved in H-bonds seems to be glucose and AC rings that may highlight their important role in the polyphenols transmembrane transport. Furthermore, it was also observed the establishment of several hydrophobic contacts (mainly π−π stacking) between the polyphenols' rings and the aromatic residues present in the inward-facing conformation of GLUT1 (Phe26, Phe72, Phe291, Tyr292, Trp388, Phe389 and Trp412) and in the outward-occluded conformation GLUT3 (Phe24, Phe70, Phe289, Tyr290, Phe377, Trp386 and Phe420). All of these interactions strongly contribute to the stability of each GLUT:polyphenol complex. Previous studies indicated that the sugar-binding residues of human GLUT1 belongs to the C-terminal domain (except the Gln161).[249, 274] However, as seen in Table 18, the binding of compounds Pn3glc, Pn3HBsoph5glc and Pn3HBCsoph5glc into the human GLUT1 involves some residues from both C- and N-terminal domains. This also happened in previous studies of the binding of anthocyanins to the human GLUT1 protein [102]. Again, this could be explained due to the larger size of anthocyanins compared to glucose.

Table 18. Intermolecular H-bonds present during more than 20% of each MD simulation. CO – carbonyl group; NH – amine group; SC – side chain. Residues that appear in more than one compound are highlighted in bold.

simulation	interaction		distance / Å	%
	receptor	polyphenol		
GLUT1:Pn3glc	**Tyr292 (SC)**	HO-C7 (AC ring)	2.80	75
	Gly384 (CO)	HO-C2 (glc-C3 ring)	2.70	67
	Gln161 (SC)	HO-C2 (AC ring)	2.89	26
	Thr30 (SC)	HO-C7 (AC ring)	2.85	26
	Asn411 (SC)	HO-C2 (glc-C3 ring)	2.89	20
GLUT1: Pn3HBsoph5glc	**Thr30 (SC)**	OH-C4 (glc-glc-C3 ring)	2.78	56
	His160 (SC)	OH-C6 (glc-C5 ring)	0.85	51
	Asn415 (SC)	OH-C3 (glc-glc-C3 ring)	2.82	48
	Tyr292 (SC)	OH-C3 (glc-glc-C3 ring)	2.76	28
	Asn288 (SC)	HO-C4' (B ring)	2.89	18
GLUT1: Pn3HBCsoph5glc	**Gly384 (CO)**	HO-C3 (glc-C3 ring)	2.69	92
	Asn317 (SC)	HO-C2 (AC ring)	2.78	67
	Glu380 (SC)	HO-C7 (AC ring)	2.68	63
	Trp388 (NH)	O-C1''' (caffeoyl ring)	2.88	48
	Glu329 (SC)	HO-C7''' (caffeoyl ring)	2.57	48
	Gln282 (SC)	O-C1''' (caffeoyl ring)	2.86	42
	Thr30 (SC)	OH-C4 (glc-C5 ring)	2.77	39
	His160 (CO)	OH-C3 (glc-glc-C3 ring)	2.73	29
	Asn288 (SC)	OH-C6 (glc-C5 ring)	2.67	27
GLUT3:Pn3glc	Asn409 (SC)	HO-C7 (AC ring)	2.69	94
	Asn413 (SC)	HO-C6 (glc-C3 ring)	2.74	25
GLUT3: Pn3HBsoph5glc	Gln281 (SC)	HO-C5'' (hydroxybenzoyl ring)	2.68	91
	Asn32 (SC)	HO-C2 (AC ring)	2.74	69
	Gln280 (SC)	OH-C6 (glc-C5 ring)	2.73	65
	Gln170 (SC)	OH-C2 (glc-glc-C3 ring)	2.75	47
	Asn413 (SC)	HO-C7 (AC ring)	2.72	31
	Thr28 (CO)	HO-C2 (AC ring)	2.7	22
GLUT3: Pn3HBCsoph5glc	Glu378 (SC)	HO-C7''' (caffeoyl ring)	2.61	100
	Gly417 (CO)	OH-C2 (glc-C5 ring)	2.67	93
	Gln159 (SC)	HO-C5'' (hydroxybenzoyl ring)	2.72	90
	Asn286 (SC)	OH-C3 (glc-C5 ring)	2.87	50
	Asn413 (SC)	HO-C2 (AC ring)	2.88	42
	Trp386 (SC)	HO-C5'' (hydroxybenzoyl ring)	2.88	37
	Gln170 (SC)	O-C1''' (caffeoyl ring)	2.87	20

4. DISCUSSION AND CONCLUSION

It is generally acknowledged that anthocyanins are beneficial to human health, although the mechanisms of their absorption are not yet fully described. The long-term view that anthocyanins could only be absorbed in their aglycon forms has been changing, since anthocyanins are unique compared with other flavonoids once that they may be absorbed as intact glycosylated forms. Native anthocyanins have been detected in both plasma and urine of human subjects few minutes after oral consumption of blackberry juice or red wine [236, 237]. Candidates for anthocyanin transporters are glucose transporters since anthocyanins possess a sugar moiety, which consists in most cases in glucose residues. Recently, Zou and coworkers reported that Cy3glc intestinal absorption decreased after *SGLT1* or *GLUT2* siRNA transfection [161]. More recently, a study with rats showed that although the overall uptake of anthocyanins was not affected by the co-administration of glucose, the kinetics of the uptake was suggesting the involvement of glucose transporters. It was also found a significant correlation between SLGT1, GLUT2 and anthocyanin absorption through computational studies [277]. Furthermore, Zhang and coworkers demonstrated the bioaccessibility and bioavailability of anthocyanins from purple roots, suggesting, once again the involvement of SLGT1 and GLUT2 as the main candidates on anthocyanins transport at the intestinal level [278].

Over the years, attention has been given to intestinal anthocyanin uptake as the main site of absorption in the body. However, the findings of anthocyanins in the bloodstream as early as 15 minutes are not compatible with an exclusive intestinal uptake.

Several studies using a human gastric model have pointed towards the possible involvement of glucose transporters in the transport of anthocyanins [238, 239]. However, the direct involvement of such transporters has not been clearly demonstrated since only indirect approaches were used to assess this matter. So, the need to have a molecular approach targeted to specific proteins/transporters becomes evident.

In this work a nano-based approach was used to clearly associate the absorption of anthocyanins with glucose transporters by silencing *GLUT1*, *GLUT3* or both.

The structurally related anthocyanins selected intended to support the importance of glucose position and substituents to the transporter binding. The hindrance effect of the sugar moieties and the substituents on PFSP anthocyanins (~8 - 7 %) are clear when compared to the native anthocyanin Pn3glc (~10 %), demonstrated by the reduction of the transport efficiency of PFSP anthocyanins at the higher incubation time.

Also, it is interesting to notice that besides this, the results for the samples treated with nanoparticles with antisense RNA for *GLUT1* or *GLUT3* showed similar trends for all the anthocyanins tested, suggesting that the position of the free glucose residue is not an important feature.

The computational results suggest that all anthocyanins are able to bind to both human GLUT1 and GLUT3 transporters, with the bigger compound Pn3HBCsoph5glc showing the highest affinity of the three evaluated compounds, since it is the one that establishes the highest number of H-bonds with the transporters. This may be easily understood by the higher number of free hydroxyl groups, consequence of the acyl moieties on the sophoroside group at C3. The AC rings and the glucose moieties seem to have the most important role in the anthocyanin transmembrane binding. These groups establish both hydrophilic (H-bonds) and hydrophobic (CH-π and π-π stacking) interactions that are crucial for the polyphenols binding into the human glucose transporters. Furthermore, although the results suggested an overall higher affinity of the compounds for GLUT1, one can observe a that Pn3HBCsoph5glc showed a more negative ΔG binding energy for GLUT3 rather than GLUT1. This suggests higher affinity.

Going back to the RNA silencing, one can see that the acylated anthocyanins transport was more decreased upon the silencing of GLUT3 when comparing to GLUT1. And this fact seems to be more pronounced in the case of Pn3HBCsoph5glc, which is in agreement with the findings of the molecular dynamics simulations.

This shows the importance and the relevance of using two completely different techniques and research areas to confirm results.

Although a clear reduction in anthocyanin transport was observed upon gold nanoparticles treatments, only when a 4 ºC treatment was applied a total reduction of active transport was observed. This is suggested by the different values for treatments with gold nanoparticles and 4 ºC treatment. So, the differences of about 4 up to 6 % depending on the cases when comparing AuNP@PEG with or without antisense *GLUT1/3* RNA's, suggest the involvement of other transporters. The treatments with inhibitors of different transporter families showed a reduced absorption of Mv3glc, although not so significant as in the case of GLUTs inhibition. This phenomenon is quite understandable since cells have a high number of mechanisms to internalize and transport different compounds, and it is virtually impossible to assess all of them to be sure of which of them are involved. In fact, Passamonti and coworkers demonstrated the involvement of bilitranslocase on anthocyanins uptake at gastric level [107].

Anthocyanins display some chemical unique features such as their dependence on pH [279]. The fact that these compounds can reach an equilibrium in different structural forms at a specific pH value, suggest that anthocyanin transport in vivo is dynamic, and cannot be attributed to a specific form. At pH 5, the working pH of the model used in this work and the average pH of the stomach at the fed state, although anthocyanins are mainly found at hemiketal neutral form, other different forms are present in equilibrium [133, 279], as it was demonstrated in Chapter I for Pn3HBsoph5glc and Pn3HBCsoph5glc. This may explain the results obtained when testing different transporter families, which highlighted that this particular class of polyphenols can be transported in different equilibrium forms by different transporters.

Hence, this study provides useful data to assist the clarification of the role of glucose transporters in the gastric absorption of anthocyanins. This data also suggests the involvement of other type of transporters that may contribute to the global transport efficiency, which should be the focus of future studies into this theme. This work brings new insights onto the paradox between the high levels of anthocyanins consumed, their low bioavailability and the reported health effects.

PART II

APPLIED STUDIES ON THE BIOACTIVITY AND BIOAVAILABILITY OF DIFFERENT FOOD BIOACTIVES FROM RED WINE AND *GARDENIA JASMINOIDES ELLIS*

The second part mainly focused on the use of different natural sources for the study of the bioactivity and bioavailability of different food bioactives and resulted in the publication of two articles in international scientific journals.

On the first chapter the study of the bioactivities using MCF-7 breast cancer cells and bioavailability using MKN-28 gastric cancer cells was directed for the differences between the anthocyanin derived compounds formed during red wine ageing.

The second chapter shows the study of the main natural bioactive compounds present in *Gardenia Jasminoides Ellis*, a flower widely used in food industry in China and approved by the Chinese Pharmacopoeia for use in traditional Chinese medicine.

The two chapters are based on the structure of each published paper. The experiments were developed abroad, during the period of internship at the Polytechnic University of Wuhan, China, in the Food Chemistry Laboratory under the supervision of Professor Jingren He.

CHAPTER I

BIOAVAILABILITY STUDIES AND ANTICANCER PROPERTIES OF MALVIDIN BASED ANTHOCYANIN, PYRANOANTHOCYANINS AND NON-OXONIUM DERIVATIVES.

Synopsis

The objective of this study, was to evaluate the gastric transport efficiency of malvidin-3-glucoside and several derivatives was assayed on MKN-28 cell model.

The work focused on the structural differences between the compounds tested and among the pyranoanthocyanin derivatives the presence of the carbonyl group and the absence of charge were important for the transport efficiency percentage of oxovitisin A and apparently compensated the negative effect associated with the additional ring.

Moreover, the antiproliferative properties of these compounds in MCF-7 cancer cell line were assayed.

Oxovitisin A showed the highest efficiency in inhibiting the proliferation of MCF-7 cells.

A study of the fluorescence properties of oxovitisin A was performed and a kinetic incorporation of oxovitisin A was assayed revealing that this pyranoanthocyanin is quickly incorporated into cells.

This study confirms the importance of the natural micro-oxidative processes that occur during ageing of anthocyanin-containing food and their impact on their bioavailability and bioactivity properties.

This chapter resulted in the following paper: ***Oliveira, H.,*** *Wu, N., Zhang, Q., Wang, J., Oliveira, J., de Freitas, V., Mateus, N., He, J., Fernandes, I. (2016). "Bioavailability studies and anticancer properties of malvidin based anthocyanins, pyranoanthocyanins and non-oxonium derivatives", Food and Function, 7, 2462-2468. DOI: 10.1039/c6fo00445h.*

1. INTRODUCTION

Red wine is a complex mixture of polyphenols (anthocyanins, tannins, catechins, etc.), so it is not surprisingly that anthocyanin absorption may be affected by their presence. In addition, anthocyanins participate in several reactions during wine aging, resulting in the formation of new pigments [280]. One of the most important groups of newly formed compounds is carboxy-pyranoanthocyanins (type A vitisins) and methyl-pyranoanthocyanins, both present in aged red wines [281, 282]. Anthocyanin pyruvic-acid adducts (carboxy-pyranoanthocyanins) can rapidly reach rat plasma after oral administration of malvidin-3-glucoside-pyruvic acid adduct [103]. Also, flavanol-anthocyanin pigments were found to be absorbed in the intestinal caco-2 cell model [160]. Although, the information about the gastric absorption of these anthocyanin-derived compounds is very scarce.

The absorbed fraction of anthocyanins or pyranoanthocyanin that reaches the systemic circulation can go to different tissues where they can exert their effects on cancer progression.

The roles of anthocyanins in breast cancer have been widely assayed [283-285]. Anthocyanins are reported to act on the inhibition of key modulators that promote breast cancer progression and development. Recently, several studies showed that these compounds can act directly on the DNA fragmentation, promoting the death of MCF-7 cancer cells while not exerting cytotoxic effects on non-cancer cell lines. Furthermore, specific anthocyanins like delphinidin can act as a potential antimetastatic agent that suppresses PMA-induced cancer cell invasion through the specific inhibition of NF-κB-dependent MMP-9 gene expression.

Considering the biological activity of pyranoanthocyanins the scenario is almost non-existent. Former data indicated that formation of anthocyanin adducts with pyruvic acid, decreases the hydroxyl and superoxide anion scavenging and thus could decrease the antioxidant potential of these compounds [286]. Recently, several pyranomalvidin-3-glucosides were suggested as good candidates as antioxidant compounds because they easily donate an H atom to the free radicals, originating stable species [287] supporting the fact that the antioxidant potential arising from anthocyanins is not impaired by some of their transformations during red wine aging. Few in vitro studies have been performed demonstrating that extracts of blueberry anthocyanin-pyruvic acid adducts possesses

anticancer properties by inhibiting breast cancer MCF-7 cell proliferation and by acting as cell anti-invasive factors and chemo-inhibitors [288].

Thus, in this study, the bioavailability in gastric cancer cell line MKN-28 of malvidin-3-*O*-glucoside (Mv3glc) and some of corresponding pyranoanthocyanins including flavylium and non-flavylium derivatives was evaluated and their biological activities against breast cancer cell line MCF-7 was also assayed. A putative structure-activity relationship was also assessed in order to better understand the role of these pigments on human health.

2. MATERIAL AND METHODS

2.1. Materials and Reagents

Toyopearl gel HW-40(s) was purchased from Tosoh (Tokyo, Japan), pyruvic acid (97%) was purchased from Sigma-Aldrich. Methanol, Ethanol, formic acid and acetonitrile, used for HPLC analysis, were of chromatographic grade (Fischer Scientific). Pyruvic acid, acetone and ethanol of analytical grade were purchased from Sinopharm Chemical Reagent Ltd (China). Rhodamine 123 and Hoescht 33342 were purchased from Life Technologies (Thermo Fischer Scientific).

2.2. Anthocyanidin-3-glucoside extraction

Grape skin extract (color value: 30) was purchased from Yunnan Tonghai Yang Natural Produces Ltd (China), malvidin-3-*O*-glucoside (Mv3glc) is the main anthocyanin in the extract as previously detected [289]. Grape skin extract was dissolved in acidic aqueous solution first. Then the sample was purified on a polyamide gel column (Mesh 80-100). The Mv3glc and other anthocyanidin-3-glucosides fractions were eluted with a methanol 10% (v/v) acidic aqueous solution. The fractions were concentrated in a Heidolph G3 rotary evaporator under vacuum in water at 35 ºC, freeze-dried and stored at -20 ºC until further purification.

2.3. Synthesis of vitisin A, methylpyrano-malvidin-3-O-glucoside (Me-py) and oxovitisin A

Oxovitisin A was achieved through a slow oxidation reaction of vitisin A (1 mg/mL) in ethanol aqueous solution, with 20% ethanol, pH 3.6, 45 ºC during 21 days according to the procedure reported, with optimization [290]. Pyranoanthocyanins (methylpyrano-malvidin-3-*O*-glucoside and oxovitisin A) were formed by reaction of the grape extract and acetone as reported by Kuang et al [291]. Vitisin A was synthesized as previously described [292]. The presence of all products was characterized by HPLC/DAD-MS as the method reported before [292].
The purity of all isolated compounds was confirmed by HPLC-DAD-MS and NMR analysis. Then the isolated compounds were frozen, freeze-dried and stored at -20 ºC until use.

2.4. Cell Culture Conditions

MKN-28 gastric cancer cell line and MCF-7 breast cancer cell line were grown as monolayer. For routine maintenance, cells were cultured in 25 cm^2 plates as monolayer and maintained in DMEM, and supplemented with 15% heat-inactivated FBS, 1% antibiotic/antimycotic solution (100 units/mL of penicillin, 100 µg/mL of streptomycin and 0.25 µg/mL of amphotericin B) at 37 °C in a humidified atmosphere with 5% CO_2. Cells were harvested by trypsinisation (0.25% (w/v) trypsin–$EDTA_4Na$) twice a week.

2.4.1. Transport experiments on MKN-28 cells

Transport experiments were performed according to previously published methods [102, 133]. Briefly, MKN-28 cells were plated on 12-well transwell inserts (0.4 µm pore size tissue culture inserts (Corning Costar, Corning, NY, USA)). Cells were cultured at 37 °C in an atmosphere of 5% CO_2, and the medium was changed every 2 days. At 7 days MKN-28 cells were fully confluent and differentiated, so experiments were initiated at that time. Experiments were conducted only in MKN-28 cell monolayers that showed a TEER > 150 Ω/cm^2 (determined at 37 °C).

In transport experiments HBSS, pH 7.4, was the main component of the basolateral medium. In the gastric cell model the apical medium was acidified to 5.0 by adding solid 2-(N-morpholino)ethanesulfonic acid (MES) to give a concentration of 25 mM and then adjusting the pH with 5 M HCl.

Medium was removed and cells were washed with Hanks' medium, pH 7.4. Malvidin-3-O-glucoside and their derivatives were dissolved in Hanks, with a final concentration of 100 µM was added to the apical side of the cells and Hanks containing 2% FBS was added to the basolateral compartment.

Transepithelial transport was followed as a function of time. A total of 150 µL was taken from the basolateral side and replaced by fresh medium (Hanks containing 2% FBS) at 30, 60, and 120 min and 180 min. Each time sample (150 µL) was acidified with HCl to a final concentration of 0.06 M. All samples, from both apical and basolateral sides, were acidified and frozen (-18°C) to ensure that the cumulative amounts of each compound that were later quantified were not altered during sample delay until uHPLC analysis.

Transport efficiency percentages were calculated as ((compound concentrations at the basolateral side overtime)/(compound concentrations at the apical side at 0 h)) × 100.

2.4.2. Sulforhodamine B assay

The effect of each anthocyanin on the growth of the two cell lines was evaluated according to the procedure adopted by the US National Cancer Institute in the "In vitro Anti- cancer Drug Discovery Screen" that uses the protein-binding dye SRB to assess cell growth, according to the procedure previously performed by Oliveira and co-workers [293]. Briefly, cells (1.5×10^5 cells/mL) were spread into 96-well plates and allowed to grow for 24 h before treatment, ensuring exponential growing state. A stock solution of each compound was prepared and kept at -20°C. Appropriate dilutions of each sample fraction were freshly prepared just prior to every assay. After, cells were incubated with the respective fraction for 2 days and exposed to five serial concentrations.
Incubation process was stopped by addition of TCA 50%, 1 h at 4°C. The plates were then washed with distilled water with 1% of acetic acid. The plates were dried and were stained with a 0.4% solution of SRB. The dye was eluted with Trizma buffer (10 mM, pH 10.5) and after 30 minutes, quantified photometrically at 492 nm in a multimode microplate reader (triplicates of each fraction sample) (Enspire, PerkinElmer, Massachusetts, USA).

2.5. Cell Imaging

All the cell images were captured using a Confocal Laser Scanning Microscope (Olympus FV1000).

2.5.1. Oxovitisin A incorporation on MCF-7 cells

The incorporation of oxovitsin A was followed by fluorescence kinetic reading using fast CCD-CMOS capture technology.
MCF-7 cells were spread in 60 mm^2 culture dishes (1.5×10^5 cells/mL) and allowed to grow for 24 h. Then, the culture medium was replaced by HBBS medium supplemented with 10% FBS. The culture dishes were placed on the microscope, and the kinetic reading started at the moment of oxovitisin A addition (375.6 μM). Time 0 represents the cells without oxovitisin A. The measure consisted in sequential pictures every 2 minutes for a

total of 30 minutes. The green channel of the fluorescence microscope was used to excite the anthocyanins and read the fluorescence emission.

2.5.2. Intracellular localization of mitochondria

MCF-7 cells were spread in 60 mm^2 culture dishes (1.5×10^5 cells/mL) and allowed to grow for 24 h. Then, the culture medium was replaced by HBBS medium supplemented with 10% FBS. Hoescht 3342 (10 µg/mL) was used to stain the nucleus and Rhodamine 123 (20 µg/mL) used to stain mitochondria. Briefly, Hoescht 3342 was added to the cells, followed by an incubation period of 30 min at 37ºC. On the last 15 min, Rhodamine 123 was added, followed by a simultaneous incubation with Hoescht 3342. The culture dishes were then washed 3x with HBBS medium supplemented with 10% FBS and submitted the confocal laser scanning microscopy. The specific parameters for the em/ex of these stains were defined using standard values on the microscope software.

2.6. Apoptotic biomarkers modulation assays

Cells were spread on 6-well plates with a density of 1.5×10^5 cells/mL and allowed to grow for 24 h. Then, the cells were treated with the respective compounds (0.2 mg/mL) for 6 h (for control, medium was renewed). The supernatants were collected and placed in ELISA plates with antibodies against Caspase-3 and Caspase-9. Further procedures were as described by the kit manufacturers (Cloud-Clone Corporation, Houston, USA).

2.7. Statistical Analysis

The experiments are expressed as the arithmetic means (n = 3-10) ± standard error mean (SEM). Statistical significance for the different incubation times for each compound was evaluated by one-way analysis of variance (ANOVA), followed by the Bonferroni's Multiple Comparison Test. Differences were considered statistically significant when #$p<0.05$.
For all other assays statistical significance between compounds was evaluated by two-way analysis of variance (ANOVA), followed by the Bonferroni posttests. Differences were considered to be statistically significant when *$p<0.05$; **$p<0.01$; ***$p<0.001$ vs Mv3glc. Each experiment was independently repeated at least 3 times. All statistical analysis were performed using GraphPad 5.01 software.

3. RESULTS

3.1. HPLC-DAD/MS characterization of the Mv3glc, vitisin A, Me-py and oxovitisin A

The structural differences of anthocyanin derivatives with precursor Mv3glc are due to the newly formed D ring and the various substituents in C10 position. In particular, oxovitisin A present a unique non-oxonium nature with additional pyranone ring and structure similarity to flavones (Figure 82).

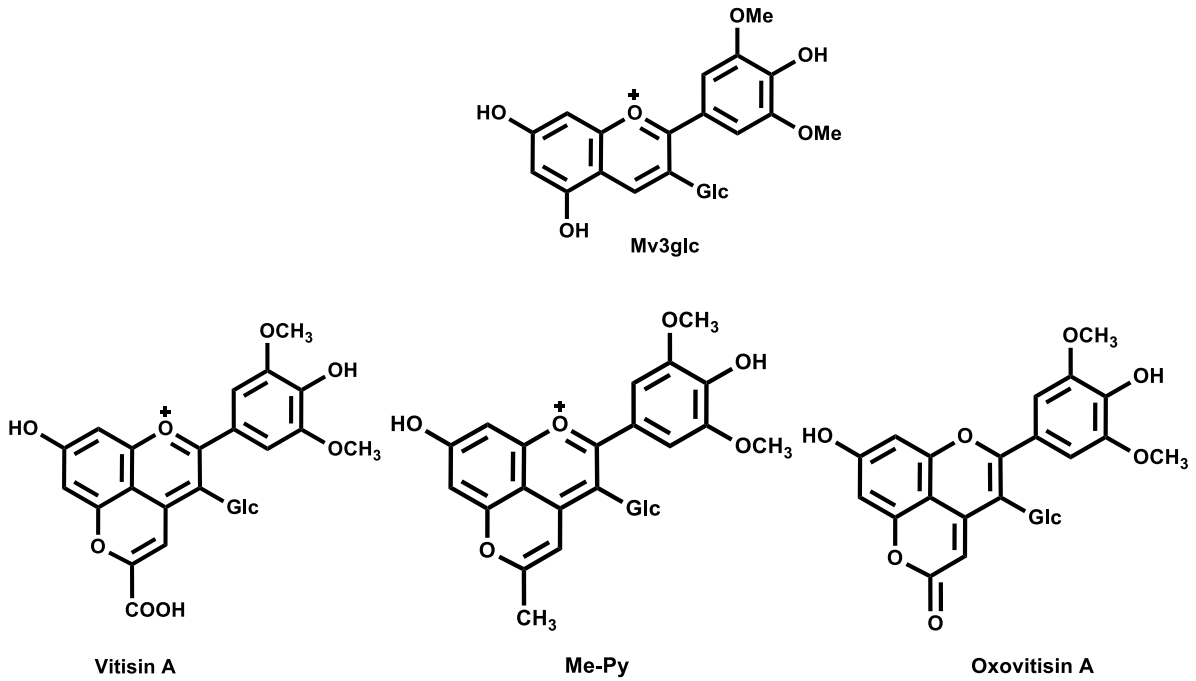

Figure 82. Chemical structures of Malvidin-3-*O*-Glucoside (Mv3glc), Metilpyrano-Malvidin (Me-py), Vitisin A, and Oxovitisin A.

Grape skin extract and anthocyanin derivatives were harvested from the respective reacting system, and then directly characterized by HPLC/DAD-MS, referring to the analytical retention time (RT), UV-visible spectroscopic data and typical fragmentation ions. The basis of the proposed identifications is shown in Table 19.

Table 19. Spectral characteristics of Malvidin-3-*O*-Glucoside (Mv3glc), Metilpyrano-Malvidin (Me-py), Vitisin A, and Oxovitisin A.

Anthocyanin	*RT/ (min)*	λ_{max}/ *(nm)*	*MS/ (m/z)*	MS^2/ *(m/z)*	MS^3/ *(m/z)*	ε/ $(mol^{-1}dm^3cm^{-1})$	*Em/Ex (nm)*
Mv3glc	13.8	531	528.4	331	-	16000[a]	-
Vitisin A	17.7	512	596.9	399	-	12900[a]	-
Me-py	21.9	478	566.4	369	-	16503	-
Oxovitisin A	30.7	373	532.4	371	343	17390	440/490

[a] As already reported [294].

3.2. Gastric transport of Mv3glc and derivatives

The transport of Mv3glc, vitisin A, Me-py and oxovitisin A was evaluated through a transwell gastric system using MKN-28 cell line model. It could be concluded that their transport efficiency increases with incubation time, with significative differences in adjacent incubation times for all the compounds tested ($p< 0.001$) (Figure 83). It could hence be assumed that formation of pyranoanthocyanins during wine aging may slightly impair transport efficiency levels in comparison with native anthocyanins.

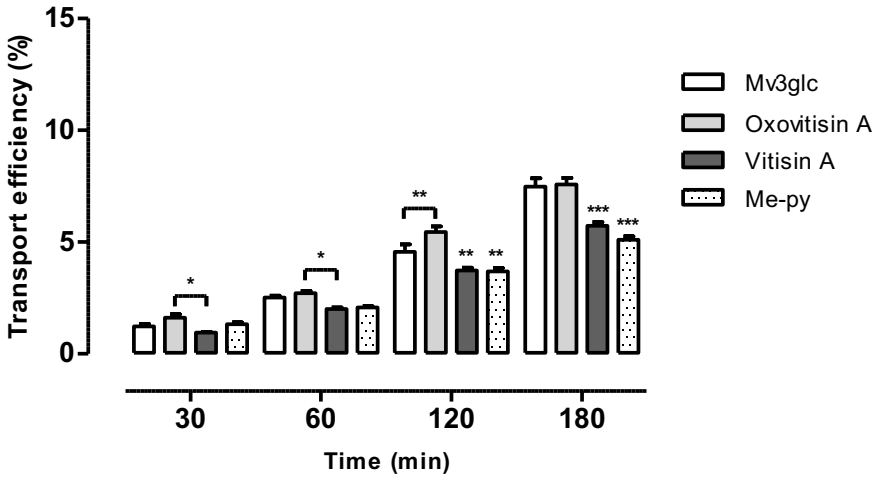

Figure 83. Transport efficiency of Mv3glc and derivatives through MKN-28 barrier (Apical → Basolateral). The experiments were conducted with apical pH 5.0 and basolateral pH 7.4. Results are presented as transport efficiency (%) (mean ± SEM). Transport efficiency percentages were calculated based on (compound concentrations at the basolateral side overtime)/(compound concentrations at the apical side at the zero hours)*100. Significantly different from Mv3glc and oxovitisin A for the same incubation time, unless otherwise indicated * $p<0.05$; ** $p<0.01$, *** $p<0.001$.

Furthermore, Mv3glc and oxovitisin A showed similar transport efficiency (Figure 83). This may be related to the small size of the original anthocyanin.

The lowest uptake levels by the gastric barrier were for Vitisin A and Me-py, with no significant differences between them. Apparently, the substitution of the carboxylic group by a methyl group is not accompanied by any effect on transport efficiency.

The higher absorption value observed for oxovitisin A among the three pyrano-anthocyanins tested may be related to the absence of charge on this molecule.

3.3. Antiproliferative capacity of Mv3glc, vitisin A, Me-py and oxovitisin A on MCF-7 cells

The antiproliferative capacity of the compounds was evaluated by the SRB method. All the compounds showed an antiproliferative activity (IC_{50} values lower than 380 μM). Mv3glc and oxovitisin A seem to be the most effective compounds in cell growth inhibition with an IC_{50} of 109.08 ± 10.69 and 177.98 ± 7.20 μM, respectively (Table 20). The results suggest that the most effective compounds on the antiproliferative effect of MCF-7 cancer cells seems to be Mv3glc and oxovitisin A, followed by vitisin A and Me-py as the least effective.

Table 20. Effect of Mv3glc and derivatives on MCF-7 cells proliferation evaluated by SRB assay. MCF-7 cells, seeded in 96 well plates, were treated with a broad concentration range (380-20 μM) of each compound for 48h. Each value represents the mean ± SEM (n=6-30). Different letters indicate the values are statistically different.

IC_{50} ± SEM (μM)	
Compound	**MCF-7**
Mv3glc	109.08 ± 10.69[a]
Vitisin A	244.97 ± 21.75[b]
Me-py	309.31 ± 9.62[c]
Oxovitisin A	177.98 ± 7.20[d]

3.4. Intracellular location of oxovitisin A

Aiming to get some insights on the mechanism involved in the antiproliferative effect of the compounds their presence within the cell components was assayed. Due to the remarkable fluorescence of oxovitisin A at 490 nm and the absence of fluorescence in the other compounds the intracellular location of oxovitisin A was followed by fluorescence microscopy during 30 min (Figure 84a).

The results revealed that after 4 minutes oxovitisin A was fully incorporated by the cells, as the fluorescence is notorious different between the background and the cells. Is also possible to see that the cells seem to keep the fluorescent signal during the 30 minutes of measurement. Furthermore, at this time a higher intensity on the fluorescence is noticeable on the nucleus and surrounding areas. The nucleus and mitochondria location within cells was also stained by (Figure 84b).

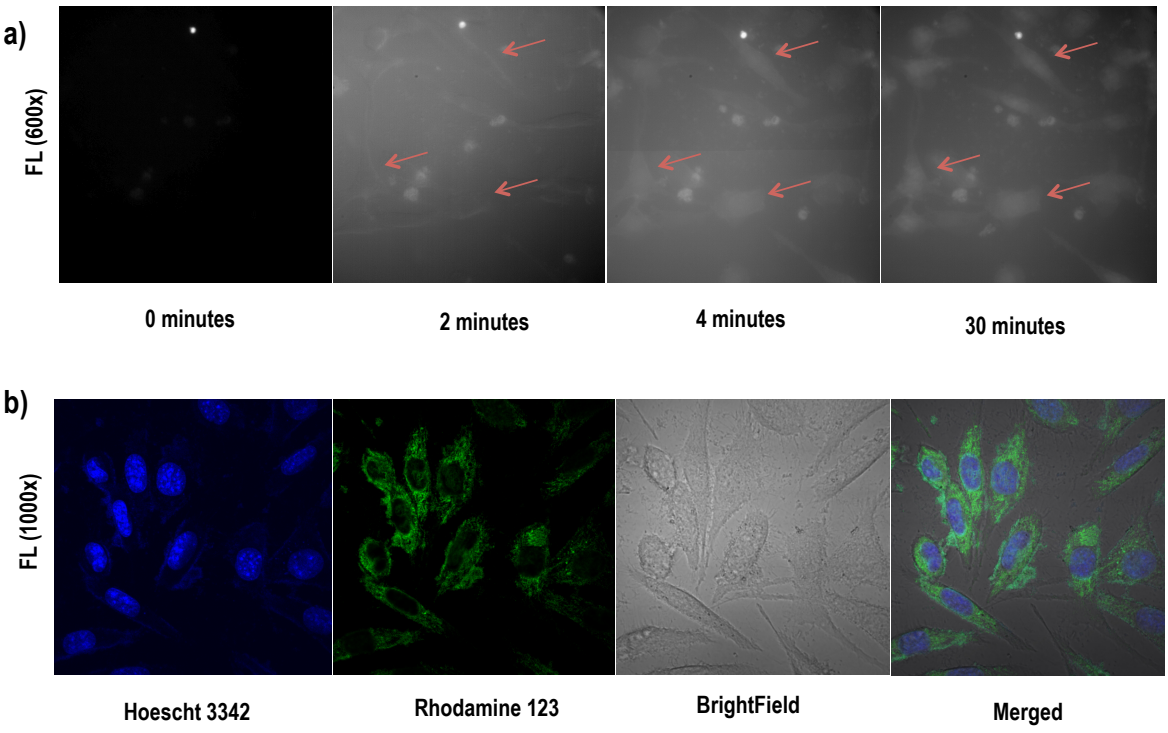

Figure 84. a) Intracellular localization of mitochondria in MCF-7 cell lines. The cells were stained with Hoechst 3342 (blue) for nucleus highlight, with Rhodamine 123 (green) for mitochondria highlight. b) Time-dependent incorporation of oxovitisin A by MCF-7 cell line during 30 minutes. A sequential capture of fluorescence microscopy images was performed using fast capture CCD-CMOS technology. Time 0 represents the cells without the addition of oxovitisin A. The green channel of the fluorescence microscope was used to visualize oxovitisin A fluorescence. The red arrows point for the compound location in the cell.

3.5. Modulation of apoptosis markers on MCF-7 cells by Mv3glc, vitisin A, Me-py and oxovitisin A

The modulation of apoptosis by the compounds was evaluated (Figure 85) measuring the levels of two different apoptotic markers, caspase-3 and caspase-9, using the ELISA assay and subsequent absorbance reading.

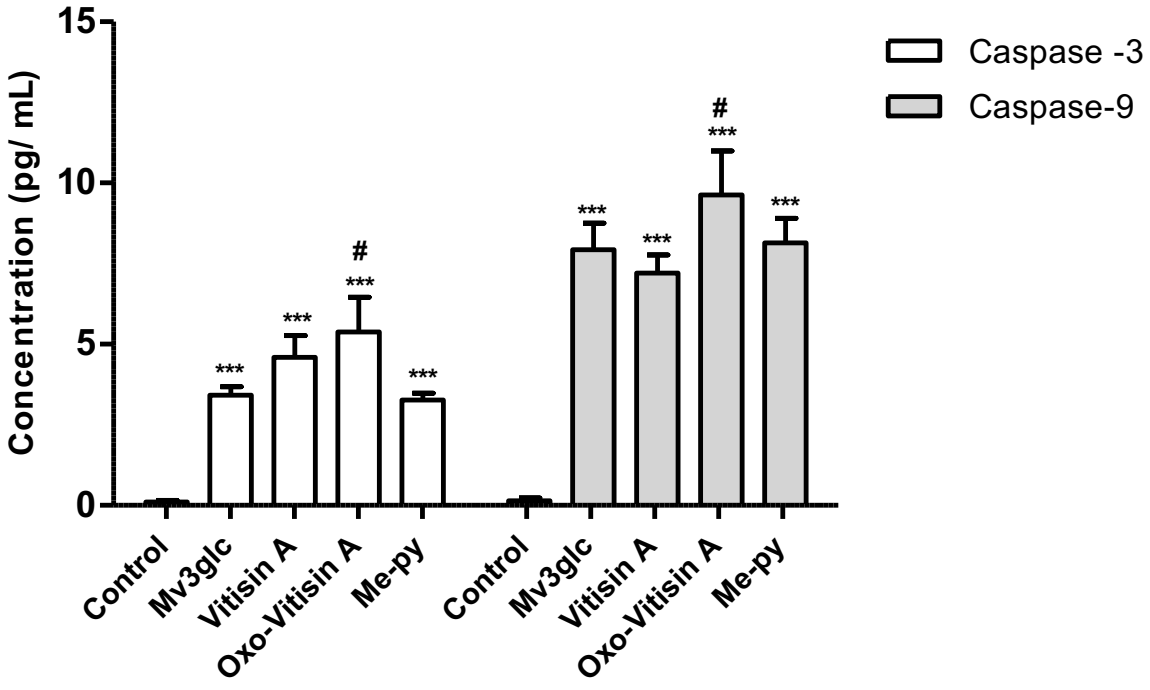

Figure 85. Modulation of Caspase-3 and Caspase-9 apoptotic markers by Mv3glc and its derivatives on MCF-7 cell line. The apoptotic experiments are expressed as the arithmetic means (n = 3) ± standard error mean (SEM). Statistical significance of the difference between compounds for the same cell line. *p<0.05, **p<0.01.

All the compounds showed a significant upregulation of caspase-3 when compared to the control cells (p<0.01 for Mv3glc, vitisin A and Me-py; p<0.001 for oxovitisin A) (Figure 85). Oxovitisin A showed the most efficiency capacity on the activation of caspase-3 among the compounds. Significant differences were found between oxovitisin A and the other pyranoanthocyanins (p<0.05). No significant differences were found between Mv3glc, vitisin A and Me-py. Furthermore, the maximum value of caspase-3 detected was 5.37 ±

1.2 ng/mL for oxovitisin A and the lowest 3.23 ± 0.38 ng/mL. The control revealed values near to undetectable.

Like in the case of caspase-3 modulation, all the compounds showed a significant upregulation of caspase-9 when compared to the control cells ($p<0.01$ for Mv3glc, vitisin A and Me-py; $p<0.001$ for oxovitisin A) (Fig. 4). Oxovitisin A showed the most efficiency capacity on the activation of caspase-9. Significant differences were found between oxovitisin A and the other pyrano-anthocyanins ($p<0.05$). No significant differences were found between Mv3glc, vitisin A and Me-py. Furthermore, the maximum value of caspase-9 detected was 9.33 ± 1.07 ng/mL for oxovitisin A and the lowest 7.67 ± 1.03 ng/mL for Me-py. The control revealed values near to undetectable.

4. DISCUSSION

The gastric absorption of pyrano-anthocyanic derivatives was slightly reduced in comparison with the parental anthocyanin possibly by some steric interference resulting from the higher size of those molecules. The slightly higher gastric absorption value observed for oxovitisin A among the three pyrano-anthocyanins tested may be related to the absence of charge on this molecule. This fact overcomes the problem of the distribution of the initial applied amount by several equilibrium forms and also the difficulty associated with the transport of a charged molecule. The importance of pH on the anthocyanin transport efficiency that may be related not only with the main anthocyanin forms present but also with the influence on the possible transporters involved in their transport was already reported [102].

Besides the proven gastric absorption of these pigments also the intestinal compartment may contribute to the circulatory appearance of anthocyanins derivative pigments [160]. After reaching the systemic circulation the compounds may exert their biological effects in different target tissues.

In this study, the SRB results revealed an interesting capacity for all the compounds in inhibiting the proliferation of breast cancer cells (MCF-7 cell line). All the IC_{50} were lower than the highest concentration tested (380 μM). The choice of this value was based on the previous reported value of around 0.4 mg/mL (around 760 μM, considering Mv3glc molar mass) of anthocyanins that can reach the stomach after the intake of a glass of red wine (200 mL) [293]. Thus, half of the concentration was chosen once breast tissue is far from the anatomical position of stomach and during the bloodstream journey, losses may happen. This first observation is interesting concerning not only the losses involved on the journey to reach breast cancer tissue *in vivo*, but also the low bioavailability of these pigments. All of this, may result in very low concentrations of effective bioactive anthocyanins that can reach far, target tissues. The results show, that even at very low concentrations the anthocyanins can be bioactive against these cancer cells.

Comparing the efficacy among the compounds, is possible to see that significant differences were found between Mv3glc and oxotivisin A, the first one has a smaller IC_{50} value, and that among the derivatives, oxovitisin A is the most effective in inhibiting the proliferation of MCF-7 cells. Concerning the structure of the compounds, oxovitisin A possess a pyranone moiety in its structure, result of a slow micro-oxidation natural process, while vitisin A possess a carboxypyrano moiety derived from the reaction with pyruvic acid,

and Me-py a methylpyrano moiety resulting from the slow oxidation of vitisin A. Furthermore, this latter does not possess an oxonium ion component. This can lead to a more stable compound once it becomes hindered from nucleophilic attacks. In fact, the molar extinction factor analysis revealed a higher colour capacity for oxovitisin A, which can be translated to a more stable compound.

The type of substituent seems to be directly related with the antiproliferative properties of these compounds. The carbonyl group on pyranone oxovitisin A seems to be the most reactive group, followed by the carboxylic acid group on vitisin A and the methyl group on Me-py seems to be the less reactive. Nevertheless, the native compound, Mv3glc, showed the highest efficacy among the compounds tested. To understand the specific, induce-death pathways that may be stimulated by the compounds and that ultimately lead to cancer cells growth inhibition and destruction some complementary approaches were performed.

Due to the remarkable fluorescent properties of oxovitisin A, the incorporation kinetics of this compound in MCF-7 cells revealed that after 4 minutes oxovitisin A was fully incorporated by the cells. Furthermore, at this time a higher intensity on the fluorescence is noticeable on the nucleus and surrounding areas. It is possible to see that the mitochondria are not evenly distributed inside the cell. They seem to be more concentrated in the surrounding areas near the cell nucleus.

Once the apoptotic events are tightly linked to mitochondria, the possible modulation of two apoptosis biomarkers the levels of two pro-apoptotic (caspase-3 and 9) were analysed. Both caspase-3 and caspase-9 were upregulated by all the compounds, however, oxovitisin A showed the highest upregulation among the anthocyanins tested. These observations are once again reinforcing the role of the pyranone ring on the bioactivity of this compound. Among the other compounds, it seems to exist a specific affinity to caspase-3 or 9 and the trend is not clear. In fact, several reports state that anthocyanins can have both pro-apoptotic effects on cells promoting or inhibiting key events on death-pathways [295-297].

Overall, these observations revealed the importance of the carbonyl group to the induction of apoptotic proteins caspase-3 and caspase-9.

Altogether the results confirm the importance of the natural micro-oxidative processes occurring during food ageing and leading to structural changes of anthocyanic compounds to their absorption and biological potential. Nevertheless, more studies are certainly needed to confirm these observations.

CHAPTER II

GASTROINTESTINAL ABSORPTION, ANTIPROLIFERATIVE AND ANTI-INFLAMMATORY EFFECT OF THE MAJOR CAROTENOID OF *GARDENIA JASMINOIDES ELLIS* ON CANCER CELLS

Synopsis

The objective of this chapter was to evaluate the gastrointestinal absorption of the main carotenoids present in *Gardenia jasminoides Ellis*, crocetin, crocin-1 and crocin-2, through transport studies on MKN-28 and caco-2 cell lines.

Overall, crocetin was the compound that presented the highest gastrointestinal transport efficiency.

Additionally, and since, after absorption, crocins is metabolized into crocetin, the antiproliferative capacity of crocetin was assayed in MKN-28 (stomach), MCF-7 (breast) and caco-2 (colon) cancer cell lines.

The results point to an antiproliferative effect of crocetin on the three cell lines tested.

Anti-inflammatory properties were also assayed. Overall, crocetin showed a potential involvement in the downregulation of IL-1β and TNF-α but not IL-6.

Altogether, the results suggest that these compounds can have an important role against cancer proliferation, highlighting the importance of *Gardenia Jasminoides Ellis* as a nutraceutical food source.

This chapter resulted in the following paper: ***Oliveira, H.,*** *Cai, X., Zhang, Q., de Freitas, V., Mateus, N., He, J., Fernandes, I. (2017). "Gastrointestinal absorption, antiproliferative and anti-inflammatory effect of the major carotenoids of Gardenia Jasminoides Ellis on cancer cells", Food and Function, 8, 1672-1679. DOI: 10.1039/c7fo00091j*

1. INTRODUCTION

Gardenia jasminoides Ellis is a flowering plant widely used by many Asian countries in traditional medicine, which belongs to the Gardenia genus and Rubiaceae family. The fruit of this plant has been used for the treatment of hepatic diseases reducing the pain, and for many other disorders like headaches, hypertension and fever [298]. The pigmentation of this herb (yellow) makes it widely used as a natural colorant in Japan and China, in many types of foods like juices, candies and noodles [299]. The major bioactive compounds in *Gardenia jasminoides* Ellis are mainly iridoid glycosides, carotenoids (such as crocetin and its derivatives), monoterpenoids, flavonoids, organic acid esters sterols, and others [300-302]. Saffron spice derived from the flower of Crocus sativus is another herb tipically consumed in Asian countries that contains the same yellow pigments of *Gardenia jasminoides* Ellis [303], but it is the most expensive spice in the world [304], which makes the latter a more attractive economic option.

The compounds responsible for the yellow pigmentation of these herbs are mainly crocetin and its derivatives [305]. Crocetin (Figure 86) belongs to the familiy of carotenoids. It is a 8,8'diapo-8,8'-carotenic acid, characterized by a diterpenic and symmetrical structure with alternating double bounds and four methyl groups, and is slightly soluble in water [306]. Crocins (Figure 86), are a group of hydrophilic carotenoids that are either mono- or di-glycosyl polyene esters of crocetin with D-glucose and/or D-gentiobiose as carbohydrate residues [307].

Several studies suggest the involvement of these compounds in health-promoting effects, mainly due to their antioxidant properties [308-312].

The role of crocetin as anticancer agents has also been assessed by several studies in which the compounds revealed interesting anti-proliferative properties in different types of cancer cell lines [313-315].

Although knowledge about the role of these compounds in cancer inhibiton is already established, some important and relevant features are lacking. To the best of our knowledge, very few is known about the role of crocetin from *Gardenia Jasminoides* Ellis in the inflammatory processes related with cancer development.

Tumour cells produce several types of cytokines that attract leukocytes, in order to get the ideal inflammatory environment state for tumour growth and progress. IL-1β, IL-6 and TNF-α are well known pro-inflammatory cytokines involved in chronic inflammation and cancer development [316, 317]. Although the main effect of these cytokines is tumour

promotion and growth, it highly depends on the overall cytokine microenvironment and network, since these cytokines can have dual roles as pro and anti-inflammatory agents [318].

The bioavailability of the compounds is also a crucial parameter to evaluate before any biological effect can be associated, once it highly defines their effective biological properties. It is important to understand if the compound can reach the target in an efficient concentration, and the effects of the absorption at the gastrointestinal level on their biological activity at internal tissues.

The objective of this study was then to evaluate the gastrointestinal bioavailability of 3 structurally related carotenoids (crocetin, crocin-1 and crocin-2) isolated from *Gardenia Jasminoides* Ellis by performing transepithelial studies, in MKN-28 and caco-2 barrier models. Aditionally, the antiproliferative effects of crocetin on three different cancer cell lines, MKN-28 (stomach), caco-2 (colon) and MCF-7 (breast) and the levels of inflammatory biomarkers, IL-6, IL-1β and TNF-α were also evaluated.

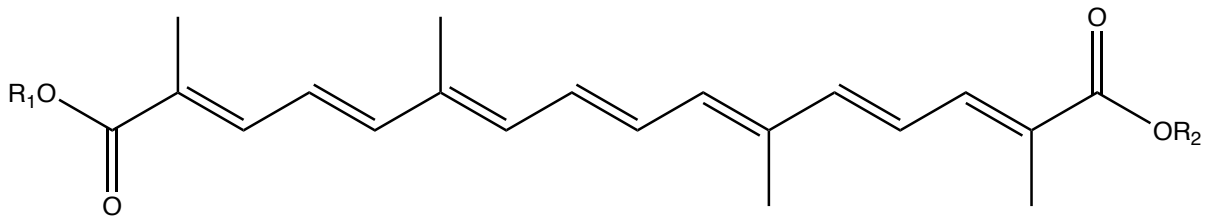

Crocetin: R_1, R_2 = H

Crocin-1: R_1, R_2 = 6-*O*-(α-*D*-glupyranosyl-)-*D*-Glucopyranose

Crocin-2: R_1 = 6-*O*-(α-*D*-glupyranosyl-)-*D*-Glucopyranose, R_2 = *D*-glucopyranose

Figure 86. Chemical structure of crocetin, crocin-1 and crocin-2.

2. MATERIALS AND METHODS

2.1. Reagents

Crocetin (>90%), Crocin-1 (>98%) and Crocin-2 (>98%), isolated from *Gardenia Jasminoides Ellis*, were obtained from Chengdu Biopurify Phytochemicals Ltd., China.

2.2. Cell Culture Conditions

Three human cancer cell lines (MKN-28 (stomach), Caco-2 (colon) and MCF-7 (breast)) were grown as monolayer. For routine maintenance, cells were cultured in 25 cm^2 plates as monolayer and maintained in RPMI-1640 (MKN-28) or DMEM (Caco-2 and MCF-7), and supplemented with 10 % or 15 % heat-inactivated FBS, 1 % antibiotic/antimycotic solution (100 units/mL of penicillin, 100 µg/mL of streptomycin and 0.25 µg/mL of amphotericin B) at 37 °C in a humidified atmosphere with 5 % CO_2. Cells were harvested by trypsinisation (0.25% (w/v) trypsin–$EDTA_4Na$) twice a week. The exponentially growing cells were obtained by plating 1.5 × 10^5 cells/mL, followed by 24 h incubation before adding the compounds. A stock solution of each compound was prepared and kept at −20°C. Appropriate dilutions of each sample fraction were freshly prepared just prior to every assay.

2.3. Transport assays

For the transport experiments, MKN-28 cells were seeded at a density of 10^5 cells/cm^2 on 12-well transwell inserts (0.4 µm pore size tissue culture inserts (Corning Costar, Corning, NY, USA)) and grow for 7 days in humidified incubator at 37ºC, 5% CO_2, before obtaining a dense and well differentiated cell monolayer. The culture medium was changed every 2 days. Caco-2 cells were grown in the same transwell system for 21 days.

Monolayers were placed in a water bath at 37°C and transepitelial electrical resistance (TEER) of the monolayer was measured using a MILLICELL-ERS epithelial voltammeter (Millipore Co.; Bedford, MA). Only monolayers with electrical resistance value > 150 Ω (MKN-28) and > 250 Ω (Caco-2) were used for experiments.

For the transport, each compound at 100 µM in Hank's buffer (pH 5.0 in gastric cell model and pH 7.4 in intestinal cell model)) was added to the apical side of the monolayers and

1.5 mL of Hank´s buffer (HBSS) with 2% fetal serum (pH 7.4) were maintained at basolateral side. Transepitelial transport was followed as a function of time: 0, 30, 60, 120 and 180 minutes (only for gastric cell model) and for each moment, samples (150 µL) were collected from the basolateral side, replaced by fresh medium, acidified (1% HCl 6 M) and frozen -20ºC until HPLC analyses.

2.4. Sulforhodamine B (SRB) assay

The effects of crocetin on the growth of the three cell lines were evaluated according to the procedure adopted by the US National Cancer Institute in the "In vitro Anti- cancer Drug Discovery Screen" that uses the protein-binding dye SRB to assess cell growth, according to the procedure previously described by Oliveira and coworkers [293]. Briefly, cells (1.5×10^5 cells/mL) were spread into 96-well plates and allowed to grow for 24 h before treatment, ensuring exponential growing state. After, cells were incubated with crocetin for 2 days and exposed to five serial concentrations (200; 100; 50; 25 and 12.5 µM) for MKN-28, Caco-2 and MCF-7 cells. Incubation process was stopped by addition of TCA 50%, 1 h at 4°C. The plates were then washed with distilled water with 1 % of acetic acid. The plates were dried and were stained with a 0.4 % solution of SRB. The dye was eluted with Trizma buffer (10 mM, pH 10.5) and after 30 minutes, quantified photometrically at 492 nm in a multimode microplate reader (triplicates of each fraction sample) (Enspire, PerkinElmer, Massachussetts, USA). Concentrations were equal in all cell lines tested to facilitate comparison between results.

2.5. 5-Bromo-2'-deoxyuridine (BrdU) assay

Briefly, cells (1.5×10^5 cells/mL) were spread into 96-well plates and allowed to grow for 24 h before treatment, ensuring exponential growing state. After, cells were incubated with crocetin for 48 h and exposed to five serial concentrations (200; 100; 50; 25 and 12.5 µM) for MKN-28, Caco-2 and MCF-7 cells).

The BrdU was added to each well at a concentration of 10 µM during 2 hours for incorporation in DNA. After that, the procedure was as described by the kit manufacturer (Cell Signaling Technology, Inc.).

2.6. Evaluation of IL-1β, IL-6 and TNF-α

Cells were spread on 6-well plates with a density of 1.5 × 10^5 cells/mL and allowed to grow for 24 h previous to the experiments. Cells were treated with the crocetin (200 μM) for 6 h (for control, medium was renewed). The supernatants were collected and placed in ELISA plates. Further procedures were as described by the kit manufacturers (Cloud-Clone Corporation, Houston, USA).
The equation curves used for the calculations were as follows:

$$\textbf{IL-1b: } y = 15.056x^2 + 186.8x - 25.666, R^2 = 0.99487$$
$$\textbf{IL-6: } y = 62.209x^2 + 7.9337x + 0.6558, R^2 = 0.99559$$
$$\textbf{TNF-α: } y = 2.9702x^2 + 35.05x - 12.282, R^2 = 0.99664$$

The results were obtained considering control as 100% of production, based on the following equation:

$$\%\, production = \frac{Concentration\ of\ sample}{Concentration\ mean\ of\ control} \times 100$$

2.7. HPLC analysis

For quantitative analysis, the HPLC-DAD determination was analyzed by SSI series 1500 HPLC system (SSI, Scientific System Inc., USA) coupled with an online degasser, two 1500 pumps, a PDA detector, a thermostatically controlled column compartment and an auto-sampler. The HPLC chromatographic separation was carried out using a Luna C18 (Phenomenex, San Francisco, CA, USA). The separation conditions were as follows: column temperature was set at 30 °C; UV-Vis spectra were recorded in the range from 220 to 780 nm; chromatograms were acquired with channel A (440 nm) for crocin-1 and crocin-2, channel B (420 nm) for crocetin; injection volume was 20 μL; 0.3% formic acid aqueous solution A and 100% acetonitrile B were used as mobile phases. The elution gradients were as follows: initially 70% of mobile phase A, 30% B; followed from 70% to 60% A, 30% to 40% B in 5 min; 0% A and 100% B at 10 min, and then returned to 70% A and 30% B at 15 min, keep for 5 min. The flow rate was 0.8 mL.min^{-1}.

2.8. Statistical Analysis

The transport studies experiments were expressed as the arithmetic means (n=6) ± standard error mean (SEM). Statistical significance of the difference between treatments was evaluated by two-way analysis of variance (ANOVA), followed by the Bonferroni's correction for multiple comparisons.

Differences were considered to be statistically significant when *p<0.05; **p <0.01; ***p <0.001 vs control for the same cell line. Each experiment was independently repeated at least 3 times.

The antiproliferative experiments (SRB and BrdU) are expressed as the arithmetic means (n = 6 or n=4) ± standard error mean (SEM). Statistical significance of the difference between cell lines was evaluated by one-way analysis of variance (ANOVA).

The evaluation of cytokines levels are also expressed as the arithmetic means (n=6) ± standard error mean (SEM). Statistical significance of the difference between crocetin vs control for each cell line was evaluated by two-way analysis of variance (ANOVA) followed by Bonferroni post-test.

3. RESULTS

3.1. Transport Studies

The gastrointestinal transport of the three carotenoids (crocetin, crocin-1 and crocin-2) (Figure 86) were evaluated using Transwell™ system with MKN-28 and Caco-2 cell lines as gastric and intestinal barriers, respectively. All transport experiments were performed in a transwell plate system introducing the Hanks buffer, pH 5 or pH 7.4, in which the compounds (100 μM) were previously dissolved, in the donor chamber.

3.1.1. Transport across MKN-28 cell line

Overall, crocetin seemed to be the compound with the highest transport efficiency. A representative chromatogram of the apical side at time zero of crocetin and each incubation time point of the basolateral side is presented in Fig. 6. After 30 minutes, significant differences between crocetin and crocin-1 and 2 are already noticeable (Figures 87 and 88). Significant differences between crocin-1 and crocin-2 are only noticeable after 120 min, revealing crocin-1 as the least transported of the three compounds tested (Figures 87 and 88)

.

3.1.2. Transport across Caco-2 cell line

The results for the intestinal transport showed a different pattern than that revealed for the gastric transport studies. Crocetin and crocin-1 seemed to be the two most efficient compounds transported across Caco-2 cell line during the time of the experiment (Figure 88). On the other hand, crocin-2 showed the lowest transport rate (Figure 88).

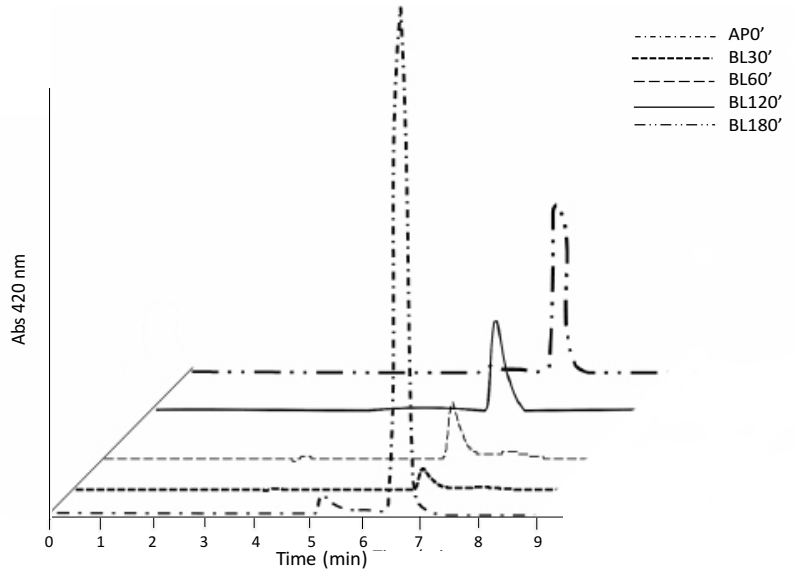

Figure 87. Representative chromatogram of the apical and basolateral sides of gastric barrier after incubation with crocetin. AP0'- Time zero, apical side. BL30'- after 30 minutes, basal side; BL60'- after 60 minutes, basal side; BL120'- after 120 minutes, basal side; BL180'- after 180 minutes, basal side.

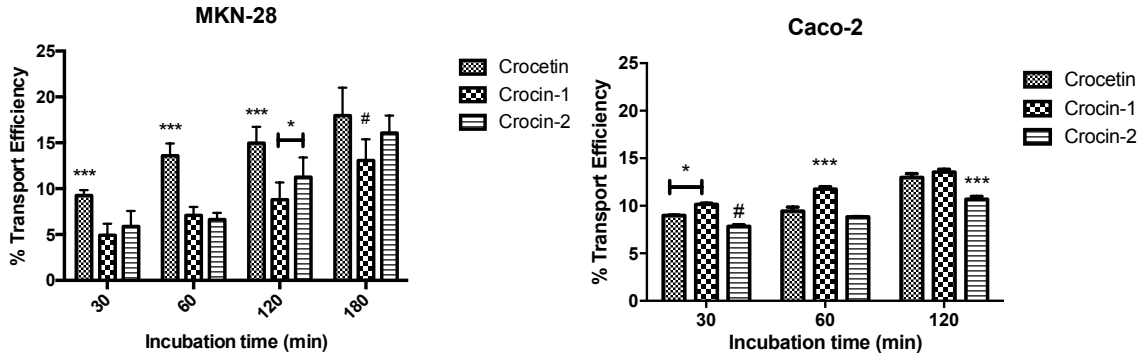

Figure 88. Transport studies on gastric and intestinal barriers. The experiments are expressed as the arithmetic means (n = 3-6) ± standard error mean (SEM). Statistical significance of the difference between compounds for the same cell line was evaluated by two-way analysis of variance (ANOVA), followed by the Bonferroni test. *p<0.05, ***p<0.001. # stands for significant different from all others.

3.2. Antiproliferative activity and S-phase arrest

The effect of crocetin, on the proliferation of three human cell cancer lines were evaluated not only in the two cell lines from the gastrointestinal system MKN-28 (gastric adenocarcinoma) and Caco-2 (colon cancer), but also in a target tissue using MCF-7 cell line as breast cancer model. Growth inhibitory effects evaluated by the SRB and BrdU methods were expressed in IC_{50} values and are represented in Figure 89 and 90. Crocetin showed a dose-dependent proliferative inhibitory effect on the three cell lines after a continuous exposure of 48h.

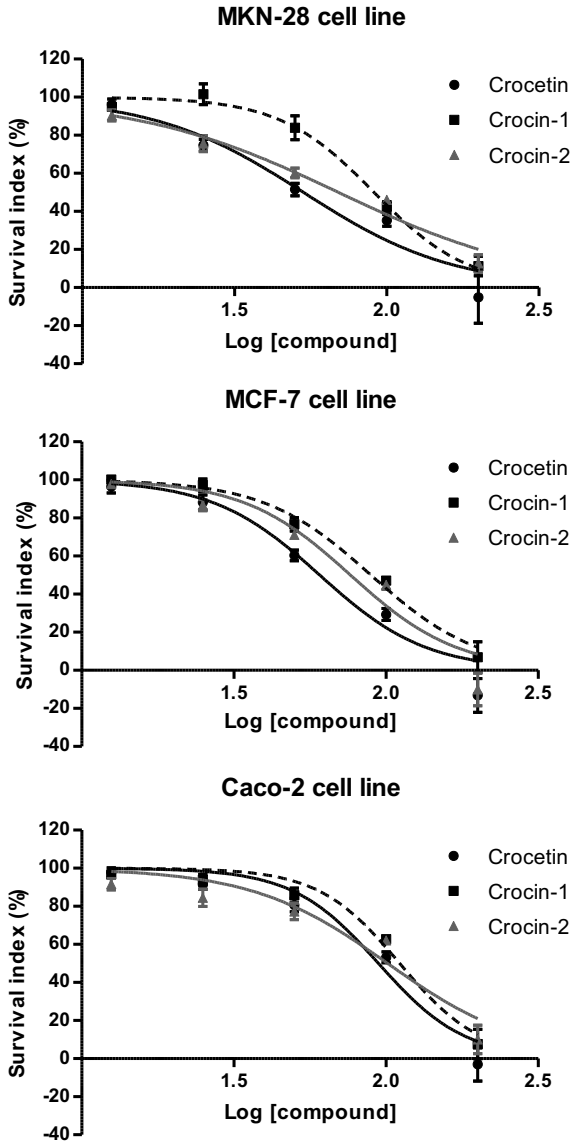

IC_{50} (Crocetin) 53.23 ± 4.45^{a} µM
IC_{50} (Crocin-1) = 90.06 ± 1.31^{b} µM
IC_{50} (Crocin-2) = 74.43.± 1.08^{c} µM

IC_{50} (Crocetin) 63.18 ± 0.54$^{a, c}$ µM
IC_{50} (Crocin-1) = 94.07 ± 2.40^{b} µM
IC_{50} (Crocin-2) = 89.55 ± 3.20$^{b, c}$ µM

IC_{50} (Crocetin) = 103.33 ± 5.30$^{b, c, d}$ µM
IC_{50} (Crocin-1) = 117.73 ± 0.91^{d} µM
IC_{50} (Crocin-2) = 107.70 ± 1.12^{d} µM

Figure 89. Effect of crocetin, in MKN-28, MCF-7 and Caco-2 cell lines proliferation by using the SRB method. The antiproliferative experiments are expressed as the arithmetic means (n = 12) ± standard error mean (SEM). Different letters means significant differences from the others.

3.2.1. Sulforhodamine B assay

Crocetin showed biological activity in the three cell lines tested (IC_{50} values lower than 110 µM). The compounds appear to have a selectivity for MKN-28 and MCF-7 cell lines. Overall, crocetin showed the lower IC_{50} value in stomach cells, followed by breast and colon cell lines. Significant differences were found between Caco-2 and both MKN-28 and MCF-7 ($p<0.001$) (Figure 89).

Thus, MKN-28 seems to be the most susceptible cell line to the effect of the compounds as it showed the overall lowest IC_{50} values. On the other hand, Caco-2 showed to have a higher resistance to the antiproliferative properties of the compounds when compared to MKN-28 and MCF-7 as revealed by the overall highest IC_{50} values.

3.2.2. 5-Bromo-2'-deoxyuridine (BrdU) assay

The effect of crocetin in cell proliferation was also tested by BrdU incorporation assay. 5-Bromo-2'-deoxy-uridine (BrdU) can be incorporated into DNA in place of thymidine. The results showed that the inhibition of cell proliferation is dose-dependent in all cell lines tested (Figure 90).

The number of cells in S phase was quantified after incubation with crocetin during 48 h. The number of cells in S phase was significantly reduced after the treatment in comparison to control cells.

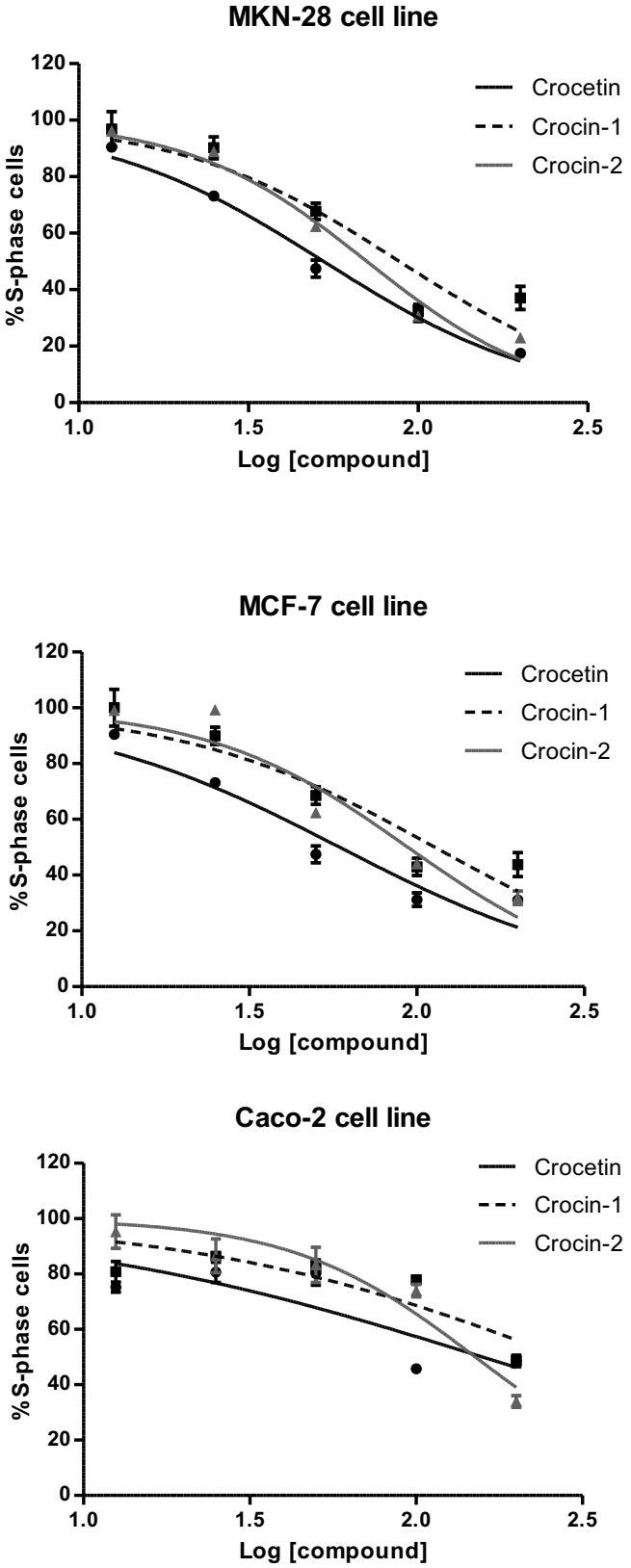

Figure 90. Effect of crocetin in S phase arrest detected by BrdU incorporation analysis. MKN-28, MCF-7 and Caco-2 cells were incubated in the presence of crocetin, crocin-1 and crocin-2 for 48h. The experiments are expressed as the arithmetic means (n = 4) ± standard error mean (SEM).

3.3. IL-1β, IL-6 and TNF-α levels modulation

3.3.1. IL-1 β

Crocetin showed inhibitory capacity on the production of IL-1β (Figure 91). For all cell lines tested the crocetin revealed a significant reduction of IL-1 β levels, when compared to control. MKN-28 seems to be the most resistant cell line to the inhibitory effect of the compounds on IL-1 β, followed by MCF-7 and Caco-2. Significant differences were found between MKN-28 and both MCF-7 and Caco-2 ($p<0.001$). Also, significant differences were found between MCF-7 and Caco-2 ($p<0.01$).

3.3.2. IL-6

The results show major differences between the cell lines tested and it is not possible to get an overall pattern (Figure 91).

For MKN-28, crocetin show no significant differences when compared to the control group. On the other hand, for MCF-7, the groups treated with the crocetin revealed a higher level of IL-6 when compared to the constitutive amounts (considered 100%) on the control group.

In Caco-2, crocetin did not show any significant effect on IL-6 levels modulation in this cell line (Figure 91). Significant differences were found between MCF-7 and MKN-28 and caco-2 cell lines for crocetin treatment ($p<0.001$). Thus, IL-6 seems to be upregulated by crocetin in MCF-7 but not in MKN-28 and Caco-2.

3.3.3. TNF-α

Crocetin showed a remarkable inhibitory capacity for TNF-α production in all cell lines tested (Figure 91)

MCF-7 seems to be the most resistant cell line among the cell lines tested, as revealed for the highest values of TNF-α production after treatment.

Although no significant differences were found for MKN-28 and Caco-2 cell line, the pattern followed seems very similar to the other cell lines, with MKN-28 being the most susceptible cell line.

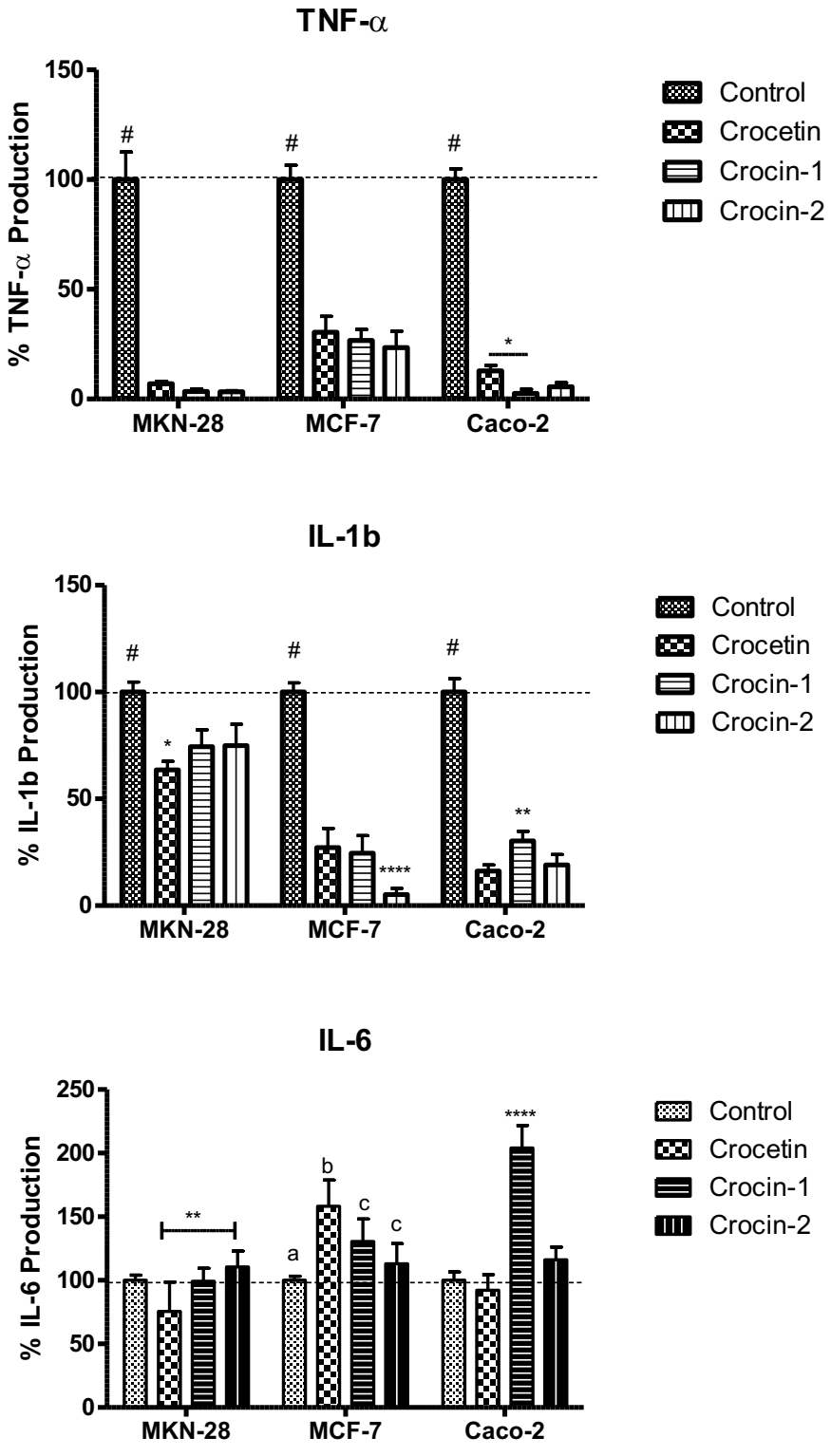

Figure 91. IL-1β, IL-6 and TNF- α levels modulation by crocetin, in MKN-28, MCF-7 and Caco-2 cell lines. The experiments are expressed as the arithmetic means (n = 3) ± standard error mean (SEM). Statistical significance of the difference between controls and for crocetin in each cell line same cell line was evaluated by two-way analysis of variance (ANOVA), followed by the Bonferroni test. *p<0.05, **p<0.01, ***p<0.001.

4. DISCUSSION

Nowadays, the evaluation of the biological properties of natural compounds present in the diet needs to be reinforced by the evaluation of their bioavailability. Thus, in this study the transport of crocetin, crocin-1 and crocin-2 was evaluated across MKN-28 (gastric) and Caco-2 (intestinal) cell lines. Overall, the transport was higher on MKN-28, which can be due to differences between cell lines and the barrier form. In fact, studies with anthocyanins also suggest that the transport is higher on gastric barriers than intestinal ones [103, 108]. Crocetin seems to be the most efficiently transported compound on gastric cell barrier, and both crocetin and crocin-1 on the intestinal barrier. Once again these observations may be due to differences on the cell phenotype. Nevertheless, the results revealed an interesting rate of absorption for all the compounds tested, which justify other biological studies on some tissues (considering ingestion) such as breast cancer cells. After absorption, crocins lose their glucose moieities and are converted into crocetin [319, 320], which justifies the option of only evaluate the biological effects of crocetin of the following experiments performed.

The antiproliferative capacity of crocetin was evaluated with the conjugation of two techniques, SRB and BrdU assays. Overall, for the SRB experiments, the results revealed that crocetin was bioactive in all cell lines tested at the range of concentrations used (200 to 12.5 μM). Similarly, a study performed with Cervical cancer cell line HeLa, non-small cell lung cancer cell line A549 and ovarian cancer cell line SKOV3, crocetin showed cytotoxic effects and potentiated the effects of vincristine [321]. In another study, it was suggested that *Crocus sativus* L. (saffron) extract and its major constituents, crocetin and crocins, significantly inhibited the growth of colorectal cancer cells while not affecting normal cells [315].

It is clear that crocetin revealed a cytotoxic effect in all the cell lines tested revelead by the IC_{50} values. This was further confirmed by the BrdU experiments. The conjugated diene that characterizes crocetin and its lipophilicity can give a high rate of reactivity that may result in the observations. Also, the structural conformation of crocetin may influence the cytotoxicity. The fact that it has hydrogen endings (reducing possible steric hindrance effects) promotes a better conformational adaptation for target-ligand interactions and may also influence the efficacy against the growth of these types of cancer cells. Nevertheless, further research is certainly needed to confirm these aspects.

Concerning the different cell lines, MKN-28 seems to be the most susceptible to the antiproliferative effects of crocetin as revealed by the lowest IC_{50} values, followed by MCF-

7 and finally by Caco-2, which revealed to be the most resistant one. This may be due to singular characteristics in the genotype and phenotype of the different cell lines tested.

Following exposure to pathogens, the imunne systems (both innate and specific) act and cooperate during the acute inflammatory responses to eliminate the cause and prevent further damage to the surrounding tissues.

When the imunne responses are not able to solve the problem, a long term chronic inflammation state is established, thus leading to an altered enviroment on the tissue, with persistent immune cells infiltrates and the release of oxidative agents such as the ROS and reactive nitrogen species (RNS) between other events that lead to DNA damage. These conditions raised through the continuous inflammatory state are ideal for cancer initiation and tumour progression [322].

Furthermore, the progression of the tumour to more agressive states can then promote inflammation in an auto-capable manner. Cancer cells will release inflammatory cytokines that will attract more immune cells and potentiate the inflammation state which will promote key events in tumour progression such as angiogenesis. Inflammatory cytokines such as IL-1β, IL-6 and TNF-α are usually high in tumour cells when compared to normal cells [323].

Thus, agents that can effectively downregulate the levels of these cytokines in cancer cells will have a potential effect on the overall inflammatory and cancer environment.

In this study, all the cells were treated with 200 μM of crocetin for 6 h to induce an acute treatment. The results revealed major differences between the several cytokines analysed. IL-6 modulation was not clear among the different cells and a pattern could not be found from cell to cell.

In the particular case of MFC-7, crocetin even raised the constitutive levels of IL-6. These may be related to specific cell-compound interactions, and may not dictate a pro-inflammatory role of these compounds. Actually, IL-6, in cancer, usually acts as a proinflammatory cytokine, promoting tumour growth and progression [324], although, this role highly depends on the extra and intracellular environment and in the balance of the overall amount of the different cytokines and chemokines. Nevertheless, the upregulation that was found in MCF-7 upon treatment with crocetin deserves further investigation.

IL-1β is a pleiotropic cytokine with numerous roles in both physiological and pathological states. It is known to be upregulated in many tumour types and has been implicated as a factor in tumour progression via the expression of metastatic and angiogenic genes and growth factors.

Cancer cells can directly produce IL-1β or induce cells within the tumour microenvironment to do so [325]. Several studies have documented a constitutive IL-1β protein production in human and animal cancer cell lines including sarcomas and ovarian and transitional cell carcinomas [326].

Overall, crocetin showed a remarkable capacity to downregulate the levels of IL-1β in all the cells tested.

It seems that crocetin can act in an effective anti-inflammatory manner against this cytokine. The fact that the results are less pronounced in MKN-28 may be due to the differences in the intracellular environment.

The pro-inflammatory cytokine TNF-α is also a key downstream mediator in inflammation. TNF-α is important in early events in tumours, regulating a cascade of cytokines, chemokines, adhesion factors, MMPs and pro-angiogenic activities [327]. Thus, TNF-α is one of the key pathways in which inflammation acts as a tumour promoter.

The results for TNF-α are similar to the other cytokines evaluated, as crocetin showed an inhibitory effect of the production of this cytokine. MCF-7 showed a higher resistance to the effect of crocetin of TNF-α production when compared to the other cells.

No correlation between the chemical structure of crocetin and the anti-inflammatory response of this compound in the different cell lines tested, was found. Nevertheless, we show here that crocetin, can downregulate the levels of IL-1β and TNF-α in the cell lines tested.

Although the IL-6 levels were not clearly downregulated, the effect on the other cytokines may dictate an overall multitarget anti-inflammatory action of crocetin.

The inhibition of these cytokines induces further alterations in the metabolism of cancer cells that can culminate in the tumour regression and death. Thus, the modulation of the inflammatory state on cancer cells can be a key event for the tumoricidal effects of crocetin. Nevertheless, it is clear that other key events are involved in the antiproliferation capacity of the compounds, once there is no correlation between the anti-inflammatory findings and the antiproliferative capacities revealed in this study.

In summary, these results show that “Gardenia Jasminoides Ellis” crocetin can act as antiproliferative and anti-inflammatory agent on the gastrointestinal tract, and that together with crocetin esters, can be effectively absorbed at gastric and intestinal level after ingestion.

CONCLUDING REMARKS

This work brought new insights on the clarification of the complex network involved on anthocyanins bioavailability.

It was demonstrated that acylated anthocyanins with high molecular weight have bioavailability properties comparable with the common anthocyanins, which is definitely very interesting due to their overall higher resistance.

This work allowed to open new perspectives and prompted the formulation of new ideas applied to this research field.

These results showed promising characteristics for both the food industry and health industry.

Anyway, several questions remain unanswered and more studies are needed to fully understand this universe of anthocyanins bioavailability.

ATTACHMENTS

ATTACHMENT I

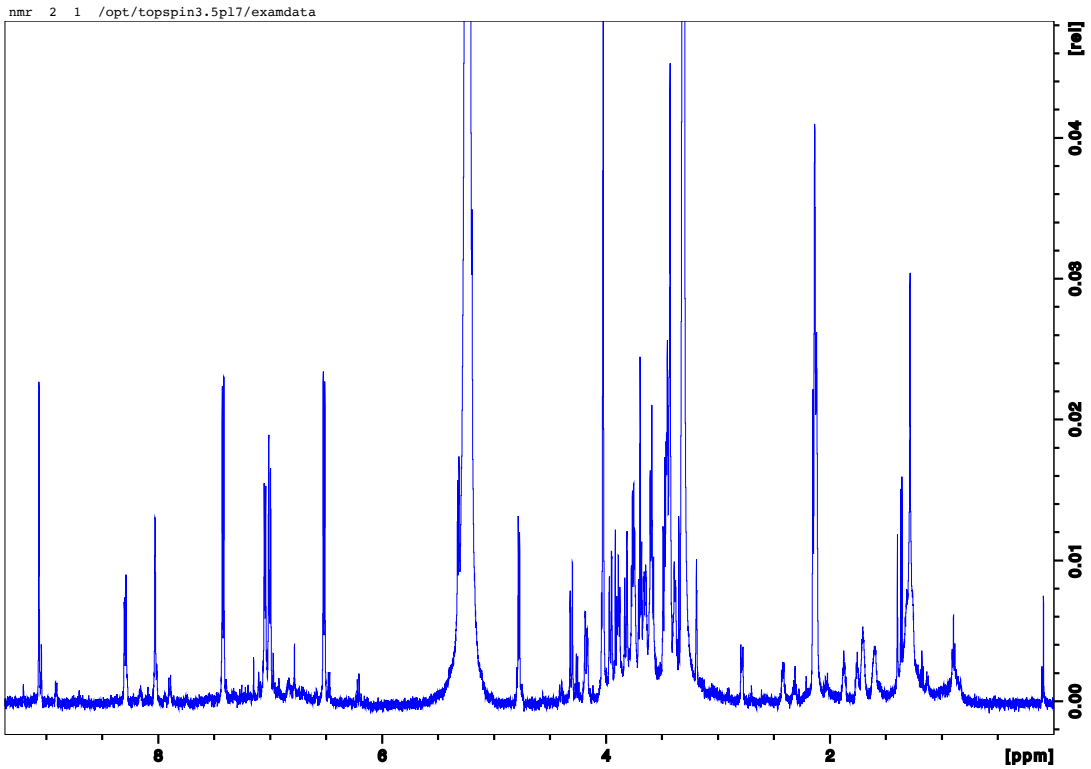

Attachment 3a. ^{1}HNMR complete spectrum of *Peonidin-3-(6'-p-hydroxybenzoyl)-sophoroside-5-glucoside.*

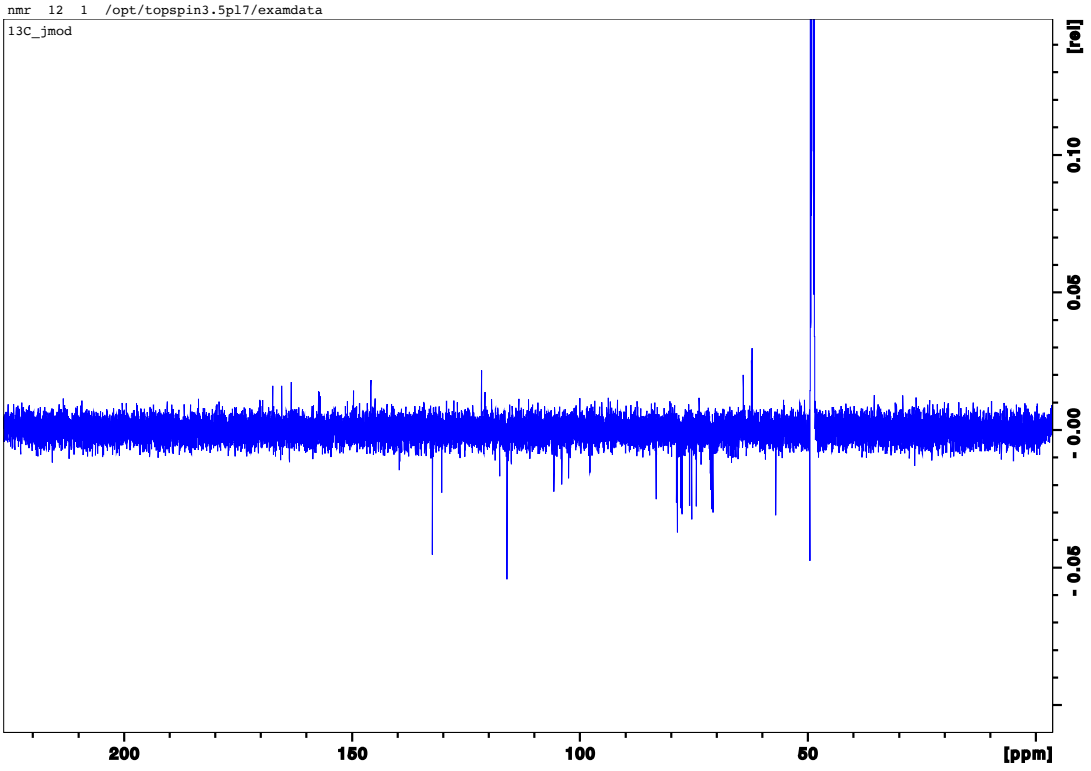

Attachment 1b. ^{13}CNMR-APT spectrum of *Peonidin-3-(6'-p-hydroxybenzoyl)-sophoroside-5-glucoside.*

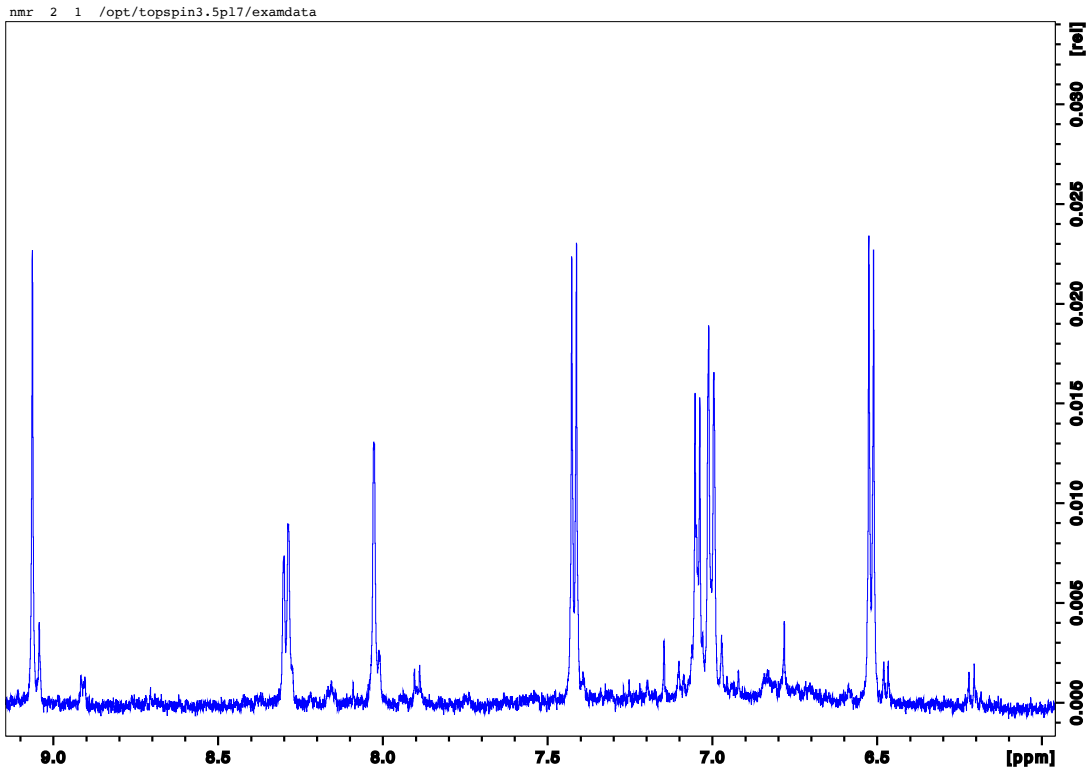

Attachment 1c. [1]HNMR spectrum of aromatic rings zone of *Peonidin-3-(6'-p-hydroxybenzoyl)-sophoroside-5-glucoside.*

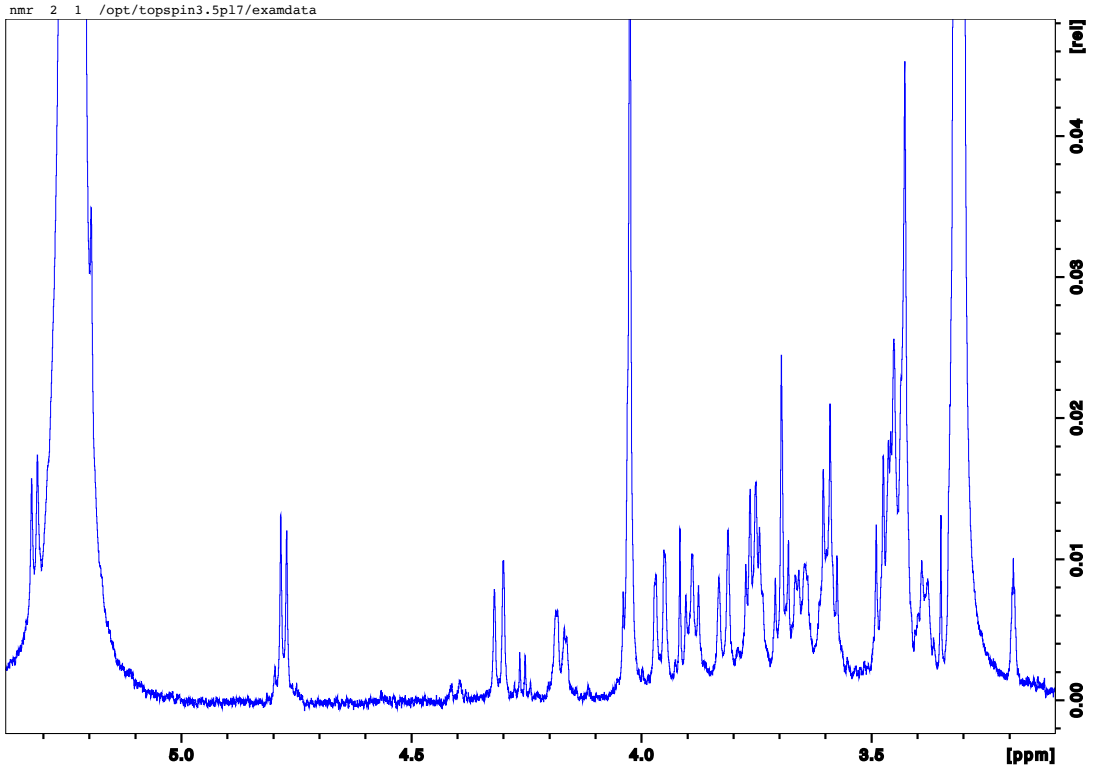

Attachment 1d. ^{1}HNMR spectrum of glucose protons zone of *Peonidin-3-(6'-p-hydroxybenzoyl)-sophoroside-5-glucoside.*

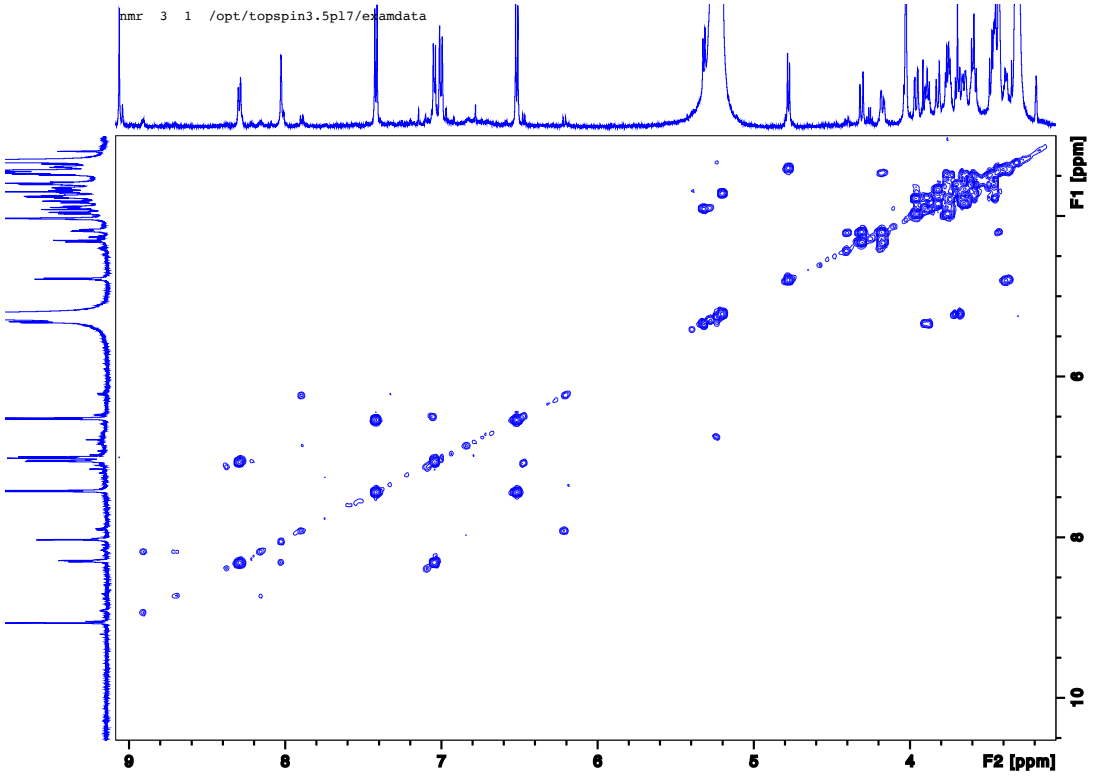

Attachment 1e. COSY complete spectrum of *Peonidin-3-(6'-p-hydroxybenzoyl)-sophoroside-5-glucoside.*

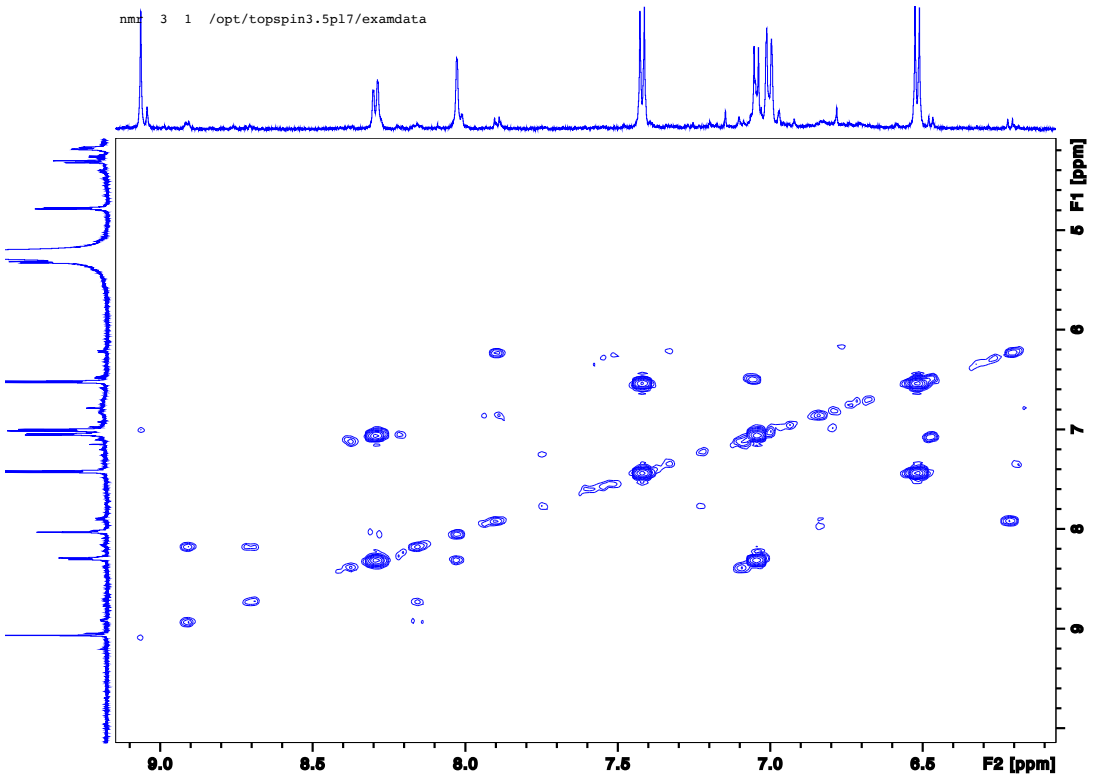

Attachment 1f. COSY spectrum with aromatic rings zone correlations evidenced for *Peonidin-3-(6'-p-hydroxybenzoyl)-sophoroside-5-glucoside.*

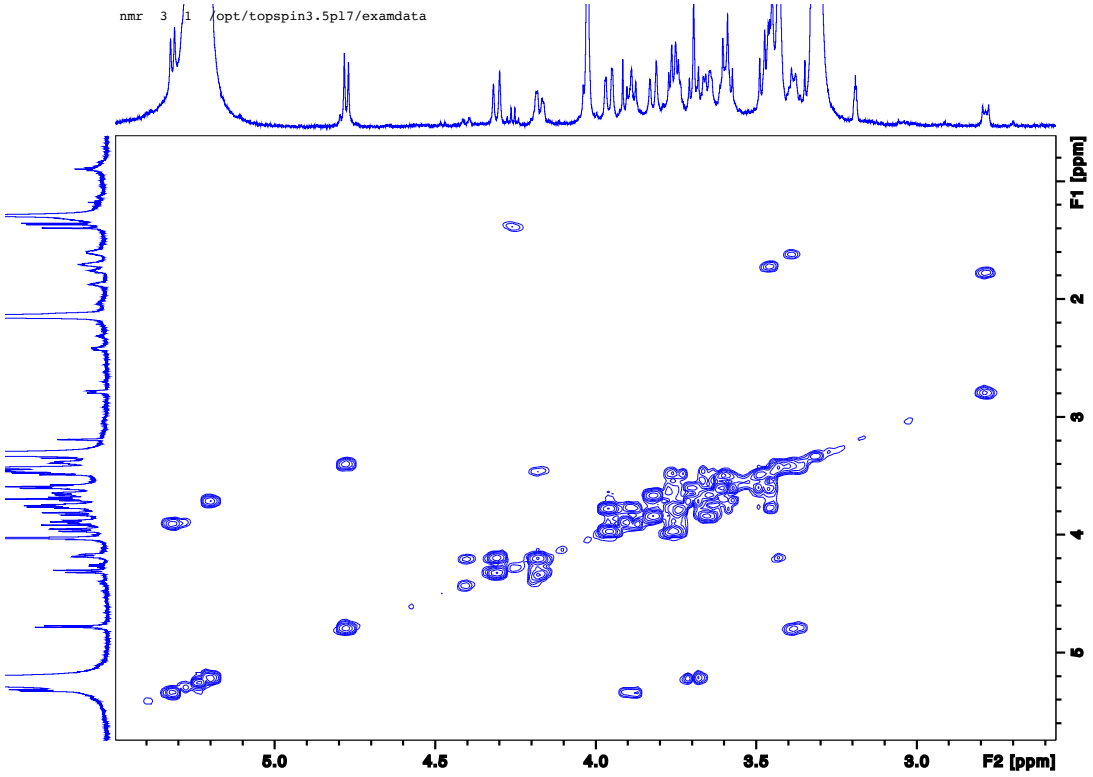

Attachment 1g. COSY spectrum with glucose protons zone correlations evidenced for *Peonidin-3-(6'-p-hydroxybenzoyl)-sophoroside-5-glucoside.*

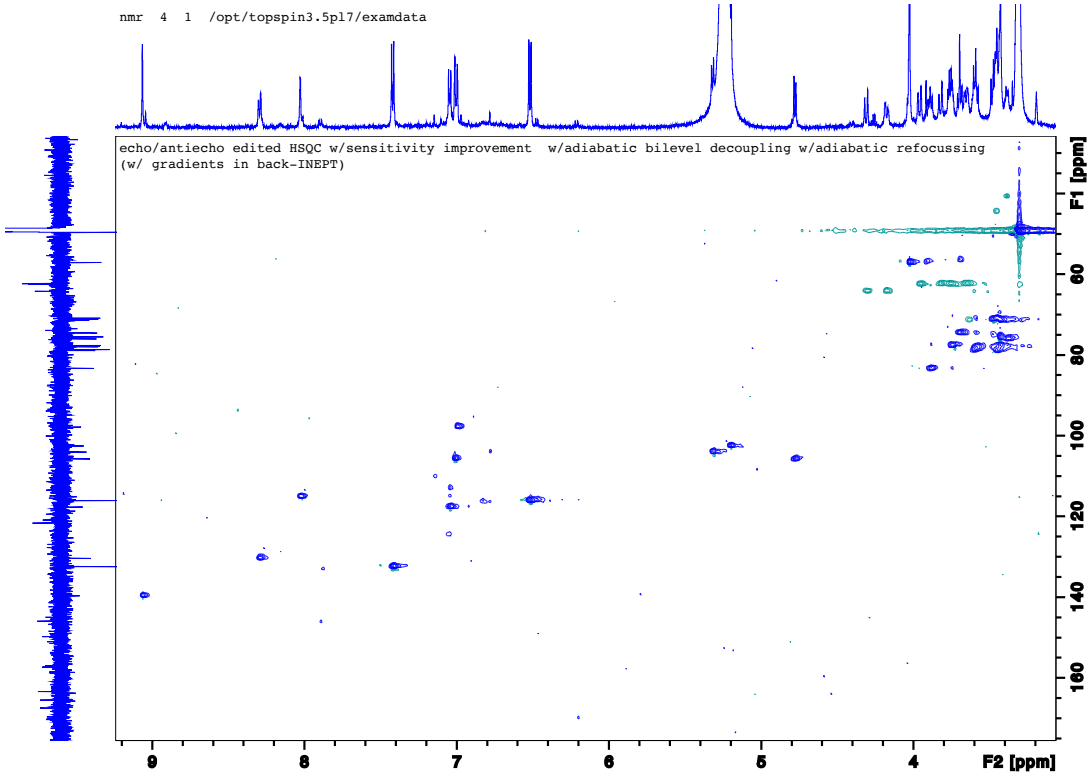

Attachment 1h. HSQC complete spectrum of *Peonidin-3-(6'-p-hydroxybenzoyl)-sophoroside-5-glucoside.*

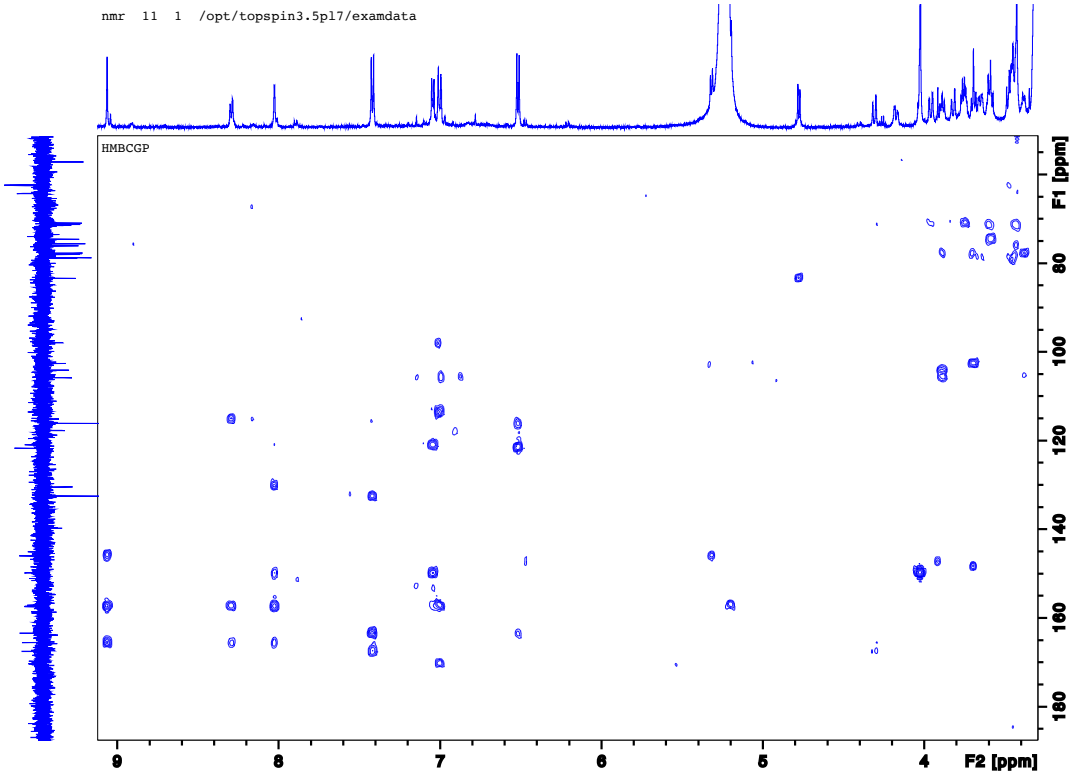

Attachment 1i. HMBC complete spectrum of *Peonidin-3-(6'-p-hydroxybenzoyl)-sophoroside-5-glucoside.*

ATTACHMENT II

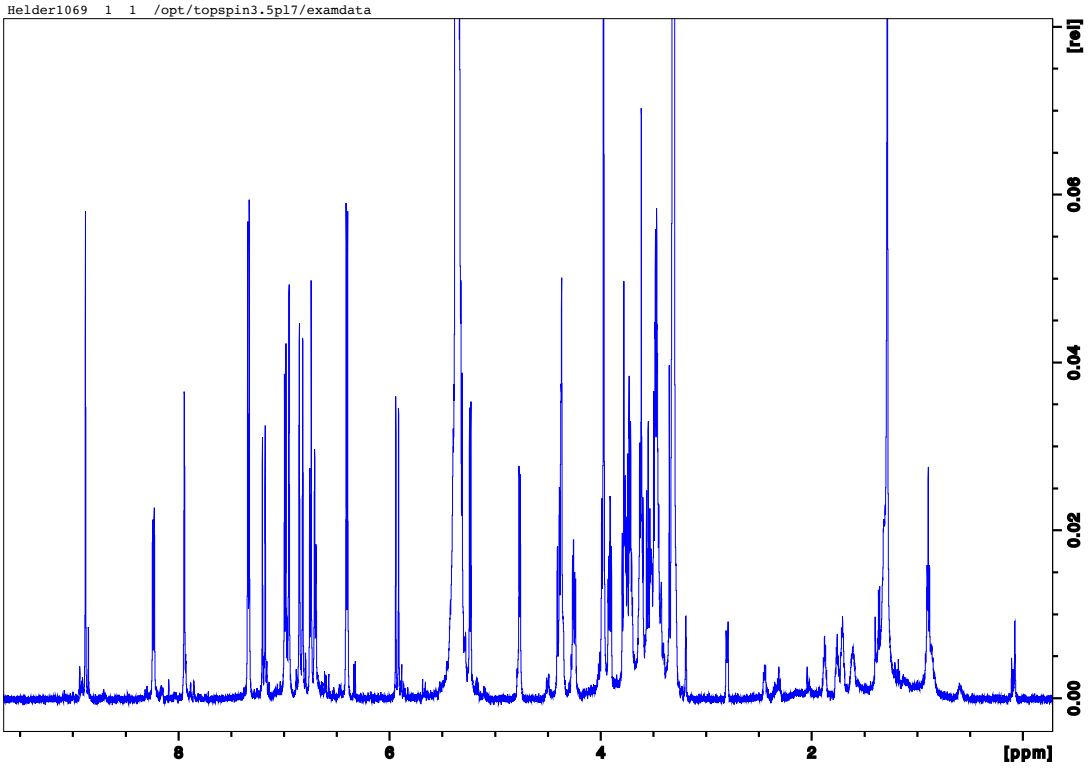

Attachment 2a. ^{1}HNMR complete spectrum of *Peonidin-3-(6'-p-hydroxybenzoyl-6''-caffeoyl)-sophoroside-5-glucoside.*

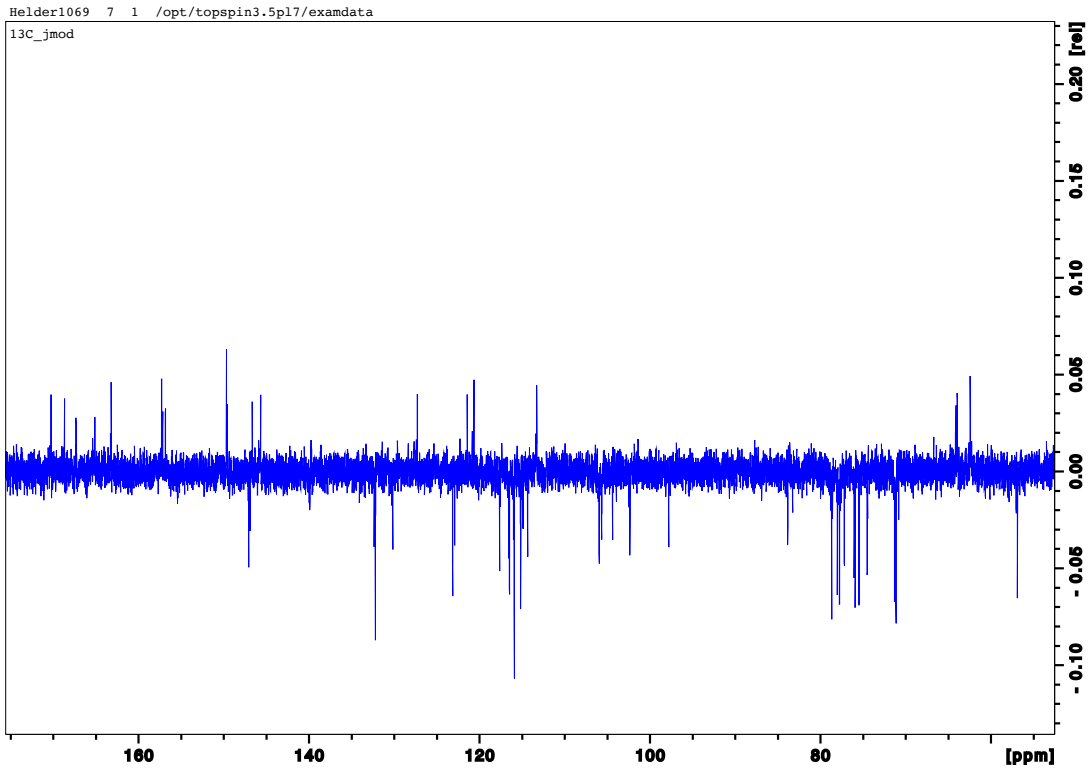

Attachment 4b. ^{13}CNMR-APT spectrum of *Peonidin-3-(6'-p-hydroxybenzoyl-6''-caffeoyl)-sophoroside-5-glucoside.*

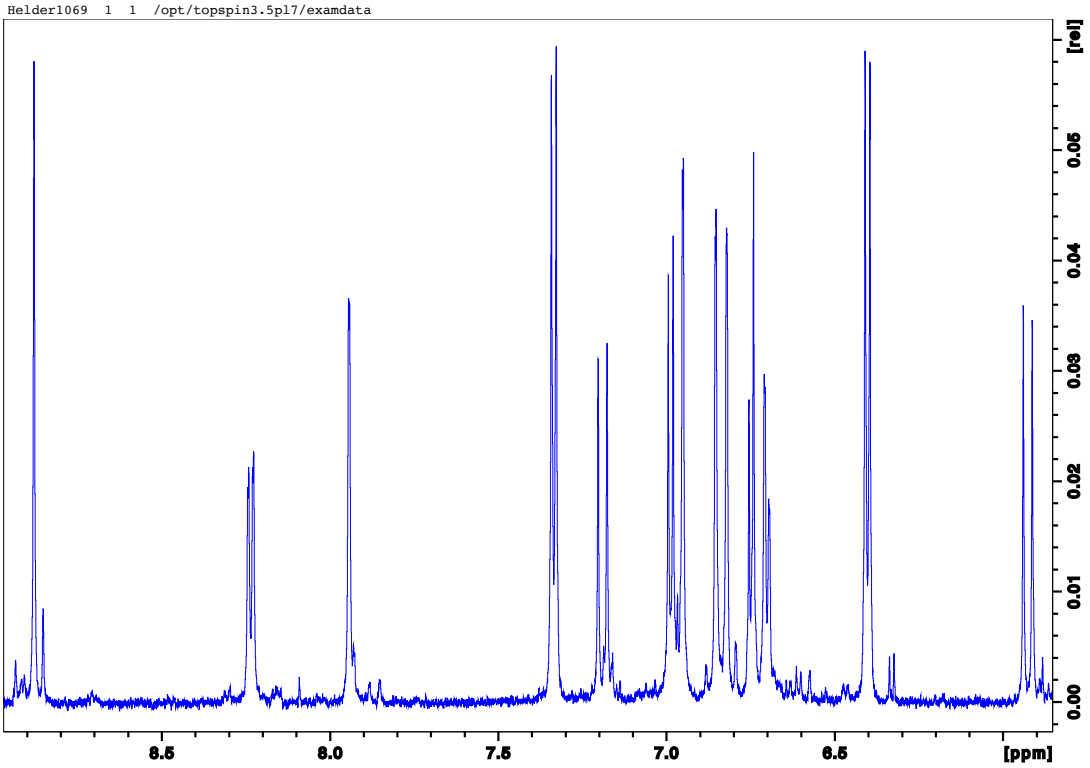

Attachment 2c. [1]HNMR spectrum of aromatic rings zone of *Peonidin-3-(6'-p-hydroxybenzoyl-6''-caffeoyl)-sophoroside-5-glucoside.*

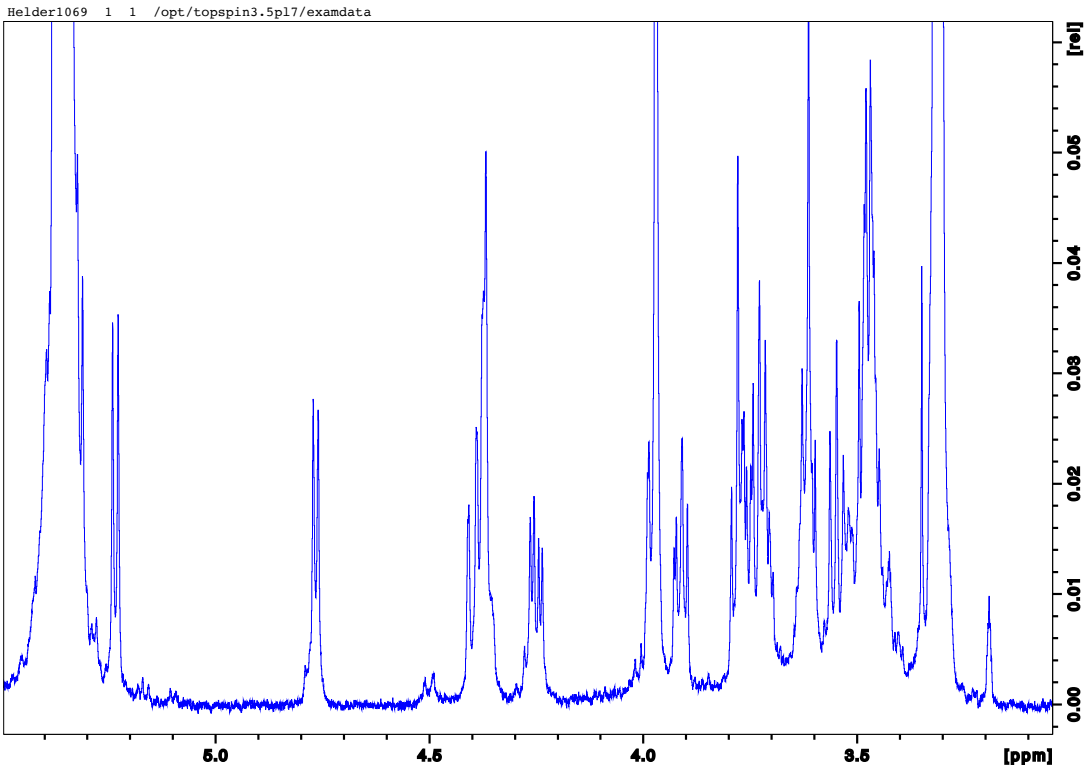

Attachment 2d. ^{1}HNMR spectrum of glucose protons zone of *Peonidin-3-(6'-p-hydroxybenzoyl-6''-caffeoyl)-sophoroside-5-glucoside.*

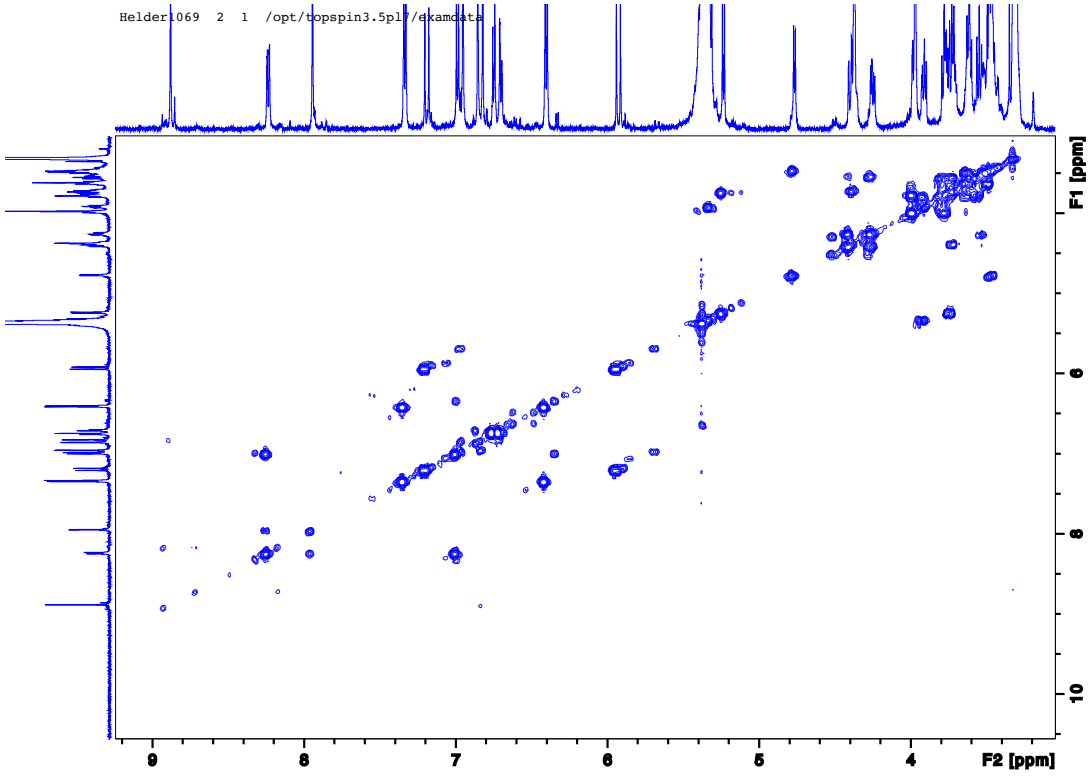

Attachment 2e. COSY complete spectrum of *Peonidin-3-(6'-p-hydroxybenzoyl-6''-caffeoyl)-sophoroside-5-glucoside.*

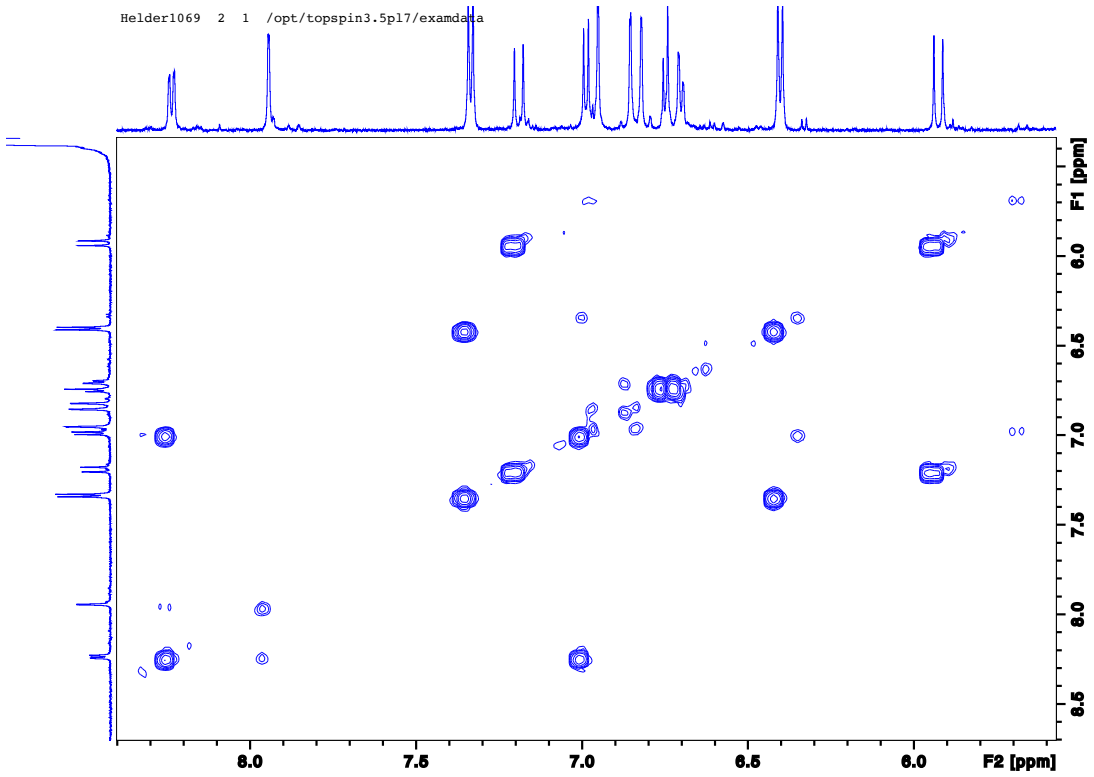

Attachment 2f. COSY spectrum with aromatic rings zone correlations evidenced for *Peonidin-3-(6'-p-hydroxybenzoyl-6''-caffeoyl)-sophoroside-5-glucoside*.

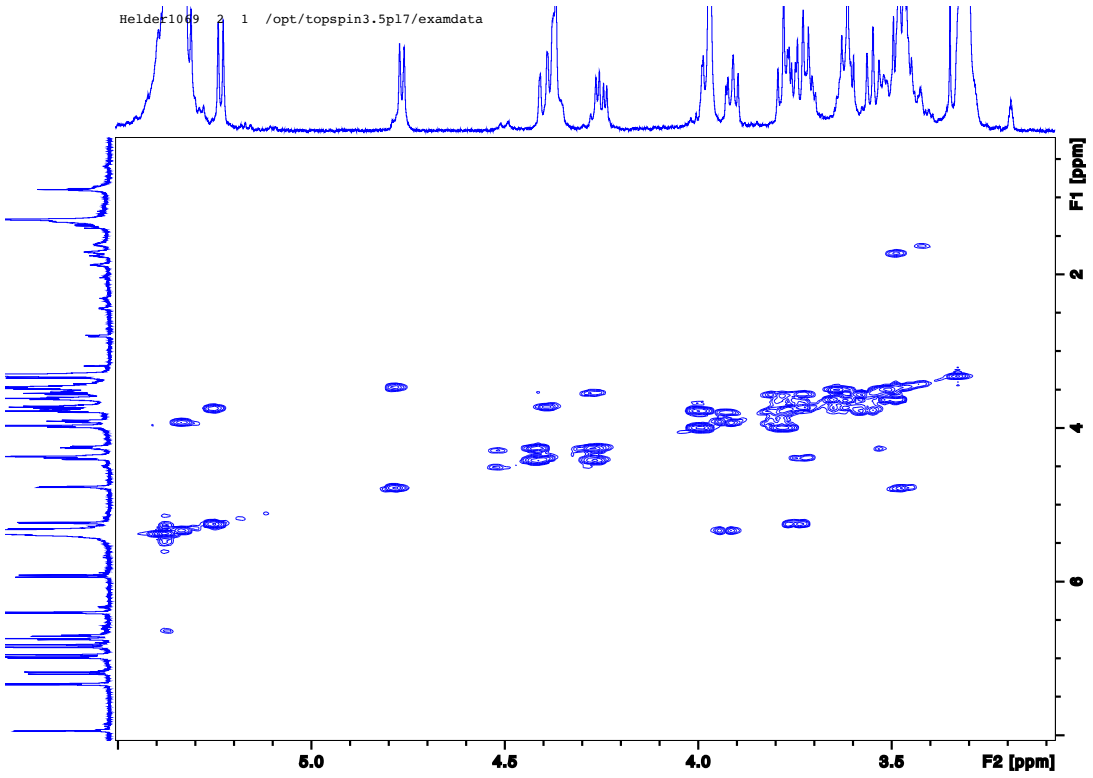

Attachment 2g. COSY spectrum with glucose protons zone correlations evidenced for *Peonidin-3-(6'-p-hydroxybenzoyl-6''-caffeoyl)-sophoroside-5-glucoside.*

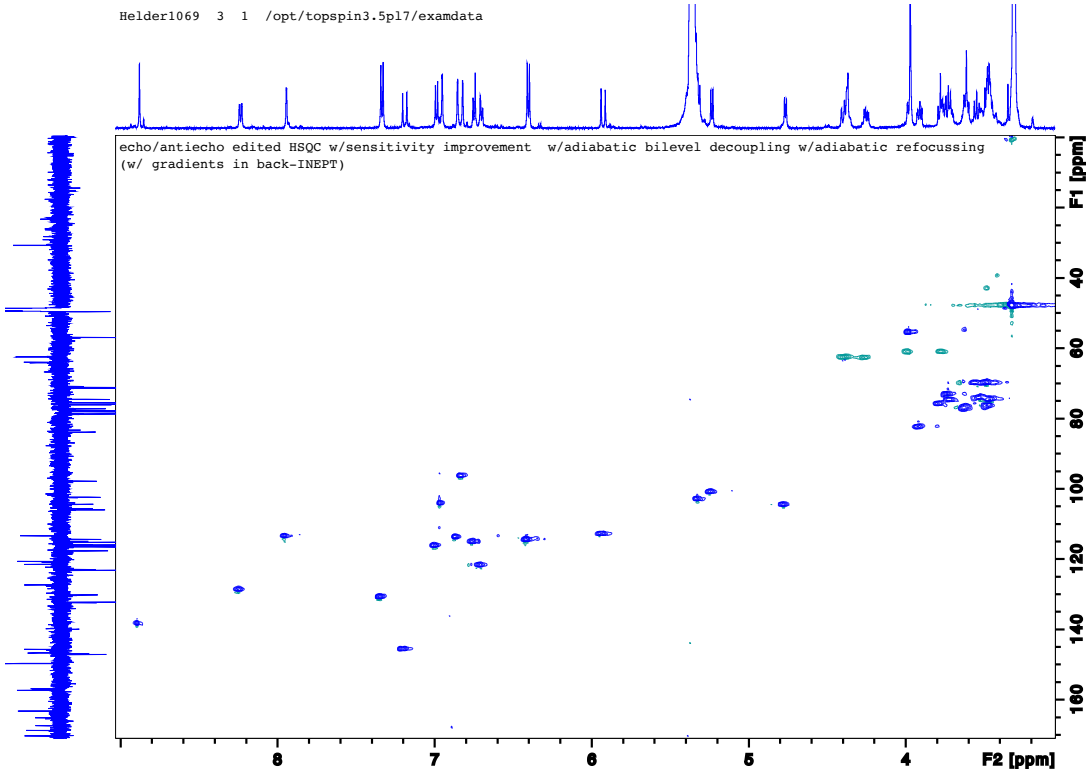

Attachment 2h. HSQC complete spectrum of *Peonidin-3-(6'-p-hydroxybenzoyl-6''-caffeoyl)-sophoroside-5-glucoside.*

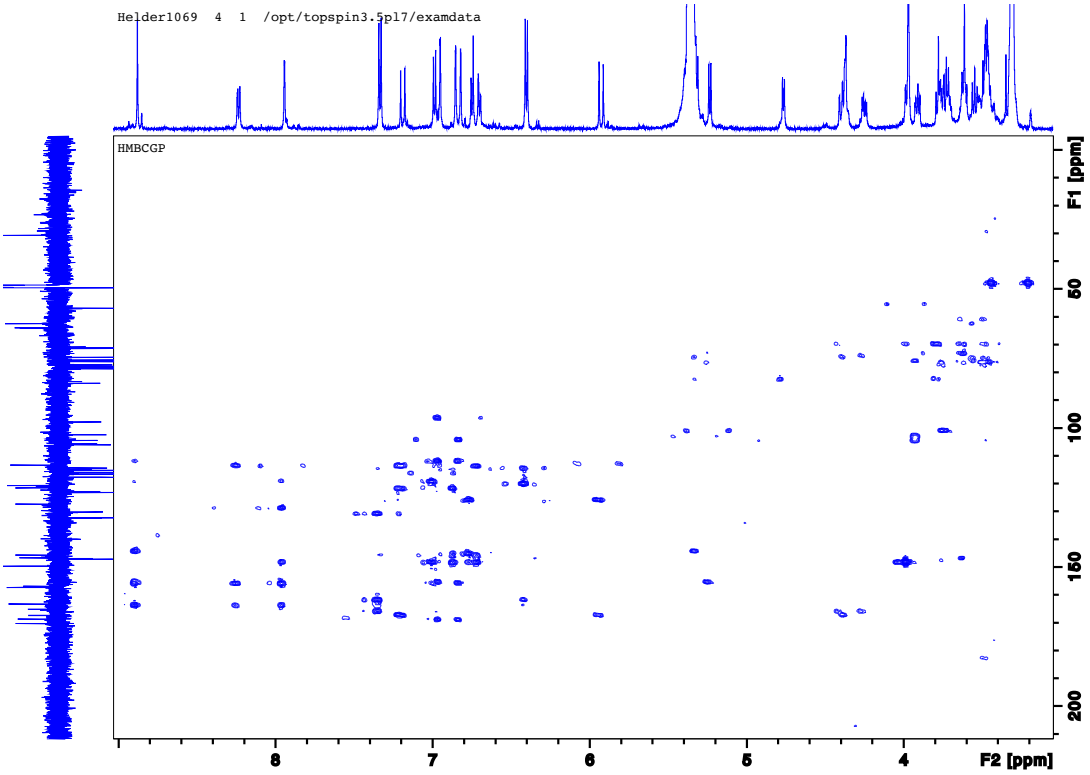

Attachment 2i. HMBC complete spectrum of *Peonidin-3-(6'-p-hydroxybenzoyl-6''-caffeoyl)-sophoroside-5-glucoside.*

ATTACHMENT III

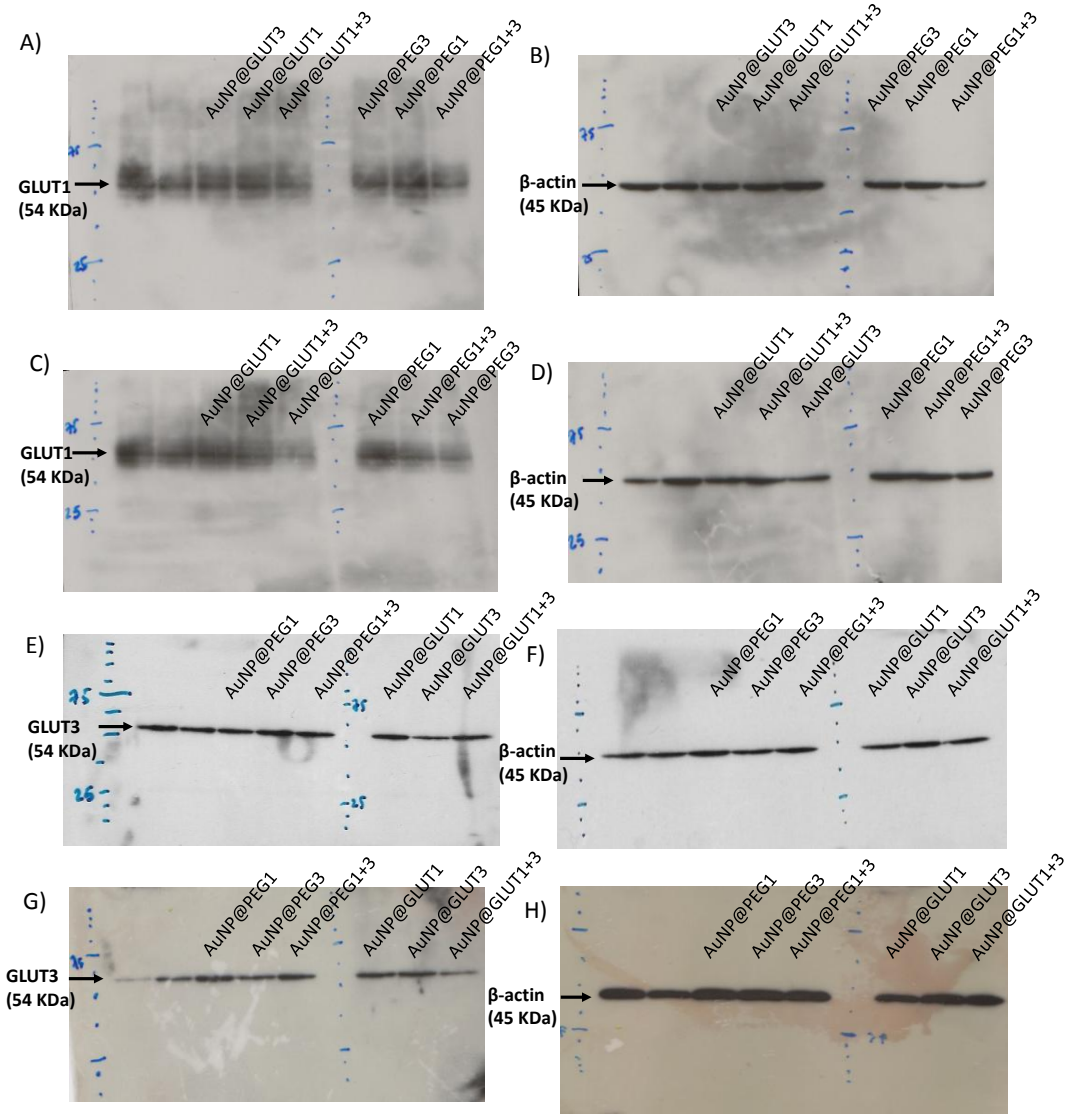

Attachment 3. Full length blots of the Western Blot analysis of A) GLUT1 after 24 h; B) β-actin, control of GLUT1 blot after 24 h; C) GLUT1 after 24h+24h and D) β-actin, control of GLUT1 blot after 24h+24h. E) GLUT3 after 24 h; B) β-actin, control of GLUT3 blot after 24 h; C) GLUT3 after 24h+24h and D) β-actin, control of GLUT3 blot after 24h+24h. Represented Western Blots correspond to 10 µg total protein of MKN-28 cells incubated for 24 h or 24 h plus 24 h with fresh RPMI medium supplemented with 5.5 mM fructose and 30 nM AuNP@PEG@anti-*GLUT1* (AuNP@GLUT1), 20 nM AuNP@PEG@anti-*GLUT3* (AuNP@GLUT3), or a mixture of 30 nM AuNP@PEG@anti-*GLUT1* and 20 nM AuNP@PEG@anti-*GLUT3* (AuNP@GLUT1+3). After 24 h cells were collected or incubated for an additional 24 h with fresh medium supplemented according to the first incubation. Control samples consist in MKN-28 cells treated with RPMI medium supplemented with 5.5 mM fructose and 0.75 nM AuNP@PEG (control of AuNP@GLUT1), 0.63 nM AuNP@PEG (control of AuNP@GLUT3), or 1.38 nM AuNP@PEG (control of AuNP@GLUT1+3), and collected at the same time point.

ATTACHMENT IV

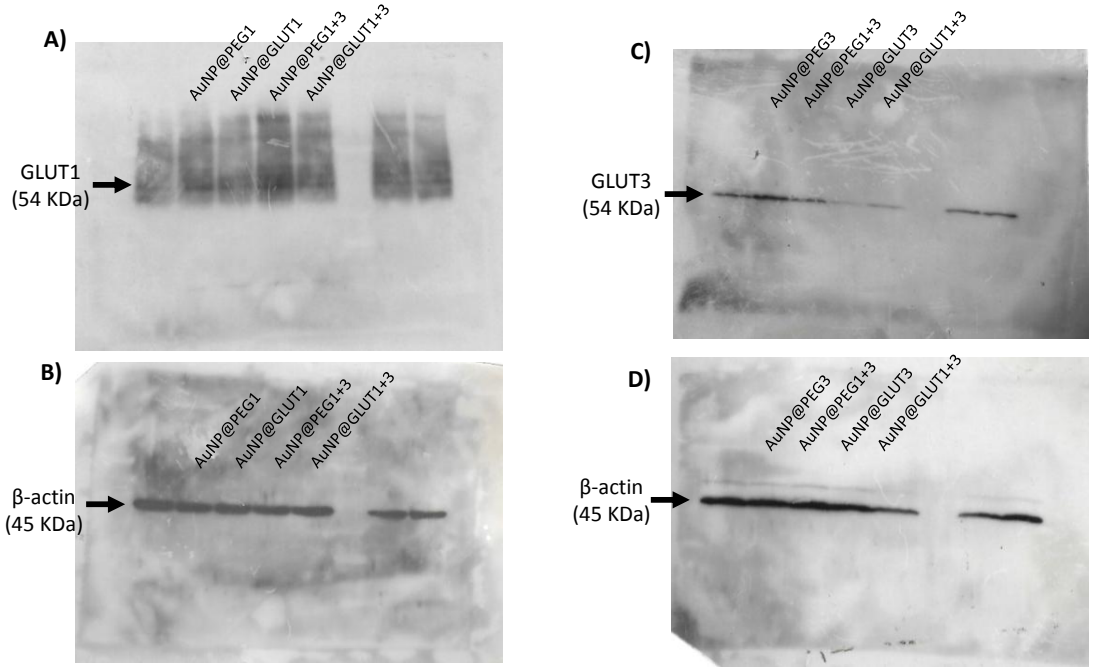

Attachment 4. Full length blots of the Western Blot analysis of A) GLUT1; B) β-actin, control of GLUT1 blot; C) GLUT3 and D) β-actin, control of GLUT3 blot. Represented Western Blots correspond to 10 µg total protein of MKN-28 cells grown on transwell plates and incubated for 24 h with fresh RPMI medium supplemented with 5.5 mM fructose and 0.75 nM AuNP@PEG (AuNP@PEG1), 0.63 nM AuNP@PEG (AuNP@PEG3), 1.38 nM AuNP@PEG (AuNP@PEG1+3), 30 nM AuNP@PEG@anti-GLUT1 (AuNP@GLUT1), 20 nM AuNP@PEG@anti-GLUT3 (AuNP@GLUT3), or a mixture of 30 nM AuNP@PEG@anti-GLUT1 and 20 nM AuNP@PEG@anti-GLUT3 (AuNP@GLUT1+3). After 24 h cells incubated for an additional 24 h with fresh medium supplemented according to the first incubation.

BIBLIOGRAPHY

1. Boudet, A.M., *Evolution and current status of research in phenolic compounds.* Phytochemistry, 2007. **68**: p. 2722-2735.
2. Harborne, J.B. and C. Williams, *Advances in flavonoid research since 1992.* Phytochemistry, 2000. **55**(6): p. 481-504.
3. Costa, G., et al., *Current evidences on the effect of dietary polyphenols intake on chronic diseases.* Food and Chemical Toxicology, 2017. **110**: p. 286-299.
4. Fiorentini, D., et al., *Polyphenols as Modulators of Aquaporin Family in Health and Disease.* Oxidative Medicine and Cellular Longevity, 2015. **196914**.
5. Bahadoran, Z.e.a., *Dietary polyphenols as potential nutraceuticals in management of diabetes: a review.* Journal of Diabetes Metabolic Disorders, 2013. **12**: p. 43.
6. Goutzourelas, N.e.a., *Polyphenolic composition of grape stem extracts affects antioxidant activity in endothelial and muscle cells.* Molecular Medicinal Reports, 2015. **12**: p. 5846-5856.
7. Leopoldini, M.e.a., *The molecular basis of working mechanism of natural polyphenolic antioxidants.* Food Chemistry, 2011. **125**: p. 288-306.
8. Kyro, C., et al., *Pre-diagnostic polyphenol intake and breast cancer survival: the European Prospective Investigation into Cancer and Nutrition (EPIC) cohort.* Breast Cancer Research Treatment, 2015. **137**: p. 225-236.
9. Thoppil, R.J., et al., *Black currant anthocyanins abrogate oxidative stress through Nrf2-mediated antioxidant mechanisms in a rat model of hepatocellular carcinoma.* Current Cancer Drug Targets, 2012. **12**: p. 1244-1257.
10. Teng, H., et al., *Red raspberry and its anthocyanins: Bioactivity beyond antioxidant capacity.* Trends in Food Science & Technology, 2017. **66**: p. 13.
11. Iwasaki, M., et al., *Plasma tea polyphenol levels and subsequent risk of breast cancer among Japanese women: a nested case-control study.* Breast Cancer Research Treatment, 2010. **124**: p. 827-834.
12. Hirvonen, T., et al., *Flavonol and flavone intake and the risk of cancer in male smokers (Finland).* Cancer Causes Control, 2001. **12**: p. 789-796.
13. Wang, L., et al., *Dietary intake of selected flavonols, flavones, and flavonoid-rich foods and risk of cancer in middle-aged and older women.* Am J Clin Nutr, 2009. **89**(3): p. 905-12.
14. Cutrim, C. and M. Cortez, *A review on polyphenols: Classification, beneficial effects and their application in dairy products.* 2018. **Dairy Technology**.
15. Karakaya, S., *Bioavailability of phenolic compounds.* Critical Reviews in Food Science and Nutrition, 2004. **44**(6): p. 453-464.

16. Natsume, M., et al., *Structures of (-)-epicatechin glucuronide identified from plasma and urine after oral ingestion of (-)-epicatechin: differences between human and rat.* Free Radical Biological Medicine, 2003. **34**: p. 840-849.
17. Setchell, K.D., et al., *Comparing the pharmacokinetics of daidzein and genistein with the use of 13c-labeled tracers in premenopausal women. .* American Journal of Clinical Nutrition, 2003. **77**: p. 411-419.
18. Manach, C., et al., *Bioavailability and bioefficacy of polyphenols in humans. I. Review of 97 bioavailability studies.* American Journal of Clinical Nutrition, 2005. **81**(1): p. 230S-242S.
19. Scalbert, A. and G. Williamson, *Dietary intake and bioavailability of polyphenols.* Journal of Nutrition, 2000. **130**.
20. Szent-Györgyi, A., *Nobel Lecture: Oxidation, Energy Transfer and Vitamins.* Nobel Media AB 2014, 1937.
21. Perez-Vizcaino, F. and C. Fraga, *Research trends in flavonoids and health.* Archives of Biochemistry and Biophysics, 2018. **646**: p. 107-112.
22. Cassidy, A., *Berry anthocyanin intake and cardiovascular health.* Molecular Aspects in Medicine, 2017.
23. Kong, J.M., et al., *Analysis and biological activities of anthocyanins.* Phytochemistry, 2003. **64**(5): p. 923-933.
24. Wallace, T. and M. Giusti, *Anthocyanins in Health and Disease* CRC Press, 2014. **ISBN: 978-1-4398-9471-2**.
25. Andersen, O.M. and M. Jordheim, *The anthocyanins.* Flavonoids 2nd edition, Chemistry, Biochemistry and applications, 2006. **CRC Press**: p. 452-471.
26. Dey, P.M. and J.B. Harborne, *1. Plant phenolics methods in plant biochemistry.* Academic Press Limited, London, 1993. **2**: p. 15.
27. Andersen, O.M., *Personal database on anthocyanins.* 2012.
28. Rein, M., *Copigmentation reactions and color stability of berry anthocyanins.* Helsinki: Uniservity of Helsinki, 2005: p. 10-14.
29. Wrolstad, R.E., *Anthocyanins.* Handbook of Food Analytical Chemistry, 2005: p. 5-69.
30. Andres, V., et al., *Colour, bioactive compounds and antioxidant cacpcity of mixed beverages on fruit juices with milk or soya.* Journal of Food Nutrition Research, 2014. **53**.
31. Peng, B. and H. Li, *Degradation of anthocyanins in foods during heating process and its mechanism.* Journal of Food Safety and Quality, 2016. **7**: p. 3851–3858.
32. Mazza, G. and R. Brouillard, *The mechanism of co-pigmentation of anthocyanins in aqueous solutions.* Phytochemistry, 1990. **29**(4): p. 6.

33. Zhao, C.L., et al., *Stability-increasing effects of anthocyanin glycosyl acylation.* Food Chem, 2017. **214**: p. 119-128.
34. Markakis, P., *Anthocyanins as Food Colours.* Academic Press, New York, 1982.
35. Furtado, P., et al., *Photochemical and thermal degradation of anthocyanidins.* Journal of Phytochemistru and Photobiology A: chemistry, 1993. **75**(2): p. 113-118.
36. Pina, F., J. Oliveira, and V. de Freitas, *Anthocyanins and derivatives are more than flavylium cations.* Tetrahedron, 2015. **71**(20): p. 14.
37. Cabrita, L., T. Fossen, and O.M. Andersen, *Colour and stability of the six commom anthocyanidin 3-glucosides in aqueous solutions.* Food Chemistry, 2000. **68**: p. 101-107.
38. Dangles, O., N. Saito, and R. Brouillard, *Anthocyanin intramolecular copigment effect.* Phytochemistry, 1993. **34**: p. 119-124.
39. Yoshida, K., M. Mori, and T. Kondo, *Blue flower color development by anthocyanins: From chemical structure to cell physiology.* Natural Products Reports, 2009. **26**: p. 884-915.
40. Nerdal, W. and O.M. Andersen, *Intermolecular aromatic acid association of an anthocyanin (petanin) evidenced by two-dimensional nuclear overhauser enhancement nucleat magnetic resonance experiments and distance geometry calculations.* Phytochemistry Analysis, 1992. **3**: p. 182-189.
41. Brouillard, R., *Anthocyanins as Food Colors.* Academic Press Limited, New York, 1982.
42. Brouillard, R. and O. Dangles, *Flavonoids and flower colour. .* The Flavonoids: Advances in Research since 1986, 1994.
43. Glover, B.J. and C. Martin, *Anthocyanins.* Current Biology, 2012. **22**(5): p. 147-150.
44. Kammerer, D., R. Carle, and A. Schieber, *Quantification of Anthocyanins in black carrot extracts and evaluation of their color properties.* European Food Research and Technology, 2004. **219**: p. 479-486.
45. Elham, G., et al., *Isolation and structure characterization of anthocyanin pigments in black carrot (daucus carota L.).* Pakistan journal of biological sciences : PJBS, 2006. **9**: p. 2905-2908.
46. Montilla, E.C., et al., *Anthocyanin composition of black carrot cultivars Antonina, Beta Sweet, Deep Purple and Purple Haze.* Journal of Agricultural and Food Chemistry, 2011. **59**: p. 3385-3390.
47. Clifford, M.N., *Anthocyanins: nature, occurence and dietary burden* Journal of Agricultural and Food Chemistry, 2000. **80**: p. 1063-1072.

48. Kim, H.-W.e.a., *Anthocyanin changes in the Korean purple-fleshed sweet potato, Shinzami, as affected by steaming and baking.* Food Chemistry, 2012. **130**: p. 966-972.
49. Fossen, T. and O.M. Andersen, *Anthocyanins from tubers and shoots of the purple potato, Solanum tuberosum.* Journal of Horticulture Science and Biotechnology, 2000. **75**: p. 360-363.
50. Steyn, W.J., *Prevalence and functions of anthocyanins in fruits.* Anthocyanins: Biosynsthesis, Functions and Applications, 2009. **Springer Science**: p. 107-168.
51. Park, J.S., et al., *Genes up-regulated during red coloration in UV-b irradiated lettuce leaves.* Plant Cell Reports, 2007. **26**: p. 507-516.
52. Kühnau, J., *The flavonoids. A class of semi-essential food components: their role in human nutrition.* World Revisions on Nutrition and Dietetics, 1976. **24**: p. 117-191.
53. Wu, X., et al., *Concentrations of anthocyanins in common foods in the United States and estimation of normal consumption.* Journal of Agricultural and Food Chemistry, 2006. **54**: p. 4069-4075.
54. Clifford, M.N. and J.E. Brown, *Dietary Flavonoids and Health- Broadening the perspectives.* Flavonoids 2nd edition, Chemistry, Biochemistry and applications, 2006: p. 319-370.
55. Gosnay, S.L., et al., *Estimation of the mean intakes of fourteen classes of dietary phenolics in a population of young British women aged 20-30 years.* Proceedings of the Nutrition Society, 2002. **61**: p. 125A.
56. Koponen, J.M., et al., *Contents of anthocyanins and ellagitannins in selected foods consumed in Finland.* Journal of Agricultural and Food Chemistry, 2007. **55**: p. 1612-1619.
57. Ovaskeinen, M.L., *Dietary intake and major food sources of polyphenols in Finnish adults.* Journal of Nutrition, 2008. **138**: p. 562-566.
58. Drossard, C., et al., *Anthocyanins in the diet of infants and toddlers: Intake, sources and trends.* European Journal of Nutrition, 2011. **50**: p. 705-711.
59. Kharadze, M., et al., *Anthocyanins and antioxidant activity of red wines made from endemic grape varieties.* Annals of Agrarian Science, 2018. **16**(2): p. 181-184.
60. Duarte, L., et al., *Molecular mechanism of action of Pelargonidin-3-O-glucoside, the main anthocyanin responsible for the anti-inflammatory effect of strawberry fruits.* Food Chemistry, 2018. **247**: p. 56-65.
61. León-González, A., et al., *Anthocyanin-rich bilberry extract induces apoptosis in acute lymphoblastic leukemia cells via redox-sensitive epigenetic modifications.* Journal of Functional Foods, 2018. **44**: p. 227-234.

62. Gowd, V., Z. Jia, and W. Chen, *Anthocyanins as promising molecules and dietary bioactive components against diabetes – A review of recent advances.* Trends in Food Science & Technology, 2017. **68**: p. 1-13.
63. Spagnuolo, C., S. Moccia, and G. Russo, *Anti-inflammatory effects of flavonoids in neurodegenerative disorders.* European Journal of Medicinal Chemistry, 2018. **153**: p. 105-115.
64. Matsumoto, H. and Y. Nakamura, *Stimulatory effect of cyanidin-3-glucoside on the regeneration of rhodopsin".* Journal of Agricultural and Food Chemistry, 2003. **51**(12): p. 3560-3563.
65. Long, H., et al., *Mulberry anthocyanins improves thyroid cancer progression mainly by inducing apoptosis and autophagy cell death.* The Kaohsiung Journal of Medical Sciences, 2018. **34**(5): p. 255-262.
66. Mazewski, C., K. Liang, and E. Mejia, *Inhibitory potential of anthocyanin-rich purple and red corn extracts on human colorectal cancer cell proliferation in vitro.* Journal of Functional Foods, 2017. **34**: p. 254-265.
67. Wang, D., et al., *Inhibition of ALV-A-induced apoptosis in DF-1 cells via inactivation of nuclear transcription factor κB by anthocyanins from purple corn (Zea mays L.).* Journal of Functional Foods, 2014. **10**: p. 274-282.
68. Pham-Huy, L., H. He, and C. Pham-Huy, *Free radicals between health and diseases.* Roman Journal of Physiology, 2007. **37**: p. 15-22.
69. Halliwell, B. and J. Gutteridge, *The definition and measurement of antioxidants in biological systems.* Free Radical Biological Medicine, 1995. **18**: p. 125-126.
70. Halliwell, B., *Free radicals and antioxidantes - Quo vadis ?* Trends in Pharmacology, 2011. **32**: p. 125-130.
71. Esfahani, A., et al., *Health effects of mixed fruit and vegetable concentrates: A systematic review of the clinical interventions.* Journal of the American College of Nutrition, 2011. **30**: p. 285-294.
72. Kahkonen, M.P. and M. Heinonen, *Antioxidant activity of anthocyanins and their algycons.* Journal of Agricultural and Food Chemistry, 2003. **51**: p. 628-633.
73. Seeram, N.P., R.H. Cichewicz, and M.G. Nair, *Cyclooxigenase inhibitory and antioxidant compounds from crabapple fruits.* Journal of Agricultural and Food Chemistry, 2001. **51**: p. 1948-1951.
74. Niki, E., *Assessment of antioxidant capacity in vitro and in vivo* Free Radical Biological Medicine, 2010. **49**: p. 503-515.
75. Elisia, I. and D.D. Kitts, *Anthocyanins inhibit peroxyl radical-induced apoptosis in Caco-2 cells.* Molecular Cell Biochemistry, 2008. **312**: p. 139-145.

76. Solomon, A., et al., *Protection of fibroblasts (NIH-3T3) agaisnt oxidative damage by cyanidin-3-rhamnoglucoside isolated from fig fruits.* Journal of Agricultural and Food Chemistry, 2010. **58**: p. 6660-6665.
77. Chen, J., et al., *Effects of tetramethylpyrazine from Chinese black vinegar on antioxidant and hypolipidemia activities in HepG2 cells.* Food and Chemical Toxicology, 2017. **109**: p. 930-940.
78. Jayakumar, R. and M.S. Kanthimathi, *Inhibitory effects of fruit extracts on nitric oxide-induced proliferation in MCF-7 cells.* Food Chemistry, 2011. **126**(3): p. 956-960.
79. Fernandes, I., et al., *Antioxidant and antiproliferative properties of methylated metabolites of anthocyanins.* Food Chemistry, 2014. **141**: p. 2923-2933.
80. Brouillard, R. and J. Lang, *The a<-cis-chalcone equilibrium of malvin, a natural anthocyanin.* Canadian Journal of Chemistry Reviews, 1990. **68**(5): p. 755-761.
81. Seeram, N.P., L.D. Bourquin, and M.G. Nair, *Degradation products of cyanidin glycosides from tart cherries and their bioactives.* Journal of Agricultural and Food Chemistry, 2001. **49**: p. 4924-4929.
82. Berger, R., et al., *Antioxidants in food: Mere myth or magic medicine?* Critical Reviews in Food Science and Nutrition, 2012. **52**: p. 162-171.
83. Prior, R.L., *Fruits and vegetables in the prevention of cellular oxidative damage.* American Journal of Clinical Nutrition, 2003. **78**: p. 570-578.
84. Mazza, G., et al., *Absorption of anthocyanins from blueberries and serum antioxidant status in human subjects.* Journal of Agricultural and Food Chemistry, 2002. **50**: p. 7731-7737.
85. Matsumoto, H., et al., *Antioxidant activity of black currant anthocyanin aglycons and their glycosides measured by chemiluminescence in a neutral pH region and in human plasma.* Journal of Agricultural and Food Chemistry, 2002. **50**: p. 5034-5037.
86. Wang, C.J., et al., *Protective effect of Hibiscus anthocyanins against tert-butyl hydroperoxide-induced hepatic toxicity in rats. .* Food Chemical Toxicolgy, 2000. **38**: p. 411-416.
87. Lionetto, M.G., et al., *Effect of the daily ingestion of a purified anthocyanin extract from grape skin on rat serum antioxidant capacity.* Physiological Research, 2011. **60**: p. 637-645.
88. Esposito, D., et al., *Inhibitory effects of wild blueberry anthocyanins and other flavonoids on biomarkers of acute and chronic inflammation in vitro.* Journal of Agricultural and Food Chemistry, 2014. **62**: p. 7022-7028.

89. Peiffer, D.S., et al., *Chemoprevention of esophageal cancer with black raspberries, their component anthocyanins, and a major anthocyanin metabolite, protocatechuic acid.* Cancer Prevention Revisions, 2014. **7**: p. 574-584.
90. Thwe, A., et al., *Effect of different agrobacterium rhizogenes strains on hairy root induction and phenylpropanoid biosynthesis in tartary buckwheat (Fagopyrum tataricum Gaertn).* Frontiers in Microbiology, 2016. **7**: p. 1-10.
91. Hou, D.X., et al., *Anthocyanidins inhibit activator protein 1 activity and cell transformation: structure–activity relationship and molecular mechanisms. .* Carcinogenesis, 2004. **25**: p. 29-36.
92. Hou, D.X., et al., *Anthocyanidins inhibit cyclooxygenase-2 expression in LPS-evoked macrophages: structure activity relationship and molecular mechanisms involved.* Biochemical Pharmacology, 2005. **70**: p. 417-425.
93. Kang, N.J., et al., *Delphinidin attenuates neoplastic transformation in JB6 Cl41 mouse epidermal cells by blocking Raf/mitogen-activated protein kinase kinase/extracellular signal-regulated kinase signaling. .* Cancer Prevention Research, 2008. **1**: p. 522-531.
94. Marko, D., et al., *The substitution pattern of anthocyanidins affects different cellular signaling cascades regulating cell proliferation.* Molecular Nutrition and Food Research, 2004. **48**: p. 318-325.
95. Chang, H., et al., *Anticancer activities of an anthocyanin-rich extract from black rice against breast cancer cells in vitro and in vivo. .* Nutrition in Cancer, 2010. **62**: p. 1128-1136.
96. Liu, J., et al., *Cyanidin 3-O-betaglucoside ameliorates ethanol-induced acute liver injury by attenuating oxidative stress and apoptosis: the role of SIRT1/FOXO1 signaling.* Alcohol Clinical Experimental Research, 2016. **40**: p. 457-466.
97. Reddivari, L., et al., *Anthocyanin fraction from potato extracts is cytotoxic to prostate cancer cells through activation of caspase-dependent and caspase-independent pathways.* Carcinogenesis, 2007. **28**: p. 2227-2235.
98. Lin, B., et al., *Effects of anthocyanins on the prevention and treatment of cancer.* British Journal of Pharmacology, 2017. **174**: p. 1226-1243.
99. Ward, R., K. Steven, and R. Lugo, *Pharmacokinetics, Pharmacodynamics, and Pharmacogenetics.* Avery's Diseases of the Newborn, 2012. **9th Edition**.
100. Srinivasan, V., *Bioavailability of Nutrients: A Practical Approach to In Vitro Demonstration of the Availability of Nutrients in Multivitamin-Mineral Combination Products.* The Journal of Nutrition, 2001. **131**(4): p. 1349-1350.

101. Scholz, S. and G. Williamson, *Interactions affecting the bioavalability on dietary polyphenols in vivo.* International Journal of Vitamins and Nutrition Research, 2000. **77**(3): p. 224-235.
102. Oliveira, H., et al., *Experimental and Theoretical Data on the Mechanism by Which Red Wine Anthocyanins Are Transported through a Human MKN-28 Gastric Cell Model.* J Agric Food Chem, 2015. **63**(35): p. 7685-92.
103. Faria, A., et al., *Absorption of anthocyanins through intestinal epithelial cells - Putative involvement of GLUT2.* Molecular Nutrition and Food Research, 2009. **53**(11): p. 7.
104. Porrini, M. and P. Riso, *Factors influencing the bioavailability of antioxidants in foods: A critical appraisal.* Nutrition, Metabolism and Cardiovascular Diseases, 2008. **18**(10): p. 647-650.
105. Morazzoni, P., et al., *Vaccinium myrtillus anthocyanosides pharmacokinetics in rats.* Drug Research, 1991. **41**: p. 128-131.
106. Lapidot, T., et al., *Bioavailability of red wine anthocyanins as detected in human urine.* Journal of Agricultural and Food Chemistry, 1998. **46**: p. 4297-4302.
107. Passamonti, S., U. Vrhovsek, and F. Mattivi, *The interaction of anthocyanins with bilitranslocase.* Biochem Biophys Res Commun, 2002. **296**(3): p. 631-6.
108. Fernandes, I., et al., *A new approach on the gastric absorption of anthocyanins.* Food and Function, 2012. **3**(5): p. 508-16.
109. Miyazawa, T., et al., *Direct intestinal absorption of red fruit anthocyanins, cyanidin-3-glucoside and cyanidin-3,5-diglucoside, into rats and humans.* Journal of Agricultural and Food Chemistry, 1999. **47**: p. 1083-1091.
110. Tsuda, T., F. Horio, and T. Osawa, *Absorption and metabolism of cyanidin-3-O-(beta)-glucoside in rats.* FEBS Letters, 1999. **449**: p. 179-182.
111. He, J., et al., *Stability of black raspberry anthocyanins in the digestive tract lumen and transport efficiency into gastric and small intestinal tissues in the rat.* Journal of Agricultural and Food Chemistry, 2009. **57**: p. 3141-3148.
112. Matsumoto, H., et al., *Orally administered delphinidin-3-rutinoside and cyanidin-3-rutinosideare directly absorbed in rats and humans and apper in the blood as the intact form.* Food Chemistry, 2001. **49**: p. 1546-1551.
113. Ichiyanagi, T., et al., *Absorption and metabolism of delphinidin-3-O-(beta)-d-glucopyranoside in rats.* Free Radical Biology and Medicine, 2004. **36**: p. 930-937.
114. Ichiyanagi, T., et al., *Extended glucuronidation is another major path of cyanidin-3-O-(beta)-d-glucopyranoside metabolism in rats.* Journal of Agricultural and Food Chemistry, 2005. **53**: p. 7312-7319.

115. Ichiyanagi, T., et al., *Metabolic pathway of cyanidin-3-O-(beta)-d-glucopyranoside in rats.* Journal of Agricultural and Food Chemistry, 2005. **53**: p. 145-150.
116. Wu, X., H.E.I. Pittman, and R.L. Prior, *Pelargonidin is absorbed and metabolized differently than cyanidin after marionberry consumption in pigs.* Journal of Nutrition, 2004. **134**: p. 2603-2610.
117. Wu, X., et al., *Aglycones and sugar moieties alter anthocyanin absorption and metabolism after berry consumption in wealing pigs.* Journal of Nutrition, 2005. **135**: p. 2417-2424.
118. Talavera, S., et al., *Anthocyanin metabolism in rats and their distribution to digestive are, kidney, and brain.* Journal of Agricultural and Food Chemistry, 2005. **53**(3902-3808).
119. Nielsen, I.L.F., et al., *Absorption and excretion of black currant anthocyanins in humans and Watanabe heritable hyperlipidemic rabbits.* Journal of Agricultural and Food Chemistry, 2003. **51**: p. 2813-2820.
120. Walton, M.C., et al., *Anthocyanin absorption and plasma antioxidant status in pigs.* Food Chemistry, 2006. **54**: p. 7940-7946.
121. McGhie, T.K., et al., *Anthocyanin glycosides from berry fruit are absorbed and excreted unmetabolized by both humans and rats.* Journal of Agricultural and Food Chemistry, 2003. **51**: p. 4539-4548.
122. Netzel, M., et al., *Urinary excretion of antioxidants in healthy humans following Queen Garnet plum juice ingestion: A new plum variety rich in antioxidant compounds.* Journal of Food Biochemistry, 2012. **20**: p. 159-170.
123. Bub, A., et al., *Malvidin-3-glucoside bioavailability in humans after ingestion of red wine, dealcoholised red wine and red grape juice.* Molecular Nutrition and Food Research, 2001. **51**: p. 714-725.
124. Cooney, J.M., D.J. Jensen, and T.K. McGhie, *LC-MS identification of anthocyanins in boysenberry extract and anthocyanin metabolites in human urine following dosing.* Journal of the Science of Food and Agriculture, 2004. **84** p. 237-245.
125. Felgines, C., et al., *Strawbeery anthocyanins are recovered in urine as glucoro- and sulfoconjugates in humans.* Journal of Nutrition, 2003. **133**: p. 1296-1301.
126. Felgines, C., et al., *Blackberry anthocyanins are mainly recovered from urine as methylated and glucuronidated conjugates in humans.* Journal of Agricultural and Food Chemistry, 2005. **53**(20): p. 7721-7.
127. Netzel, M., et al., *Bioactive anthocyanins detected in human urine after ingestion of blackcurrant juice.* Journal of Environment Pathology, Toxicology and Oncology, 2001. **20**: p. 89-95.

128. Frank, T., et al., *Bioavailability of anthocyanins-3-glucosides following consumption of red wine and red grape juice.* Canadian Journal of Physiology and Pharmacology, 2003. **81**: p. 423-435.
129. Stevenson, D.E., A. Scheepens, and R.D. Hurst, *Bioavailability and metabolism of dietary flavonoids - Much known- much more to discover.* Flavonoids: Biosynthesis, Biological Effects and Dietary sources, 2009. **Nova Science Publishers**.
130. Czank, C., et al., *Human metabolism and elimination of the anthocyanin, cyanidin-3-glucoside, a 13C-tracer study.* American Journal of Clinical Nutrition, 2013. **97**: p. 995-1003.
131. de Ferrars, R.M., et al., *The pharmacokinetics of anthocyanins and their metabolites in humans.* British Journal of Pharmacology, 2014. **171**: p. 3268-3282.
132. Talavera, S., et al., *Anthocyanins are effectively absorbed from the stomach in anesthetized rats.* Journal of Nutrition, 2003. **133**: p. 4178-4182.
133. Fernandes, I., et al., *Bioavailability of anthocyanins and derivatives.* Journal of Functional Foods, 2014. **7**(Supplement C): p. 54-66.
134. Cao, G. and R.L. Prior, *Anthocyanins are detected in human plasma after oral administration of an elderberry extract.* Clinical Chemistry, 1999. **45**: p. 237-245.
135. Murkovic, M., U. Adam, and W. Pfannhauser, *Analysis of anthocyan glycosides in human serum.* Fresenius Journal of Analytical Chemistry, 2000. **366**: p. 379-381.
136. Mulleder, U., M. Murkovic, and W. Pfannhauser, *Urinary excretion of cyanidin glycosides.* Journal Biochemical and Biophysical Methods, 2002. **53**(1-3): p. 61-6.
137. Milbury, P.E., et al., *Bioavailablility of elderberry anthocyanins.* Mechanisms of Ageing and Development, 2002. **123**(8): p. 997-1006.
138. Wu, X. and R.L. Prior, *Absorption and metabolism of anthocyanins in elderly women ater consumption of elderberry or blueberry.* Journal of Nutrition, 2002. **132**: p. 1865-1871.
139. Kay, C.D., et al., *Anthocyanin metabolites in humans urine and serum* British Journal of Nutrition, 2004. **91**: p. 933-942.
140. Mullen, W., et al., *Bioavailability of pelargonidin-3-O-glucoside and its metabolites in humans following the ingestion of strawberries with or without cream* Journal of Agricultural and Food Chemistry, 2008. **56**: p. 713-716.
141. Azzini, E., et al., *Bioavailability of strawberry antioxidants in human subjects.* British Journal of Nutrition, 2010. **104**: p. 1165-1173.
142. Milbury, P.E. and J.A. Vita, *Anthocyanins are bioavailable in humans following an acute dose of cranberry juice.* Journal of Nutrition, 2010. **140**(6).

143. Nurmi, T. and J. Mursu, *Metabolism of Berry anthocyanins of phenolic acids in humans.* Journal of Agricultural and Food Chemistry, 2009. **57**(6): p. 2274-2281.
144. Kay, C.D., et al., *Anthocyanins and Flavanones Are More Bioavailable than Previously Perceived: A Review of Recent Evidence.* Annual Reviews On Food Science and Technology, 2017. **8**: p. 35.
145. Kay, C.D., P.A. Kroon, and A. Cassidy, *The bioactivity of dietary anthocyanins is likely to be mediated by their degradation products.* Molecular Nutrition and Food Research, 2009. **53**(suppl.1): p. S92-S101.
146. McDougall, G.J., et al., *Assessing potential bioavailability of raspberry anthocyanins using an in vitro digestion system.* Journal of Agricultural and Food Chemistry, 2005. **53**: p. 5896-5904.
147. Kay, C.D., *Aspects of anthocyanin absorption, metabolism and pharmacokinetics.* Nutrition Research Reviews, 2006. **19**: p. 137-146.
148. Kuntz, S., et al., *Inhibition of low-grade inflammation by anthocyanins from grape in an in vitro epithelial-endothelial co-culture model.* Food & Function, 2015. **6**: p. 1136-1149.
149. Kuntz, S., et al., *Uptake and bioavailability of anthocyanins and phenolic acids from grape/blueberry juice and smoothie in vitro and in vivo.* British Journal of Nutrition, 2015. **113**: p. 1044-1055.
150. Fang, J., *Bioavailability of anthocyanins.* Drug Metabolism Reviews, 2014. **46**: p. 508-520.
151. Esposito, D., et al., *Black currant anthocyanins attenuate weight gain and improve glucose metabolism in diet-induced obese mice with intact, but not disrupted, gut microflora.* Journal of Agricultural and Food Chemistry, 2015. **63**: p. 6172-6180.
152. Amin, H.P., et al., *Anthocyanin and its physiologically relevant metabolites alter the expression of IL-6 and VCAM-1 in CD40L and oxidized LDL challenged vascular endothelial cells.* Molecular Nutrition and Food Research, 2015. **59**: p. 1095-1106.
153. Ludwig, I.A., et al., *New insights into the bioavailability of red raspberry anthocyanins and ellagitannins.* Free Radical Biological Medicine, 2015. **89**: p. 758-759.
154. Kepler, K. and H.U. Humpf, *Metabolism of Anthocyanins and their phenolic degradation products by the intestinal microflora.* Bioorganic and Medicinal Chemistry, 2005. **12**(17): p. 5195-5205.
155. Felgines, C. and S. Talavera, *Absorption and metabolism of red orange juice anthocyanins in rats.* British Journal of Nutrition, 2006. **95**(5): p. 898-904.
156. Gonzalez-Barrio, R., C.A. Edwards, and A. Crozier, *Colonic catabolism of ellagitannins, ellagic acid, and raspberry anthocyanins: in vivo and in vitro studies.* Drug Metabolism & Disposition, 2011. **58**: p. 1680-1688.

157. Yi, W. and C.C. Akoh, *Absorption of anthocyanins from blueberry extracts by caco-2 human intestinal cell monolayers.* Journal of Agricultural and Food Chemistry, 2006. **54**(15): p. 5651-5658.
158. Steinert, R.E., et al., *Absorption of black currant anthocyanins by monolayers of human intestinal epithelial Caco-2 cells mounted in ussing type chambers. .* Journal of Agricultural and Food Chemistry, 2008. **56**: p. 4995-5001.
159. Pacheco-Palencia, L.A., S.U. Mertens-Talcott, and S.T. Talcott, *In vitro absorption and antiproliferative activities of monomeric and polymeric anthocyanin fractions from açai fruit (Euterpe oleracea Mart.).* Food Chemistry, 2010. **119**: p. 1071-1078.
160. Fernandes, I., et al., *On the bioavailability of flavonols and anthocyanins: Flavonol-anthocyanin dimers.* Food Chemistry, 2012. **135**: p. 812-818.
161. Zou, T.-B., et al., *The Role of Sodium-Dependent Glucose Transporter 1 and Glucose Transporter 2 in the Absorption of Cyanidin-3-O-β-Glucoside in Caco-2 Cells.* Nutrients, 2014. **6**(10): p. 4165-4177.
162. Kosińska-Cagnazzo, A., et al., *Identification of bioaccessible and uptaken phenolic compounds from strawberry fruits in in vitro digestion/Caco-2 absorption model.* Food Chemistry, 2015. **170**: p. 288-294.
163. Alzaid, F., et al., *Regulation of glucose transporter expression in human intestinal Caco-2 cells following exposure to an anthocyanin-rich berry extract. .* PLoS ONE, 2013. **8**: p. e78932.
164. Passamonti, S. and A. Vanzo, *Hepatic uptake of grape anthocyanins and the role of bilitranslocase.* Food Chemistry and Toxicolgy, 2005. **38**: p. 953-960.
165. Yoshikawa, T., et al., *Comparative expression of hexose transporters (SGLT1, GLUT1, GLUT2 and GLUT5) throughout the mouse gastrointestinal tract.*
. Histochemistry and Cell Biology,, 2011. **135**: p. 183–194.
166. Eraly, S.A., et al., *The molecular pharmacology of organic anion transporters: From dna to fda? .* Molecular Pharmacology, 2004. **65**: p. 479-487.
167. Mazza, G. and E. Miniati, *Anthocyanins in Fruits, Vegetables and Grains.* CRC Press, 1993.
168. Xu, J., et al., *Characterisation and stability of anthocyanins in purple-fleshed sweet potato P40.* Food Chemistry, 2015. **186**: p. 6.
169. Steed, L.E. and V.-D. Truong, *Anthocyanin Content, Antioxidant Activity, and Selected Physical Properties of Flowable Purple-Fleshed Sweetpotato Purees.* Journal of Food Science, 2008. **73**(5): p. 6.

170. He, W., et al., *Identification and Quantitation of Anthocyanins in Purple-Fleshed Sweet Potatoes Cultivated in China by UPLC-PDA and UPLC-QTOF-MS/MS.* J Agric Food Chem, 2016. **64**(1): p. 171-7.
171. Gould, K., K.M. Davies, and C. Winefield, *Anthocyanins: Byosinthesis, functions and applications.* New York: Springer, 2008.
172. Maçanita, A.L., F. Pina, and A.J. Parola, *Proton transfer in anthocyanins and related flavylium salts. Determination of ground-state rate constants with nanosecond laser flash-photolysis.* Journal of Physical Chemistry 2002. **106**(7): p. 1248-1255.
173. Basílio, N. and F. Pina, *Chemistry and Photochemistry of Anthocyanins and Related Compounds: A thermodynamic and kinetic approach.* Molecules, 2016. **21**: p. 1502.
174. Pina, F., *Recent Advance in Polyphenols Research.* Wiley-Blackwell, 2014. **Vol.4**.
175. Brouillard, R. and J.E. Dubois, *Mechanism of the Structural Transformations of Anthocyanins in Acidic Media.* Journal of the American Chemical Society, 1977. **99**: p. 1359-1364.
176. McClelland, R.A. and G.H. McGall, *Hydration of flavylium ion .2. The 4'-hydrroxyflavylium ion. .* Journal of Organic Chemistry, 1982. **47**(19): p. 3730-3736.
177. Pina, F., *Thermodynamics and kinetics of flavylium salts - Malvin revisited.* Journal of Chemical Society -Faraday Transitions, 1998. **94**: p. 2109-2116.
178. Leydet, Y., et al., *The effect of self-aggreagtion on the determination of the kinetic and thermodynamic constants of the network of chemical reactions in 3-glucoside anthocyanins.* Phytochemistry, 2012. **83**: p. 125-135.
179. Dangles, O., N. Saito, and R. Brouillard, *Kinetic and Thermodynamic control of flavylium hydration in the pelargonidin-cinnamic acid complexation. Origin of the extraordinary flower color diversity of Pharbitis Nil.* Journal of the American Chemical Society, 1993. **115**: p. 3125-3132.
180. Mendoza, J., et al., *Rationalizing the Color in Heavenly Blue Anthocyanin: A Complete Kinetic and Thermodynamic Study.* Journal of Physical Chemistry B, 2018. **122**: p. 4982-4992.
181. Drabent, R., B. Pliszka, and T. Olszewska, *Fluorescence properties of plant anthocyanin pigments. I. Fluorescence of anthocyanins in Brassica oleracea L. extracts.* Journal of Photochemistry and Photobiology, 1999. **50**: p. 53-58.
182. Drabent, R., et al., *Ultraviolet Fluorescence of Cyanidin and Malvidin Glycosides in Aqueous environment.* Spectroscopic Letters, 2007. **40**: p. 165-182.
183. Cherepy, N.J., et al., *Ultrafast Electron Injection: Implications for a photoelectrochemical cell utilizing an anthocyanin dye-sensitized TiO2 nanocrystalline electrode. .* Journal of Physical Chemistry B, 1997. **101**: p. 9342-9351.

184. Figueiredo, P., et al., *Fluorescence spectra and decays of malvidin 3,5diglucoside in aqueous solutions.* Journal of Photochemistry and Photobiology, 1990. **52**: p. 411-424.
185. Agati, G., et al., *Fluorescence Approach for Measuring Anthocyanins and Derived Pigments in Red Wine.* Journal of Agricultural and Food Chemistry, 2013. **61**: p. 10156-10162.
186. Xu, J., et al., *Characterisation and stability of anthocyanins in purple-fleshed sweet potato P40.* Food Chem, 2015. **186**: p. 90-6.
187. Kubow, S., et al., *Biotransformation of anthocyanins from two purple-fleshed sweet potato accessions in a dynamic gastrointestinal system.* Food Chemistry, 2016. **192**: p. 171-177.
188. Esatbeyoglu, T., et al., *Fractionation, enzyme inhibitory and cellular antioxidant activity of bioactives from purple sweet potato (Ipomoea batatas).* Food Chemistry, 2017. **221**: p. 447-456.
189. Drake, E. and C. Brown, *Application of nmr to biochemical kinetics. A laboratory experiment in physical biochemistry.* Journal of Chemical Education, 1977. **54**(2): p. 124.
190. Salas, E., et al., *Structure and properties of a flavanol-anthocyanin adduct.* 228th national meeting of the amercian-chemical-society, 2004.
191. Gonzalez-Manzano, S., et al., *Flavanol–anthocyanin pigments in corn: NMR characterisation and presence in different purple corn varieties.* Journal of Food Composition and Analysis, 2008. **21**(7): p. 521-526.
192. McClelland, R.A., D.B. Devine, and P.E. Sorensen, *Hemiacetal fromation with a phenol nucleophile - simple proton transfers as rate-limiting steps.* Journal of American Chemical Society, 1985. **107**(19): p. 5459-5463.
193. Pina, F., et al., *Photochemistry of 3,4'-dimethoxy-7-hydroxyflavylium chloride - Photochromism and excited-state proton transfer.* Journal of the Chemical Society, Farady Transactions, 1996. **92**(10): p. 1693-1699.
194. Nave, F. and e. al, *Thermodynamic and Kinetic Properties of a Red Wine Pigment: Catechin-(4,8)-malvidin-3-O-glucoside.* The Journal of Physical Chemistry B, 2010. **114**(42): p. 13487-13496.
195. Torkskangerpoll, K. and O.M. Andersen, *Colour stability of anthocyanins in aqueous solutions at various pH values.* Food Chemistry, 2005. **89**: p. 427-440.
196. Andersen, O.M., et al., *Anthocyanins with unusual furanose sugar (apiose) from leaves of Synadenium grantii (Euphorbiaceae).* Phytochemistry, 2010. **71**(13): p. 1558-63.
197. Noda, Y., et al., *Antioxidant activity of nasunin, an anthocyanin in egg plants.* Toxicology, 2000. **148**: p. 119-123.

198. Matsui, T., et al., *α-Glucosidase inhibitory action of natural acylated anthocyanins. 1. Survey of natural pigments with potent inhibitory activity.* 49, 2001: p. 4.
199. Lima, J., et al., *Excited states of anthocyanins: the chalkone isomers of malvidin 3,5-diglucoside.* Journal of Photochemistry and Photobiology, 1994. **59**: p. 412-418.
200. De Rosso, V.V., *Bioactivities of Brazilian fruits and the antioxidant potential of tropical biomes.* Food and Public Health, 2013. **3**(1): p. 37-51.
201. Philpott, P., et al., *Enhanced col- oration reveals high antioxidant potential in new sweetpotato cultivars.* Journal of Science Food and Agriculture, 2003. **83**: p. 6.
202. Cevallos-Casals, B.A. and L. Cisneros-Zevallos, *Stability of anthocyanin-based aqueous extracts of Andean purple corn and red-fleshed sweet potato compared to synthetic and natural colorants.* Food Chemistry, 2004. **86**(1): p. 8.
203. McGhie, T.K. and M.C. Walton, *The bioavailability and absorption of anthocyanins: towards a better understanding.* Mol Nutr Food Res, 2007. **51**(6): p. 702-13.
204. Fardet, A., et al., *Influence of food structure on dairy protein, lipid and calcium bioavailability: A narrative review of evidence.* Critical Reviews in Food Science and Nutrition, 2018.
205. Pissarra, J., et al., *Reaction Between Malvidin 3-Glucoside and (+)-Catechin in Model Solutions Containing Different Aldehydes.* Journal of Food Science, 2003. **68**(2): p. 476-481.
206. Soares, S., et al., *Reactivity of human salivary proteins families toward food polyphenols. .* Journal of Agricultural and Food Chemistry, 2011. **59** (10): p. 12.
207. Brandão, E., et al., *Human saliva protein profile: Influence of food ingestion.* Food Research International, 2014. **64**: p. 6.
208. Minekus, M., et al., *A standardised static in vitro digestion method suitable for food - an international consensus.* Food Funct, 2014. **5**(6): p. 1113-24.
209. Fernandes, I., et al., *A new approach on the gastric absorption of anthocyanins.* Food Funct, 2012. **3**(5): p. 508-16.
210. He, F., et al., *Anthocyanins and Their Variation in Red Wines I. Monomeric Anthocyanins and Their Color Expression* Molecules, 2012. **17**: p. 30.
211. Arroyo-Maya, I.J., et al., *Characterization of flavonoid-protein interactions using fluorescence spectroscopy: Binding of pelargonidin to dairy proteins.* Food Chemistry, 2016. **213**: p. 8.
212. Tsukita, S. and M. Furuse, *Pores in the wall: claudins constitute tight junctions strands containing aqueous pores.* Journal of Cellular Biology, 2000. **149**: p. 13-16.

213. Lemieux, M., et al., *The NCI-N87 cell line as a gastric epithelial barrier model for drug permeability assay.* Biochemical and Biophysical Research Communications, 2011. **412**(3): p. 429-434.
214. Michaelis, L. and M. Menten, *Die Kinetik der Invertinwirkung.* Biochemische Zeitschrift, 1913. **49**: p. 333-369.
215. Bhaswant, M., et al., *Anthocyanins in chokeberry and purple maize attenuate diet-induced metabolic syndrome in rats.* Nutrition, 2017. **41**: p. 24-31.
216. Fernandes, I., et al., *Wine Flavonoids in Health and Disease Prevention.* Molecules, 2017. **22**(2).
217. Udenigwe, C.C. and V. Fogliano, *Food matrix interaction and bioavailability of bioactive peptides: Two*
faces of the same coin? Journal of Functional Foods, 2017. **35**: p. 4.
218. Soares, S., N. Mateus, and V. de Freitas, *Interaction of different classes of salivary proteins with food tannins.* Food Research International, 2012. **49**(2): p. 7.
219. Soares, S., et al., *Study of human salivary proline-rich proteins interaction with food tannins.* Food Chemistry, 2018. **243**: p. 11.
220. Ferrer-Gallego, R., et al., *New Anthocyanin-Human Salivary Protein Complexes.* Langmuir, 2015. **31**(30): p. 8392-401.
221. Sasaki, N., et al., *The role of acyl-glucose in anthocyanin modifications.* Molecules, 2014. **19**(11): p. 18747-66.
222. Liu, Y., et al., *Stability and absorption of anthocyanins from blueberries subjected to a simulated digestion process.* Int J Food Sci Nutr, 2014. **65**(4): p. 440-8.
223. Sirisena, S., S. Ajloun, and K. Ng, *Simulated gastrointestinal digestion and in vitro colonic fermentation of date (Phoenix dactylifera L.) seed polyphenols.* International Journal of Food Science and Technology, 2018. **53**(2): p. 10.
224. Mandalari, G., et al., *Food Matrix Effects of Polyphenol Bioaccessibility from Almond Skin during Simulated Human Digestion.* Nutrients, 2016. **8**(9).
225. Sengul, H., E. Surek, and D. Nilufer-Erdil, *Investigating the effects of food matrix and food components on bioaccessibility of pomegranate (Punica granatum) phenolics and anthocyanins using an in-vitro gastrointestinal digestion model.* Food Research International, 2014. **62**: p. 11.
226. Pineda-Vadillo, C., et al., *The food matrix affects the anthocyanin profile of fortified egg and dairy matrices during processing and in vitro digestion.* Food Chem, 2017. **214**: p. 486-496.
227. Milbury, P.E., et al., *Bioavailablility of elderberry anthocyanins.* Mech Ageing Dev, 2002. **123**(8): p. 997-1006.

228. Maeshima, M. and T. Ashi, *Characterization of major proteins in sweet potato tuberous roots.* Phytochemistry, 1985. **24**(9): p. 4.
229. Senthilkumar, R. and K.W. Yeh, *Multiple biological functions of sporamin related to stress tolerance in sweet potato (Ipomoea batatas Lam).* Biotechnol Adv, 2012. **30**(6): p. 1309-17.
230. Sun, Y.-L., J.-M. Sun, and Q.-P. Li, *Purification and Trypsin Inhibitor Activity of a Sporamin B from Sweet Potato (Ipomoea batatas Lam. 55-2).* Agricultural Sciences in China, 2012. **8**(7): p. 12.
231. Hou, W.C., et al., *Glutathione peroxidase-like activity of 33 kDa trypsin inhibitor from roots of sweet potato* Plant Science, 2004. **166**: p. 5.
232. Garcia-Estévez, I., et al., *First evidences of interaction between pyranoanthocyanins and salivary proline-rich proteins.* Food Chemistry, 2017. **228**: p. 7.
233. Dauchet, L., P. Amouyel, and J. Dallongeville, *Fruit and vegetable consumption and risk of stroke: a meta-analysis of cohort studies.* Neurology, 2005. **65**(8): p. 1193-7.
234. Pandey, K.B. and S.I. Rizvi, *Plant polyphenols as dietary antioxidants in human health and disease.* Oxidative Medicine and Cellular Longevity, 2009. **2**(5): p. 270-278.
235. Fernandes, I., et al., *Multiple-approach studies to assess anthocyanin bioavailability.* Phytochemistry Reviews, 2015: p. 1-21.
236. Marques, C., et al., *Pharmacokinetics of blackberry anthocyanins consumed with or without ethanol: A randomized and crossover trial.* Mol Nutr Food Res, 2016.
237. Fernandes, I., et al., *Pharmacokinetics of table and Port red wine anthocyanins: a crossover trial in healthy men.* Food & Function, 2017. **8**(5): p. 2030-2037.
238. Fernandes, I., et al., *A new approach on the gastric absorption of anthocyanins.* Food & Function, 2012. **3**(5): p. 508-516.
239. Oliveira, H., et al., *Experimental and Theoretical Data on the Mechanism by Which Red Wine Anthocyanins Are Transported through a Human MKN-28 Gastric Cell Model.* Journal of Agricultural and Food Chemistry, 2015. **63**(35): p. 7685-7692.
240. Conde, J., et al., *15 years on siRNA delivery: Beyond the State-of-the-Art on inorganic nanoparticles for RNAi therapeutics.* Nano Today, 2015. **10**(4): p. 421-450.
241. Mendes, R., A.R. Fernandes, and P.V. Baptista, *Gold Nanoparticle Approach to the Selective Delivery of Gene Silencing in Cancer—The Case for Combined Delivery?* Genes, 2017. **8**(3): p. 94.
242. Conde, J., J.M. de la Fuente, and P.V. Baptista, *Nanomaterials for reversion of multidrug resistance in cancer: a new hope for an old idea?* Frontiers in Pharmacology, 2013. **4**: p. 134.

243. Vinhas, R., A.R. Fernandes, and P.V. Baptista, *Gold Nanoparticles for BCR-ABL1 Gene Silencing: Improving Tyrosine Kinase Inhibitor Efficacy in Chronic Myeloid Leukemia.* Molecular Therapy. Nucleic Acids, 2017. **7**: p. 408-416.
244. Roma-Rodrigues, C., et al., *Tumor Microenvironment Modulation via Gold Nanoparticles Targeting Malicious Exosomes: Implications for Cancer Diagnostics and Therapy.* International Journal of Molecular Sciences, 2017. **18**(1): p. 162.
245. Child, H.W., et al., *Gold nanoparticle-siRNA mediated oncogene knockdown at RNA and protein level, with associated gene effects.* Nanomedicine, 2015. **10**(16): p. 2513-2525.
246. Lee, P.C. and D. Meisel, *Adsorption and surface-enhanced Raman of dyes on silver and gold sols.* The Journal of Physical Chemistry, 1982. **86**(17): p. 3391-3395.
247. Livak, K.J. and T.D. Schmittgen, *Analysis of relative gene expression data using real-time quantitative PCR and the 2(-Delta Delta C(T)) Method.* Methods, 2001. **25**(4): p. 402-8.
248. Roberts, T.C., et al., *Quantification of nascent transcription by bromouridine immunocapture nuclear run-on RT-qPCR.* Nat Protoc, 2015. **10**(8): p. 1198-211.
249. Deng, D., et al., *Crystal structure of the human glucose transporter GLUT1.* Nature, 2014. **510**(7503): p. 121-5.
250. Deng, D., et al., *Molecular basis of ligand recognition and transport by glucose transporters.* Nature, 2015. **526**(7573): p. 391-6.
251. Gaussian Inc., C.O.P., Bldg. 6, Pittsburgh, PA 15106, USA.
252. Cerqueira, N., et al., *vsLab-An Implementation for Virtual High-Throughput Screening Using AutoDock and VMD.* International Journal of Quantum Chemistry, 2011. **111**(6): p. 1208-1212.
253. Morris, G.M., et al., *AutoDock4 and AutoDockTools4: Automated docking with selective receptor flexibility.* Journal of Computational Chemistry, 2009. **30**(16): p. 2785-91.
254. Humphrey, W., A. Dalke, and K. Schulten, *VMD: Visual molecular dynamics.* Journal of Molecular Graphics & Modelling, 1996. **14**(1): p. 33-38.
255. Jo, S., et al., *CHARMM-GUI: a web-based graphical user interface for CHARMM.* Journal of Computational Chemistry, 2008. **29**(11): p. 1859-65.
256. Frisch, M.J., G. W. Trucks, H. B. Schlegel, Scuseria, G. E.; Robb, M. A.; Cheeseman, J. R.; Scalmani, G.; Barone, V.; Mennucci, B.; Petersson, G. A.; Nakatsuji, H.; Caricato, M.; Li, X.; Hratchian, H. P.; Izmaylov, A. F.; Bloino, J.; Zheng, G.; Sonnenberg, J. L.; Hada, M.; Ehara, M.; Toyota, K.; Fukuda, R.; Hasegawa, J.; Ishida, M.; Nakajima, T.; Honda, Y.; Kitao, O.; Nakai, H.; Vreven, T.; Montgomery, Jr., J. A.; Peralta, J. E.;

Ogliaro, F.; Bearpark, M.; Heyd, J. J.; Brothers, E.; Kudin, K. N.; Staroverov, V. N.; Kobayashi, R.; Normand, J.; Raghavachari, K.; Rendell, A.; Burant, J. C.; Iyengar, S. S.; Tomasi, J.; Cossi, M.; Rega, N.; Millam, N. J.; Klene, M.; Knox, J. E.; Cross, J. B.; Bakken, V.; Adamo, C.; Jaramillo, J.; Gomperts, R.; Stratmann, R. E.; Yazyev, O.; Austin, A. J.; Cammi, R.; Pomelli, C.; Ochterski, J. W.; Martin, R. L.; Morokuma, K.; Zakrzewski, V. G.; Voth, G. A.; Salvador, P.; Dannenberg, J. J.; Dapprich, S.; Daniels, A. D.; Farkas, Ö.; Foresman, J. B.; Ortiz, J. V.; Cioslowski, J.; Fox, D. J., *Gaussian 09*. 2009, Gaussian, Inc.: Wallingford CT.

257. Bayly, C.I., et al., *A Well-Behaved Electrostatic Potential Based Method Using Charge Restraints for Deriving Atomic Charges - the Resp Model.* Journal of Physical Chemistry, 1993. **97**(40): p. 10269-10280.
258. Hornak, V., et al., *Comparison of multiple amber force fields and development of improved protein backbone parameters.* Proteins-Structure Function and Bioinformatics, 2006. **65**(3): p. 712-725.
259. Wang, J.M., et al., *Development and testing of a general amber force field.* Journal of Computational Chemistry, 2004. **25**(9): p. 1157-1174.
260. Jambeck, J.P. and A.P. Lyubartsev, *An Extension and Further Validation of an All-Atomistic Force Field for Biological Membranes.* Journal of Chemical Theory and Computation, 2012. **8**(8): p. 2938-48.
261. Ryckaert, J.P., G. Ciccotti, and H.J.C. Berendsen, *Numerical-Integration of Cartesian Equations of Motion of a System with Constraints - Molecular-Dynamics of N-Alkanes.* Journal of Computational Physics, 1977. **23**(3): p. 327-341.
262. Izaguirre, J.A., et al., *Langevin stabilization of molecular dynamics.* Journal of Chemical Physics, 2001. **114**(5): p. 2090-2098.
263. Essmann, U., et al., *A SMOOTH PARTICLE MESH EWALD METHOD.* Journal of Chemical Physics, 1995. **103**(19): p. 8577-8593.
264. Case, D.A., et al., *AMBER 12, University of California, San Francisco*. 2012.
265. Roe, D.R. and T.E. Cheatham, 3rd, *PTRAJ and CPPTRAJ: Software for Processing and Analysis of Molecular Dynamics Trajectory Data.* Journal of Chemical Theory and Computation, 2013. **9**(7): p. 3084-95.
266. Kollman, P.A., et al., *Calculating structures and free energies of complex molecules: Combining molecular mechanics and continuum models.* Accounts of Chemical Research, 2000. **33**(12): p. 889-897.
267. Sanz, V., et al., *Effect of PEG biofunctional spacers and TAT peptide on dsRNA loading on gold nanoparticles.* Journal of Nanoparticle Research, 2012. **14**(6): p. 917.

268. Kuang, T., et al., *Molecular Beacon Nano-Sensors for Probing Living Cancer Cells.* Trends Biotechnol, 2017. **35**(4): p. 347-359.
269. Cordeiro, M., et al., *Gold Nanobeacons for Tracking Gene Silencing in Zebrafish.* Nanomaterials, 2017. **7**(1): p. 10.
270. Garnett, M.J., et al., *Systematic identification of genomic markers of drug sensitivity in cancer cells.* Nature, 2012. **483**(7391): p. 570-5.
271. Jeong, S.H., et al., *OCT-1 overexpression is associated with poor prognosis in patients with well-differentiated gastric cancer.* Tumour Biol, 2014. **35**(6): p. 5501-9.
272. Wei, Z., et al., *The impact of insulin on chemotherapeutic sensitivity to 5-fluorouracil in gastric cancer cell lines SGC7901, MKN45 and MKN28.* Journal of Experimental & Clinical Cancer Research : CR, 2015. **34**(1): p. 64.
273. Loike, J.D., et al., *Role of facilitative glucose transporters in diffusional water permeability through J774 cells.* J Gen Physiol, 1993. **102**(5): p. 897-906.
274. Park, M.S., *Molecular Dynamics Simulations of the Human Glucose Transporter GLUT1.* PLoS One, 2015. **10**(4): p. e0125361.
275. Hruz, P.W. and M.M. Mueckler, *Cysteine-scanning mutagenesis of transmembrane segment 11 of the GLUT1 facilitative glucose transporter.* Biochemistry, 2000. **39**(31): p. 9367-72.
276. Mueckler, M. and C. Makepeace, *Analysis of transmembrane segment 10 of the Glut1 glucose transporter by cysteine-scanning mutagenesis and substituted cysteine accessibility.* J Biol Chem, 2002. **277**(5): p. 3498-503.
277. Baron, G., et al., *Pharmacokinetic profile of bilberry anthocyanins in rats and the role of glucose transporters: LC-MS/MS and computational studies.* J Pharm Biomed Anal, 2017. **144**: p. 112-121.
278. Zhang, H., et al., *Bioaccessibility, bioavailability, and anti-inflammatory effects of anthocyanins from purple root vegetables using mono- and co-culture cell models.* Mol Nutr Food Res, 2017. **61**(10).
279. Pina, F., *Chemical applications of anthocyanins and related compounds. A source of bioinspiration.* Journal of Agricultural and Food Chemistry, 2014. **62**(29): p. 6885-97.
280. He, J., et al., *Oxovitisins: a new class of neutral pyranone-anthocyanin derivatives in red wines.* Journal of Agricultural and Food Chemistry, 2010. **58**: p. 8814-8819.
281. Mateus, N., et al., *Structural diversity of anthocyanin-derived pigments in port wines.* Journal of Agricultural and Food Chemistry, 2002. **76**: p. 335-342.
282. Oliveira, J., et al., *Pyranoanthocyanin dimers: a new family of turquoise blue anthocyanin-derived pigments found in Port wine.* Journal of Agricultural and Food Chemistry, 2010. **58**: p. 5154-5159.

283. Seeram, N.P., et al., *Blackberry, black raspberry, blueberry, cranberry, red raspberry, and strawberry extracts inhibit growth and stimulate apoptosis of human cancer cells in vitro.* Journal of Agricultural and Food Chemistry, 2006. **54**: p. 9329-9339.
284. Zhang, Y., S.K. Vareed, and M.G. Nair, *Human tumor cell growth inhibition by nontoxic anthocyanidins, the pig- ments in fruits and vegetables.* Life Sciences, 2005. **76**: p. 1465-1472.
285. Huang, W.Y., et al., *Inhibitory effect of Malvidin on TNF-alpha-induced inflam- matory response in endothelial cells.* European Journal of Pharmacology, 2014. **723**: p. 67-72.
286. Garcia-Alonso, M., et al., *Electron spin resonance spectroscopy studies on the free radical scavenging activity of wine anthocyanins and pyranoanthocyanins.* Molecular Nutrition and Food Research, 2005. **49**: p. 1112-1119.
287. Azevedo, J., et al., *Antioxidant features of red wine pyranoanthocyanins: experimental and theoretical approaches.* Journal of Agricultural and Food Chemistry, 2014. **62**: p. 7002-7009.
288. Faria, A., et al., *Blueberry anthocyanins and pyruvic acid adducts: anticancer properties in breast cancer cell lines.* Phytotherapy Research, 2010. **24**: p. 1862-1869.
289. Zhu, Z., et al., *Preparation and toxicological evaluation of methyl pyranoanthocyanin.* Food and Chemical Toxicology, 2015. **83**: p. 125-132.
290. He, J., et al., *Oxidative formation and structural characterisation of new α-pyranone (lactone) compounds of non-oxonium nature origi- nated from fruit anthocyanins.* Food Chemistry, 2011. **127**: p. 984-992.
291. Min, K., et al., *Optimized method for preparation of methyl pyranoanthocyanins and analyzed by HPLC-MS/MS.* Science and Technology of Food Industry, 2014: p. 257-262.
292. Oliveira, J., et al., *Color properties of four cyanidin-pyruvic acid adducts.* Journal of Agricultural and Food Chemistry, 2006. **54**: p. 6894-6903.
293. Oliveira, H., et al., *Ageing impact on the antioxidant and antiproliferative properties of Port wines.* Food Research International, 2015. **67**(0): p. 199-205.
294. Mateus, N. and V. De Freitas, *Evolution and stability of anthocyanin-derived pigments during Port wine aging.* Journal of Agricultural and Food Chemistry, 2001. **49**: p. 5217-5222.
295. Léon-Gonzalez, A.J., C. Auger, and V.B. Schini-Kert, *Pro-oxidant activity of polyphenols and its implication on cancer chemoprevention and chemotherapy.* Biochemical Pharmacology, 2015.

296. Garcia-Alonso, M., et al., *Antioxidant and cellular activities of anthocyanins and their corresponding vitisins A--studies in platelets, monocytes, and human endothelial cells.* Journal of Agricultural and Food Chemistry, 2004. **52**: p. 3378-3384.
297. Chen, J., et al., *Protective effect of blueberry anthocyanins in a CCL4-induced liver cell model.* LWT - Food Science and Technology, 2015. **60**(2, Part 2): p. 1105-1112.
298. Lelono, R.A., S. Tachibana, and K. Itoh, *Isolation of antifungal compounds from Gardenia jasminoides.* Pakistan journal of biological sciences : PJBS, 2009. **12**(13): p. 949-56.
299. Watanabe, T. and S. Terabe, *Analysis of natural food pigments by capillary electrophoresis.* Journal of chromatography. A, 2000. **880**(1-2): p. 311-22.
300. Machida, K., et al., *Studies on the constituents of Gardenia species. III. New iridoid glycosides from the leaves of Gardenia jasminoides cv. fortuneana Hara.* Chemical & pharmaceutical bulletin, 2003. **51**(12): p. 1417-9.
301. Takeda, Y., H. Nishimura, and H. Inouye, *Two new iridoid glucosides from Ixora chinensis.* Phytochemistry, 1975. **14**(12): p. 2647-2650.
302. Qin, F.M., et al., *Three new iridoid glycosides from the fruit of gardenia jasminoides var. radicans.* Chemical & pharmaceutical bulletin, 2013. **61**(10): p. 1071-4.
303. Selim, K., M. Tsimidou, and C.G. Biliaderis, *Kinetic studies of degradation of saffron carotenoids encapsulated in amorphous polymer matrices.* Food Chemistry, 2000. **71**(2): p. 199-206.
304. Ordoudi, S.A. and M.Z. Tsimidou, *Saffron Quality: Effect of Agricultural Practices, Processing and Storage*, in *Production Practices and Quality Assessment of Food Crops Volume 1: Preharvest Practice*, R. Dris and S.M. Jain, Editors. 2004, Springer Netherlands: Dordrecht. p. 209-260.
305. Kyriakoudi, A., et al., *Changes in Total and Individual Crocetin Esters upon in Vitro Gastrointestinal Digestion of Saffron Aqueous Extracts.* Journal of Agricultural and Food Chemistry, 2013. **61**(22): p. 5318-5327.
306. Gutheil, W.G., et al., *Crocetin: an agent derived from saffron for prevention and therapy for cancer.* Current Pharmaceutical Biotechnology, 2012. **13**(1): p. 173-9.
307. Alavizadeh, S.H. and H. Hosseinzadeh, *Bioactivity assessment and toxicity of crocin: a comprehensive review.* Food and Chemical Toxicology 2014. **64**: p. 65-80.
308. Debnath, T., et al., *Antioxidant activity of Gardenia jasminoides Ellis fruit extracts.* Food Chemistry, 2011. **128**(3): p. 697-703.
309. Ozaki, A., et al., *Genotoxicity of gardenia yellow and its components.* Food and Chemical Toxicology, 2002. **40**(11): p. 1603-10.

310. Bors, W., M. Saran, and C. Michel, *Radical intermediates involved in the bleaching of the carotenoid crocin. Hydroxyl radicals, superoxide anions and hydrated electrons.* International journal of radiation biology and related studies in physics, chemistry, and medicine, 1982. **41**(5): p. 493-501.

311. Bors, W., C. Michel, and M. Saran, *Inhibition of the bleaching of the carotenoid crocin a rapid test for quantifying antioxidant activity.* Biochimica et Biophysica Acta (BBA) - Lipids and Lipid Metabolism, 1984. **796**(3): p. 312-319.

312. Bountagkidou, O., et al., *An on-line high performance liquid chromatography-crocin bleaching assay for detection of antioxidants.* Journal of Chromatography A, 2012. **1237**: p. 80-85.

313. Konoshima, T., et al., *Crocin and crocetin derivatives inhibit skin tumour promotion in mice.* Phytotherapy Research, 1998. **12**(6): p. 400-404.

314. Escribano, J., et al., *Crocin, safranal and picrocrocin from saffron (Crocus sativus L.) inhibit the growth of human cancer cells in vitro.* Cancer Letters, 1996. **100**(1–2): p. 23-30.

315. Aung, H.H., et al., *Crocin from Crocus sativus possesses significant anti-proliferation effects on human colorectal cancer cells.* Experimental Oncology, 2007. **29**(3): p. 175-80.

316. Coussens, L.M. and Z. Werb, *Inflammation and cancer.* Nature, 2002. **420**(6917): p. 860-7.

317. Grivennikov, S., et al., *IL-6 and Stat3 are required for survival of intestinal epithelial cells and development of colitis-associated cancer.* Cancer Cell, 2009. **15**(2): p. 103-13.

318. Tse, B.W.C., K.F. Scott, and P.J. Russell, *Paradoxical Roles of Tumour Necrosis Factor-Alpha in Prostate Cancer Biology.* Prostate Cancer, 2012. **2012**: p. 8.

319. Zhang, Y., et al., *Sensitive analysis and simultaneous assessment of pharmacokinetic properties of crocin and crocetin after oral administration in rats.* Journal of Chromatography B, 2017. **1044–1045**: p. 1-7.

320. Khorasany, A.R. and H. Hosseinzadeh, *Therapeutic effects of saffron (Crocus sativus L.) in digestive disorders: a review.* Iran J Basic Med Sci, 2016. **19**(5): p. 455-69.

321. Zhong, Y.J., et al., *Crocetin induces cytotoxicity and enhances vincristine-induced cancer cell death via p53-dependent and -independent mechanisms.* Acta Pharmacol Sin, 2011. **32**(12): p. 1529-36.

322. Kipanyula, M.J., et al., *Signaling pathways bridging microbial-triggered inflammation and cancer.* Cellular Signalling, 2013. **25**(2): p. 403-16.

323. Ashizawa, T., et al., *Study of interleukin-6 in the spread of colorectal cancer: the diagnostic significance of IL-6.* Acta Medica Okayama, 2006. **60**(6): p. 325-30.
324. Atsumi, T., et al., *Inflammation amplifier, a new paradigm in cancer biology.* Cancer Research, 2014. **74**(1): p. 8-14.
325. Dinarello, C.A., *Biologic basis for interleukin-1 in disease.* Blood, 1996. **87**(6): p. 2095-147.
326. Apte, R.N., et al., *Effects of micro-environment- and malignant cell-derived interleukin-1 in carcinogenesis, tumour invasiveness and tumour-host interactions.* European journal of cancer (Oxford, England : 1990), 2006. **42**(6): p. 751-9.
327. Shanahan, J.C. and W. St Clair, *Tumor necrosis factor-alpha blockade: a novel therapy for rheumatic disease.* Clinical immunology (Orlando, Fla.), 2002. **103**(3 Pt 1): p. 231-42.